V. P. I. LIBRARY
DEC 18 1961
BLACKSBURG, VA.

JOURNAL OF FLUID MECHANICS

VOLUME 11 PART 3

NOVEMBER 1961

PUBLISHED BY

CAMBRIDGE UNIVERSITY PRESS

BENTLEY HOUSE, 200 EUSTON ROAD, LONDON, N.W.1

AMERICAN BRANCH: 32 EAST 57TH STREET, NEW YORK 22, N.Y.

Price 30*s.* (*U.S.A.* $5.00)

The JOURNAL OF FLUID MECHANICS exists for the publication of theoretical and experimental investigations of all aspects of the mechanics of fluids, and is issued in four parts per volume.

EDITORS

DR G. K. BATCHELOR, DR T. BROOKE BENJAMIN

Department of Applied Mathematics and Theoretical Physics, University of Cambridge, Free School Lane, Cambridge, England

ASSISTANT EDITORS

DR J. R. A. PEARSON, DR O. M. PHILLIPS

ASSOCIATE EDITORS

PROF. G. F. CARRIER

Pierce Hall, Harvard University, Cambridge 38, *Massachusetts, U.S.A.*

DR W. C. GRIFFITH

Lockheed Missiles and Space Division, Palo Alto, California, U.S.A.

M. J. LIGHTHILL

Royal Aircraft Establishment, Farnborough, Hampshire, England

PROF. R. R. LONG

School of Engineering, The Johns Hopkins University, Baltimore 18, *Maryland, U.S.A.*

DR P. G. SAFFMAN

Department of Mathematics, King's College, London, W.C. 2, *England*

Authors wishing to have papers published in the JOURNAL should communicate them to any one of the persons named above, choosing one in their own country where possible.

Authors are urged to ensure that their papers are written clearly and attractively, in order that their work will be readily accessible to readers.

Manuscripts should be typed in double spacing on one side of the paper only, with references listed at the end in alphabetical order of authors. Drawings should be done on a large scale in Indian ink on tracing cloth or drawing paper, the lettering being shown clearly in pencil for reproduction by the printer; the list of captions should be typed at the end of the manuscript. Proofs of papers from overseas will usually be despatched to authors by airmail. There is no charge for publication. Authors are entitled to receive 50 offprints of a paper in the JOURNAL free of charge, and additional offprints can be purchased if ordered in advance.

SUBSCRIPTIONS

The subscription price for a volume of four parts is £5. 10*s*. net, post free, payable in advance; separate parts 30*s*. net, plus postage. Subscriptions may be sent to any bookseller, or to the Cambridge University Press, Bentley House, 200 Euston Road, London, N.W.1.

Subscribers in the United States should send their orders to the Cambridge University Press, American Branch, 32 East 57th Street, New York 22, N.Y. The subscription price per volume is $18.50, post free, payable in advance; separate parts $5.00, plus postage.

Quotations for available back volumes and parts may be obtained on application to the Cambridge University Press.

The mechanism of transition in the wake of a thin flat plate placed parallel to a uniform flow

By HIROSHI SATO AND KYOICHI KURIKI
Aeronautical Research Institute, University of Tokyo, Japan

(Received 10 February 1961)

A study was made of the laminar-turbulent transition of a wake behind a thin flat plate which was placed parallel to a uniform flow at subsonic speeds. Experimental results on the nature of the velocity fluctuations have made it possible to classify the transition region into three subregions: the linear region, the non-linear region and the three-dimensional region.

In the linear region there is found a sinusoidal velocity fluctuation which is antisymmetrical with respect to the centre-line of the wake. The frequency of fluctuation is proportional to the $\frac{3}{2}$ power of the free-stream velocity, and the amplitude increases exponentially in the direction of flow. The behaviour of small disturbances in the linear region was investigated in detail by inducing velocity fluctuation with an external excitation—actually sound from a loudspeaker. Solutions of the equation of a small disturbance superposed on the laminar flow were obtained numerically and compared with the experimental results. The agreement between the two was satisfactory.

When the amplitude of fluctuation exceeds a certain value, the growth rate deviates from being exponential due to non-linear effects. Although velocity fluctuations in the non-linear region are still sinusoidal and two-dimensional, the experimental results on the distributions of amplitude and phase indicate that the flow pattern may be described by the model of a double row of vortices. This configuration lasts until three-dimensional distortion takes place in the final subregion, the three-dimensional region, in which the fluctuation loses regularity and gradually develops into turbulence without being accompanied by abrupt breakdown or turbulent bursts.

1. Introduction

The laminar-turbulent transition of boundary layers is a well-known phenomenon which has been investigated theoretically and experimentally since the beginning of this century. The detailed process of transition, however, still remains unclarified. In the initial period of investigation, interest lay mainly in determining the transition Reynolds number, which was important from the practical viewpoint. Modern developments in experimental techniques of flow measurement have made it possible to make detailed observations of velocity fluctuations in the boundary layer. Thus, investigations in the last decade have been focused on the understanding of the mechanism of transition. Recent

experimental results have indicated that two typical patterns of velocity fluctuation are essential in the transition. One is the regular sinusoidal fluctuation of small amplitude, and the other is the instantaneous turbulent burst of much higher intensity.

Sinusoidal fluctuations were first discovered experimentally by Schubauer & Skramstad (1948) in the boundary layer along a flat plate. They obtained good agreement between their results and the linearized stability theory which had been developed by Tollmien, Schlichting and others. Since then, extended studies have been made on the properties of sinusoidal fluctuations both experimentally and theoretically. Sinusoidal velocity fluctuations have been found in various flow fields at subsonic and supersonic speeds, and agreement between linearized theory and the experimental results is satisfactory (Sato 1959*a*, *b*; Laufer & Vrebalovich 1960). It is now well established that the behaviour of fluctuations of small amplitude in the boundary layer is described by the linearized theory. On the other hand, our knowledge on the turbulent burst is poor. Experimental results obtained by various investigators sometimes show disagreements, and no concrete conclusions have been obtained on the origin and the law of development of a burst. Moreover, in the transition region of free boundary layers, no bursts have been observed so far (Sato 1959*a*, *b*). In order to obtain a full understanding of the detailed mechanism of transition, more extensive studies are wanted.

The present investigation has been undertaken with the intention of clarifying the process of transition in wakes. A thin flat plate was placed in a uniform flow with zero angle of attack so as to produce a simple, well-defined wake. It is obvious that the wake of a cylinder is inadequate for detailed studies of transition since the flow field behind a cylinder is much too complicated owing to boundary-layer separation and rolling up of vortices in the wake. The velocity profile of a laminar wake was calculated by Goldstein (1933), and stability calculations based on the Orr–Sommerfeld equation were carried out by Hollingdale (1940) and McKoen (1956) in the case of large Reynolds number. It was Hollingdale (1940) who made the first systematic observation of velocity fluctuations in the wake of a flat plate by taking pictures in a water tank. Taneda (1958) has extended these observations to a wider range of Reynolds number with an improved experimental arrangement. He has found sinusoidal velocity fluctuations whose frequency is proportional to $\frac{3}{2}$ power of the flow speed. The present work was started in order to make a more detailed survey of velocity fluctuations in wakes, using modern techniques of hot-wire anemometry in a low-turbulence wind-tunnel. The first part of this paper gives a general view of the transition phenomenon. The second part deals with the sinusoidal velocity fluctuations, and the third and fourth parts are devoted to clarifying the role of non-linear effects and three-dimensional distortion in the process of development into turbulence.

2. Experimental arrangement

The experiment was conducted in a 60×60 cm low-turbulence wind-tunnel which was newly constructed at the Aeronautical Research Institute. The tunnel is of non-return type with the test-section downstream of the fan. The contraction ratio, i.e. the ratio of cross-sectional area of the settling chamber to that of the test-section, is 16:1. Eleven damping screens were installed in the settling chamber. These arrangements, incorporated with a proper design of air-intake, fan and diffuser, diminished the turbulence level at the test-section to 0·05 % at a flow velocity of 10 m/sec. Background noise and mechanical vibrations were carefully reduced by suitable construction, since they have a great influence on the transition process. The wind speed at the test-section was

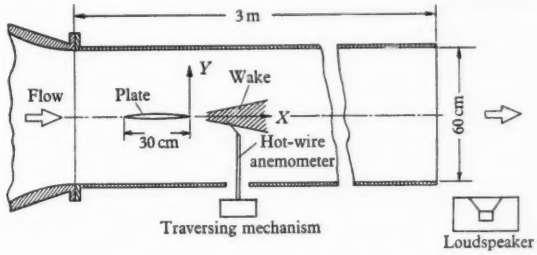

FIGURE 1. Layout of test-section.

variable from 1 to 30 m/sec. The general layout of the test-section is shown in figure 1, in which X is the distance downstream from the trailing edge of the plate, Y is measured perpendicular to the plate, and Z is the spanwise distance from the central point of the trailing edge.

The side walls of the test-section were made of aluminum plates which were adjusted in order to keep the streamwise static-pressure distribution constant. One of the side walls had slits parallel and normal to the flow which allowed the insertion and traversing of hot-wire anemometers and pressure probes in the X-, Y- and Z-directions.

The two-dimensional wake was realized behind a thin flat plate which was spanned vertically along the centre-line of the wind-tunnel. The parallel alignment between the plate and the direction of flow was accomplished by measuring the mean-velocity distribution at the trailing edge of the plate. Three kinds of flat plate were used in order to clarify the effect of the thickness of the plate, as well as the sharpness of trailing edge, on the transition process. Dimensions of these plates are summarized in table 1.

The chord and span of all plates were 30 and 60 cm, respectively. Plate I was made of aluminium, carefully machined into a thin airfoil over the whole length and polished to a mirror-like surface. Plate II was a thin brass foil without machining. Plate III was made of aluminium and was sharpened at the leading edge, with the remaining part kept at the same thickness until the square trailing edge. The Reynolds number based on the length of plate ranged from 6×10^4 to 4×10^5.

For the measurement of the mean-velocity distribution, both fine Pitot tubes and hot-wire anemometers were used, although the measurements by Pitot tubes formed a very small part of the present experiment. For the hot-wire anemometers, use was made of 10 % rhodium-platinum wire, 5 μ in diameter and about 2 mm in length. For the measurement of the w-component of velocity, the hot-wire was rotated around the axis of support.

	Maximum thickness (mm)	Thickness ratio (%)	Thickness at the trailing edge (mm)
Plate I	3	1	0·1
Plate II	0·3	0·1	0·3
Plate III	3	1	3

TABLE 1. Dimensions of plate.

The mean velocity and the root-mean-square of the fluctuating velocity were measured by conventional hot-wire equipment which has been previously reported (Sato, Kobashi, Iuchi, Yamamoto & Onda 1954). The spectral distribution of the velocity fluctuation was observed by a band-pass filter. The mean-cube of the fluctuation was measured by a newly constructed unit in which the cubic curve was approximated by the superposition of the plate currents of ten triodes which were properly biased and loaded. A mean-square output meter was constructed on the same principle. This type of circuit had the advantages of higher input impedance and lower power consumption compared with similar circuits constructed by diodes. The fluctuation patterns were observed and recorded by a dual-beam cathode-ray oscilloscope.

The anemometers were traversed in the X-, Y- and Z-directions. The X- and Z-positions were determined by scales, and the Y-position was indicated by a precision dial gauge. The accuracy of positioning was 0·2 mm in the X- and Z-directions, and 0·01 mm in the Y-direction.

The flow was artificially excited by the sound radiated from a 10 W loud-speaker placed at the exit of the test-section as shown in figure 1. The maximum available intensity of the sound was about 100 db, although a much weaker sound was enough to induce transition in the laminar wake. The excitation frequency was varied from 500 to 1000 c/s, excluding the resonance frequency of the wind-tunnel, which was about 200 c/s. The intensity of sound was uniform throughout the test-section, and no resonance effect was detected in the above-mentioned frequency range.

3. General aspects of transition

At first, measurements were made in the boundary layer along the surface of the plate. The streamwise static-pressure variation along the surface was very small because the plates were very thin. The boundary layer was laminar everywhere on the plate, and no traces of a velocity fluctuation were found even at the

highest wind-speed. The velocity profile was of Blasius-type, and the streamwise development of the boundary layer was in good agreement with the well known theoretical calculation for a flat plate. These results were quite satisfactory as regards fixing the initial condition of the laminar two-dimensional wake.

After separation at the trailing edge, the boundary layers from both sides coalesced and formed a wake, which still remained laminar to some distance downstream. The velocity profile gradually changed from Blasius-type into laminar-wake type. Velocity distributions at various X-stations are shown in figure 2, where U_0 denotes the free-stream velocity. At $X = 0$, the distribution is of Blasius-type. Until $X = 30$ or 40 mm, the distribution varies slowly, while a sharp increase of central velocity is found from $X = 40$ to 60 mm. In the figure two unusual facts are demonstrated. First the velocity at the outer part of the wake sometimes exceeds the free-stream velocity (for example, at $X = 120$ mm, $Y = 4$ to 5 mm). Secondly, the central velocity is approximately equal at $X = 60$, 120 and 150 mm.

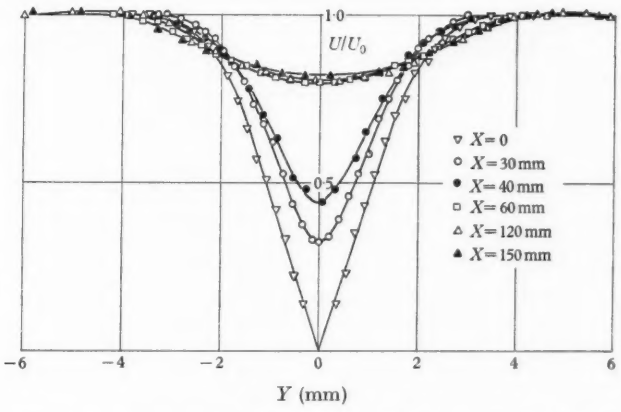

FIGURE 2. Mean-velocity distribution. Plate I, $U_0 = 10{\cdot}0$ m/sec.

In order to illustrate the streamwise variation of velocity distribution more clearly, the velocity U_c on the centre-line is plotted against X in figure 3. Curves for various experimental conditions show the same trend. The theoretical curve for the laminar wake given by Goldstein (1933) is in agreement with the experimental results when X is small. As X is increased, the experimental curves deviate from Goldstein's result, reach maxima, decrease and again increase gradually. The point of deviation from the theoretical curve may be called the 'transition point'. It must be kept in mind, however, that the transition never takes place at a point and, moreover, that the definition of transition itself is arbitrary. A more detailed account of the velocity distribution in the transition region will be given in the following paragraphs.

At $X = 5$ to 30 mm, depending on experimental conditions, there appears a velocity fluctuation whose wave-form is regular and sinusoidal. By careful investigation it was confirmed that the observed sinusoidal fluctuation was not

the result of either mechanical vibrations of the hot-wire or of acoustical resonance in the wind-tunnel. The frequency of fluctuation was the same throughout the whole region in which the wave-form was sinusoidal. The amplitude increased downstream until the wave-form was distorted into an irregular pattern. Since similar sinusoidal fluctuations have been already found in separated layers (Sato 1956, 1959*b*) and jets (Wehrmann & Wille 1958; Sato 1959*a*), the existence of sinusoidal fluctuations in the wake is not surprising. It has also been pointed out that the frequency of such fluctuations is proportional to the $\frac{3}{2}$ power of the flow velocity according to dimensional reasoning

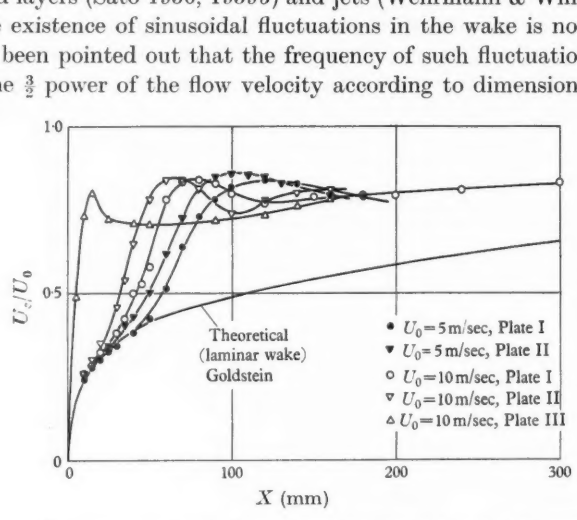

FIGURE 3. Streamwise variation of mean velocity U_c on the centre-line under various experimental conditions.

(Sato 1956). The logarithmic plot of frequency in the wake verified the same power law, as is shown in figure 4. The difference in frequency for three different plates was due to the difference in the thickness of the trailing edge. For a thick trailing edge, such as on Plate III, the thickness of the wake is comparatively large, and therefore the frequency of fluctuation is lower.

The development of the velocity fluctuations is illustrated in figures 5 and 6, which show results obtained with slight artificial excitation at the 'natural' frequency (i.e. the frequency of the sinusoidal fluctuations observed in the natural transition). Since the excitation was very slight, it had little effect on the transition process. On the other hand, the excitation improved the reproducibility of the flow field, and it was also used as a phase standard in the measurement of the phase relation of the velocity fluctuations. A detailed discussion concerning the interrelation between natural and excited transition is given in § 7. The wave-form of the u-fluctuation (figure 5) shows a gradual development from sinusoidal into irregular patterns. No turbulent bursts or momentary breakdowns have been observed. This type of transition is in contrast to that of a boundary layer on a solid wall, and is in accordance with transitions in separated layers and jets. Figure 6 is a map of fluctuation patterns at various X- and Y-positions. The sinusoidal fluctuation was observed from $X = 20$ to about 400 mm. Near the centre-line the second-harmonic component

prevailed as shown in figure 5. The irregular fluctuation first appeared near the centre-line and spread, as X was increased, until about $X = 400$ mm, where the whole wake was covered by irregular fluctuations.

It is worth while to note that at low Reynolds numbers the velocity fluctuation decays by viscous dissipation before the wave-form becomes irregular. In this case, no turbulent region exists in the wake even though the intensity of sinusoidal fluctuation may be considerable. This is another sharp contrast to the transition of a boundary layer on a solid wall, in which the continuous energy supply due to Reynolds stresses and velocity gradient is maintained. In the low

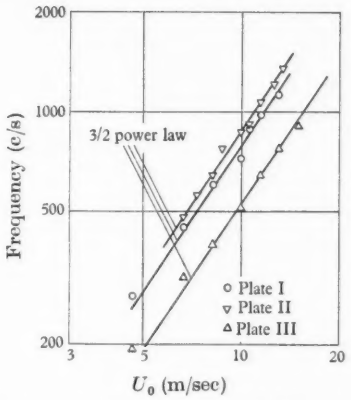

FIGURE 4. Frequency of natural sinusoidal fluctuations plotted against free-stream velocity U_0.

Reynolds number wake, the velocity gradient as well as the Reynolds stresses becomes progressively smaller downstream, and the viscous dissipation becomes pronounced. At higher Reynolds number, the wave-form of the fluctuations becomes irregular before it dies out, but it is still doubtful whether the wake becomes 'fully turbulent' or not. Moreover, even when the central part of the wake becomes turbulent, the regular fluctuation can persist in the outer part, as shown in figure 6. In these cases the definition of transition is vague. If the existence of a fully-turbulent region is a prerequisite of transition, there occurs no transition in the above-mentioned cases. Nevertheless, a high-level regular fluctuation exists in the wake and the mean-velocity distribution is different from that of laminar wake. We might call the region which is neither laminar nor turbulent the 'transition region'. In so far as we use the term 'transition' in this sense, the transition point might be the end point of the laminar region and not the beginning point of turbulent region.

The intensity of the u-fluctuations, with Plate I and $U_0 = 10{\cdot}0$ m/sec, is plotted in figure 7. When X was small, the distribution was almost similar, and positions of peak values approximately coincided with positions of maximum gradient in the mean-velocity distribution. As X was increased, the intensity increased until about $X = 60$ mm and then decreased. Distributions from $X = 60$ to 150 mm have maxima on the centre-line. This is due to the increase

of the second-harmonic component, which is shown in figures 5 and 6. The intensity of fluctuation in the present experiment was rather small compared with that in the wake behind a cylinder. This fact might be explained by the

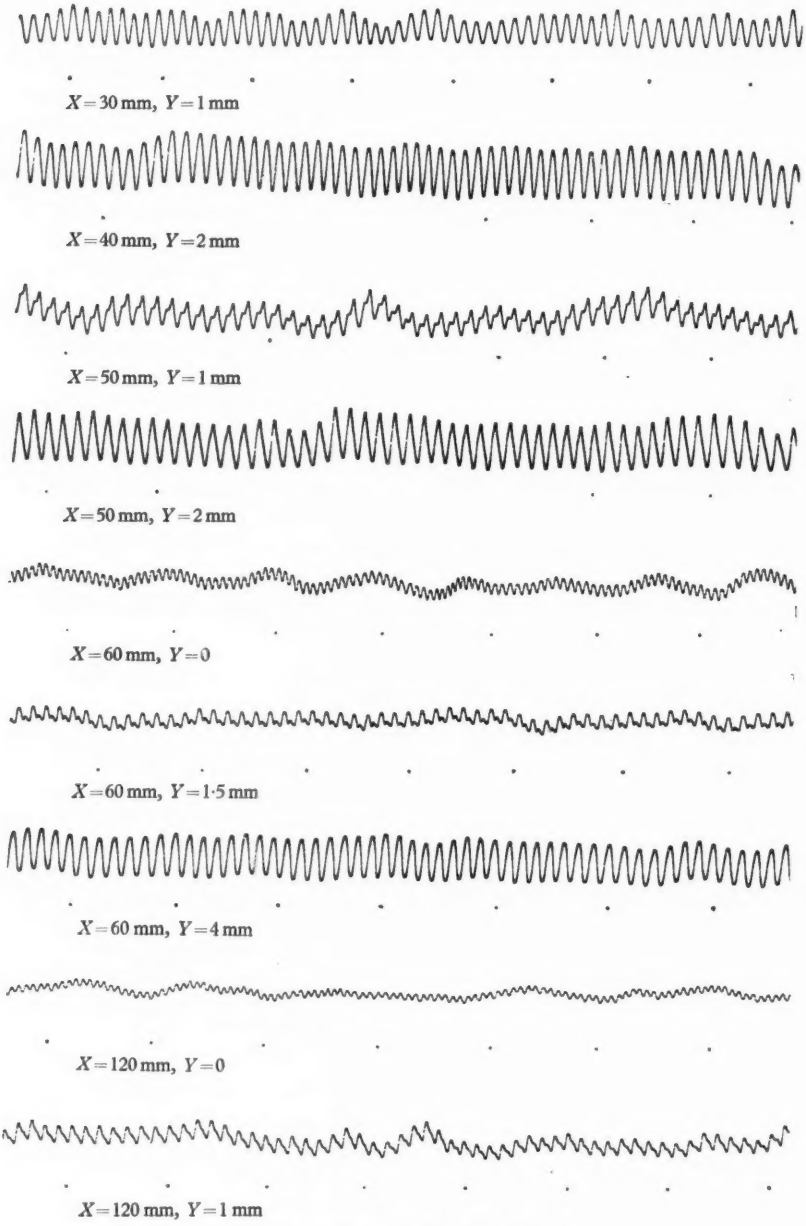

FIGURE 5. For legend see facing page.

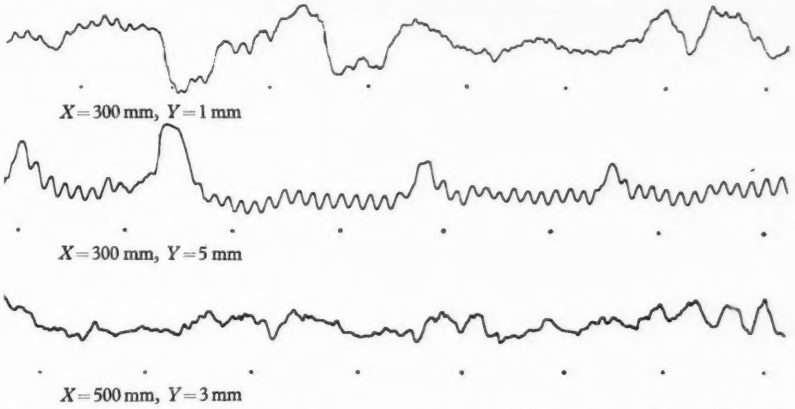

FIGURE 5. Oscillographic records of u-fluctuations in wake. Plate I, $U_0 = 10{\cdot}0$ m/sec. Time goes from left to right and time interval between dots is 0·01 sec.

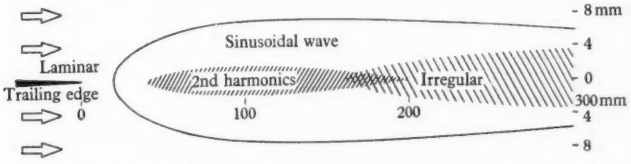

FIGURE 6. Map of fluctuation patterns. Plate I, $U_0 = 10{\cdot}0$ m/sec.

disturbance at the trailing edge of a flat plate being smaller than that behind a cylinder.

After these investigations were made on the velocity fluctuation in the transition region, we found it convenient to consider a division into three sub-regions, i.e. the linear region, the non-linear region, and the three-dimensional region, which are characterized by the pattern of fluctuations.

1. *Linear region.* In this region were observed two-dimensional sinusoidal velocity fluctuations which were amplified exponentially downstream. Referring to the previous investigations on free boundary layers (Sato 1959*a*, *b*), it is expected that these sinusoidal fluctuations may be described by the linearized theory. This region ends at the X-station where the amplitude of fluctuation reaches the 'linearity limit': in other words, where the law of amplification deviates from being exponential. The mean-velocity distribution in this region is in agreement with Goldstein's theoretical result.

2. *Non-linear region.* As a result of amplification of the sinusoidal fluctuations, second and higher harmonics are found in the wave-form, as shown in figure 5. Two-dimensionality is still maintained, that is, $\overline{w}^2$ is small compared with $\overline{u}^2$ and $\overline{v}^2$ and the phase difference of the velocity fluctuations in the Z-direction is small. The variation of mean velocity is remarkable in this region, being the result of intense energy supply from the mean flow to the velocity fluctuations.

3. *Three-dimensional region.* Further downstream the velocity fluctuation becomes three-dimensional, while some periodicity still persists. The wave-form

is irregular in the central part and is sinusoidal at the outer part of the wake. The turbulent region starts where the remaining regularity diminishes.

In the following paragraphs the mechanism of transition will be made clearer by describing in detail these three regions.

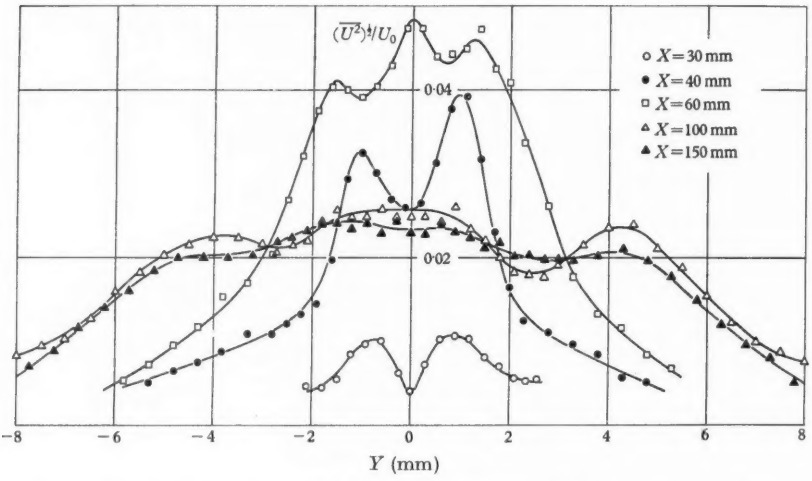

FIGURE 7. Distribution of intensity of u-fluctuations. Plate I, $U_0 = 10{\cdot}0$ m/sec.

4. The linear region

As shown in the previous paragraph, sinusoidal fluctuations are found in the transition region of the wake. They are weak at first, grow as the distance downstream is increased, and finally develop into irregular fluctuations still further downstream. The nature of the sinusoidal fluctuations has been clarified by both experimental and theoretical investigations.

4.1. *Experimental results*

Experiments on sinusoidal fluctuations have been made in two cases, one for natural transition and the other for transition caused by the external artificial disturbance. The latter is important for the experimental verification of linearized theory, which in turn is useful for clarifying the mechanism of the linear region in natural transition. Since natural transition results from the development of small unknown and uncontrollable disturbances, there is no essential difference between the natural and excited transition except the nature of the original disturbances. However, before detailed measurements are made with artificial excitations, it should be ascertained that the flow field is not changed too much by them. If the intensity of the artificial disturbance is too high, non-linear effects set in at X-stations that would lie in the linear region of natural transition. On the other hand, if the incoming sound is too weak, the induced fluctuation is masked by natural fluctuations, and in this case accurate measurements are difficult. The proper level of exciting sound was carefully decided as a compromise between these two considerations.

Experiments were carried out using Plate I at $U_0 = 10{\cdot}0$ m/sec. The frequency of natural fluctuations in this case was around 730 c/s. The frequency range of the artificial excitation was from 480 to 850 c/s. Outside this range the observed fluctuation was hardly affected by the sound.

The phase of the sinusoidal fluctuations was not constant in the X-direction, that is, the fluctuation was in fact a travelling wave. The propagation velocity was measured by moving a hot-wire anemometer in the X-direction. Since the

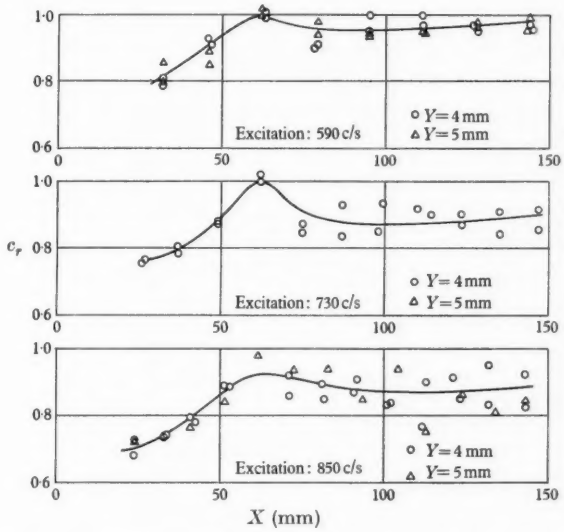

FIGURE 8. Propagation velocity of sinusoidal waves induced by artificial excitation. Plate I, $U_0 = 10{\cdot}0$ m/sec.

variation of phase in the Y-direction was remarkably large near the centre-line, as shown later, the phase difference in the X-direction had to be determined at large Y. Results for various frequencies of excitation are shown in figure 8, in which the propagation velocity c_r, expressed as a fraction of U_0, is plotted against X. The value of c_r increases as X is increased, reaches a maximum at about $X = 60$ to 70 mm, and settles at about 0·9 for larger X. It is interesting to note that the variation of c_r in the X-direction is similar to that of U_c. Detailed discussion of the values of c_r is found in § 4.3.

The increase in amplitude of the spectral components in the X-direction is illustrated in figure 9, in which $(\overline{u_f^2})^{\frac{1}{2}}_{\max}$ is the maximum value of the Y-distribution, of root-mean-square intensity of the spectral component at each X-station in the presence of excitation, whose frequency was as indicated. The value was obtained by adjusting the central frequency of a band-pass filter to be exactly equal to the frequency of the sound excitation, and then traversing the hot-wire in the Y-direction. Since $(\overline{u_f^2})^{\frac{1}{2}}_{\max}$ is plotted on an arbitrary scale, comparison between values at different frequencies would be meaningless, although the relative values for the same frequency are correctly expressed. Each spectral

component was amplified exponentially at small X and deviated from the exponential form at $X = 30$ to 35 mm due to non-linear effects. From the gradient of each curve the rate of amplification in the X-direction is calculated.

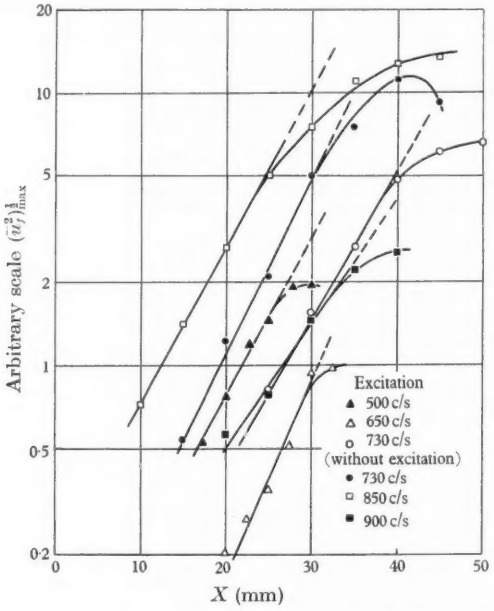

FIGURE 9. Growth of spectral components. Plate I, $U_0 = 10{\cdot}0$ m/sec.

Distributions in the Y-direction of amplitude and phase of natural sinusoidal fluctuations are shown in figure 10. The amplitude distribution has two peaks at about $Y = \pm 1$ mm, and becomes nearly zero on the centre-line. A change in phase is observed at -3 mm $< Y < 3$ mm. This is the reason why the variation of phase in the X-direction had to be measured at $Y = 4$ or 5 mm. Although a phase shift of about 70 degrees existed between $Y = -1$ and -5 mm, the phase difference at any two symmetrical points with respect to the centre-line was always approximately 180 degrees. These results are to be compared presently with the linearized theory.

Figure 11 shows distributions of amplitude and phase of the second-harmonic component (1460 c/s) which is found predominantly near the centre-line, as described before. The amplitude is a maximum at $Y = 0$, and the phase distribution shows that this component is symmetrical with respect to the centre-line. For the generation of the harmonic component the non-linear effect might be responsible. A full discussion of this point is given in the following sections.

4.2. *Theoretical considerations*

A theoretical investigation of the stability of wakes to small disturbances has been carried out by Hollingdale (1940) and McKoen (1956). Their work is restricted to the case of neutrally stable disturbances and, moreover, their

methods of approximation are rather crude. Therefore, in order to compare the foregoing experimental results with theory, calculations extending to the non-neutral case have been made with improved accuracy. Only the case of infinite Reynolds number has been considered.

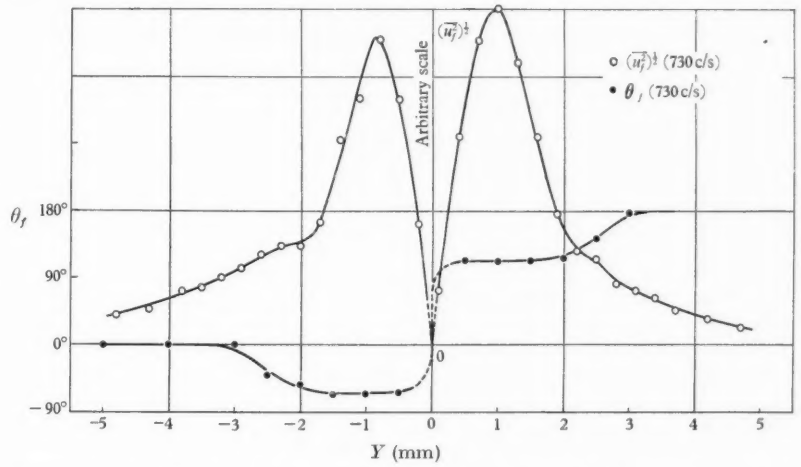

FIGURE 10. Amplitude and phase distributions of fundamental component. Plate I, $U_0 = 10{\cdot}0$ m/sec, $X = 40$ mm.

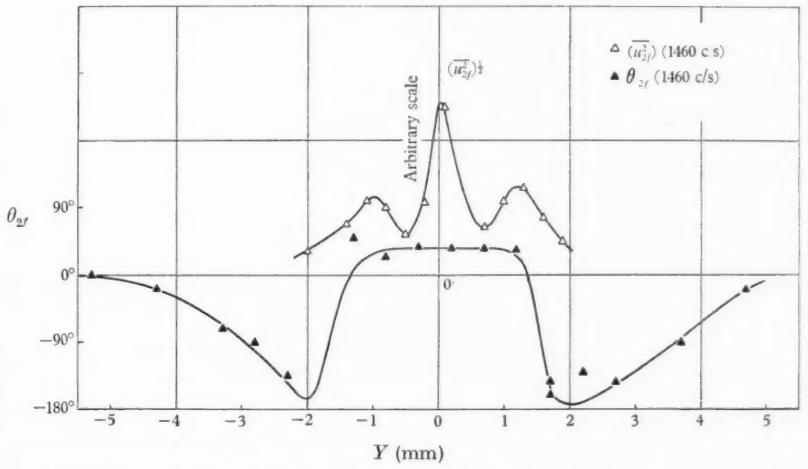

FIGURE 11. Amplitude and phase distributions of second-harmonic component. Plate I, $U_0 = 10{\cdot}0$ m/sec, $X = 40$ mm.

We follow the procedure of conventional linearized stability calculations. The basic flow is assumed to be two-dimensional and a function of y only, and lateral disturbance velocities are neglected. The disturbance velocities u and v are assumed to be functions of x, y and time t. Quantities in the equations of

motion and continuity are made non-dimensional by taking as units of velocity and length the free-stream velocity U_0 and the half-breadth b of the mean-velocity distribution. If X, Y, Z and T are the dimensional coordinates and time, the corresponding dimensionless quantities are written $x = X/b$, $y = Y/b$, $z = Z/b$ and $t = TU_0/b$.

We define a stream-function ψ such that the velocity perturbations are given by

$$u = \frac{\partial \psi}{\partial y}, \quad v = -\frac{\partial \psi}{\partial x},$$

and we assume that u and v are small enough to justify linearization of the equations of motion. We further assume that the Reynolds number is large enough for the viscous terms in the equations of motion to be neglected. (The justification for this is based on the fact that the stability characteristics of free boundary layers become insensitive to viscous effects when the Reynolds number is fairly high.) Then, assuming ψ to take the form

$$\psi = \phi(y) \exp [i\alpha(x-ct)], \tag{1}$$

in which α is the wave-number and $c = c_r + ic_i$, where c_r is the propagation velocity and c_i a measure of the rate of amplification of the disturbance, we find that ϕ satisfies the equation

$$\left(\frac{U}{U_0} - c\right)(\phi'' - \alpha^2\phi) - \frac{U''}{U_0}\phi = 0, \tag{2}$$

which is the 'inviscid' form of the well-known Orr–Sommerfeld equation.

The boundary conditions are

$$\left.\begin{aligned} \phi(0) = 1, \quad \phi'(0) = 0, \\ \phi'(\pm\infty) + \alpha\phi(\pm\infty) = 0, \end{aligned}\right\} \tag{3}$$

and the mean velocity distribution is assumed to be

$$\frac{U}{U_0} = 1 - \frac{U_0 - U_c}{U_0} \exp(-ay^2),$$

in which a is taken as 0·69315 so as to make $(U_0 - U)/(U_0 - U_c) = \frac{1}{2}$ at $y = \pm 1$. The validity of this expression is indicated in figure 13. Since, in a wake, symmetrical disturbances are more stable than antisymmetrical ones, calculations have been made only for the latter.

In order to find a set of eigenvalues which satisfies the boundary conditions, numerical integrations have been repeated by a high-speed electronic computer. The computed results for the eigenvalues α and c, taking $(U_0 - U_c)/U_0 = 0{\cdot}692$, are shown in figure 12.

Before we compare these theoretical results with experiment, we have to make a transformation of time axis and X-axis according to the relation $x = c_r t$, since the flow in a wind-tunnel is stationary and the disturbance is amplified as it travels in the X-direction. Therefore the spatial rate of amplification $\alpha c_i/c_r$ must be used instead of αc_i for the comparison with experimental results.

4.3. *Comparison of experimental results with linearized theory*

A non-dimensional plot of the velocity defect in the linear region of the wake is shown in figure 13. The theoretical distribution for a fully developed laminar wake is in the form $\exp(-ay^2)$, which is indicated by a solid line. The velocity distribution at $X = 30$ mm according to the calculation by Goldstein (1933) is

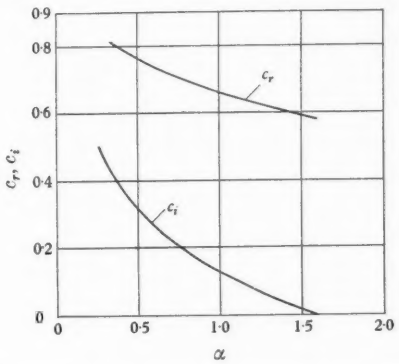

FIGURE 12. Theoretical rate of amplification and propagation velocity.

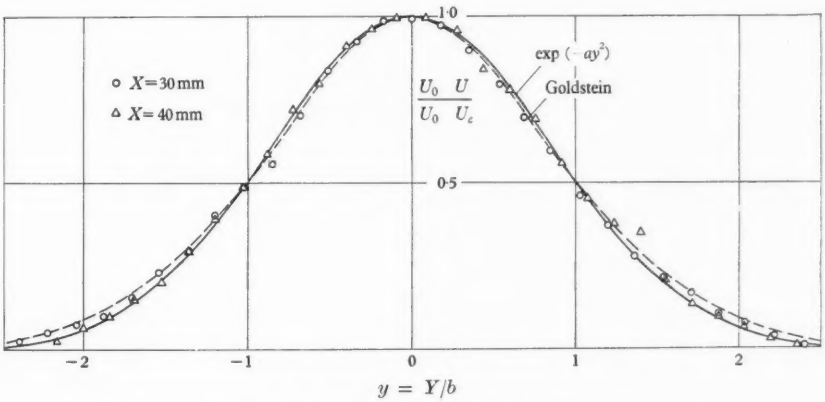

FIGURE 13. Non-dimensional mean-velocity distribution in linear region.

as shown by a broken line. The two theoretical curves are very close, and the experimental data are in good agreement with these curves. Since the distribution given by the broken line has no simple analytical expression, the exponential distribution is preferable as a basic flow for the calculation of disturbance properties.

The non-dimensional frequency αc_r of the observed natural fluctuations is plotted against Reynolds number in figure 14. Since the theoretical value of αc_r for neutral oscillations at infinite Reynolds number is 0·92, the frequency of the natural fluctuations can be assumed to lie inside the unstable zone of the

theoretical stability diagram, although the curve of neutral stability for finite Reynolds numbers has not been derived. To the right of the figure is shown the theoretical spatial amplification rate at infinite Reynolds number, which has a maximum at about $\alpha c_r = 0{\cdot}5$. Thus it is confirmed that the frequency of the sinusoidal fluctuations found in natural transition approximately corresponds to the frequency of the small disturbance which receives maximum spatial amplification according to the linearized theory.

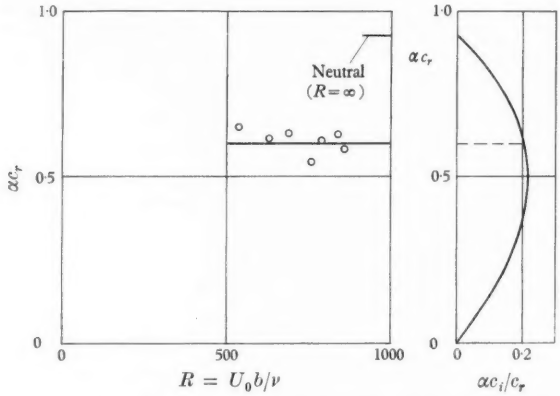

FIGURE 14. Comparison of theoretical and experimental results. Frequency of velocity fluctuation, $\alpha c_r = 2\pi f b/U_0$.

When sound waves were used as artificial excitation, it was impossible to observe the damping of disturbances just beyond the critical condition since the induced velocity fluctuations were not sufficiently strong. Therefore the neutral point was determined experimentally by the method introduced in a previous paper (Sato 1959*b*). The ratio of the intensities of spectral components with and without excitation is plotted against non-dimensional frequency in figure 15. The neutral frequency is determined as the point where the ratio becomes unity. Arrows on the abscissa indicate the theoretical values which have been obtained by various investigators: e.g. by Hollingdale (1940) who obtained two values with different methods of approximation, and by McKoen (1956). The present value of αc_r determined by numerical integration is the smallest among the four given values. The experimental results obtained under four different conditions are fairly consistent, and they agree most closely with the present theoretical estimate.

Figure 16 shows the propagation velocity and spatial rate of amplification which are obtained from experimental data such as figures 8 and 9. The solid lines are theoretical results for amplified disturbances at infinite Reynolds number. The agreement between theory and experiment is fairly good in both c_r and $\alpha c_i/c_r$.

Distributions of amplitude and phase in Y-direction are compared in figure 17. Experimental points denote the root-mean-square values of spectral components of the u-fluctuations in the natural transition, taking the maximum value as

unity and, for the phase angle of the spectral components, taking the value at $Y = -5$ mm as zero. Theoretical results are given for amplified disturbances for which $\phi(y)$ is complex. The amplitude function and phase angle for the u-fluctuations were calculated from the real and imaginary parts of $\phi'(y)$. As shown by a solid line in the figure, a gradual phase shift in the y-direction exists for the

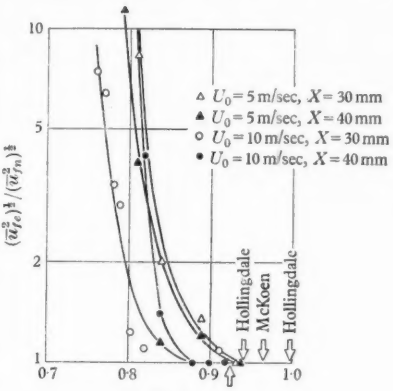

FIGURE 15

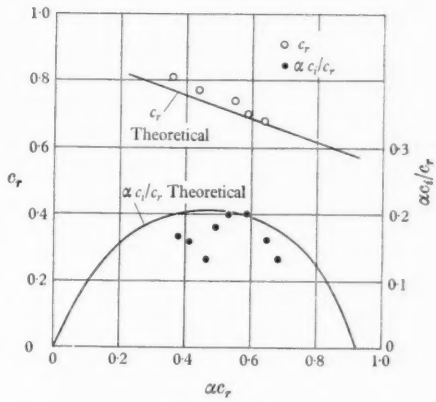

FIGURE 16

FIGURE 15. Determination of frequency of neutral oscillation. Plate I. $(\overline{u}^2_{fe})^{\frac{1}{2}}$ and $(\overline{u}^2_{fn})^{\frac{1}{2}}$ denote root-mean-square values of spectral components of frequency f with and without artificial excitation respectively.

FIGURE 16. Propagation velocity c_r and spatial rate of amplification $\alpha c_i/c_r$.

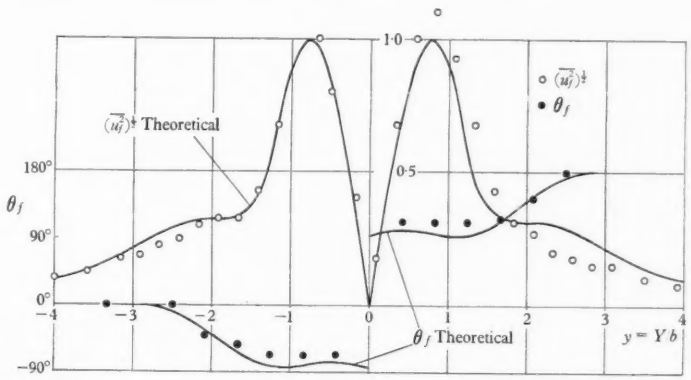

FIGURE 17. Amplitude function. In theoretical results, $\alpha = 0{\cdot}832$ and $c_i = 0{\cdot}168$.

amplified disturbance, in contrast to the case of neutral disturbances. Theoretical eigenvalues in the present case are $\alpha = 0{\cdot}832$, $c_i = 0{\cdot}168$, $c_r = 0{\cdot}692$, which correspond to a disturbance with approximately the maximum spatial rate of amplification. The agreement between theory and experiment is excellent.

Thus the experimental results on the properties of sinusoidal fluctuations in the linear region are properly described by the linearized theory. Considering

the previous results on the separated layer and jet, it is now obvious that in the transition region of a free boundary layer there exists a linear region in which sinusoidal fluctuations grow as predicted by the theory of the Orr–Sommerfeld equation.

5. The non-linear region

The upstream boundary of the non-linear region is the X-station where the growth rate of velocity fluctuations deviates from being exponential. This deviation demonstrates the role of non-linear terms in the equation of motion. This initial point of the non-linear region might be called the 'transition point' since the non-linearity is an essential feature of turbulent motion. On the other hand, the transition point defined as the end-point of laminar region in the preceding section is determined from, for instance, the streamwise variation of velocity on the centre-line such as is shown in figure 3. These two kinds of transition point, one defined from the velocity fluctuation and the other from the time-mean velocity, are found experimentally to be very close. This fact has been already pointed out in the case of separated layers and jets (Sato 1956, 1959*a*). From the experimental results it has been confirmed that the two-dimensionality of the fluctuations is still maintained in the non-linear region. The downstream boundary of the non-linear region is defined as the X-station where the fluctuations become three-dimensional so that, for instance, $\overline{u}^2$ and $\overline{w}^2$ become comparable. With Plate I and $U_0 = 10{\cdot}0$ m/sec, the extent of the non-linear region was found to be about $X = 40$ to 150 mm.

5.1. *Non-linear development of sinusoidal fluctuations*

As shown in figure 5, the non-linear effect on the wave-form of the fluctuations is observed in the vicinity of the centre-line as an increase of low-frequency irregular fluctuations. In the outer part of the wake the sinusoidal fluctuation persists with the same frequency. The non-linear effect seems to be slight between $X = 40$ and 150 mm as far as the wave-form is concerned. However, remarkable changes take place in the distributions of amplitude and phase of the spectral components, as is shown in figures 18 and 19. In figure 18, the root-mean-square values of the spectral component at the fundamental frequency are plotted on an arbitrary scale, while the relative values at various X-stations are correctly expressed. The distribution changes in a rather peculiar way as X is increased. From $X = 40$ to 80 mm, the variation is gradual. The positions of the two peaks move outwards, maintaining a roughly similar type of distribution. At $X = 120$ and 150 mm, the distribution shows three minima, at $Y = 0$ and $Y = \pm 2{\cdot}5$ mm. Referring to figure 19, we see that a 180-degree phase reversal takes place at these three points. At each X-station, 180-degree reversal is observed at $Y = 0$, except at $X = 80$ mm which is in some sense a dividing line. Now it seems possible to classify the non-linear region into two parts. The upstream part more or less resembles the linear region, although the exponential amplification of fluctuations is no longer observed. In the downstream part, the distribution functions of amplitude and phase are completely different from

those in the upstream part. It is obvious that in the non-linear region a new equilibrium is established at about $X = 100$ mm.

The next step of the investigation is to clarify the nature of the harmonic components in the non-linear region. An increase of harmonic components is expected as a result of non-linear interaction. In figure 20, the distribution of second harmonics is shown. While a remarkable increase in $(\overline{u_{2f}^2})^{\frac{1}{2}}$ takes place

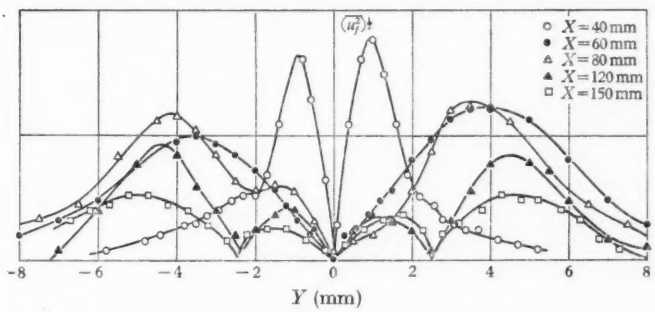

FIGURE 18. Amplitude distribution of fundamental component in non-linear region. The ordinate scale is arbitrary.

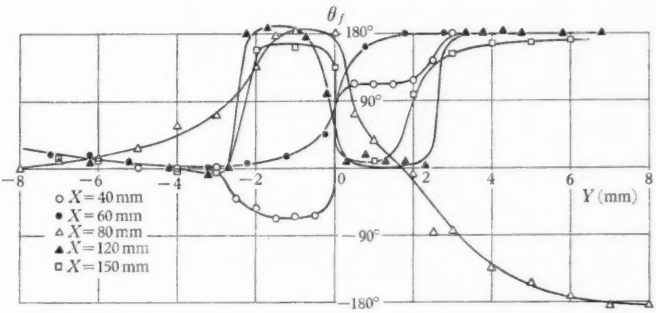

FIGURE 19. Phase distribution of fundamental component in non-linear region.

from $X = 40$ to 60 mm, it decreases downstream from $X = 60$ mm. This is a curious situation since the fundamental component still increases or only slightly decreases from $X = 60$ to 100 mm. The ratio of harmonic component to fundamental component becomes a maximum at $X = 60$ mm and decreases as X is increased further. Although non-linear effects might always be expected to increase the harmonic content, we here observe a contrary result. The distribution function of the second-harmonic component $(\overline{u_{2f}^2})^{\frac{1}{2}}$ in the Y-direction shows a reduction in the extent of the distribution from $X = 60$ to 120 mm. This fact is also unusual. A more detailed discussion of figure 20 is hardly justified, however, since the accuracy of measurement of the harmonic components was not high, owing to the unavoidable non-linearity of the characteristics of the hot-wire anemometer itself. The necessary correction for this non-linearity reached 50% of the value of $(\overline{u_{2f}^2})^{\frac{1}{2}}$, while the harmonic component was very small compared with the fundamental component.

Another quantity which characterizes the non-linear distortion of sinusoidal fluctuations is $(\overline{u^3})^{\frac{1}{3}}$. When the wave-form remains symmetrical with respect to the zero line, the value of $(\overline{u^3})^{\frac{1}{3}}$ is zero. Thus $(\overline{u^3})^{\frac{1}{3}}$, which was determined by the use of a cubing unit, is a measure of asymmetry of the wave-form. Due to the inevitable non-linearity of the hot-wire, as mentioned before, the measured value of $(\overline{u^3})^{\frac{1}{3}}$ was not zero even for sinusoidal fluctuations when the amplitude was fairly large. Moreover, the wave-form distortion was usually accompanied by slow irregular velocity fluctuation. For these reasons, a high accuracy was not expected in the measurement of $(\overline{u^3})^{\frac{1}{3}}$. Figure 21 is the result obtained in the non-linear region. At $X = 60$ mm, the distribution is different from those at $X = 80$ and 120 mm, which again suggests the peculiar character of the region

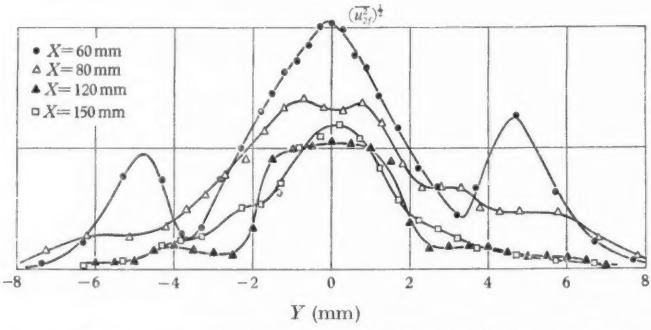

FIGURE 20. Amplitude distribution of second harmonics in the non-linear region. The ordinate scale is arbitrary.

$X = 80$ to 150 mm. It is worth while to note that in the distribution at $X = 120$ mm, the zeros of $(\overline{u^3})^{\frac{1}{3}}$ at about $Y = \pm 2$ mm coincide approximately with the phase-reversal points for the fundamental component. Outside $Y = \pm 2$ mm, the second-harmonic component is very small, so that non-linearity is manifested as the asymmetry of the wave-form. Inside $Y = \pm 2$ mm, $(\overline{u_{2f}^2})^{\frac{1}{2}}$ is nearly constant, whereas $(\overline{u^3})^{\frac{1}{3}}$ changes sign. From these facts it is expected that the generation of harmonics and asymmetrical distortion of wave-form have no simple relation, although both are undoubtedly results of non-linear interactions.

In order to clarify the situation at $X = 120$ mm, the non-dimensionalized mean-velocity distribution (figure 22) may be closely examined. We find two facts. One is the over-shoot of velocity between $y = 1{\cdot}6$ and $2{\cdot}5$, and the other is the flat distribution near the centre-line. The distribution at $X = 40$ mm is added for comparison. The peculiarity of the distribution at $X = 120$ mm is clearly seen.

5.2. *Vortex model*

The curious features of the flow field in the region $X = 40$ to 150 mm are summarized as follows:

1. Before the experiment was made, it seemed probable that in the wake the central velocity U_c increases monotonically and approaches U_0 at large X. But

at about $X = 80$ mm, U_c becomes a maximum, begins to decrease, and reaches a minimum at $X = 120$ mm before it gradually increases again.

2. The mean-velocity distribution at $X = 120$ mm is very different from that at smaller or larger X. The distribution has a flat part near the centre-line, and the velocity over-shoots the free-stream velocity at the edge of the wake.

3. The fundamental component of the velocity fluctuations at $X = 120$ to 150 mm becomes zero not only at $Y = 0$ but also at $Y \doteqdot \pm 2$ mm. The phase reversal also takes place there.

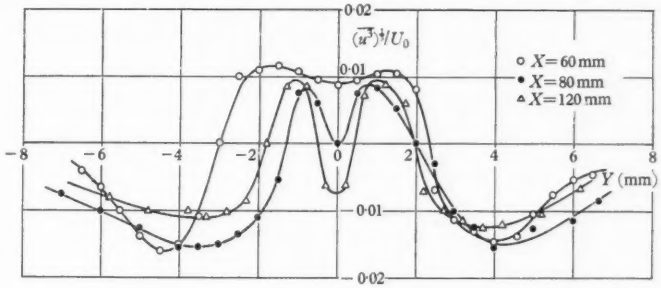

FIGURE 21. Distribution of $(\overline{u^3})^{\frac{1}{3}}$ in non-linear region.

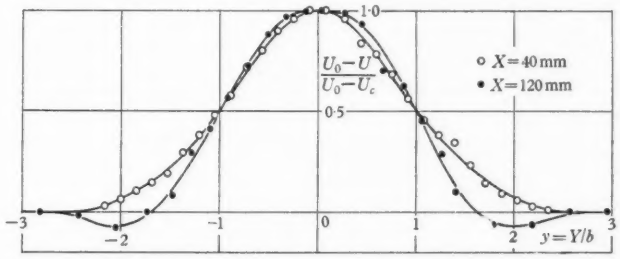

FIGURE 22. Non-dimensional mean-velocity distributions in linear and non-linear regions.

4. As X is increased, the second-harmonic component increases until $X = 60$ mm, decreases, reaches a minimum, and increases a little again as X is increased further. The distribution in the Y-direction shows a systematic change over the range $X = 40$ to 150 mm.

These features might be explained by an analytical method taking account of non-linear terms in the equation of motion. Since the linearized theory has had substantial experimental verification in the linear region, the mechanism of the non-linear region might also be clarified by an appropriate theoretical model. Practically, however, analysis of the non-linear equations of motion is very difficult, and no satisfactory theory has been reported so far. Thus we are inclined to take a tentative empirical model which explains the above-mentioned experimental facts.

In the past, many investigators have observed the formation of vortices in the wake of two-dimensional bodies, including a thin flat-plate (Hollingdale

1940; Taneda 1958). It is usually accepted that the sinusoidal fluctuations in the signal from a hot-wire anemometer corresponds to the moving vortex which is observed visually. In order to make such a correspondence apply in the present case, the physical properties posed on the vortex must be sufficiently complex to explain the wave-form of the hot-wire output. The usual simple vortex model is obviously inadequate. In order to approximate the linear region, a single row of vortices which travels in the X-direction as shown in figure 23(*a*) is useful. The adjacent vortices rotate in opposite direction and the radial distribution of circumferential velocity is assumed as shown. This model roughly explains the calculated and observed distributions of amplitude and phase of the velocity fluctuations in the linear region. The nature of the fluctuations in the non-linear region is explained as follows by the development of the single row into a double row as shown in figure 23(*b*).

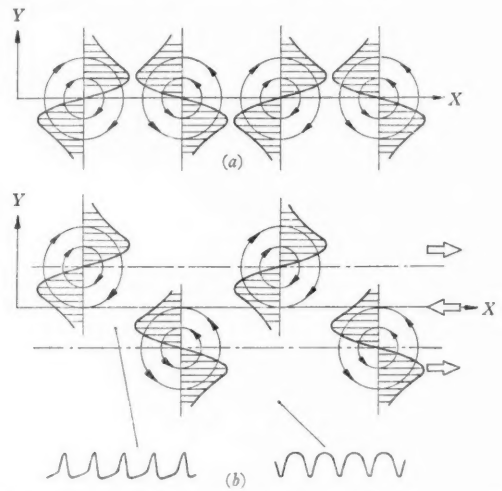

FIGURE 23. Vortex model. (*a*) Single row; (*b*) double row of vortices.

In the single row, the superposition of vortices has no effect on the mean-velocity field. On the other hand, in the double-row configuration a velocity is induced in the negative X-direction between rows of vortices, as shown by the arrow. This results in a decrease of U_c. Furthermore, a positive velocity is induced at the outer part of the wake. These facts explain the mean-velocity distribution at about $X = 120$ mm as shown in figure 22. In the double row of vortices, the phase inversion of the fundamental component takes place not only on the centre-line but on lines connecting centres of vertices in each row if the lateral spacing is large. The generation of second harmonics in the vicinity of the centre-line is also easily understood. Typical wave-forms of velocity fluctuations as expected from the vortex model are shown at the bottom of figure 23, depending on the location of hot-wire. These are in accord with the experimental observations. The change of sign of $(\overline{u}^3)^{\frac{1}{3}}$ on the line connecting centres of vortices is understood from these wave-forms. Thus the process in the non-

linear region is explained by the development of the single row into a double row of vortices, and if once the double row is established, the configuration is stable and remains unchanged until three-dimensional deformation begins.

It is worth while to calculate an important geometrical parameter of a double row of vortices, that is, the ratio of lateral to longitudinal spacings. The value is 0·281 in von Kármán's analysis, whereas in the present experiment it is about 0·39. This comparatively large lateral spacing allows the phase inversion of the fundamental component on the lines connecting centres of vortices. This fact is in contrast to the case of the wake of a circular cylinder, in which the phase reversal is found only at $Y = 0$ (Roshko 1954).

5.3. *Interaction between spectral components*

In the linear region, spectral components of different frequencies are damped or amplified independently. In the non-linear region, however, two spectral components may interact with each other through the non-linear terms in the

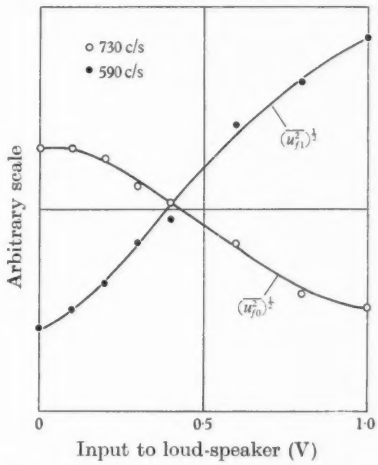

FIGURE 24. Variation of intensity of natural and excited spectral components in the non-linear region. $X = 120$ mm.

equations of motion. This interaction was experimentally investigated by superposing an artificial disturbance, that is, sound from the loudspeaker at a frequency other than that of the natural fluctuations.

At first, as the result of non-linear interaction, we expected the generation of spectral components of frequency $f_0 \pm f_1$, where f_0 and f_1 denote the frequencies of the natural and artificial disturbances respectively. However, no peaks were observed experimentally at $f_0 \pm f_1$ in the energy spectrum of the u-fluctuations. By varying the intensity of sound from the loudspeaker, the wave-form and intensity of the velocity fluctuations in the non-linear region have been investigated. Figure 24 shows the change in the root-mean-square values of two spectral components. The induced spectral component $(\overline{u_{f1}^2})^{\frac{1}{2}}$ (590 c/s) increases monotonically as the input voltage to the loudspeaker is increased. On the

other hand, the component of natural fluctuation (730 c/s) diminishes when the intensity of excitation is increased. This 'suppression effect' is more remarkable when f_1 is close to f_0. This effect means, in other words, the supply of energy from the component at f_0 to that at f_1. The detailed mechanism of the energy exchange is not yet known.

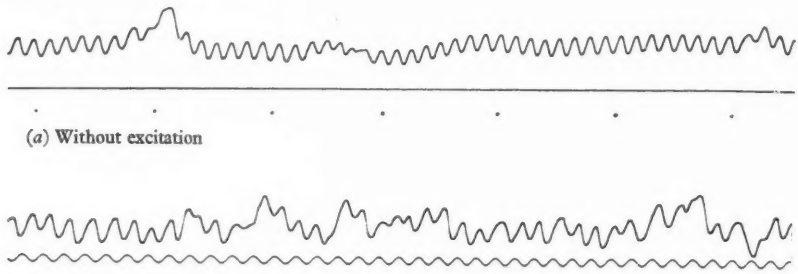

(*a*) Without excitation

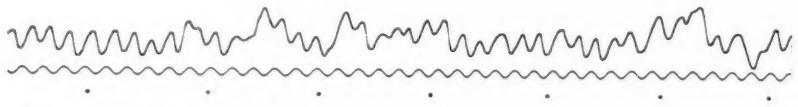

(*b*) Input to loud-speaker 1 V.

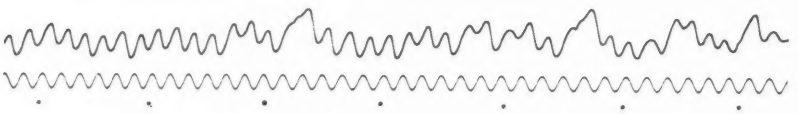

(*c*) Input to loud-speaker 2 V.

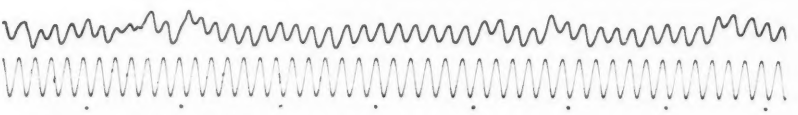

(*d*) Input to loud-speaker 3 V.

FIGURE 25. Oscillographic records of u-fluctuations in the non-linear region at $X = 120$ mm and $Y = 5$ mm. Excitation 590 c/s. Upper trace is the output from the hot-wire anemometer, and lower trace is the input to the loudspeaker. Time goes from left to right and the time interval between dots is 0·01 sec.

The wave-form in the presence of artificial excitation is shown in figure 25. Without artificial excitation the frequency of fluctuation is about 730 c/s (*a*). When the incoming sound is weak, the component of f_1 appears in a small fraction of time, while the f_0 component prevails (*b*). By increasing the intensity of sound, the probability of finding the f_1 component increases (*c*), and with the maximum intensity of sound the f_0 component is hardly found (*d*). From these records, it is obvious that the probability of finding induced fluctuation is a function of intensity of the artificial disturbance. No periodicity was found in the occasional change of the frequency of fluctuation.

6. Three-dimensional region

In the linear and non-linear regions, velocity fluctuations are approximately two-dimensional. The distortion of two-dimensional waves—in other words, the three-dimensional deformation of the row of vortices—takes place in the final

subregion of transition, the three-dimensional region, in which regularities in the fluctuations gradually diminish until the fully turbulent wake is formed. If the Reynolds number of flow is small, the fluctuation energy decays by viscous dissipation before the development into turbulence is completed. In this case, there is no turbulent region and the three-dimensional region is also hardly observed.

With the use of Plate I at $U_0 = 10{\cdot}0$ m/sec, the physical process which takes place in the three-dimensional region was as follows.

The double row of vortices formed in the non-linear region became unstable at about $X = 150$ mm. As a first sign of the deformation of the vortices, irregular wave-forms were observed near the centre-line of the wake while the fluctuation was still sinusoidal in the outer part. As X was increased, the region of irregular fluctuations extended into the outer part until the whole breadth of the wake was covered. At the same time, the phase relation of the sinusoidal fluctuations with respect to the Z-direction became irregular, and w-fluctuations became comparable in magnitude with u-fluctuation. The turbulent wake was thus established at about $X = 400$ mm, although the intensity of fluctuation was much less there compared with that in the non-linear region. No instantaneous turbulent bursts have been observed so far in this region. The change of wave-form was gradual.

Before we go into the quantitative discussion, we may suitably introduce some physical quantities to characterize the three-dimensionality. From the consideration that the difference in mean-velocity distribution at various Z-stations is small, three quantities concerning the velocity fluctuation have been used. They are the relative magnitude of $(\overline{u^2})^{\frac{1}{2}}$ and $(\overline{w^2})^{\frac{1}{2}}$, the phase relation in the Z-direction, and the distribution of spectral components at various Z-stations.

The ratio $(\overline{w^2})^{\frac{1}{2}}/(\overline{u^2})^{\frac{1}{2}}$ is plotted against Y in figure 26. At $X = 150$ mm, u- and w-fluctuations are nearly the same in magnitude, or $(\overline{w^2})^{\frac{1}{2}}$ is even greater in the region -2 mm $< Y < 2$ mm, and outside this region $(\overline{w^2})^{\frac{1}{2}}$ is very small compared with $(\overline{u^2})^{\frac{1}{2}}$. Therefore, the irregular fluctuation observed in the central region is three-dimensional, but the sinusoidal fluctuation in the outer part of the wake is still two-dimensional. At $X = 300$ mm, the ratio is close to unity over the whole breadth of the wake. This fact resulted from the faster decay of $(\overline{u^2})^{\frac{1}{2}}$ rather than the growth of $(\overline{w^2})^{\frac{1}{2}}$ in the three-dimensional region. The value of $(\overline{w^2})^{\frac{1}{2}}/(\overline{u^2})^{\frac{1}{2}}$ at $X = 300$ mm is close to that in the fully developed wake behind a cylinder.

The straightness of the front of the sinusoidal wave is expressed by the phase relation in the Z-direction at large Y. The experimental result is shown in figure 27, in which the phase angle at $Z = 0$ is taken to be zero. At small X, the variation in the Z-direction is small. This means that the wave is approximately two-dimensional and propagates in the X-direction. At larger X, a phase difference of more than 180 degrees is observed at some Z-station, while the direction of propagation as a whole still remains in the X-direction. As mentioned before, the wave-form at large X is irregular near the centre-line of the wake. This means that the double row of vortices is first distorted in the region between rows. For instance, the phase of the velocity fluctuations at $X = 250$ mm could

not be determined experimentally because of the irregularity in the central part of the wake. The phase distribution in the Z-direction at large Y might still be significant, since it expresses the three-dimensional distortion in a large scale. As shown in figure 27, the Z-station of the phase lag or advance is approximately fixed at various X-stations. This fact might have arisen from imperfections of

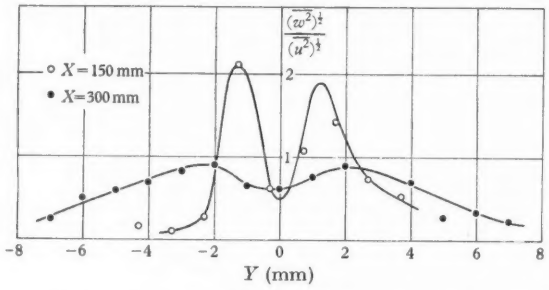

FIGURE 26. Distribution of $(\overline{w^2})^{\frac{1}{2}}/(\overline{u^2})^{\frac{1}{2}}$ at $X = 150$ and 300 mm.

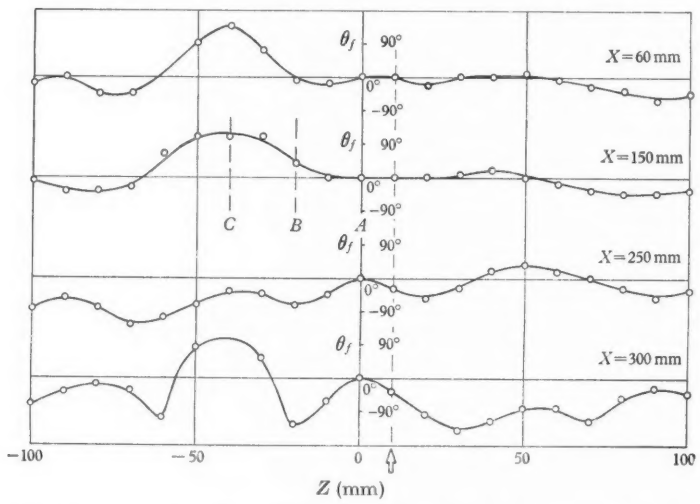

FIGURE 27. Spanwise distribution of phase of fundamental component at various X-stations in the outer part of the wake. Arrow indicates the station where detailed measurements were made.

the flat plate. Upon careful inspection of the plate, a slight waviness (about 0·2 mm in height) was found in the trailing edge at about $Z = -40$ mm. Since all measurements in the linear and non-linear regions were made at $Z = 10$ mm, as indicated by an arrow in figure 27, the experimental results described in preceding sections were uninfluenced by disturbances produced by this waviness. However, since the slightest spanwise irregularity can have a decisive effect on the breakdown of the laminar boundary layer on a solid wall (Schubauer 1958; Tani 1960), a measurement has been made on the distribution of spectral com-

ponents at three Z-stations A, B and C as denoted in figure 27. A and C are stations of maximum lag and advance respectively, and B is the midway station. The experimental results obtained at A and C are in good accordance with those at $Z = 10$ mm where all systematic measurements have been made. On the other hand, the distribution at B with $X = 150$ mm is somewhat different. The 180-degree phase shift is observed only at $Y = 0$ and the maximum value of amplitude is about 1·3 times that at $Z = 10$ mm. The phase configuration suggests the single-row configuration at B, although it is accompanied by an appreciable distortion. At $X = 200$ mm, the difference between the three Z-stations is not observed any more. From the observations made so far, the peculiar region around station B has no decisive effect on the transition process in the whole wake. This fact is in contrast to the case of transition of the boundary layer along a solid wall, which depends to an important extent on the three-dimensionality in the layer.

The three-dimensional region is succeeded by the turbulent region, on which no detailed measurements have been made in the course of the present investigation.

7. Discussion

First of all, the relation between natural and artificially excited transition must be clarified, because in the present experiment the transition was often initiated by sound from a loudspeaker. Generally speaking, in wind-tunnels there are various kinds of residual disturbance such as the free-stream turbulence, acoustic noise, mechanical vibration, etc., which undoubtedly have great influence on the transition process. These residual disturbances usually change day by day, and the reproducibility of transition pattern is sometimes very poor. And, moreover, the magnitude and nature of these disturbances are not the same for different wind-tunnels; therefore, experimental results on so-called natural transition obtained at different places are usually not comparable. We may assume that transition would take place in a similar way if levels of residual disturbances were smaller than certain limits. But even if this assumption is true, no one knows these limits, and it is probable that disturbances in existing wind-tunnels are almost always too great.

The advantages of artificial disturbances are twofold; one is to specify the nature and intensity of the predominant disturbance which induces the transition, and the other is to improve the reproducibility of the transition process. When the intensity of the artificial disturbance is considerably higher than that of residual disturbances, the reproducibility of the transition pattern is improved remarkably. However, if the intensity is too high, the pattern of transition is completely changed from that of natural transition. The frequency and amplitude of artificial disturbances are therefore to be determined by consideration of these two conditions.

A sound wave is one of the simplest and most convenient forms of artificial disturbance, since the frequency and intensity can be changed very easily. However, the excitation by sound extends uniformly over the whole flow field, and a point of excitation cannot be specified. Sometimes, the applicability is restricted by acoustical resonance of the wind-tunnel. In these respects the

vibrating ribbon (Schubauer & Skramstad 1948) is a more satisfactory measure than sound waves. But it is difficult to apply the ribbon technique to a wake and, moreover, the disturbance generated by a ribbon is undesirably large in such highly unstable flows as wakes and jets. The transition might be induced by the ribbon even when it does not vibrate, and the growth of disturbances is completed in a small region which is not suitably large compared with the dimensions of the ribbon. Although the excitation by sound is not localized, its effect is greatest at the X-station where the spatial amplification of the impressed disturbance is a maximum. As a matter of fact, the velocity amplitude of the sound may be extremely small: for instance, 0·1 cm/sec for sound at 80 db. Therefore, the induced velocity fluctuation is observable only when it is

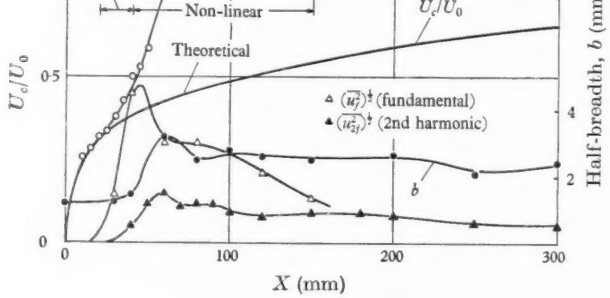

FIGURE 28. Streamwise variation of various quantities in the transition region. $U_0 = 10{\cdot}0$ m/sec, Plate I. $(\overline{u_f^2})^{\frac{1}{2}}$ is the maximum value at each X-station, and $(\overline{u_{2f}^2})^{\frac{1}{2}}$ is the value at $Y = 0$. Both are plotted on an arbitrary scale.

amplified about 100 times. Thus, it is possible to consider that the excitation is applied at an original point of amplification. The propagation velocity, rate of amplification and distribution function of spectral components in the linear region were determined in our experiments by the use of sound excitation. Wave-forms, the mean-velocity distribution and the distribution of total energy $\overline{u}^2$ were observed without sound excitation.

Some of the experimental results described in the preceding sections are summarized in figure 28, which provides a general view of the mechanism of transition. The transition region is classified into three subregions, linear, non-linear and three-dimensional. The linear region in which the sinusoidal velocity fluctuation was amplified exponentially extended from $X = 20$ to 40 mm, and this was followed by the non-linear region in which a two-dimensional double row of vortices was established as a stable configuration. The three-dimensional region started at about $X = 150$ mm and was succeeded by a turbulent region at about $X = 400$ mm. This result was found with Plate I at $U_0 = 10{\cdot}0$ m/sec, the corresponding Reynolds number based on the length of plate being $2{\cdot}1 \times 10^5$. Under different experimental conditions, the relative extent of each subregion

was, of course, different. However, the essential features of transition were concluded to be identical. In order to obtain a better understanding of the transition phenomenon, the mechanism of transition in other flow fields is now to be compared with the present result.

First, the wake of a circular cylinder is considered. Many extensive investigations have been carried out on the double row of vortices in the wake of the cylinder since the pioneering work by von Kármán. Hot-wire measurements were made by Kovásznay (1949) and Roshko (1954). Roshko has pointed out the great difference in the flow pattern behind cylinders with different Reynolds number. Therefore, before we make a comparative discussion, we have to establish the correspondence of Reynolds number between the two types of wake. It seems reasonable to compare the drags of a cylinder and flat plate in uniform flow, which are expressed by

$$D_{\text{plate}} = 1{\cdot}328\sqrt{(U_0^3\mu\rho l)},$$
$$D_{\text{cylinder}} = C_D\tfrac{1}{2}\rho U_0^2 d,$$

in which l and d are the streamwise length of the plate and the diameter of the cylinder respectively. The boundary layer on the plate is assumed laminar everywhere. Since the drag is a measure of energy taken out of the flow, the velocity defect and velocity fluctuation might well be of the same level if the drag is equal. Thus, by putting $D_{\text{plate}} = D_{\text{cylinder}}$, we have

$$l/d = 0{\cdot}38C_D\sqrt{R_l},$$

in which $R_l = U_0 l/\nu$. The present experimental conditions for a plate, $l = 30$ cm, $U_0 = 10{\cdot}0$ m/sec, may thus correspond to $d = 0{\cdot}18$ cm and $U_0 = 10{\cdot}0$ m/sec for a cylinder, the Reynolds number $U_0 d/\nu$ being 1200. According to the classification by Roshko, this Reynolds number belongs to the 'irregular range' in which the periodic vortex shedding is accompanied by irregular velocity fluctuations.

In the wake of a cylinder there exists no linear region in the present sense, that is, the sinusoidal fluctuation is of high intensity and always decays downstream. The mechanism of generation of vortices is different for the two types of wake. Behind a cylinder there are two separated layers from the wall, which are laminar at first and become turbulent before the rolling-up into vortices is completed at Reynolds numbers below 10^5. The continuity of the boundary layer into the wake is much smoother for the case of a flat plate. Besides these differences in the mechanism of generation, the double row of vortices in the wake of a cylinder might correspond to that in the non-linear region of the wake of a flat plate. Thus, in the wake-like velocity distribution, the anti-symmetrical two-dimensional double row of vortices is a stable configuration. The three-dimensional distortion of these vortices leads the gradual change into turbulence.

The transition of a two-dimensional jet has also been found to be characterized by sinusoidal velocity fluctuations which grow exponentially and develop gradually into turbulence (Sato 1959*b*). Observed features of the sinusoidal fluctuations were in good agreement with predictions of linearized theory. Generally speaking, the nature of transition of a jet is very close to that of a wake behind a thin plate. The separated layer from a sharp edge, though it is not a

symmetrical flow field, exhibits a similar nature of transition to jets and wakes (Sato 1959*a*). Thus, in free boundary layers including wakes, jets and separated layers, the process of transition is to a large extent similar, although in the wake behind a cylinder there is some difference, as mentioned above.

We now compare the transition of the boundary layer along a solid wall. The early work by Schubauer & Skramstad (1948) on the boundary layer along a flat plate has verified the linearized theory in the linear region of transition. Concerning the non-linear region, we can point out many essential differences between free and 'fixed' boundary layers. Modern investigations on the boundary layer along a flat plate indicate the importance of three-dimensional distortion of two-dimensional waves in the process of transition (Hama, Long & Hegarty 1957; Schubauer 1958; Tani 1960). The pre-existing three-dimensionality in the laminar layer—for instance, the spanwise variation of layer thickness—is a decisive factor in the distortion of two-dimensional waves and, therefore, in the onset of turbulence. Although the role of three-dimensionality in the transition of free boundary layers is not yet fully understood, it might be much less significant than in the case of fixed boundary layers. One of the most important features in the transition of a fixed boundary layer is the generation of turbulent bursts or, in other words, sudden breakdowns of laminar flow. It is now established that the breakdown is closely related to the complicated three-dimensional distortion of originally two-dimensional waves. The development of a small patch of turbulence has been made clear experimentally (Schubauer & Klebanoff 1956). These features of the non-linear region have no counterparts in the transition of free layers. Thus it is concluded that the linear development of sinusoidal fluctuations is verified in both free and fixed boundary layers, whereas the mechanism in the non-linear region is completely different.

The formation of a double row of vortices in the wake is a peculiar fact. As mentioned in a previous paper (Sato 1959*b*), there might be some mechanism which suppresses the deformation of vortices due to a non-linear effect. The vortex theory, such as that originated by von Kármán and modified by many other investigators, might explain some of the observed results. However, it is far from a complete explanation since it fails to describe the continuity from the linear region, or to predict wavelength, etc., in relation to the mean-velocity distribution of the wake. Thus we are inclined to think that a stability calculated for disturbances of finite amplitude is required. It is expected that the observed formation of a double row of vortices is the result of a selective action which is closely related to the initial conditions and mean-velocity distribution.

The three-dimensional distortion of two-dimensional vortices is initiated by pre-existing three-dimensionality in the flow. Recently, Benney & Lin (1960) have developed a non-linear theory and calculated second-order terms assuming a periodic variation in the Z-direction for the primary fluctuations. From the present measurements of the distributions of $\overline{u}^2$ and $\overline{w}^2$ in the Y- and Z-directions, no definite conclusion was reached concerning the validity of the theory, because the calculation was made for a different type of flow field and the assumed distribution of primary fluctuation was not realized in the present experiment.

In the wake of a thin plate, the process of three-dimensional distortion is gradual in contrast to the sudden breakdown in fixed boundary layers. In boundary layers along solid walls, there is a great difference in the equilibrium mean-velocity distribution of laminar and turbulent layers. This implies a more complicated variation of energy flow in the process of transition of fixed layers than that of free layers, in which thickening of the layer takes place without appreciable change in the shape of the mean-velocity distribution. The three-dimensional region of free layers is to be investigated in the future in more detail by determining the energy balance in the region.

8. Conclusion

The experimental and theoretical investigation of the wake developed behind a flat plate placed parallel to the uniform flow indicated the following conclusions.

1. The observed mean-velocity distribution in the laminar region of a wake is in coincidence with Goldstein's calculation.

2. At a certain Reynolds number, the transition region is classified into three subregions: (1) the linear region, (2) the non-linear region, and (3) the three-dimensional region.

3. The frequency of sinusoidal velocity fluctuations found in natural transition is proportional to the $\frac{3}{2}$ power of free-stream velocity. The fluctuations correspond to the disturbance with maximum amplification according to the linearized stability theory.

4. The sinusoidal velocity fluctuations induced by artificial excitation are amplified exponentially in the linear region when the frequency of excitation lies inside the unstable zone of the stability diagram. The observed propagation velocity, rate of amplification and amplitude function of fluctuations at various frequencies are in good agreement with the predictions of linearized theory.

5. Vortex models, a single row of vortices in the linear region and an anti-symmetrical double row in the non-linear region, are useful for explaining many of the experimental results. The double row of vortices is similar to that found in the wake of a circular cylinder.

6. In the non-linear region, an increase of intensity of the artificial excitation results not only in the increase of induced velocity fluctuation of identical frequency, but also in a decrease in the amplitude of the natural velocity fluctuations. This 'suppression effect' is remarkable when the frequency of the artificial disturbance is close to that of natural fluctuation.

7. In the three-dimensional region, the double row of vortices, which is two-dimensional in the non-linear region, is subject to three-dimensional distortion. The velocity fluctuation gradually develops into turbulence without being accompanied by sudden breakdown or turbulent bursts.

The authors appreciate the stimulating discussions occurring throughout the whole course of the investigation with members of the Boundary Layer Research Group in Japan, which is directed by Professor Itiro Tani. Thanks are extended to Mr Y. Onda and Mr O. Okubo who helped to carry out the experimental work. The research was financially supported by the Ministry of Education of Japan.

REFERENCES

Benney, D. J. & Lin, C. C. 1960 *Phys. Fluids*, **3**, 656.

Goldstein, S. 1933 *Proc. Roy. Soc.* A, **142**, 545.

Hama, F. R., Long, J. D. & Hegarty, J. C. 1957 *J. Appl. Phys.* **28**, 388.

Hollingdale, S. H. 1940 *Phil. Mag.* (7) **29**, 209.

Kovásznay, L. S. G. 1949 *Proc. Roy. Soc.* A, **198**, 174.

Laufer, J. & Vrebalovich, T. 1960 *J. Fluid Mech.* **9**, 257.

McKoen, C. H. 1956 *Aero. Res. Coun., Lond., Rep.* no. 303.

Roshko, A. 1954 *Nat. Adv. Comm. Aero., Wash., Rep.* no. 1191.

Sato, H. 1956 *J. Phys. Soc. Japan*, **11**, 702.

Sato, H. 1959*a* *J. Phys. Soc. Japan*, **14**, 1797.

Sato, H. 1959*b* *J. Fluid Mech.* **7**, 53.

Sato, H., Kobashi, Y., Iuchi, M., Yamamoto, K. & Onda, Y. 1954 *Rep. Inst. Sci. Tech., Univ. Tokyo*, **8**, 271.

Schubauer, G. B. 1958 *Proc. Boundary Layer Symposium, Freiburg*, p. 85.

Schubauer, G. B. & Klebanoff, P. S. 1956 *Nat. Adv. Comm. Aero., Wash., Rep.* no. 1289.

Schubauer, G. B. & Skramstad, H. K. 1948 *Nat. Adv. Comm. Aero., Wash., Rep.* no. 909.

Taneda, S. 1958 *J. Phys. Soc. Japan*, **13**, 418.

Tani, I. 1960 Paper presented at 2nd Int. Congr. Aero. Sci. Zürich (Switzerland), September.

Wehrmann, O. & Wille, R. 1958 *Proc. Boundary Layer Symposium, Freiburg*, p. 387.

A study of natural convection above a line fire

By SHAO-LIN LEE

Department of Mechanical Engineering, North Carolina State College

AND H. W. EMMONS

Pierce Hall, Harvard University

(Received 17 April 1961)

The behaviour of a natural convection plume above a line fire is studied both theoretically and experimentally. In the theoretical treatment, a turbulent plume above a steady two-dimensional finite source of heated fluid in a uniform ambient fluid is investigated. By the use of the lateral entrainment assumption, a quadrature solution has been obtained for each of two separate ranges of a source Froude number, $F > 1$ or $F < 1$. In neither of these cases can the finite width line source be accurately represented by an equivalent mathematical line source at a lower level. Only the special case, $F = 1$, can be so represented and its solution is discussed.

In the experimental treatment, hot gases, resulting from the burning of a liquid fuel in a long channel burner, are driven upwards by buoyancy and gradually cooled down by the entrainment of ambient air. The average temperature along lines parallel to the channel burner was measured by a piece of resistance wire. For the case of a non-luminous diffusion flame, the effective radiation loss to the surroundings was assumed to be negligible, and, by a comparison of the energy flux supplied from the fuel and the energy flux contained in the plume, the characteristic turbulence entrainment coefficient is determined. By the alternate use of either an absorbing or a reflecting surface for the table-top surrounding a luminous flame, a measurement was made of the energy radiated from the flame that was intercepted by the fire surroundings and subsequently returned to the buoyancy plume by heating the ingested air. These measurements agree with estimates computed from such data as are available. The experimental results relating to the behaviour of the convection plume agree closely with the theoretical predictions in all cases.

1. Introduction

A line fire exhibits a complex interaction of diverse phenomena. Hot combustion products are driven upwards by natural convection, thus inducting air and fuel for further combustion. Heat is transferred downward by various mechanisms to maintain the combustion temperature in the fresh fuel and air and, if the fuel is liquid, to continue the evaporation process. Simultaneously, interchange of energy between the fire and the various elements of its environment also occur. One of the effects of this phenomenon is the instability of the inflowing air, which results from heat transferred from luminous flames to the surrounding

surface by radiation and thence to the inducted air by conduction and convection as noted by Emmons (1959).

No attempt is made to solve the flame-fuel evaporation problem, but rather attention is given only to the natural convection above the flames. Only the turbulent flow régime is considered. Experimentally, measurements are made above the level of the flames while theoretically the whole fire process is replaced by a horizontal source of heat, momentum and energy, infinitely long and of finite width. In the theory presented these may be varied independently. Since the experiments were conducted in the laboratory, the plumes were only a few metres high and atmospheric variations were negligible. The present work, therefore, extends previous work by the inclusion of arbitrary fire width, and arbitrary momentum and energy sources, rather than the line fire only.

2. Theoretical investigation

It is assumed that turbulent flow is fully developed and thus, as a consequence, molecular transfer mechanisms are negligible relative to the turbulent transfer. It is also assumed that local density variations are everywhere small compared to some reference density in the field. Although natural convection of this nature is produced by a source of heat, it is the buoyancy rather than the thermal properties of the flow which is fundamental to the phenomenon. Therefore, although the buoyant force due to density difference is sufficiently great to produce vertical acceleration, the corresponding variation in the mass density of the fluid undergoing acceleration is sufficiently small, in comparison with the density itself, to be neglected in the continuity and energy equations and the inertia term of the momentum equation.

In addition, we make the 'boundary-layer' assumption that transverse accelerations are small in comparison with those in the vertical direction, and that turbulent mixing in the vertical direction is small in comparison with that in the horizontal direction. A consequence of this is that the pressure has essentially no horizontal variation.

Let the origin O represent the location of the centre of a two-dimensional finite source of width b_0 (accurately defined by equation (8) applied at $x = 0$). The local mean component of velocity in the vertical direction x is denoted by u, and that in the y-direction (in the horizontal plane, normal to the fire) is denoted by v.

Under the foregoing assumptions the fundamental equations of motion reduce to the equation of continuity

$$\frac{\partial u}{\partial x}+\frac{\partial v}{\partial y}=0, \tag{1}$$

the simplified equation of conservation of vertical momentum

$$u\frac{\partial u}{\partial x}+v\frac{\partial u}{\partial y}=\frac{\Delta\gamma}{\rho_1}+\frac{1}{\rho_1}\frac{\partial \tau}{\partial y}, \tag{2}$$

and the simplified equation of conservation of energy

$$u\frac{\partial(\Delta T)}{\partial x}+v\frac{\partial(\Delta T)}{\partial y}=\frac{1}{\rho_1 C_p}\frac{\partial w}{\partial y}. \tag{3}$$

Here ρ_1 is the mass density of undisturbed ambient fluid, and

$$\Delta\gamma = g\Delta\rho = g(\rho_1 - \rho)$$

is the local buoyancy, where ρ is the local mass density, γ the local weight density, and g the gravitational acceleration. Also, $\tau = -\rho_1\overline{u_f v_f}$ is the Reynolds stress, u_f, v_f being fluctuating velocities in the x- and y-directions respectively; $\Delta T = T - T_1$, where T is the local time-mean temperature, and T_1 the temperature of undisturbed ambient fluid. Lastly, C_p is the specific heat at constant pressure, and $w = -\rho_1 C_p \overline{v_f \Delta T_f}$ is the eddy heat transfer, where ΔT_f is the fluctuating temperature difference.

Since $v = 0$ at $y = 0$ by symmetry, integration of equation (1) with respect to y gives

$$\frac{d}{dx}\int_0^\infty u\,dy + v(x,\infty) = 0. \tag{4}$$

This equation states that the increase of ascending mass in a heated plume is due to the lateral entrainment of the ambient fluid.

Since no work is applied at either $y = 0$ or $y = \infty$ and the flow is symmetrical with respect to $y = 0$, therefore $\tau = 0$ at both $y = 0$ and $y = \infty$. Integration of equation (2) with respect to y by parts, with use of equation (1), gives

$$\frac{d}{dx}\int_0^\infty u^2 dy = \int_0^\infty \frac{\Delta\gamma}{\rho_1} dy. \tag{5}$$

This equation states that the increase of vertical momentum of ascending mass of heated fluid is due to the buoyancy effect caused by the density difference.

Since no heat is added at either $y = 0$ or $y = \infty$ and the flow is symmetrical with respect to $y = 0$, therefore $w = 0$ at both $y = 0$ and $y = \infty$. By the assumption that the ambient fluid is undisturbed, $\Delta T = 0$ at $y = \infty$. Integration of equation (3) with respect to y, using equation (1) and the assumption of small density variation, gives

$$\frac{d}{dx}\int_0^\infty u\Delta\gamma\,dy = 0. \tag{6}$$

This equation states that the buoyancy flux of an ascending mass of heated fluid is conserved.

When a stream of fluid is in contact with another stream, the eddies which cause transfer of matter between them are characterized by velocities proportional to the relative velocity of the two streams. This can be seen from dimensional considerations, since if the mutual entrainment is turbulent the only quantity determining the motion is the relative velocity of the two streams. This was also shown by the experiment of Kuethe (1935) on the mixing at the edge of a jet. The rate at which the bounding edge of a heated plume expands and absorbs the surrounding fluid into the plume may similarly be assumed proportional to the velocity at that level. As first suggested by Taylor (1945) and later adopted by Morton, Taylor & Turner (1956) and Morton (1959), the rate at which fluid is entrained into the heated plume is taken as proportional to the vertical velocity on the axis of the plume, thus

$$v(x,\infty) = \alpha u(x,0), \tag{7}$$

where α is the entrainment constant.

Rouse, Yih & Humphreys (1952) have obtained velocity and temperature measurements of heated plumes above a line of small gas flames designed to simulate a line heat source. Their results show the Gaussian profiles

$$\exp(-32y^2/x^2) \quad \text{and} \quad \exp(-41y^2/x^2)$$

for the velocity and temperature measurements, respectively. Since the entrainment constant α is by definition associated with the velocity profile rather than the temperature profile, it will be appropriate to seek a similarity solution for which α measures the rate of flow into a heated plume, with velocity profile characterized by a horizontal length-scale b, and with an associated buoyancy profile of the same shape but with a length-scale λb. α and λ are assumed to be universal constants.

Consider a two-dimensional heated plume generated from a finite source in an incompressible environment. The plume will be assumed to have Gaussian profiles of time-mean vertical velocity and time-mean buoyancy: thus

$$u(x, y) = u(x)\exp(-y^2/b^2), \tag{8}$$

where $u(x) = u(x, 0)$ is the time-mean vertical velocity on the axis of symmetry of the plume, and

$$\Delta\gamma(x, y) = \Delta\gamma(x)\exp(-y^2/\lambda^2 b^2), \tag{9}$$

where $\Delta\gamma(x) = \Delta\gamma(x, 0)$ is the time-mean buoyancy on the plume axis. The finite source will be characterized by $b(0) = b_0$, $u(0) = u_0$ and $\Delta\gamma(0) = \Delta\gamma_0$. Substituting equations (8) and (9) into equations (4), (5) and (6), we have the equations of continuity, conservation of vertical momentum and conservation of energy

$$\frac{d}{dx}[ub] = \frac{2}{\pi^{\frac{1}{2}}}\alpha u, \tag{10}$$

$$\frac{d}{dx}[u^2 b] = 2^{\frac{1}{2}}\lambda g b\frac{\Delta\gamma}{\gamma_1}, \tag{11}$$

$$\frac{d}{dx}[ub\Delta\gamma] = 0, \tag{12}$$

subject to the boundary conditions

$$b = b_0, \quad u = u_0, \quad \Delta\gamma = \Delta\gamma_0 \quad \text{at} \quad x = 0. \tag{13}$$

With the following transformations designed to remove all unnecessary coefficients,

$$\left.\begin{aligned} x' &= (2/\pi^{\frac{1}{2}})\,\alpha\, x/b_0, \\ b' &= b/b_0, \\ p' &= (\Delta\gamma/\gamma_1)/(\Delta\gamma_0/\gamma_1), \\ u' &= \left(\frac{2^{\frac{1}{2}}}{\pi^{\frac{1}{2}}}\frac{1}{g}\frac{\alpha}{\lambda}\frac{1}{b_0}\frac{\gamma_1}{\Delta\gamma_0}\right)^{\frac{1}{2}} u, \end{aligned}\right\} \tag{14}$$

we have, from equations (10) to (13), the equations

$$\frac{d}{dx'}[u'b'] = u', \tag{15}$$

$$\frac{d}{dx'}[u'^2 b'] = b'p', \tag{16}$$

$$\frac{d}{dx'}[u'b'p'] = 0, \tag{17}$$

subject to the boundary conditions

$$b' = 1, \quad u' = F, \quad p' = 1 \quad \text{at} \quad x' = 0, \tag{18}$$

where

$$F = \left(\frac{2}{\pi}\right)^{\frac{1}{4}} \left(\frac{1}{g}\frac{\alpha}{\lambda}\frac{1}{b_0}\frac{\gamma_1}{\Delta\gamma_0}\right)^{\frac{1}{2}} u_0.$$

We note that this group can be written

$$F = \left(\frac{2}{\pi}\right)^{\frac{1}{4}} \left(\frac{\alpha}{\lambda}\frac{\gamma_1}{\Delta\gamma_0}\right)^{\frac{1}{2}} \frac{u_0}{(gb_0)^{\frac{1}{2}}},$$

a source Froude number of the usual form $u_0/(gb_0)^{\frac{1}{2}}$ modified by factors $(2/\pi)^{\frac{1}{4}}$ to account for the Gaussian distribution, $(\alpha/\lambda)^{\frac{1}{2}}$ to account for the difference between velocity and buoyancy profiles, and $(\Delta\gamma_0/\gamma_1)^{\frac{1}{2}}$ to account for the actual effective density difference. This Froude number plays an essential role in what follows. Equation (17) can be immediately integrated to give

$$u'b'p' = F, \tag{19}$$

by the use of which equation (16) becomes

$$\frac{d}{dx}[u'^2b'] = \frac{F}{u'}. \tag{20}$$

To solve equations (15) and (20) introduce the 'mass flux' and 'momentum flux' as two new variables

$$N = u'b', \quad M = u'^2b'. \tag{21}$$

Thus we get

$$\frac{dN}{dx'} = \frac{M}{N}, \tag{22}$$

$$\frac{dM}{dx'} = \frac{FN}{M}, \tag{23}$$

subject to the boundary conditions

$$N = F, \quad M = F^2 \quad \text{at} \quad x' = 0. \tag{24}$$

By eliminating x' and integrating, we find that

$$FN^3 = M^3 + c, \tag{25}$$

where $c = F^4(1 - F^2)$. We note that both mass and momentum flux are positive and by equations (22) and (23) increase with increasing x', although c may be zero or have either sign.

The position in the plume is now found by integrating equation (22), i.e.

$$x' = \int_F^N \frac{N\,dN}{M} = \int_F^N \frac{N\,dN}{(FN^3 - c)^{\frac{1}{3}}}. \tag{26}$$

It is convenient to consider separately three cases, $c < 0$, $c = 0$, $c > 0$, and arrange the integral for graphical or numerical evaluation. The three ranges correspond to $F < 1$, $F = 1$, and $F > 1$, respectively.

Case I. $F = 1$, the line source

For $F = 1$, $c = 0$, equations (25) and (26) give

$$N = M \tag{27}$$

and

$$x' = N - I, \tag{28}$$

which together with equations (19) and (21) give

$$u' = 1, \quad b' = x' + 1, \quad p' = \frac{1}{x'+1}. \tag{29}$$

These equations are plotted in figure 1.

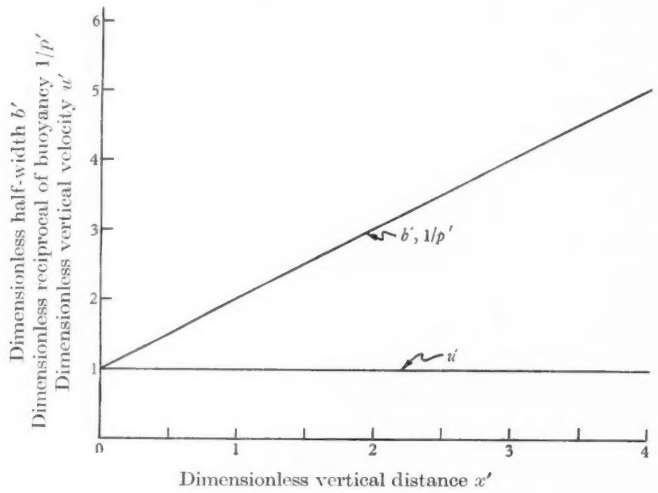

FIGURE 1. Graphical representation of the theoretical solution for a plume issuing from a neutral source, $F = 1$.

If we introduce the conserved buoyancy flux across any horizontal cross-section

$$Q = \int_{-\infty}^{\infty} gu(x,y)\frac{\Delta\gamma(x,y)}{\gamma_1}dy = \pi^{\frac{1}{2}}\frac{\lambda g}{(1+\lambda^2)^{\frac{1}{2}}}F\frac{b_0\Delta\gamma_0}{\gamma_1}, \tag{30}$$

we have, from equation (29), the familiar forms

$$\left.\begin{aligned} u &= \{\tfrac{1}{2}(1+\lambda^2)\}^{1/\gamma}\alpha^{-\frac{1}{3}}Q^{\frac{1}{3}}, \\ b &= 2\pi^{-\frac{1}{2}}\alpha x + b_0, \\ \frac{\gamma_1}{\Delta\gamma} &= \frac{(2)^{\frac{5}{6}}g\lambda\alpha^{\frac{2}{3}}}{(1+\lambda^2)^{\frac{1}{3}}Q^{\frac{2}{3}}}\left(x+\frac{\pi^{\frac{1}{2}}}{2\alpha}b_0\right). \end{aligned}\right\} \tag{31}$$

If some arbitrary point in the plume were regarded as the source at which the convection started, we would compute a source Froude number of $F = 1$ independent of location. Thus, the above solution describes the convection above a line source $b_0 = 0$ in which case the velocity $u = \text{const.}$, the plume 'width' b is proportional to x, while the buoyancy $\Delta\gamma/\gamma_1$ is inversely proportional to x.

Furthermore, for a finite width line source, the whole convection column can be regarded as arising from a line source situated a distance $x_0 = \pi^{\frac{1}{2}} b_0/2\alpha$ below the real source. We note that the equivalent line source has a finite buoyancy flux if $b_0 \Delta\gamma_0$ is constant; i.e. if the density difference becomes infinitely great as the source width goes to zero.

Case II. Plume issuing from a restrained source ($F < 1$)

The integral of equation (26) is expressible as an incomplete beta function. However, direct numerical integration is more convenient. For this purpose the parameters are removed by setting

$$N = \beta\nu, \tag{32}$$

with

$$\beta = \left(\frac{C}{F}\right)^{\frac{1}{3}} = F(1-F^2)^{\frac{1}{3}}.$$

There results

$$x' = \{F^2(1-F^2)\}^{\frac{1}{3}} \int_{\nu_0}^{\nu} \frac{\nu\, d\nu}{(\nu^3-1)^{\frac{1}{3}}}, \tag{33}$$

where

$$\left.\begin{aligned} \nu &= (1-F^2)^{-\frac{1}{3}} \frac{N}{F}, \\ \nu_0 &= (1-F^2)^{-\frac{1}{3}}. \end{aligned}\right\} \tag{34}$$

These integration limits are both greater than 1, the upper limit being larger than the lower limit. Since for the Froude number limits of this case $F = 0$, $F = 1$, ν has limits of 1 and ∞, we define

$$I_1(\nu) = \int_1^{\nu} \frac{\nu\, d\nu}{(\nu^3-1)^{\frac{1}{3}}}, \tag{35}$$

and the height scale in the convection plume is given by

$$x' = \{F^2(1-F^2)\}^{\frac{1}{3}} \{I_1(\nu) - I_1(\nu_0)\}. \tag{36}$$

Thus the actual plume may be regarded as a section of the plume arising from a virtual source at a distance $\{F^2(1-F^2)\}^{\frac{1}{3}} I_1(\nu_0)$ below the real source. The strength of the real source is specified by its 'mass flux' $N_0 = F$, while the 'mass flux' increases along the plume as $N = F(1-F^2)^{\frac{1}{3}}\nu$ increases.

From equations (19), (21), (25) and (32), the physically interesting quantities are given as follows:

$$\left.\begin{aligned} &\text{plume half-width} && b' = \{F^2(1-F^2)\}^{\frac{1}{3}} \frac{\nu^2}{(\nu^3-1)^{\frac{1}{3}}}, \\ &\text{velocity} && u' = F^{\frac{1}{3}} \frac{(\nu^3-1)^{\frac{1}{3}}}{\nu}, \\ &\text{buoyancy} && p' = \frac{1}{(1-F^2)^{\frac{1}{3}}\nu}. \end{aligned}\right\} \tag{37}$$

The integral $I_1(\nu)$ was evaluated graphically and the physical plume characteristics are plotted in figure 2. The real plume may be visualized from this figure

by imagining the actual source located at a distance to the right of the origin given by

$$x_0'' = \frac{x_0'}{\{F^2(1-F^2)\}^{\frac{1}{3}}} = I_1\{(1-F^2)^{-\frac{1}{3}}\}, \tag{38}$$

while other higher plume points appear to the right of the actual source. The plume shape is particularly interesting. For a real source with $F < 2^{-\frac{1}{2}}$ the plume width first decreases and then increases again. Furthermore, any plume at great height behaves as though it arose from a line source located at a distance (in the scale of equation (37)) of 0·7 below the virtual origin.

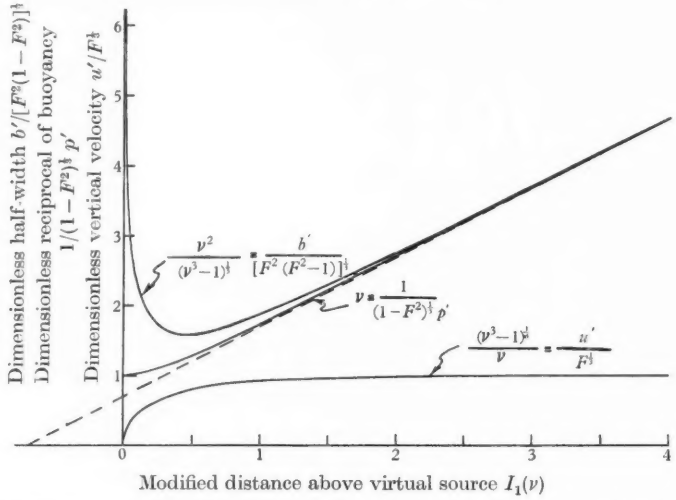

FIGURE 2. Graphical representation of the theoretical solution for a plume issuing from a restrained source (see equation (33)), $F < 1$.

Case III. Plume issuing from an impelled source ($F > 1$)

We again remove the parameters from the integral of equation (26) by setting

$$N = \beta\nu, \tag{39}$$

where now $\beta = F(F^2-1)^{\frac{1}{3}}$.

The resulting integral for graphical evaluation is

$$x' = \{F^2(F^2-1)\}^{\frac{1}{3}} \int_{\nu_0}^{\nu} \frac{\nu d\nu}{(\nu^3+1)^{\frac{1}{3}}}, \tag{40}$$

with

$$\left.\begin{aligned} \nu &= (F^2-1)^{-\frac{1}{3}}\frac{N}{F}, \\ \nu_0 &= (F^2-1)^{-\frac{1}{3}}, \end{aligned}\right\} \tag{41}$$

where $0 < \nu_0 < \nu < \infty$.

For this case we use zero as the lower limit and define

$$I_2(\nu) = \int_0^{\nu} \frac{\nu d\nu}{(\nu^3+1)^{\frac{1}{3}}}, \tag{42}$$

from which the position in the plume is computed as

$$x' = \{F^2(F^2-1)\}^{\frac{1}{3}}\{I_2(\nu) - I_2(\nu_0)\}. \tag{43}$$

By equations (19), (21), (25) and (39), the physically interesting quantities are obtained:

$$\left.\begin{aligned} &\text{plume half-width} && b' = \{F^2(F^2-1)\}^{\frac{1}{3}} \frac{\nu^2}{(\nu^3+1)^{\frac{1}{3}}}, \\ &\text{velocity} && u' = F^{\frac{1}{3}} \frac{(\nu^3+1)^{\frac{1}{3}}}{\nu}, \\ &\text{buoyancy} && p' = \frac{1}{(F^2-1)^{\frac{1}{3}}\nu}. \end{aligned}\right\} \tag{44}$$

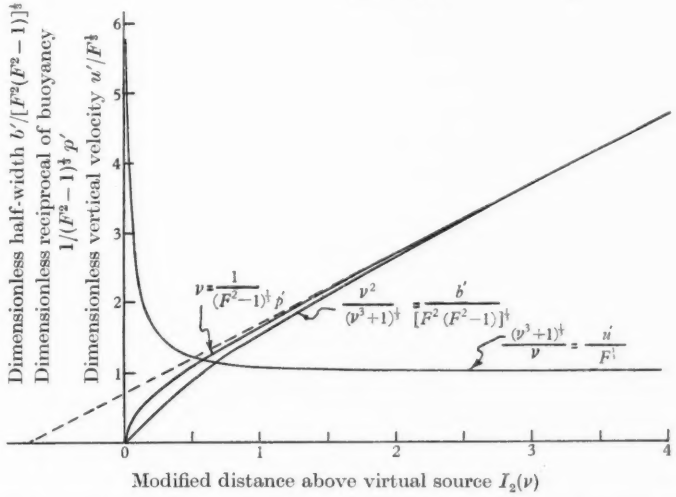

FIGURE 3. Graphical representation of the theoretical solution for a plume issuing from an impelled source (see equation (43)), $F > 1$.

Curves of these plume properties are given in figure 3. Again the origin of the distance scale may be regarded as a virtual source with the real source located at a distance

$$x_0'' = \frac{x_0'}{\{F^2(F^2-1)\}^{\frac{1}{3}}} = I_2\{(F^2-1)^{\frac{1}{3}}\}, \tag{45}$$

and the real plume given by the curves from the real source to infinity. The plume grows in size rapidly at first and then more and more slowly. In this case too, the plume at great heights becomes like the plume from a line source located at a distance of 0·7 below the *virtual* source.

We note that both cases II and III approach the case of $F = 1$ as height increases. $F = 1$ corresponds to a balance between inducted mass increase and buoyancy which just maintains the vertical velocity constant. If the plume velocity is relatively too small, i.e. $F < 1$, the plume grows slowly or even contracts to raise the local Froude number. If, on the other hand, the plume velocity is too high, as in a heated jet, i.e. $F > 1$, the plume grows more rapidly, decreasing the velocity.

3. Experimental investigation

The channel burner, 0·564 in. wide, 0·282 in. deep and 78 in. long, is cooled on the sides by a water-jacket, which controls the fuel consumption rate, and is connected by inlets underneath to a metered steady fuel supply system. On either side of the channel burner there is an 18 in. wide asbestos side plate set flush with the sides of the channel burner to prevent any entrainment of air from below. Against each end of the channel burner stands a vertical asbestos end plate to prevent the entrainment from the ends. A view of the apparatus is shown as figure 4 (plate 1). Except for cases with very low fuel consumption rates, the flame from the channel burner fluctuates both with time and location along the length of the channel burner. The average temperature at different heights was measured with a 40 in. piece of pure nickel resistance wire 0·002 in. in diameter suspended parallel to the channel burner. Two fuels were chosen, acetone and methyl alcohol, because they differ considerably from one another in radiation from the flames. Two different kinds of surface were chosen for the side plates, aluminium foil surface and bare asbestos surface, because they react very differently to radiation.

(*A*) *Analyses of asymptotic behaviour of plumes*

For either methyl alcohol or acetone, Gaussian profiles of the natural convection plume are found to prevail at all measurable heights and the corresponding values of the characteristic buoyancy half-width are thus computed. For each plume the values of the slopes $d(\gamma_1/\Delta\gamma)/dx$ and $d(\lambda b)/dx$ were obtained graphically from the measured centre-line buoyancy and Gaussian width respectively and are found to approach their respective asymptotic values.

These asymptotic values are given in a convenient form by equation (31)

$$\left.\begin{aligned}\left[\frac{d(\gamma_1/\Delta\gamma)}{dx}\right]_{\lim} &= \frac{(2)^{\frac{5}{3}} g\lambda\alpha^{\frac{2}{3}}}{(1+\lambda^2)^{\frac{1}{3}} Q^{\frac{2}{3}}},\\ \left[\frac{d(\lambda b)}{dx}\right]_{\lim} &= 2\pi^{-\frac{1}{2}}\alpha\lambda.\end{aligned}\right\} \tag{46}$$

The energy flux Q in this equation could be computed from the rate of fuel use and the fuel properties if it were not for radiation losses. If radiation is negligible, the energy flux from the fuel $\bar{Q}$ is

$$\bar{Q} = \frac{qg(H-\delta h)}{C_p\rho_1 T_1}, \tag{47}$$

where q represents the mass consumption rate of fuel per unit length of burner, H the heat of combustion per unit mass of fuel, and δh the heat removed by the cooling water per unit mass of fuel burned.

(*a*) *Convection plumes above a non-luminous diffusion flame of methyl alcohol*

Since radiation is relatively unimportant in the process of heat transfer from a non-luminous flame, the surface condition of the side plates would be expected to have relatively little effect on the behaviour of the convection plume above

the flame. Experiments with asbestos board side plates and bright aluminium foil side plates gave nearly identical convection plumes with the methyl alcohol flames. Thus the heat released from chemical reaction minus the amount removed by cooling water is carried away by the convection plume and Q equals $\bar{Q}$. Therefore the values of the assumed universal constants α and λ can be computed from equation (46) and the asymptotic data. We find $\alpha = 0{\cdot}16$, $\lambda = 0{\cdot}9$, which check very well with values computed from results of velocity and temperature measurements by Rouse *et al.* (1952) from natural convection plumes above a simulated line buoyancy source. Furthermore, the value of α also checks very well with a value computed from velocity measurements of a turbulent two-dimensional free jet by Reichardt (1942).

(*b*) *Convection plumes above a luminous diffusion flame of acetone*

Since in a luminous flame carbon particles radiate energy to the surroundings, the value of Q in the convection plume is usually smaller than that of $\bar{Q}$. The difference $\bar{Q} - Q$ is the net radiation loss from the flame-plume system to the surroundings. The results of experimental measurements with asbestos and with aluminium side plates are shown in figure 5.

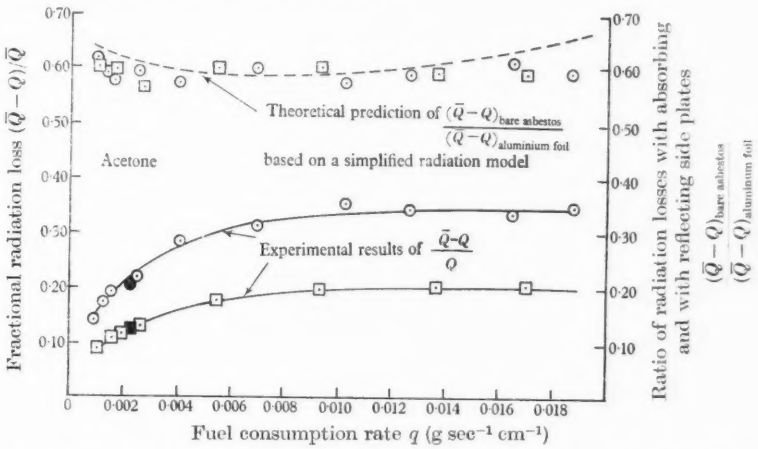

FIGURE 5. Radiation loss computed from measurements of the plume above a luminous diffusion flame of acetone: ⊡, with bare asbestos side plates; ⊙, with aluminium foil-covered side plates (estimates based on average temperature of carbon particles and emissivity measured by Tankin 1960).

It is readily seen that the net loss to the surroundings is lower for the case with bare asbestos side plates, than for those covered with aluminium foil. This can be explained by the difference in the way radiant energy is dealt with by the surface of the side plates in the two cases. The bare asbestos surface has a very high emissivity ($\epsilon = 0{\cdot}96$) and thus absorbs almost all of the radiant energy from the flame intercepted by it. The asbestos surface thus heated will give up heat by conduction to the adjacent air, which is then convected into the flame-plume. On the other hand, the aluminium foil surface has a very low emissivity

($\epsilon = 0{\cdot}087$) and will reflect almost all of the radiant energy from the flame intercepted by it. Thus all radiation from the flame not directly intercepted by the fuel is permanently lost from the convection column.

To estimate the flame radiation loss, use is made of measurements by Tankin (1960) with a bolometer of the average temperature of flame carbon particles, and of the emissivity of a luminous diffusion flame of acetone. A simplified line radiation source was used to estimate the radiation loss of a flame of approximately the same brightness, over the channel burner. The results, shown as solid points in figure 5, are in good agreement with findings of the plume measurements. The ratio of radiation losses with absorbing and with reflecting side plates based on the same simplified radiation model, is also shown in figure 5 as the broken curve which checks quite well with findings of the plume measurements at all values of fuel consumption rate.

(*B*) *Comparison of theoretical and experimental convection plume results*

It is predicted by the theoretical analysis that the behaviour of a plume above a finite source depends on a parameter F which is a function of the source characteristics, b_0, u_0 and $\Delta\gamma_0/\gamma_1$. It is then desirable to determine the values of F by comparing the theoretical predictions with the experimental data.

It is seen from figures 2 and 3 that the solutions for the variation of plume half-width with vertical distance and the location of the actual source above a virtual source, when all dimensionless quantities are converted back to physical quantities, depend only on two of the three independent characteristics of the source, F and b_0. For an origin assumed to be at the mean flame height, experimental data on the plume half-width are plotted against theoretical predictions based on different pairs of trial values of F and b_0. By the principle of least squares, the best-fit values of F and b_0 are determined for each case. The corresponding best-fit value of $\Delta\gamma_0/\gamma_1$ is then determined by comparing the theoretical predictions and experimental data on the variation of buoyancy with vertical distance. The values of F thus found for an origin assumed to be at the mean flame height are listed in table 1.

The plumes from a methyl alcohol flame are seen to lie in the region of $F < 1$, while the plumes from an acetone flame are found to lie in the region of $F < 1$ for low burning rates and $F > 1$ for high burning rates. Very good agreement has been found between theoretical predictions and experimental measurements for all the experiments performed as shown by the sample comparisons made in figures 6 and 7.

(*C*) *Interpretation of experimental results with the introduction of a simplified flame model*

The rigorous analysis of a flame is extremely complicated. However, if the main interest is in the study of the convection plume then the flame itself serves merely as a supplier of heated fluid to the source at the mean flame height for the convection problem. Therefore, if we introduce a simplified flame model with uniform temperature and vertical velocity distributions along a mean flame contour as shown in figure 8, the characteristics of the source can be determined.

Based on such a simplified flame model, the energy flux from the flame is

$$Q = 2g\bar{b}_0 u_0 \frac{\Delta\gamma_0}{\gamma_1}, \tag{48}$$

where $\bar{b}_0$ is the half-channel width of the inside burner. The energy flux contained in the plume, from equation (30), is

$$Q = (\pi)^{\frac{1}{2}} \frac{\lambda g}{(1+\lambda^2)^{\frac{1}{2}}} b_0 u_0 \frac{\Delta\gamma_0}{\gamma_1}. \tag{49}$$

Fuel	Side plates	q (g sec^{-1} cm^{-1})	F
Acetone	Bare asbestos	0·00110	0·79
		0·00163	0·98
		0·00191	1·33
		0·00268	1·83
		0·0055	3·56
		0·0093	5·85
		0·0138	8·67
		0·0170	10·7
Acetone	Aluminium foil	0·00100	0·65
		0·00134	0·85
		0·00157	0·98
		0·00254	1·49
		0·0041	2·14
		0·0070	3·74
		0·0103	5·37
		0·0127	6·75
		0·0165	8·82
		0·0187	10·3
Methyl alcohol	Bare asbestos	0·000716	0·39
		0·000885	0·48
		0·00158	0·85
Methyl alcohol	Aluminium foil	0·0074	0·40
		0·00158	0·85

TABLE 1. Values of Froude number at the effective source obtained from plume measurements.

Comparing equations (48) and (49), we have

$$b_0 = \frac{2}{(\pi)^{\frac{1}{2}}} \frac{(1+\lambda^2)^{\frac{1}{2}}}{\lambda} \bar{b}_0. \tag{50}$$

Eliminating u_0 and b_0 among equations (18), (49) and (50), we then have

$$F = \frac{\alpha^{\frac{1}{2}}}{(2)^{\frac{5}{4}} g^{\frac{3}{4}} (1+\lambda^2)^{\frac{1}{4}}} \frac{1}{\bar{b}_0^{\frac{3}{4}}} \left(\frac{\gamma_1}{\Delta\gamma_0}\right)^{\frac{3}{4}} Q. \tag{51}$$

The values of F of the source computed from equation (51) with such data as available check closely with those determined from plume measurements as shown by the sample comparison in figure 9.

4. Conclusions

(*a*) *Theoretical conclusions*

A quadrature solution for a two-dimensional turbulent natural convection plume above a finite source has been obtained with the assumptions of lateral entrainment and similar Gaussian velocity and temperature profiles. A characteristic parameter F based on the characteristics of the finite source, has been found to describe the behaviour of the plume above that source. Plumes for cases where $F < 1$ and $F > 1$ behave differently but both approach asymptotically the case where $F = 1$. The solution for the case where $F = 1$ is identified as the solution for a plume above a line buoyancy source situated at a lower level.

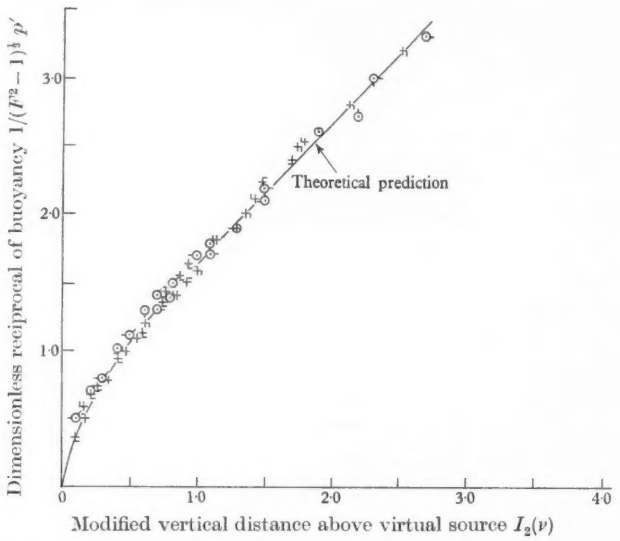

FIGURE 6. Example of comparison between theoretical and experimental results for the buoyancy in the plume above an acetone flame, $F > 1$.

	q (g sec^{-1} cm^{-1})	F		q (g sec^{-1} cm^{-1})	F
Bare asbestos side plates	0·00191	1·33	Side plates covered with aluminium foil	0·00254	1·49
	0·00268	1·83		0·0041	2·14
	0·0055	3·56		0·0070	3·74
	0·0093	5·85		0·0103	5·37
	0·0138	8·67		0·0127	6·75
	0·0170	10·70		0·0165	8·82
				0·0187	10·33

(*b*) *Experimental conclusions*

(i) A Gaussian profile was found to prevail at all measurable heights.

(ii) Values of the entrainment constant α and the auxiliary constant λ obtained from methyl alcohol burnings agree closely with those evaluated from the previously established data.

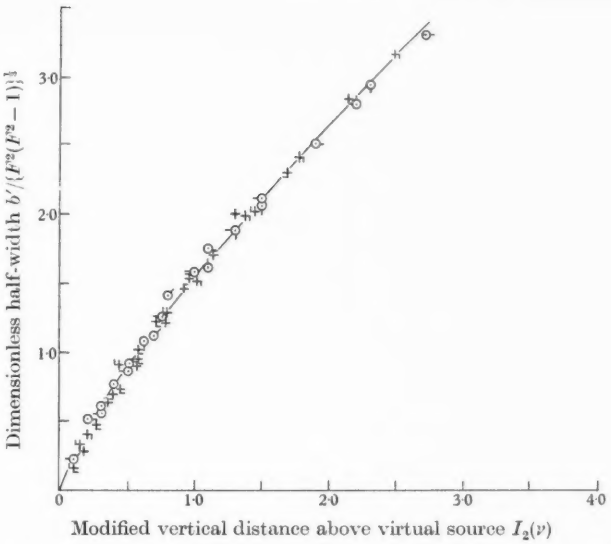

FIGURE 7. Example of comparison between theoretical and experimental results for the half-width of the plume above an acetone flame, $F > 1$. The theoretical curve is drawn in a continuous line.

		q (g sec^{-1} cm^{-1})	F
Bare asbestos side plates	⊙	0·00191	1·33
	⊙	0·00268	1·83
	⊙	0·0055	3·56
	⊙	0·0093	5·85
	⊙	0·0138	8·67
	⊙	0·0170	10·70
Side plates covered with aluminium foil	+	0·00254	1·49
	+	0·0041	2·14
	+	0·0070	3·74
	+	0·0103	5·37
	+	0·0127	6·75
	+	0·0165	8·82
	+	0·0187	10·33

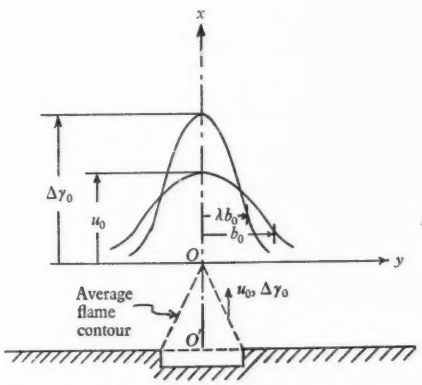

FIGURE 8. Simplified flame model and the effective finite source for the convection plume.

(iii) The radiant heat loss from a luminous flame to its surroundings determined from measurements on convection plumes agrees with estimates computed from such data as are available. The effect the surface condition of the side plates has on the behaviour of the plume from plume measurements checks very well with that from an estimate based on a simplified radiation source.

(iv) Experimental results for the natural convection plumes above a line fire are found in all cases in good agreement with theoretical predictions for the two-dimensional natural convection above a steady finite source of heated fluid. An interpretation is provided by the assumption of an effective source based on a simplified flame model.

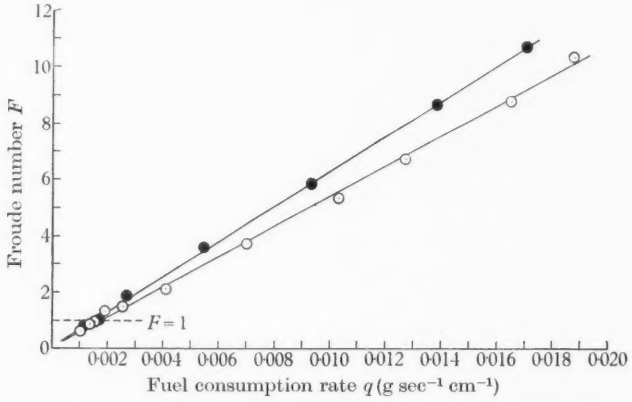

FIGURE 9. Example of comparison between the computed Froude number based on a simplified flame model and the experimentally determined Froude number of an effective source for the convection plume above an acetone flame: ●, with bare asbestos side plates; ⊙, with aluminium foil covered side plates. The two theoretical curves are drawn as continuous lines, the respective curve being the one closest to the experimental results.

REFERENCES

EMMONS, H. W. 1959 *National Fire Research Committee Report.*

KUETHE, A. M. 1935 *Trans. Amer. Soc. Mech. Engrs*, **2**, 87–98.

MORTON, B. R. 1959 *J. Fluid Mech.* **5**, 151–63.

MORTON, B. R., TAYLOR, G. I. & TURNER, J. S. 1956 *Proc. Roy. Soc.* A, **234**, 1–22.

REICHARDT, H. 1942 *VDI-Forschungeheft*, p. 414.

ROUSE, H., YIH, C. S. & HUMPHREYS, H. W. 1952 *Tellus*, **4**, 201–9.

TANKIN, R. S. 1960 Ph.D. Thesis, Harvard University.

TAYLOR, G. I. 1945 U.S. Atomic Energy Commission, MDDC-919, LADC-276.

L

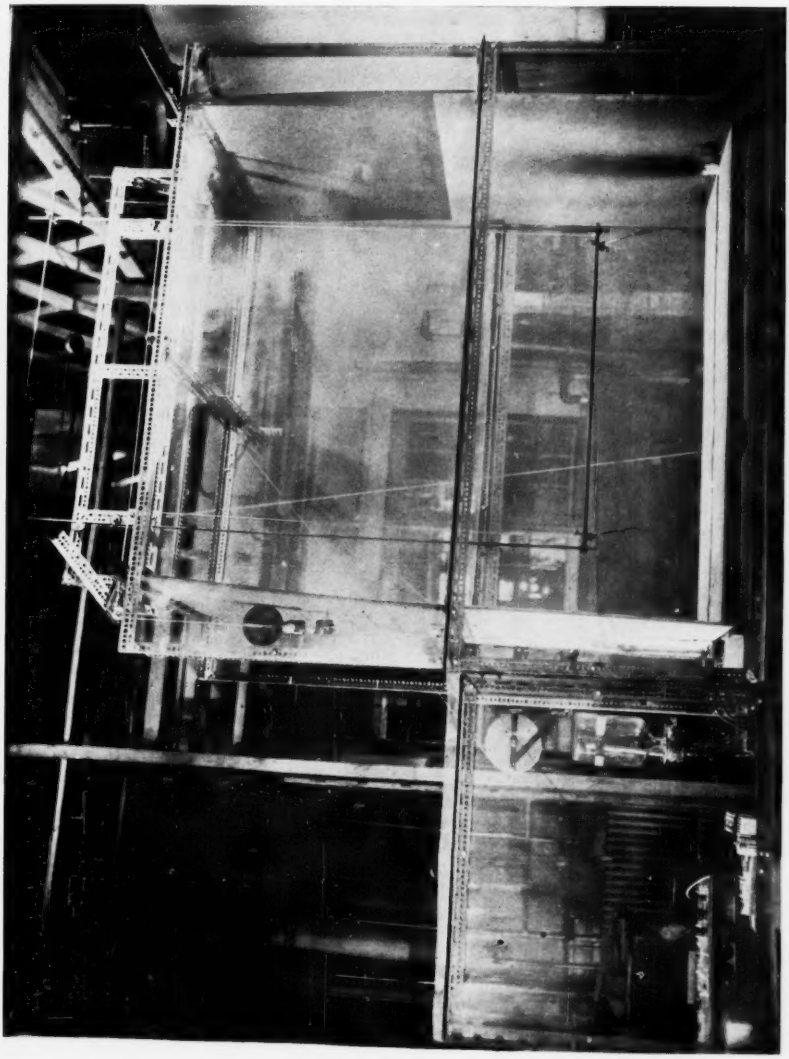

FIGURE 4 (plate 1). Experimental arrangements.

Experiments on the penetration of an interface by buoyant thermals

By J. M. RICHARDS

Department of Meteorology, Imperial College, London*

(Received 3 January 1961 and in revised form 11 April 1961)

Isolated masses of a dense aqueous solution (i.e. thermals) were released at the surface of a freshwater layer overlying one of salt water. While the whole of a thermal remained in the upper layer, the equations $z = n_1 r$, $z^2 = k_1 t$, with $k_1 = C_1 n_1^{\frac{3}{2}} (Mg/\rho)^{\frac{1}{2}}$, were obeyed, where z is the distance travelled, $2r$ the width of the thermal, t the elapsed time, M the mass excess (the difference between the masses contained within and displaced by the thermal while in the upper layer), and ρ the density of the displaced fluid. n_1 was constant for any one thermal, but varied between thermals over the range 1·9 to 7·5. C_1 had roughly the same value (0·73) for all thermals.

The behaviour after the leading extremity of the thermal (the 'front') entered the lower layer depended on the value of the parameter $S = V\Delta\rho/M$, where $\Delta\rho$ is the density difference between the upper and lower layers and V is the volume of the thermal when the widest part is at the level of the discontinuity. It was found that $Y = 0$ if $S > \beta$ ('weak' thermals), and $Y = 0{\cdot}95 - \frac{1}{2}S$ if $0{\cdot}1 < S \leqslant \beta$ ('strong' thermals), where Y is the fraction of the mass of the substance released which penetrated indefinitely into the lower layer. The constant β was approximately equal to 1·90.

In weak thermals, the equation $z - s = a_1(t - t_s)^2$ was obeyed while the front was in the lower layer, until the culminating point $z = s$ was reached at $t = t_s$. The acceleration a_1 was always negative, and constant for any one thermal, but varied between thermals. Also for weak thermals, $x = C_2 V^{\frac{1}{3}}/S$, where x is the distance from the interface to the culminating point and C_2 is a constant. C_2 was approximately equal to 3·5. For strong thermals, the distance travelled while the front was in the lower layer obeyed the equation $z^2 = k_2 t$. The origins of z and t usually differed from those found in the upper layer, and generally $k_2 \neq k_1$.

1. Introduction

In recent years, early attempts to describe the convection processes in the atmosphere which are responsible for the initiation and growth of cumulus clouds have led to 'bubble' and later 'thermal' models of buoyant convection (Bjerknes 1938; Stommel 1947; Davies & Taylor 1950; Scorer & Ludlam 1953; Scorer 1958).

In the experiments on the thermal model described by Scorer (1957), masses of marked salt solution were observed as they moved from rest at a free surface, under the action of buoyancy forces alone, into initially still water of uniform

* Now at Department of Electrical Engineering, Loughborough College of Technology.

density. It was seen that most of the marked fluid entered a well-defined region, or 'thermal', which moved through the surroundings in the direction of the buoyancy force. After an initial acceleration the shape of the thermal remained nearly constant, but its size increased continually and the rate of growth and speed of advance decreased continually.

In the experiments reported here, masses of opaque solutions were released at the surface of a comparatively shallow layer of water superimposed on a deep layer of sodium chloride solution of uniform density. As the lowest part of the thermal ('the front') approached the interface, the varying pressure distribution over the interface created waves, but the maximum displacement of the interface was always very small compared with any linear dimension of the thermal cloud while this remained entirely within the upper layer.

2. Motion in the upper layer

Dimensional analysis

The greatest linear dimension of every thermal was initally much less than the depth of the water layer, and we may therefore assume that the effect of the interface upon the early part of the motion was negligible. The accelerated part of the motion was brief, and will not be discussed. It will be assumed that the remainder of the motion may be sufficiently described by the following physical variables: the speed of advance of the front, dz/dt; the rate of increase of the maximum horizontal dimension of the thermal, $2dr/dt$; the total buoyancy force, Mg; the density of the surrounding fluid, ρ; and r. As usual, it is assumed that the fluid density may be taken as substantially equal to ρ everywhere except for the evaluation of buoyancy forces, and that the fluid viscosity is irrelevant to the motion.

A straightforward dimensional analysis then gives

$$r(dr/dt) = f_1(n_1)\,(Mg/\rho)^{\frac{1}{2}}, \tag{1}$$

where n_1 is defined by

$$dz/dt = n_1(dr/dt). \tag{2}$$

It was observed (see below) that n_1 was approximately constant only within experiments. Since Mg/ρ was also constant in each experiment, (1) indicates that $r(dr/dt)$ was constant within experiments. The Reynolds number $r(dr/dt)/\nu$ was therefore constant within experiments; and if the distribution of fluid velocities in each experiment is assumed to have been similar at all times, it follows that the circulation K round a circuit passing along the axis of an axisymmetric thermal and returning in the surrounding fluid, having the same dimensions as $r(dr/dt)$, was also constant within experiments. The dimensionless parameter $K^2\rho/Mg$ was therefore constant within experiments, but may be supposed to have varied between experiments as a result of variations in the initial conditions.

Vortex-ring model

A kinematic model of thermal motion has been advanced by Turner (1960). According to this model, a thermal may be regarded as a buoyant vortex ring having axisymmetric distributions of velocity and buoyancy. It is assumed that

these distributions are similar at all stages of the motion and that the circulation K, already defined, is constant within thermals. Turner showed that, for such a ring,

$$x_1 = (K^2\rho/Mg)\,mR, \tag{3}$$

where R is the radius of the circular axis of the vortex system (Lamb 1932, § 162), x_1 is the distance of the plane of the circular axis from a fixed virtual origin, and m is a dimensionless function of the vorticity distribution. Since, by the similarity assumption,

$$R = ar, \quad z = bx_1, \tag{4}$$

where a and b are constant within thermals, (3) may be written

$$z = abm(K^2\rho/Mg)\,r;$$

that is,

$$n_1 = abm(K^2\rho/Mg). \tag{5}$$

If the term abm is constant between thermals, this equation shows that n_1 is directly proportional to $(K^2\rho/Mg)$.

Experiments

Thermals having various mass excesses were released from a hemispherical cup. The cup was pivoted about a diametral axis which lay slightly above the free surface of the water in an experimental tank. This surface was initially coplanar with the surface of the fluid contained in the cup. Release was effected by rapidly inverting the cup about its fixed pivots.

The mass excess in the cup was found by measuring the volumes and densities of the solutions used. Standard gravimetric draining-error determinations showed that the mass excess released was always approximately 99 % of the mass excess in the cup. The corresponding values of $(z-z_0)$, $2r$ and $(t-t_0)$ were measured from enlarged images of cine photographs (z_0 is the vertical displacement of a fixed mark from the virtual origin $z = r = 0$, and $t = t_0$ at an arbitrary fixed instant). The separation of the images of two fixed marks at a known distance apart was measured to determine the scale of the photographic image. A graph of the observed values of $(z-z_0)$ was plotted against $2r$, and in each case a straight line fairly represented all except the earliest observations. The corresponding value of n_1 was found as twice the slope of this line (see (2)), and z_0 was determined as minus the intercept of the line on $2r = 0$.

From (1) and (2), we have

$$z^2 = k_1 t, \quad \text{where} \quad k_1 = f(n_1)\,(Mg/\rho)^{\frac{1}{2}}. \tag{6}$$

Graphs of z^2 against $(t-t_0)$ were plotted from the observations of each experiment. Straight lines fairly represented all except the earliest observations. This confirmed that the interface had little effect on the motion in the upper layer. The value of $f(n_1)$ for each experiment was found from the slope of the corresponding graph and the measured value of M, use being made of (6). The pair of graphs relating to one particular experiment are shown in figure 1.

Figure 2 shows a graph of the corresponding values of $f(n_1)$ and n_1 for each experiment. It will be seen that a wide range of values of n_1 was obtained, and that an equation of the form

$$f(n_1) = C_1 n_1^{\frac{3}{4}}, \quad \text{with} \quad C_1 = 0{\cdot}73, \tag{7}$$

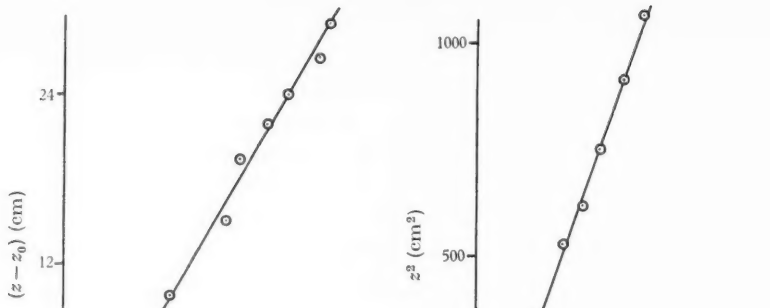

FIGURE 1. An example of motion in the upper layer.

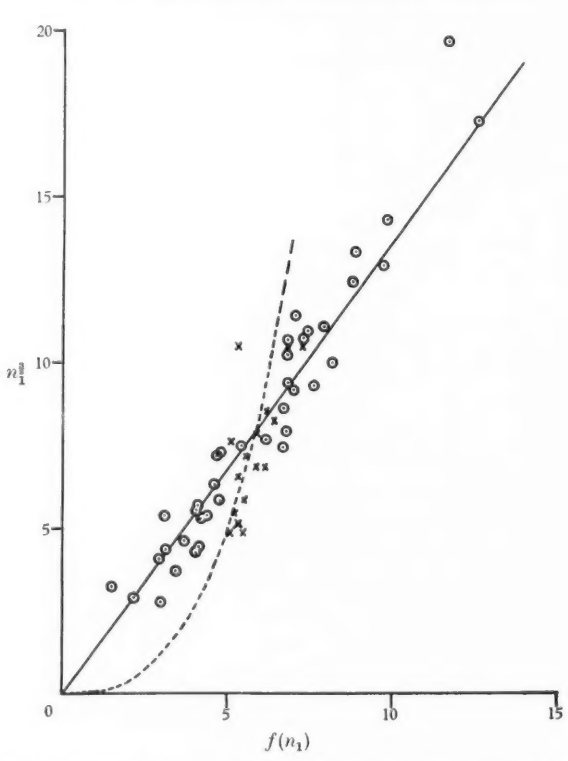

FIGURE 2. Relation between the angle of spread and rate of progress of thermals moving from a free surface into unstratified surroundings. The curve shown by the broken line is that suggested by Scorer (1957). ⊙, Richards; ×, Scorer.

fits the observations reasonably well. The value of C_1 was found as the reciprocal of the slope of the line in figure 2. Figure 2 also shows the observations reported by Scorer (1957). These are consistent with (7) and the present observations, but the latter are inconsistent with the empirical relation, $f(n_1) = 2{\cdot}9n_1^{\frac{1}{2}}$ (shown in figure 2 by a broken line) which was suggested in Scorer's paper.

Expt.	M (g)	$\Delta\rho$ (g/c.c. $\times 10^{-3}$)	V (l.)	Y	k_1 (cm^2/sec)	n_1	c	h (cm)
7	18·5	5·74	1·78	0·49	501	2·8	0·76	24
8	11·2	5·74	3·40	0·09	501	2·9	0·45	29
9	14·9	1·27	6·98	0·70	362	2·0	0·79	24
10	22·3	1·27	3·86	0·84	—	—	0·69	—
11	15·0	1·27	3·41	0·83	829	4·7	0·85	39
12	45·3	1·27	4·20	0·89	658	2·7	0·75	26
13	15·0	1·27	2·84	0·77	421	2·4	0·60	27
14	15·0	5·80	1·20	0·74	1085	5·6	0·60	41
15	11·3	5·80	1·19	—	714	4·8	0·84	37
16	15·2	5·80	2·68	0·77	912	4·9	0·78	41
21	15·1	3·92	3·03	0·60	496	2·6	0·72	27
22	15·1	3·84	4·23	0·38	756	3·9	0·87	35
23	15·1	3·65	1·66	0·67	1080	5·4	0·66	40
24	15·1	3·68	3·91	0·42	565	3·4	0·75	33
25	15·2	3·95	3·23	0·51	511	2·7	0·90	26
26	11·3	3·74	2·68	0·49	468	3·1	0·85	29
27	9·47	2·10	1·89	0·69	652	4·0	0·79	32
28	4·83	0·81	1·99	0·71	459	3·8	0·76	31
29	4·87	1·42	2·07	0·48	475	4·5	0·60	38
30	6·04	1·07	2·60	0·73	326	3·1	0·76	26
31	4·83	1·51	2·03	0·64	319	3·7	0·84	30
32	15·1	1·51	3·46	0·77	464	2·9	0·66	25
34	12·0	4·93	2·05	0·53	891	4·6	0·57	37
35	10·6	5·83	2·98	0·07	551	3·8	0·89	32
36	10·6	5·97	2·99	0·21	747	4·9	0·74	39
38	9·01	5·44	3·16	0·04	721	4·4	0·77	41
39	9·01	4·27	1·33	0·57	1048	7·3	0·63	45

TABLE 1. Measurements on strong thermals.

Note: c is the quotient (distance from level of widest part of thermal to virtual origin) ÷ (distance from front to virtual orgin).

It may be shown that the vortex-ring model leads to the equation

$$\pi z^2 = n_1^{\frac{3}{4}}(a^{-3}bm)^{\frac{1}{2}}\,(Mg/\rho)^{\frac{1}{4}}\,t. \tag{8}$$

This is consistent with (6) and (7) if $a^{-3}bm = (0{\cdot}73\pi)^2$ for all thermals. It is natural to suppose that the value of n_1 in each experiment is related to the manner of release. The controllable variables are the initial volume of the buoyant mass, the radius of the cup, and the speed with which the cup is overturned. The same cup (radius 2 in.) was used throughout. The density of the solution released was roughly 1·3 g/cm^3 in most experiments, so that the initial volume was roughly proportional to the mass excess for the experiment. However, according to the set of experimental results presented in table 1, there is no evidence of a relationship between the configuration at release and the corresponding value of n_1.

Preliminary trials showed that if the cup was inverted slowly, part of the fluid mass moved appreciably while part was still retained by the cup. The release then had the character of a pouring, and this tended to initiate plume-like rather than thermal motion. The release was so rapid in the main experiments that there was no visible distortion or descent of the buoyant mass while the cup was being overturned. However, the rate of overturning was not closely controlled or measured, and it is therefore possible that variations in this rate may have affected the value of n_1. In either case we should conclude that a wide variety of thermal motions may result from only slightly different initial circumstances.

3. Separation at the interface

The junction between the two layers of surrounding fluid was not strictly a discontinuity of density. However, we shall assume that the effect of the interface upon the thermal is determined only by the over-all difference in density between the layers, $\Delta\rho$. This assumption implies that, whenever any part of the thermal was being appreciably affected by the interface, a vertical dimension of the thermal should be large compared with the depth over which the density of the surroundings varied. This thermal thickness was at least four times the interface thickness in these experiments, so that the assumption seems reasonable.

If V_1 is the volume of the thermal as its front leaves the upper layer, the mean density excess in the thermal is then M/V_1. Material having this density excess would be neutrally buoyant in the lower layer if $M/V_1 = \Delta\rho$, that is if $V_1\Delta\rho/M = 1$. An increase in the parameter $V_1\Delta\rho/M$ therefore increases the difficulty with which a thermal may progress into the lower layer. If $V_1\Delta\rho/M$ is sufficiently great, the whole thermal will be buoyant in the lower layer, and must eventually return towards the interface. The magnitude of this critical value of $V_1\Delta\rho/M$ will depend on the rate at which the particular thermal entrains external fluid during its passage through the interface, and on the distribution of the intensity of this entrainment over the thermal surface. Some allowance for these factors will be obtained if the parameter is replaced by $V\Delta\rho/M$, where V is the volume of the thermal when its widest part is just leaving the upper layer. Let

$$V\Delta\rho/M = S. \tag{9}$$

Also let N_1 be the number of marked particles released, and let N_2 be the number which would still be moving downwards as $t \to \infty$ if the lower layer were of unlimited depth. Let

$$N_2/N_1 = Y, \tag{10}$$

where Y will be called 'the yield'. Evidently $Y = 1$ when $S = 0$, since the whole motion then takes place in unstratified surroundings. By the argument already given, $Y = 0$ for $S > \beta$, where β is a positive constant. We therefore distinguish two classes of thermals:

$$\left.\begin{aligned} &\text{'strong' thermals, for which } 0 \leqslant S \leqslant \beta \quad \text{and} \quad Y = F(S); \\ &\text{'weak' thermals, for which } S > \beta \quad \text{and} \quad Y = 0. \end{aligned}\right\} \tag{11}$$

The experiments were intended to determine the function F and the value of β.

Experimental method

The substance released was a solution of cobalt chloride in water, so that in our case N_1 was the number of cobalt ions released. The solution was strongly coloured, and visual and photographic observations were therefore possible without the use of added dyes.

After each experiment, the cobalt had become divided into two layers. The first layer was relatively shallow and was situated about the interface. This layer therefore contained $(N_1 - N_2)$ ions of cobalt. The second, deeper, layer rested on the bottom of the experimental tank, about 1·5 m below the interface. This layer, which contained the ions which would have penetrated indefinitely into an unbounded medium, was discarded by partly draining the tank. The remaining contents of the tank were stirred thoroughly so as to produce a homogeneous solution, the volume of this solution (about 320 l.) was found geometrically, and a number of 20 ml. samples were removed.

The concentration of cobalt in the samples was estimated by the method originally proposed by Haywood & Wood (1943) as modified by Eborall (1946). Briefly, the cobalt ions in the solution were caused to form a chemical complex by reaction with 'sodium nitroso-R salt' (sodium 1 nitroso 2 hydroxynaphthalene-3:6 disulphonate). The resulting substance, in weak solution, has an absorption coefficient for blue light which is directly proportional to its concentration. A measurement of the absorption over a known path length therefore gave the concentration of cobalt in the samples, and so the total amount of cobalt which had collected near the interface was determined. The method is not absolute, and the necessary calibration was carried out by mixing known small volumes of the stock solution of cobalt chloride into 320 l. of water, sampling and estimating the cobalt in the manner just described. The amount of cobalt remaining near the interface after an experiment was then expressed as a volume of the stock solution to which it was equivalent. This volume was divided by the volume of solution released to obtain the value of $(1 - Y)$ for the experiment.

Determination of $\Delta\rho$

The difference in density between the two layers was usually about 10^{-3} g/cm^3. A long uniform glass tube was partly filled with paraffin wax and weighted so as to weigh about 20 g when sealed at both ends and submerged in water. This sinker was suspended in the tank by two nylon monofilaments, one of which, attached near one end of the tube, was used to make the tube axis horizontal, as indicated by a spirit level fixed inside the tube. The other filament was attached near the middle of the tube and led to one arm of a balance. An application of the principle of moments determined what proportion of any change in the upthrust on the sinker would act on the filament attached to the balance. The tank contents being at rest, a change in the weight of the sinker was related, by Archimedes' principle, to a corresponding change in the 'mean density' of the surroundings. Terms of odd order in the distribution of density with depth did not affect the upthrust because the axis of the sinker was horizontal and the sinker was geometrically symmetrical about its axis. If any terms of even order are sufficiently small, the

mean density found from the upthrust approximates to the density at the level of the axis. This approximation was always sufficiently accurate in these experiments.

The sensitivity of the arrangement was 1 g change in balance for about 10^{-3} g/cm^3 change in density. The sinker was accordingly weighed at various depths, a typical graph of density change against depth being shown in figure 3. It will be seen that the interface was about 3 cm thick in this case.

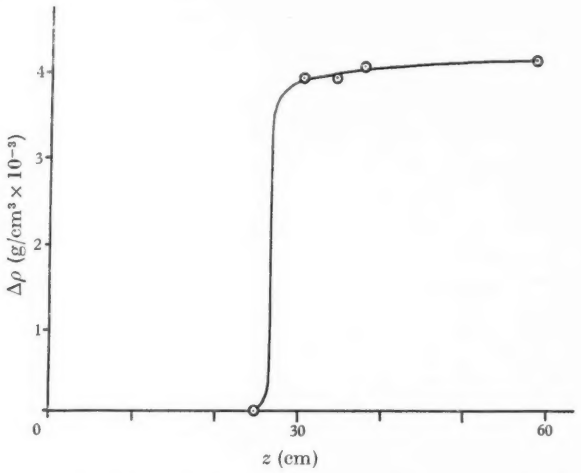

FIGURE 3. An example of the variation of the density of the surrounding fluid with depth. In the upper layer (low values of z) the density was constant. The lower layer had a slightly stable stratification.

Determination of V

Two cameras, so placed that their optic axes were respectively perpendicular to the front wall and to one of the side walls of the tank, made simultaneous exposures at the instant when the widest part of the thermal profile seen from the front of the tank was level with the top of the interface. Profile sketches like those shown in figure 4*a* were made from the enlarged images of these photographs. The profiles often indicated marked departures from axial symmetry.

With respect to the axes shown in figure 4*a*, Δx and Δy were measured at several levels z_1 in the thermal. Then V was found from the approximate expression

$$V \doteq \tfrac{1}{4}\pi \int (\Delta x\, \Delta y)\, dz_1. \tag{12}$$

The right-hand side of (12) was evaluated as $\frac{1}{4}\pi$ times the area under a graph such as figure 4*b*. Equation (12) is accurate in the case of axial symmetry, and may be accurate, depending on the orientation of axes, when horizontal cross-sections of the thermal are elliptical.

Experimental results

The graph of Y against S is given in figure 5, which shows that Y varies roughly linearly with S over a certain range. The slope of the line is approximately $-0{\cdot}5$. The results in figure 5 and table 2 may be expressed in the form

$$\left.\begin{aligned} Y &= 0{\cdot}95 - \tfrac{1}{2}S \quad \text{when} \quad 0{\cdot}1 < S \leqslant 1{\cdot}9, \\ Y &= 0 \qquad\qquad\quad \text{when} \qquad\quad S > 1{\cdot}9. \end{aligned}\right\} \tag{13}$$

Additionally, we know that $Y = 1$ at $S = 0$, but the experiments have not revealed the relation between Y and S in the range $0 < S \leqslant 0{\cdot}1$.

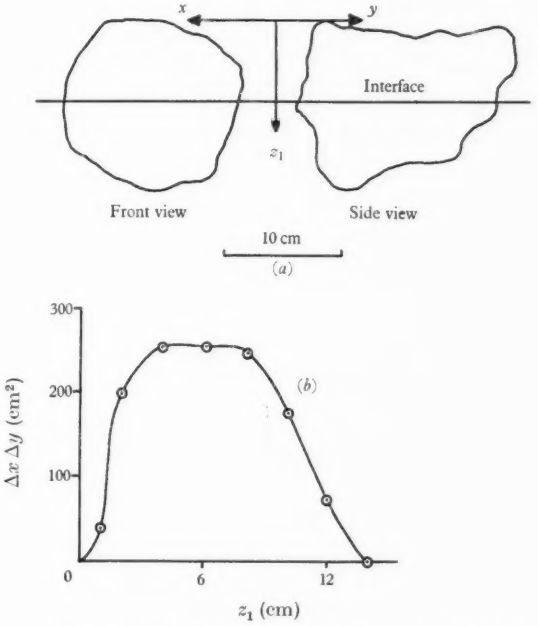

FIGURE 4. (*a*) Simultaneous profiles of a typical thermal. (*b*) Graphical determination of the thermal volume V (Δx and Δy are the widths across the profiles at the level z_1).

Now, S is not the only dimensionless parameter which can be constructed from the conditions of the experiments. For example, $h/V^{\frac{1}{3}}$ is another such parameter, where h is the vertical distance of the interface from the virtual origin of the thermal motion. Although $h/V^{\frac{1}{3}}$ varied between 1·0 and 4·1 in these experiments, the variations appear to have had no significant effect upon Y.

4. Motion in the lower layer: weak thermals

In this case there is a lower limit to the progress of any part of the thermal mass. Outline sketches of a typical weak thermal at successive instants are shown in figure 6. The distance z of the front from the virtual origin of motion in the upper

layer increases to a maximum (at the 'culminating point') and then decreases. Let s be the value of z, and t_s the value of t, at the culminating point. It was found that, for every weak thermal when $t < t_s$, the graph of $(z-s)$ against $(t-t_s)^2$ was a straight line in the lower layer. An example is shown in figure 7.

This was motion with a constant deceleration, such as might be expected when a parcel of fluid moves through uniform surroundings in the direction opposed to that of the buoyancy force. Since mixing at the front between the parcel and its

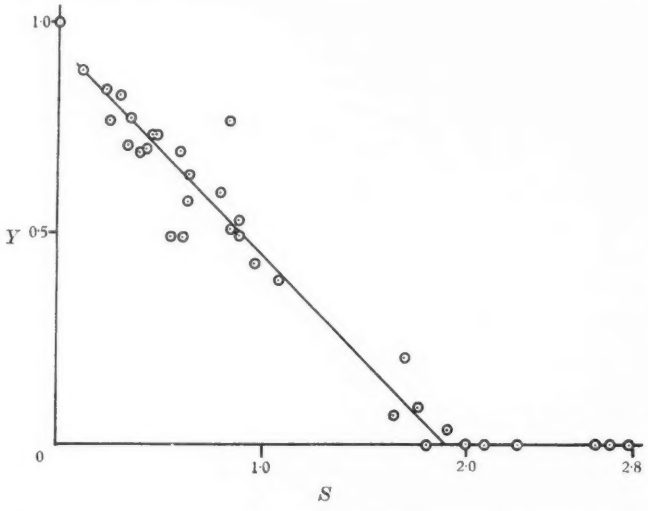

FIGURE 5. Relation between the fraction of the mass released which penetrated the inversion and the relative strength of the thermal.

Expt.	M (g)	$\Delta\rho$ (g/c.c. $\times 10^{-3}$)	V (l.)	k_1 (cm²/sec)	n_1	x (cm)	h (cm)	a_1 (cm/sec²)	v_2/v_1
6	8·07	5·62	3·79	594	4·2	16·5	31	0·66	0·48
17	11·4	5·89	4·01	505	3·8	31·3	33	0·32	0·50
51	1·05	1·64	5·72	224	4·4	8·8	39	0·15	0·58
52	2·10	1·64	2·84	572	6·7	16·4	57	0·21	0·53
53	3·10	1·62	3·78	223	3·1	25·3	29	0·14	0·73
54	2·48	1·62	4·98	154	3·1	16·6	30	0·17	0·92
55	0·64	1·69	4·36	74	2·6	4·7	24	0·14	0·73
56	1·48	1·69	3·81	304	5·0	17·2	38	0·29	0·80
57	1·25	4·12	2·20	248	5·1	7·9	36	0·42	0·74
58	2·89	4·12	2·30	—	—	12·9	—	0·66	—
59	4·08	4·01	1·81	624	5·9	27·2	39	0·23	0·60
60	6·66	4·01	4·32	121	2·2	20·9	16	0·58	1·28
61	4·16	4·29	4·29	138	2·1	9·9	20	0·69	1·06
62	6·22	4·29	3·98	760	5·5	22·9	46	0·35	0·48

TABLE 2. Measurements on weak thermals ($Y = 0$).

Note: x is the distance from the interface to the culminating point.

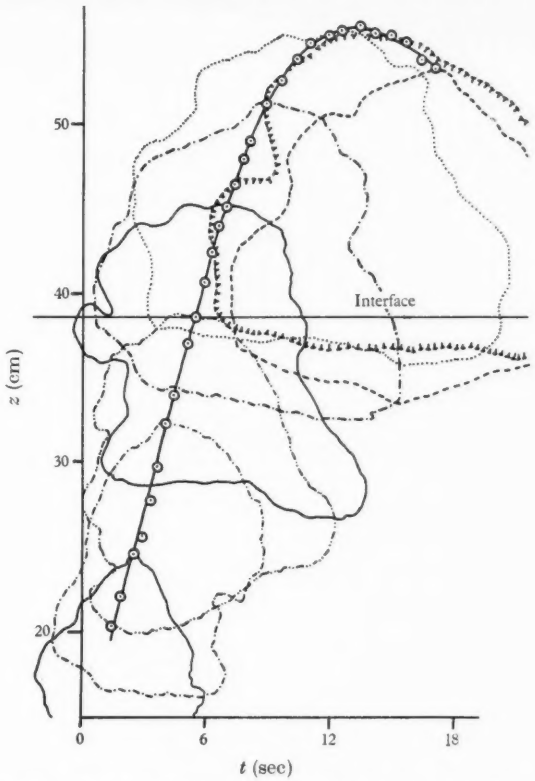

FIGURE 6. The motion of a weak thermal above and below an interface. The solid curve shows the (z, t)-variation, and the other symbols distinguish the successive thermal profiles. Low values of z refer to the upper layer.

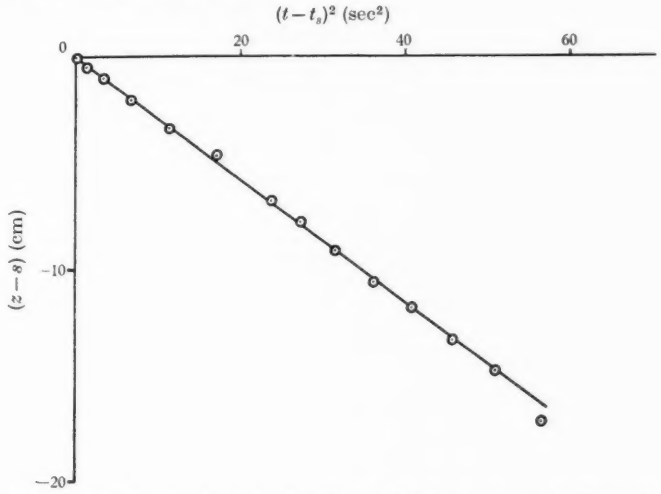

FIGURE 7. The constant deceleration of the front of a weak thermal while in the lower layer.

surroundings then has the effect of working more rapidly against the buoyancy force, the intensity of such mixture may be expected to decrease rapidly as the thermal moves into the lower layer.

In the lower layer,

$$z - s = a_1(t - t_s)^2. \tag{14}$$

Accordingly, let x be the distance from the interface to the culminating point. If (14) held near the interface, the velocity of the front at the interface would be

$$v_2 = \sqrt{(-2a_1 x)}, \tag{15}$$

which will be called the 'virtual velocity'. But, from (6), the actual velocity of the front at the interface is

$$v_1 = k_1/2h, \tag{16}$$

since $z = h$ at the interface.

It will now be assumed that the particle of fluid which is at the front when the weak thermal touches the interface remains at the front until the culminating point is reached, and that there is no mixture between other fluid and this particle while it is in the lower layer.

The density difference between the particle and its environment, which consists largely of fluid of the lower layer, is

$$(K_1 M/V) - \Delta\rho, \tag{17}$$

where K_1 is a numerical constant.

The kinetic energy per unit volume of the particle is some fraction of the average potential energy per unit volume given up by the thermal in its progress from the virtual origin to the interface. The kinetic energy per unit volume of the particle at the interface is therefore

$$C_2 V^{\frac{1}{3}} Mg/V, \tag{18}$$

where C_2 is a numerical constant. If the energy which the particle gains while in the lower layer is negligible, the kinetic energy density (18) is equal to the potential energy density of the particle at the culminating point, so that

$$-\{(K_1 M/V) - \Delta\rho\} gx = C_2 V^{\frac{1}{3}} Mg/V.$$

That is,

$$V^{\frac{1}{3}}/x = (S - K_1)/C_2. \tag{19}$$

Experimental results

These are shown in table 2. The value of a_1 was determined as the slope of the corresponding graph like figure 7, x was measured directly from the photographic images, and v_2 and v_1 were calculated from (15) and (16).

It will be noticed that v_2/v_1 varied between 0·48 and 1·28. This seems consistent with Miss Woodward's observation (1959) that the maximum mean vertical component of the fluid velocity in a thermal moving through unstratified surroundings is about twice the velocity of the thermal front.

The experimental values of $V^{\frac{1}{3}}/x$ have been plotted against S in figure 8, for both strong and weak thermals. It will be noticed that there is a sharp break, corresponding to the division between strong and weak thermals, near $S = 1{\cdot}9$. In the weak-thermal region, to the right of this break, a roughly linear relationship is

evident. If the line were produced, it would pass through or near the origin, and $V^{\frac{1}{3}}/x$ is therefore roughly directly proportional to S. This is the form taken by (19) if K_1 is much less than the minimum value of S which is possible in weak thermals, namely $S = 1{\cdot}9$. The value of C_2, obtained from the slope of the graph in figure 8, is 3·6.

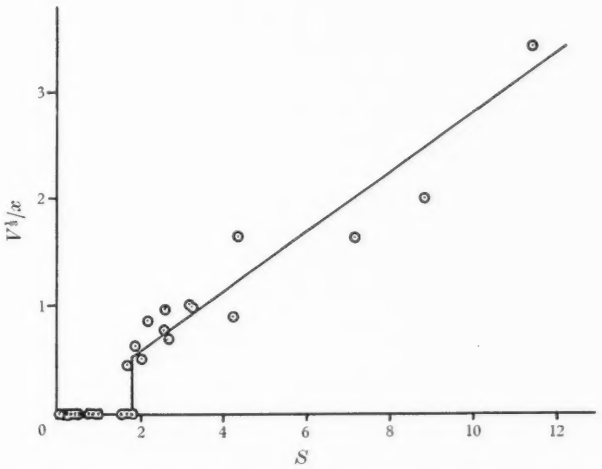

FIGURE 8. The penetration of an interface by thermals. Points to the left and right of the step represent strong and weak thermals respectively.

5. Motion in the lower layer: strong thermals

Substantially all that part of a strong thermal which would proceed indefinitely into the lower layer is denser than the surrounding fluid. If the advancing part had not been stopped, the momentum which it had on leaving the interface would eventually have become a small fraction of the total momentum, which would have been continually augmented by the action of the buoyancy force. It therefore seemed possible to suppose that thermal motion might be resumed in the lower layer at a sufficient distance below the interface.

This motion would be described by the equations

$$z = n_2 r, \tag{20}$$

$$z^2 = k_2 t, \quad \text{where} \quad k_2 = C_1 n_2^{\frac{3}{2}} (M_2 g/\rho_2)^{\frac{1}{2}}. \tag{21}$$

Equations (2), (6) and (7) have been used with a suffix 2 to refer to variables in the lower layer. C_1 would have the value obtained from the experiments in the upper layer.

Experiments

The observations in each experiment were reduced to graphs of $(z - z_0)$ against $2r$ and of z^2 against t. Typical results are shown in figures 9 and 10. In both these experiments it will be seen that $z = n_2 r$ throughout the motion in the lower layer, verifying (20). In most experiments, however, r seemed to be nearly constant in the earliest part of the motion in the lower layer, while the advancing part was

separating from the remainder of the marked fluid. The first equation of (21) was always approximately obeyed in the lower layer, typical cases being shown in figures 9*b* and 10*b*. It is therefore reasonable to suppose that (20) was also always approximately obeyed, but that the lateral extent of the advancing part was

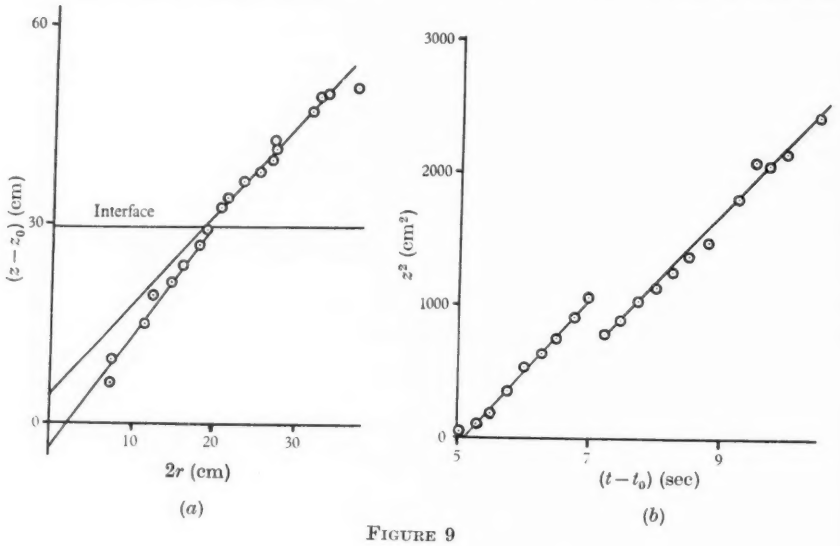

FIGURE 9

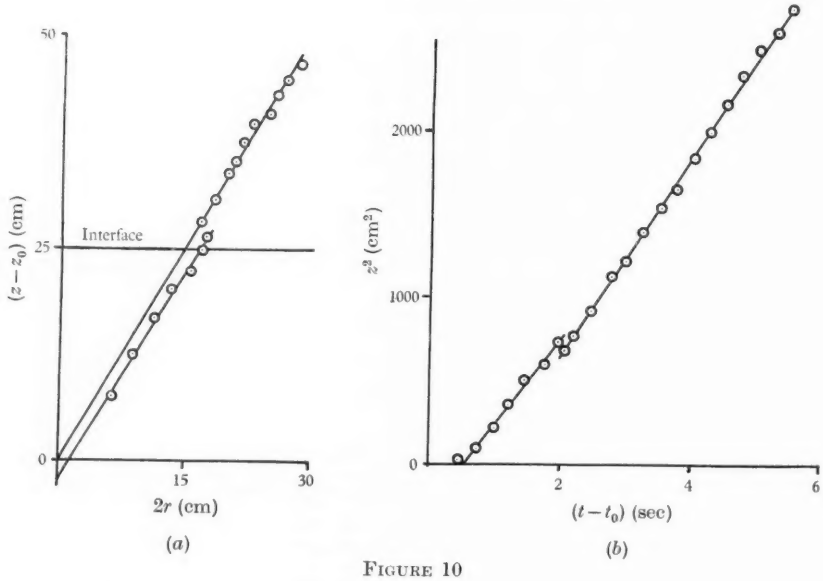

FIGURE 10

FIGURES 9 and 10. The motions of two strong thermals above and below an interface.

obscured by the remainder for a varying interval. In some cases this transitional behaviour persisted throughout the observed motion in the lower layer, so that no estimate of n_2 could be obtained.

From (6), (7) and (21), if thermal motion is resumed in the lower layer, we have

$$k_2 n_1^{\frac{3}{2}}/k_1 n_2^{\frac{3}{2}} = (M_2/M)^{\frac{1}{2}}, \tag{22}$$

since $\rho \doteqdot \rho_2$ in all experiments. The mass excess in the lower layer was always less than M since, first, the yield was always less than unity, and secondly, the surrounding fluid in the lower layer was always denser than that in the upper, so that the mass displaced by the advancing part of the thermal was increased and its mass excess therefore reduced. Hence, if thermal motion is resumed in the lower layer,

$$k_2 n_1^{\frac{3}{2}}/k_1 n_2^{\frac{3}{2}} < 1. \tag{23}$$

The experimental values of $k_2 n_1^{\frac{3}{2}}/k_1 n_2^{\frac{3}{2}}$ are shown in table 3, where it will be seen that about half these values are greater than unity.

Expt.	k_2 (cm²/sec)	n_2	$k_2 n_1^{\frac{3}{2}}/k_1 n_2^{\frac{3}{2}}$	Expt.	k_2 (cm²/sec)	n_2	$k_2 n_1^{\frac{3}{2}}/k_1 n_2^{\frac{3}{2}}$
7	584	3·6	0·81	26	283	1·7	1·41
8	680	4·1	0·79	27	708	—	—
9	531	—	—	28	459	3·8	1·00
11	958	4·7	1·15	29	319	—	—
12	1238	3·4	1·23	30	382	3·1	1·17
13	704	—	—	31	447	4·2	1·19
14	710	4·2	0·99	32	613	3·4	1·15
16	551	3·0	1·44	34	576	4·6	0·65
21	720	—	—	35	282	2·3	1·13
22	499	3·1	0·92	36	412	3·4	0·93
23	834	4·1	1·15	38	388	3·2	0·93
24	527	2·7	1·31	39	270	2·1	1·68
25	331	2·3	0·87				

TABLE 3. Comparison of motions above and below an interface (strong thermals).

We conclude that the motion of the advancing part of a strong thermal differs from thermal motion from rest at a horizontal surface into unstratified fluid. Returning to the vortex-ring model, we see from (8) that values of $k_2 n_1^{\frac{3}{2}}/k_1 n_2^{\frac{3}{2}}$ greater than unity may occur if, and only if, the value of $a^{-3}bm$ is sufficiently increased by the passage through the interface. This means that, according to the vortex-ring model, the distributions of velocity are sometimes necessarily different in the two layers.

I wish to thank Dr R. S. Scorer for many helpful discussions and Professor P. A. Sheppard for the use of experimental facilities, also Dr J. F. Herringshaw for advice and the use of apparatus and Mr S. J. Farnsworth for assistance in the determination of draining errors. My thanks are further due to Mr E. G. Jennings and his staff for workshop assistance, and to the D.S.I.R. for financial provision for this research and for permission to publish the results.

REFERENCES

Bjerknes, J. 1938 *Quart. J. Roy. Met. Soc.* **64**, 325.

Davies, R. M. & Taylor, G. I. 1950 *Proc. Roy. Soc.* A, **200**, 375.

Eborall, F. E. 1946 *Metallurgia*, **39**, 104.

Haywood, F. W. & Wood, A. A. R. 1943 *J. Soc. Chem. Ind.* **62**, 37.

Lamb, H. 1932 *Hydrodynamics*, 6th ed. Cambridge University Press.

Scorer, R. S. 1957 *J. Fluid Mech.* **2**, 583.

Scorer, R. S. 1958 *Natural Aerodynamics.* London: Pergamon.

Scorer, R. S. & Ludlam, F. H. 1953 *Quart. J. Roy. Met. Soc.* **79**, 94.

Stommel, H. 1947 *J. Met.* **4**, 91.

Turner, J. S. 1960 *J. Fluid Mech.* **7**, 419.

Woodward, B. 1959 *Quart. J. Roy. Met. Soc.* **85**, 144.

The effect of a sudden density change on a slightly non-uniform flow

By W. R. HAWTHORNE AND P. J. BANKS
Engineering Department, University of Cambridge

(Received 22 June 1960 and in revised form 24 March 1961)

The effect of combustion or heating on a slightly non-uniform flow in a tube of constant radius is explored by examining a simplified model, in which a density decrease occurs across a plane actuator-disk normal to the axis of the tube. The flow is considered to be steady, axi-symmetric, incompressible and inviscid and to originate at an injector-plate which is situated upstream of the disk. This paper analyses and discusses the effects caused by the density decrease when the velocity of flow through the injector-plate has a fractional non-uniformity u_e, when there is a curvature θ_e of the injector-plate, and when the density decrease has a fractional non-uniformity δ_2. It is shown that the non-uniformity of the flow far downstream of the disk caused by the disturbances u_e and θ_e is diminished by the density decrease; while that due to the disturbance δ_2 is increased, unless the density decrease occurs close to the injector-plate. The distance separating the injector-plate and actuator-disk is found to be an important parameter. When this distance is small, compared to the radius of the tube, and the density decrease is severe, a small disturbance u_e, θ_e or δ_2 may set up a pressure variation at the injector-plate of many times the inlet dynamic pressure of the flow. It is conjectured that this pressure variation could affect the uniformity of velocity and composition of the flow through the injector-plate, and thus cause the disturbances u_e and δ_2 to grow or diminish.

1. Introduction

In rockets, ramjets and turbo-jet combustion chambers a flow with large density changes occurs. The decrease in density caused by combustion considerably affects the pattern of flow. Such effects have been studied by Scurlock (1948), Tsien (1951), Emmons, Ball & Maier (1952) and others, in connexion with flow through a V-shaped flame-front stabilized at the centre of a duct. In these studies, the effect of the flame-front on the flow is due to the shape of the flame-front rather than to any non-uniformity of the approaching flow.† In practical cases the flow approaching the flame-front is generally non-uniform; for instance in rocket combustion chambers the flow of oxidant and fuel through the injector-plate varies with radial distance.

The effect of combustion or heating on non-uniform flows is explored in this paper by examining a simplified model in which a density change occurs across

† Ball (1951) considered the effect of shear in the flow approaching a V-shaped flame-front.

a plane actuator-disk normal to the main-flow direction. This actuator-disk would represent a flame-front if the non-uniformity of the flow at the front was identical with the flame-speed variation in the approaching flow, caused for instance by non-uniform mixture strength.

In the model examined (see figure 1), a steady, axi-symmetric, incompressible, inviscid and slightly non-uniform flow in a tube of constant radius approaches a density-change actuator-disk normal to the axis of the tube. On the upstream

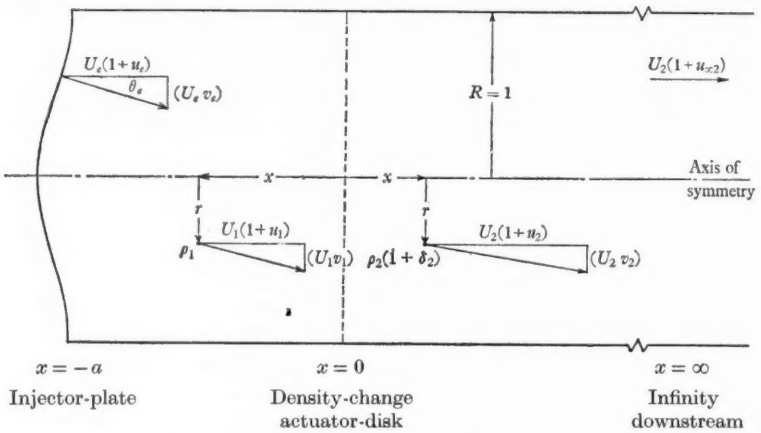

FIGURE 1. Diagram showing flow model and nomenclature.

side of the disk the flow is assumed to be of uniform density. Downstream the density may be either uniform or may vary owing to a slight non-uniformity in the density change at the disk. In accordance with the assumption of inviscid flow there will be no heat transfer, so that, since the flow is also assumed to be incompressible, the density may be considered to be constant along a streamline, except across the disk. Thus the flow on either side of the disk is obtained by a small perturbation of a flow with uniform velocity and density, and the problem may be linearized by neglecting the products of perturbations in the equations defining the flow. The effect of gravity on the flow is neglected. The disk is supposed to be stabilized at a finite distance downstream of a plate through which the fluid is injected, and the flow is assumed to continue for an infinite distance downstream of the disk.

2. Solution for flow on either side of the density-change actuator-disk

The type of flow, downstream of the disk, described above is termed stratified or non-homogeneous; the flow upstream may be regarded as a particular case of such a flow. Long (1953) has shown that the vorticity η in a steady, stratified, plane two-dimensional flow varies along the streamlines as the velocity, of magnitude q, changes, in accord with a relation of the form

$$\eta = H(\Psi) + \frac{1}{\rho}\frac{d\rho}{d\Psi}\frac{q^2}{2}; \tag{1}$$

where ρ is the density, Ψ a stream function such that $d\Psi/dn = -q$ with n measured normal to a streamline, and H is constant along a streamline. Equation (1) is equation (8) of Long (1953) with η replacing $(-\nabla^2\Psi)$, q^2 replacing $(\nabla\Psi)^2$, and the term due to gravity omitted. The equation is also applicable to axi-symmetric flow with the stream function defined by $d\Psi/dn = -qr$, because of the similarity between axi-symmetric and plane two-dimensional flow. The vorticity η is then the circumferential component.

In the problem considered in this paper, the flow is axi-symmetric and involves a small perturbation of a uniform flow, with velocity U and density ρ, in the axial direction. We define the velocity components in the axial, x, and radial, r, directions to be $U(1+u)$ and Uv respectively, and the density to be $\rho(1+\delta)$, where u, v and $\delta \ll 1$; then, by substituting in equation (1) and neglecting products of perturbations, one obtains the equation

$$\eta = H + \frac{d\delta}{d\Psi}\tfrac{1}{2}U^2. \tag{2}$$

Now U is constant and H and δ depend only on Ψ, so that the vorticity is constant along the streamlines of the perturbed flow, to first order in the perturbations. These streamlines depart only slightly from the streamlines of the unperturbed flow, which are lines of constant radius. Hence in the perturbed flow the vorticity is a function of radius alone to first order in the perturbations, and may be expressed as

$$\eta = U\left(\frac{\partial v}{\partial x} - \frac{\partial u}{\partial r}\right) = -U\frac{\partial u_\infty}{\partial r}, \tag{3}$$

where Uu_∞ is the value of the axial velocity perturbation at a plane where v and $\partial v/\partial x = 0$.

The flow may be considered to be the sum of the unperturbed flow and a perturbation flow, and, since the products of perturbations are being neglected, the perturbation flow may be resolved into a number of parts. Thus if we write $u = u_\infty + u'$, where u' and v both approach zero at the same plane, then equation (3) shows that Uu' and Uv are the velocity components of the irrotational part of the perturbation flow. The rotational part is seen to have axial velocity Uu_∞ and zero radial velocity. Therefore a perturbation stream function ψ, defined by

$$ru' = -\partial\psi/\partial r \quad \text{and} \quad rv = \partial\psi/\partial x, \tag{4}$$

satisfies Laplace's equation, which in axi-symmetric co-ordinates is

$$r\frac{\partial}{\partial r}\left(\frac{1}{r}\frac{\partial\psi}{\partial r}\right) + \frac{\partial^2\psi}{\partial x^2} = 0. \tag{5}$$

The solution of this equation which satisfies the boundary conditions, $v = 0$ at $r = 0$ and $r = 1$, the radius of the tube containing the flow being taken as the unit of length, is

$$\psi = \sum_{n=1}^{\infty} (A_n e^{k_n x} + B_n e^{-k_n x})\, rJ_1(k_n r)/k_n, \tag{6}$$

where A_n and B_n are arbitrary constants, and k_n are a series of constants determined from

$$J_1(k_n) = 0, \tag{7}$$

so that $k_1 = 3{\cdot}832$, $k_2 = 7{\cdot}016$, $k_3 = 10{\cdot}174$, etc. Therefore the perturbation flow may be considered as the sum of a series of Fourier–Bessel harmonics. The nth harmonic of the perturbation stream-function, and of the radial velocity, has a radial form defined by the Bessel function $J_1(k_n r)$, which has $(n-1)$ zeros between the tube axis and the tube wall. The factor (in any harmonic) which is independent of the radius r, e.g. $k_n^{-1}\{A_n e^{k_n x} + B_n e^{-k_n x}\}$ in equation (6), will be referred to as the amplitude of the harmonic.

Using equations (4) and (6) the velocity perturbations Uu and Uv in the flow on either side of the density-change actuator-disk are found to be given by expressions of the form

$$u = \sum_{n=1}^{\infty} u_n J_0(k_n r), \tag{8}$$

and

$$v = \sum_{n=1}^{\infty} v_n J_1(k_n r), \tag{9}$$

where the amplitudes u_n and v_n of the nth harmonics are

$$u_n = u_{\infty n} + u_n' \quad \text{with} \quad u_n' = -(A_n e^{k_n x} + B_n e^{-k_n x}) \tag{10}$$

and

$$v_n = (A_n e^{k_n x} - B_n e^{-k_n x}). \tag{11}$$

The amplitude $u_{\infty n}$ of the nth harmonic of u_∞ is defined by equation (8). The quantities u and v will be referred to as the axial and radial velocity perturbation fractions respectively, and u will be used to define the non-uniformity of axial velocity.

An expression for the pressure-perturbation fraction p, that is the static pressure-perturbation divided by the dynamic pressure of the unperturbed flow, may be derived by equating the terms containing perturbations on either side of the equation of motion in the radial direction, and neglecting products of perturbations, from which one obtains

$$-(\tfrac{1}{2}\rho U^2)\frac{\partial p}{\partial r} = (\rho U^2)\frac{\partial v}{\partial x}.$$

Combination of this result with equation (3) gives

$$\frac{\partial u'}{\partial r} = \frac{\partial v}{\partial x} = -\frac{1}{2}\frac{\partial p}{\partial r}, \tag{12}$$

from which it may be concluded that

$$p = -2u', \tag{13}$$

the constant vanishing because, at the plane where $u' = 0$, the flow is parallel to the axis.

3. Application of boundary conditions

The quantities $u_{\infty n}$, A_n and B_n in the expressions for the perturbation fractions are determined by the boundary conditions at the injector-plate, at the density-change actuator-disk, and at an infinite distance downstream. The additional

suffixes 1, 2, a, and e will be used to denote conditions upstream of the actuator-disk, downstream of the actuator-disk, at the actuator-disk, and at the injector-plate respectively.

The boundary conditions at the injector-plate are determined by the non-uniformity of the flow through the plate and the geometry of the plate. The plate is assumed to be symmetrical about the axis of the tube, and to be slightly curved. Hence the perturbation of the axial velocity at the plate $U_1 u_e$ arises directly from the non-uniformity of the flow through the plate, and can be defined by

$$u_e = \sum_{n=1}^{\infty} u_{en} J_0(k_n r). \tag{14}$$

The curvature of the plate will produce a radial velocity at the plate, which, as a fraction of U_1, may be written

$$-v_e = \theta_e = \sum_{n=1}^{\infty} \theta_{en} J_1(k_n r), \tag{15}$$

where θ_e is the angle by which the entering flow is deflected inwards from the axial direction due to the curvature of the plate. It is equal to the angle by which the surface of the plate deviates from that of a flat plate. Near the tube wall θ_e must approach zero so that the flow adjacent to the wall is injected parallel to the wall.

The flows upstream and downstream of the density-change actuator-disk are matched at the disk by the conditions of conservation of mass and momentum. From conservation of mass, we derive that

$$\rho_1 U_1(1+u_{a1}) = \rho_2(1+\delta_2)\, U_2(1+u_{a2}).$$

By neglecting the term containing a product of perturbations, and equating the terms corresponding to the unperturbed and the perturbation flows on either side of the equation, one obtains the results

$$\rho_1 U_1 = \rho_2 U_2 \tag{16}$$

and

$$u_{a1} = u_{a2} + \delta_2. \tag{17}$$

Hence, using equation (8), the non-uniformity of the density change may be expanded into harmonics, to give

$$\delta_2 = \sum_{n=1}^{\infty} \delta_{2n} J_0(k_n r). \tag{18}$$

From the conservation, across the disk, of mass and radial momentum, it is apparent that the radial velocity is continuous across the disk, so that, using equation (16),

$$\lambda v_{a1} = v_{a2}, \tag{19}$$

where $\lambda = \rho_2/\rho_1$ defines the ratio of the densities of the unperturbed flow on either side of the actuator-disk.

Conservation of momentum normal to the plane of the disk gives an equation which, on neglecting terms containing products of perturbations, equating the

terms corresponding to the perturbation flow on either side of the equation, and using equation (16), becomes

$$\lambda p_{a1} - p_{a2} = 2(2u_{a2} + \delta_2 - 2\lambda u_{a1}),$$

which, with equations (13) and (17), reduces to

$$\lambda u_{\infty 1} - u_{\infty 2} = (1-\lambda)\, u_{a1}. \tag{20}$$

This equation defines the change, at the actuator-disk, of the rotational part of the perturbation flow, u_∞, which is otherwise invariant along the tube, in terms of the conditions at the disk. Thus it leads directly to an expression for the change in the vorticity of the flow at the disk, and the relation of this result to the work of other authors is discussed in § 4.2.

At an infinite distance downstream from the disk, the streamlines are assumed to be parallel. Thus at $x = \infty$, u', v and $\partial v/\partial x = 0$, and $U_2 u_{\infty 2}$ is the only remaining velocity perturbation, so that, from equation (11),

$$A_{2n} = 0. \tag{21}$$

By substitution of the solutions for the velocity perturbation fractions, equations (8) to (11), in the boundary conditions, equations (14), (15), (17), (19) and (20), and by use of equations (18) and (21), expressions for $u_{\infty n}$, A_n and B_n can be obtained in terms of λ, $e^{-k_n a}$, u_{en}, θ_{en} and δ_{2n}, where a is the distance separating the injector-plate and actuator-disk. These expressions are shown in the Appendix, in which $u_{\infty n}$, A_n and B_n are related to u_{en}, θ_{en} and δ_{2n} by influence coefficients. The equations stating the dependence of u, v and p on x, r, $u_{\infty n}$, A_n and B_n are also summarized in the Appendix. Using the Appendix, the flow pattern arising from any combination of the disturbing non-uniformities, u_e, θ_e and δ_2, can be assessed. The number of terms required in the summations for u, v and p will depend on the number of Fourier–Bessel harmonics required to form each disturbing non-uniformity.

4. Discussion of solution

4.1. *Assumption of incompressible flow*

The effect of the compressibility of the fluid will become appreciable when the Mach number of the unperturbed flow downstream of the density-change actuator-disk exceeds a value of about 0·3. The ratio of the Mach numbers of the unperturbed flow on either side of the disk is given by

$$\frac{M_2}{M_1} = \frac{U_2}{U_1}\left(\frac{T_1}{T_2}\right)^{\frac{1}{2}} = \lambda^{-\frac{1}{2}},$$

if the fluid is assumed to be a semi-perfect gas, since then $\rho_1 T_1 = \rho_2 T_2$, for small M_1 and M_2. Hence the solution is adequate for

$$\lambda < 10 M_1^2. \tag{22}$$

If the temperature downstream of the density change were 4500 °K, a very high value for flame temperature, then λ would equal 0·07 and the above con-

dition would require $M_1 < 0{\cdot}08$. Combustion reactions in gas mixtures proceed at Mach numbers much less than this value, so that the assumption of incompressible flow is justified for the flow of gas mixtures normally through an actuator-disk at which combustion takes place.

In rocket combustion chambers, the Mach number of the flow when combustion is completed is determined by the ratio of the cross-sectional areas of the combustion chamber and the nozzle throat, where $M = 1$. If this area ratio equals 3 or more then $M_2 < 0{\cdot}3$ and compressibility effects may be neglected.

4.2. *Vorticity change at density-change actuator-disk*

The change in the vorticity of the flow at the disk is given by equation (20) with equations (3) and (16), from which

$$\eta_2 - \eta_1 = U_1 \frac{(1-\lambda)}{\lambda} \frac{\partial u_{a1}}{\partial r}. \tag{23}$$

Hence the vorticity of the flow is changed at the disk by an amount determined by the radial gradient of axial velocity just upstream of the disk and the density ratio across the disk. The vorticity change is zero if the density change is small, and does not depend directly on any small non-uniformity in the density change at the disk, to first order in the perturbations.

Hayes (1957) has studied the general case of rotational compressible flow through a surface of discontinuity in density. Hayes shows that only the component of vorticity tangential to the surface experiences a change as the flow passes through the surface, and that this change is made up of two parts, both of which depend on the ratio of the densities on either side of the surface. One part of the change is proportional to the gradient along the surface of the mass velocity normal to the surface, and this part reduces to equation (23) for the conditions of the problem considered in this paper. The other part varies with the product of the component of velocity tangential to the surface and its gradient in its own direction, which in this paper is $v(\partial v/\partial r)$ and so is zero to first order. This latter part provided a vorticity change at the flame-fronts studied by the authors cited in § 1. In the papers by these authors, the flame speed, which is the velocity of flow normal to and into a stationary flame-front, and the density upstream of the flame, were considered constant, so that the part of the vorticity change which is important in this paper was identically zero.

4.3. *Case of injector-plate and actuator-disk at an infinite distance apart* ($a = \infty$)

If the injector-plate is at an infinite distance from the actuator-disk, then there is some point between them at which the radial velocity approaches zero. Hence the relevant disturbing non-uniformities in this case are upstream vorticity, represented by $u_{\infty 1}$, and non-uniform density change at the disk, δ_2. The upstream vorticity may be caused by either or both of the disturbances u_e and θ_e at the injector-plate, and the expression for the amplitude of the nth harmonic of $u_{\infty 1}$ is, from the Appendix,

$$u_{\infty 1n} = u_{en} + \theta_{en}. \tag{24}$$

The main results of the analysis in this case do not depend on the *form* of radial variation of the disturbances. For with $a = \infty$, so that $\epsilon_n = e^{-k_n a} = 0$, it is seen from the table in the Appendix that $u_{\infty n}$, A_n and B_n are independent of k_n. Therefore at $x = -\infty, x = 0$ and $x = +\infty$, where $e^{k_n x} = 0$, $e^{\pm k_n x} = 1$ and $e^{-k_n x} = 0$ respectively, the amplitude of the velocity perturbation caused by a disturbance consisting of a single harmonic of unit amplitude is the same for all harmonics. Thus the radial *form* of a velocity perturbation is identical at the disk and at an infinite distance upstream and downstream of the disk, even if the disturbance

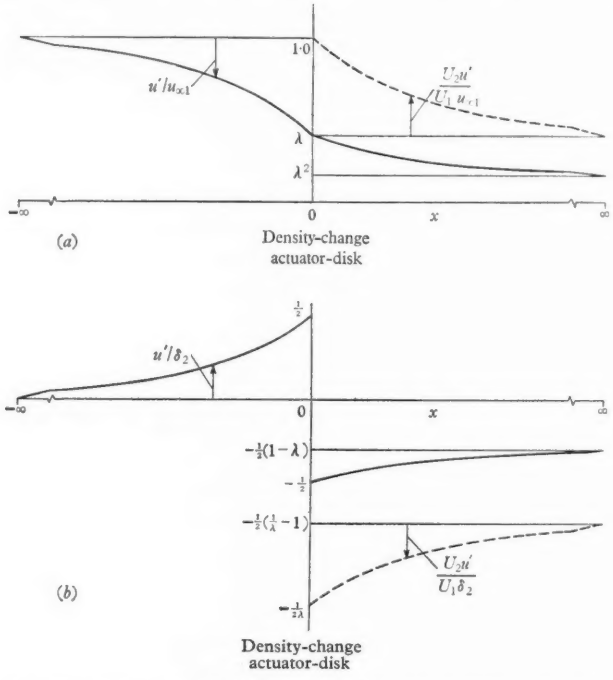

FIGURE 2. Axial velocity perturbations caused when the injector-plate is at an infinite distance upstream of the density-change actuator-disk. The figure is to scale for $\lambda = 0{\cdot}4$. (*a*) ——, $u/u_{\infty 1}$; – – – –, $U_2u/U_1u_{\infty 1}$. (*b*) ——, u/δ_2; – – – –, $U_2u/U_1\delta_2$.

consists of more than one harmonic. For example the amplitude of the nth harmonic of the axial velocity perturbation fraction just upstream of the actuator-disk is, from equation (10),

$$u_{a1n} = u_{\infty 1n} - A_{1n} - B_{1n},$$

which, using the influence coefficients in the Appendix, becomes, with $\epsilon_n = 0$,

$$u_{a1n} = (u_{en} + \theta_{en}) - (1-\lambda)(u_{en} + \theta_{en}) + \tfrac{1}{2}\delta_{2n},$$

and, with equations (24), (8) and (18), this can be summed to give

$$u_{a1} = \lambda u_{\infty 1} + \tfrac{1}{2}\delta_2. \tag{25}$$

The variation of the axial velocity perturbation fraction, expressed as $u/u_{\infty 1}$, and of the perturbation, expressed as $Uu/U_1 u_{\infty 1}$, in the axial, x, direction along a line of constant radius takes the form shown in figure 2, which shows separately the effects of $u_{\infty 1}$, figure 2 (*a*), and δ_2, figure 2 (*b*). The perturbation fraction is indicated by full lines, and the perturbation by full lines upstream of the disk and broken lines downstream. The ordinates of significant points on the curves are shown in terms of the density ratio λ, and the curves are drawn to scale for $\lambda = 0{\cdot}4$. The scale of x is omitted since the various Fourier–Bessel harmonics of a perturbation differ in their manner of variation with x, though the harmonics behave identically at $x = -\infty$, $x = 0$ and $x = +\infty$ as explained above.

At equal distances on either side of the disk the irrotational part of the perturbation Uu' is equal in magnitude and opposite in sign, for either of the disturbances δ_2 and $u_{\infty 1}$. From figure 2 it may be seen that these disturbances cause identical values of Uu' at the disk, and thus everywhere in the flow, for a particular Fourier–Bessel harmonic, if

$$\delta_2 = -2(1-\lambda)\, u_{\infty 1}. \tag{26}$$

Identical values of Uu' lead to identical values of v and p, from equation (12). Hence the radial velocities and pressure perturbations in the flow produced by a disturbance $u_{\infty 1}$ may be identically reproduced by a disturbance δ_2 which satisfies equation (26), and vice versa. The exceptional case $\lambda = 1$ is discussed in § 4.4.4 in connexion with the similar result obtained when a is finite.

From figure 2 (*a*), for which $u_{\infty 1} \neq 0$ and $\delta_2 = 0$, it is seen that a disturbing non-uniformity of axial velocity $u_{\infty 1}$ is severely attenuated by density decrease, since $u_{\infty 2} = \lambda^2 u_{\infty 1}$; the axial velocity perturbation is also attenuated by the ratio λ. The axial variation of the perturbation is seen to be of very simple form, the perturbation just upstream of the disk being equal to that far downstream, and vice versa.

From figure 2 (*b*), for which $u_{\infty 1} = 0$ and $\delta_2 \neq 0$, it is seen that a disturbance δ_2, representing a non-uniform density change at the disk, causes an irrotational upstream flow, $u_{\infty 1} = 0$, to become rotational downstream of the disk. The magnitude of the rotational part of the downstream axial velocity perturbation fraction or non-uniformity $u_{\infty 2}$ increases as the density ratio λ decreases, and approaches the maximum value of $(\frac{1}{2}\delta_2)$ as the downstream density approaches zero, $\lambda \to 0$.

4.4. *General case*

4.4.1. *The effect on the results of the radial form of a disturbance*

The distance a separating the injector-plate and the density-change actuator-disk is an important parameter in the problem, and appears in the results of the analysis in the quantity $\epsilon_n = e^{-k_n a}$. Hence the effect of a on the velocity perturbations caused by a disturbance consisting of a particular Fourier–Bessel harmonic depends on the number n of the harmonic. If a disturbance consists of more than one harmonic, then, in general, the radial form of a resulting velocity perturbation will differ at the injector-plate, the disk, and infinity downstream, in contrast to the result obtained in the special case $a = \infty$, § 4.3. The

factor $k_n a$, which determines the effect of a on the results for the nth harmonic of a disturbance, is approximately equal to π times the ratio of a and the radial distance between adjacent zeros of the radial velocity perturbation resulting from that harmonic. This rough equality becomes more exact with increase of the value of $(n-1)$, the number of zeros of the radial velocity perturbation between the tube axis and the tube wall.

The effect on the results of a being finite rather than infinite is greatest for the primary disturbance harmonic, $n = 1$, so that in the following discussion the disturbances are considered to consist of this harmonic alone. The results for a disturbance consisting of the nth harmonic alone can be obtained from those for the primary harmonic simply by multiplying the values of a by the ratio (k_1/k_n). The flows resulting from each disturbance acting singly are discussed in the following sections.

4.4.2. *Flow caused by non-uniform axial velocity at the injector-plate (disturbance u_e)*

The variation of (u/u_e) and (Uu/U_1u_e) with x is shown in figure 3 for values of a of 0, $\frac{1}{2}\beta$, β and ∞, where $\beta = k_1^{-1}\ln 2$. The arrangement of this figure is similar to that of figure 2 (*a*) and the curves from figure 2 (*a*), for $a = \infty$, are repeated on it. The variation of the axial velocity non-uniformity (u'/u_e) is shown by the full lines, and it is seen that as a is reduced so is the attenuation $\{1-(u_{\infty 2}/u_e)\}$ of the disturbance by the density decrease. The attenuation increases as the density ratio λ is decreased, for all values of a except zero. In the limiting case of $a = 0$, the density change occurs immediately after injection and the flow is invariant along the tube. The axial velocity perturbation (Uu/U_1u_e) is shown on figure 3 by full lines upstream of the disk and broken lines downstream. It is seen that the axial velocity perturbation is greater at infinity downstream than at the injector-plate for $a < \beta$, and less for $a > \beta$.

The variation with a of the upstream value of the rotational part of the axial velocity perturbation fraction, $u_{\infty 1}$, is also indicated on figure 3. It is seen that $u_{\infty 1}$ increases as a decreases; therefore, since u is nowhere greater than u_e, $u_1' = (u_1 - u_{\infty 1})$ also increases in magnitude as a decreases. Hence, from equation (13), it is seen that the pressure perturbations upstream of the disk increase in magnitude as a decreases. The radial pressure variation set up at the injector plate by the disturbance is of particular interest, since this variation may alter the uniformity of injection, and thus the disturbance, if the rate of injection of fluid at the plate is pressure controlled, as in liquid rockets. The pressure perturbation fraction at the injector-plate, p_e, is shown on figure 4, plotted against a, for various values of λ. It is seen that for $a < 0{\cdot}1$ and $\lambda < 0{\cdot}2$, conditions which may occur in liquid rockets, then $p_e \gg u_e$. Hence under these conditions a radial pressure variation of many times the inlet dynamic pressure $(\frac{1}{2}\rho_1 U_1^2)$ may be obtained at the injector-plate, even if u_e is small.

The maximum value of the radial velocity occurs at the disk, since u' defines $\partial v/\partial x$, equation (12), and is of constant sign on either side of the disk, changing sign at the disk (see figure 3). The variation of v_{a1}, the radial velocity at the disk as a fraction of U_1, with a and λ is shown in figure 5. Because of the difference in the radial forms of v_{a1} and u_e, the maximum values $\hat{v}_{a1}$ and $\hat{u}_e$ are used for com-

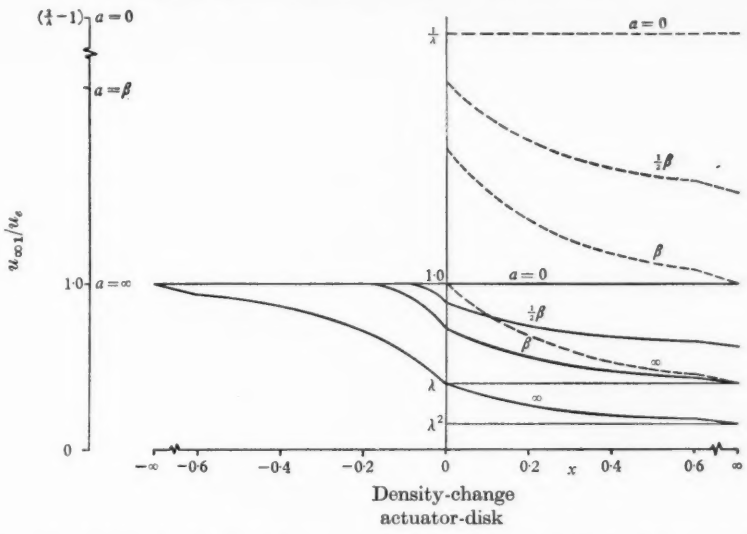

FIGURE 3. Axial velocity perturbations caused by a disturbance u_e of primary form. $\beta = k_1^{-1} \ln 2 = 0{\cdot}181$. The figure is to scale for $\lambda = 0{\cdot}4$. ——, u/u_e; – – –, $Uu/U_1 u_e$.

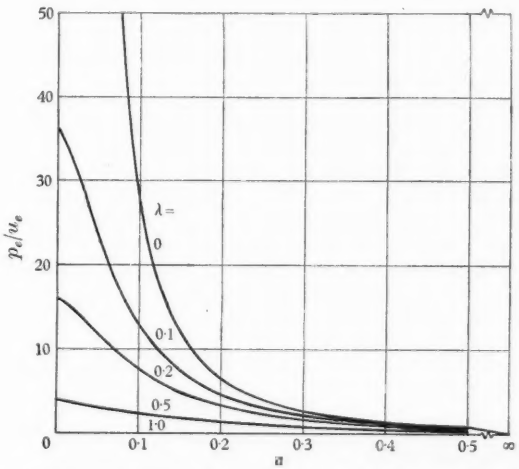

FIGURE 4. Pressure-perturbation fraction at the injector-plate caused by a disturbance u_e of primary form.

parison. In the analysis, it is assumed that $v \ll 1$. From figure 5 it is apparent that this assumption is not valid for $\lambda \ll 0{\cdot}1$ and $0 < a < 0{\cdot}1$, since under these conditions $v_{a1} \gg u_e$. However, this range of conditions is more restricted than those stated above for which $p_e \gg u_e$, so that appreciable radial pressure variations may be caused at the injector-plate, though the radial velocity is everywhere small.

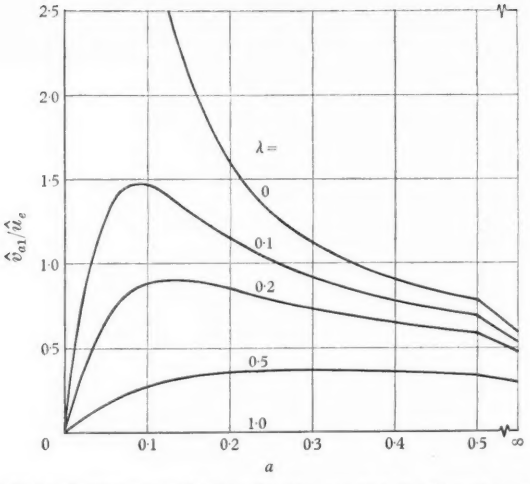

FIGURE 5. Radial velocity perturbation fraction at the density-change actuator-disk caused by a disturbance u_e of primary form. Maximum values are compared.

4.4.3. *Flow caused by a curved injector-plate (disturbance θ_e)*

In the absence of density change a curved injector-plate is seen, from equation (24), to cause a uniform flow to develop a non-uniformity of axial velocity with the same amplitude as θ_e. This non-uniformity will be attenuated in the manner described in § 4.3 by a density decrease occurring at a plane far downstream of the injector-plate. The change in this attenuation when the density decrease takes place at a finite distance downstream of the injector-plate is shown by figure 6, in which the variation with a of u_{x2}, the non-uniformity of axial velocity far downstream of the disk, is shown for various values of λ. The attenuation $\{1-(\hat{u}_{x2}/\hat{\theta}_e)\}$ of the disturbance is seen to decrease with a except near $a = 0$, and to increase as the density ratio λ is reduced, for all values of a.

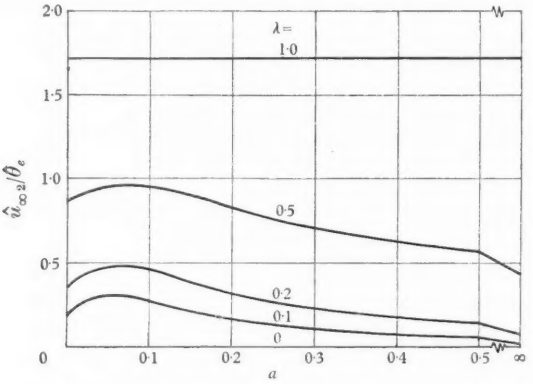

FIGURE 6. Non-uniformity of axial velocity far downstream of the density-change actuator-disk, caused by a disturbance θ_e of primary form. Maximum values are compared.

It may be shown that the velocity perturbation fractions u and v are everywhere of the same order of magnitude as the disturbance θ_e for all values of a and λ. However, an appreciable radial pressure variation may be set up at the injector-plate, as shown by figure 7 where p_e is plotted against a for various values of λ. It is seen that a radial pressure variation of many times the inlet dynamic pressure may be obtained at the injector-plate for $\lambda < 0{\cdot}1$ and $0 < a < 0{\cdot}1$, even if θ_e is small.

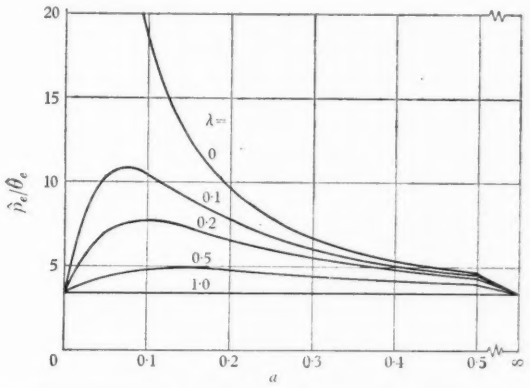

FIGURE 7. Pressure-perturbation fraction at the injector-plate caused by a disturbance θ_e of primary form. Maximum values are compared.

4.4.4. *Flow caused by a non-uniform density change (disturbance δ_2)*

It is apparent from the table of influence coefficients in the Appendix that the values of A_n and B_n, and therefore of the irrotational part of a velocity perturbation, caused by a disturbance δ_2 are identical with those caused by a disturbance u_e, if

$$\delta_2 = -2(1-\lambda)\,u_e. \tag{27}$$

Hence, in view of equation (12), the discussion in § 4.4.2 of the radial velocities and pressure perturbations caused by a disturbance u_e applies also to the flow caused by a disturbance δ_2, except when $\lambda = 1$. The exception arises because if there is no density change in the unperturbed flow, the disturbance u_e is invariant along the tube, whereas the disturbance δ_2 necessarily sets up a discontinuity in u at the disk (see equation (17)). However, the radial velocities and pressure perturbations due to δ_2 are small when $\lambda = 1$, so that the conditions for an appreciable pressure variation to be set up at the injector-plate by δ_2 are as stated for u_e. For density change caused by combustion it is possible that such a pressure variation may alter the non-uniformity of the mixture ratio of the injected fluid and thus cause the non-uniformity of the density change to grow or diminish.

The non-uniformity of axial velocity far downstream, $u_{\infty 2}$, caused by this disturbance is shown on figure 8 plotted against a for various values of λ. It is seen that if there is no density change in the unperturbed flow, $\lambda = 1$, then $u_{\infty 2}$ varies from zero when $a = \infty$ to the value of $-\delta_2$ when $a = 0$. The effect of density decrease is to amplify this non-uniformity for $a > \beta$ and attenuate it for $0 < a < \beta$,

where $\beta = k_1^{-1} \ln 2 = 0{\cdot}181$. Thus $u_{\infty 2}$ approaches the value of $-\frac{1}{2}\delta_2$ for all values of a as λ approaches zero.

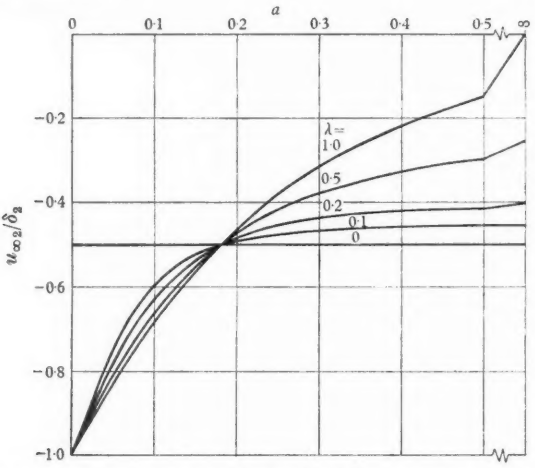

FIGURE 8. Non-uniformity of axial velocity far downstream of the density-change actuator-disk, caused by a disturbance δ_2 of primary form.

The authors wish to acknowledge the assistance of Mrs P. Camm in carrying out the calculations for the figures.

REFERENCES

BALL, G. A. 1951 *Rep. Dep. Engng Sci. and Appl. Phys., Harvard University.*

EMMONS, H. W., BALL, G. A. & MAIER, A. D. 1952 Development and use of a combustion tunnel. *Final Summary Rep., Div. Appl. Sci., Harvard University.*

HAYES, W. D. 1957 *J. Fluid Mech.* **2**, 595.

LONG, R. R. 1953 *Tellus*, **5**, 42.

SCURLOCK, A. C. 1948 *Meteor Report*, no. 19, *M.I.T.*

TSIEN, H. S. 1951 *J. Appl. Mech.* **18**, 188.

Appendix: summary of solution

Disturbing non-uniformities

$$u_e = \sum_{n=1}^{\infty} u_{en} J_0(k_n r), \quad \theta_e = \sum_{n=1}^{\infty} \theta_{en} J_1(k_n r)$$

and

$$\delta_2 = \sum_{n=1}^{\infty} \delta_{2n} J_0(k_n r).$$

Resulting perturbation fractions

$$u_j = \sum_{n=1}^{\infty} u_{jn} J_0(k_n r), \quad v_j = \sum_{n=1}^{\infty} v_{jn} J_1(k_n r) \quad \text{and} \quad p_j = -2u'_j,$$

with

$$u_{jn} = u_{\infty jn} + u'_{jn}, \quad u'_{jn} = -(A_{jn} e^{k_n x} + B_{jn} e^{-k_n x}),$$

$$v_{jn} = A_{jn} e^{k_n x} - B_{jn} e^{-k_n x},$$

where

$$j = 1 \text{ for } -a \leqslant x \leqslant 0, \quad j = 2 \text{ for } 0 \leqslant x \leqslant \infty.$$

Influence coefficients

	u_{en}/E	θ_{en}/E	δ_{2n}/E
$u_{\infty 1n}$	$\dfrac{1}{(1-\lambda)}+\epsilon_n^2$	$\dfrac{1}{(1-\lambda)}-\epsilon_n^2$	$-\dfrac{\epsilon_n}{(1-\lambda)}$
$u_{\infty 2n}$	$\lambda\left\{\dfrac{\lambda}{(1-\lambda)}+\epsilon_n^2\right\}$	$\lambda\left\{\dfrac{\lambda}{(1-\lambda)}+\epsilon_n-\epsilon_n^2\right\}$	$-\dfrac{1}{2}\left\{1-2\,\dfrac{(1-2\lambda)}{(1-\lambda)}\,\epsilon_n+\epsilon_n^2\right\}$
A_{1n}	1	$1-\epsilon_n$	$-\dfrac{1}{2(1-\lambda)}$
B_{1n}	ϵ_n^2	$\dfrac{\epsilon_n}{(1-\lambda)}-\epsilon_n^2$	$-\dfrac{\epsilon_n^2}{2(1-\lambda)}$
A_{2n}	0	0	0
B_{2n}	$-\lambda(1-\epsilon_n^2)$	$-\lambda\left\{1-\dfrac{(2-\lambda)}{(1-\lambda)}\,\epsilon_n+\epsilon_n^2\right\}$	$\dfrac{\lambda(1-\epsilon_n^2)}{2(1-\lambda)}$

Here k_n are the roots of $J_1(k_n)=0$, thus $k_1=3{\cdot}832$, $k_2=7{\cdot}016$, $k_3=10{\cdot}174$, etc.,

$$\lambda=\rho_2/\rho_1, \quad \epsilon_n=e^{-k_n a} \quad \text{and} \quad E=\{[1/(1-\lambda)]-2\epsilon_n+\epsilon_n^2\}.$$

On corner eddies in plane inviscid shear flow

By L. E. FRAENKEL

Aeronautics Department, Imperial College, London

(Received 11 March 1961)

Local solutions are found for the inviscid shear flow past an acute corner (of included angle $\leqslant \frac{1}{2}\pi$ on the side of the fluid) on an otherwise arbitrary boundary. Unlike irrotational 'corner flows', these solutions are determinate locally, provided that the vorticity is known. Under certain circumstances the existence of a corner eddy may be inferred.

1. Introduction

Yih (1959) has shown that a certain inviscid shear flow in a channel (figure 1*a*) includes closed streamlines. The same phenomenon is seen in the shear flow past a semicircular projection on a plane wall (figure 1*b*: details of this solution will be given in § 4).† The purpose of this paper is to point out that such eddies may always be expected under certain conditions, which will be described, and to give simple expressions for the stream function in the immediate neighbourhood of the corner.

We are concerned throughout with plane, inviscid, incompressible shear flow, and mainly with the case of constant vorticity. Then, writing

$$\psi = \int (u\,dy - v\,dx), \quad z \doteq x + iy = re^{i\theta},$$

for the stream function and coordinates, we have

$$\nabla^2\psi = \text{const.} = \omega > 0, \quad \text{say.} \tag{1}$$

We suppose that at some point the tangents to a solid boundary (or to some other streamline) make an angle $\beta \leqslant \frac{1}{2}\pi$, measured on the side of the fluid. Near the corner the fluid is sufficiently stagnant for its motion to be determined by the rotation, so that (for $\omega > 0$) an observer moving with the fluid near the corner keeps the boundary on his *left*. We shall see that the dominant term in the expression for the velocity near the corner is independent of the boundary shape away from the corner, and that this term dominates no matter what irrotational flow past the boundary is added. If now the main flow further out from the corner is such that an observer moving with it keeps the boundary on his *right*, a corner eddy occurs. In this case the local solution near the corner implies the existence of an eddy, but of course the size of the eddy depends on the flow as a whole.

† Despite the apparent similarity of figure 1*b* to figure 1 of Yih (1960) the stream functions in question are quite different.

Flows with constant vorticity are easy to treat analytically, and viscous flows bounded by closed streamlines are known to have constant vorticity in the limit of infinite Reynolds number (Batchelor 1956). Accordingly the behaviour of solutions of (1) near acute corners will be studied in some detail.

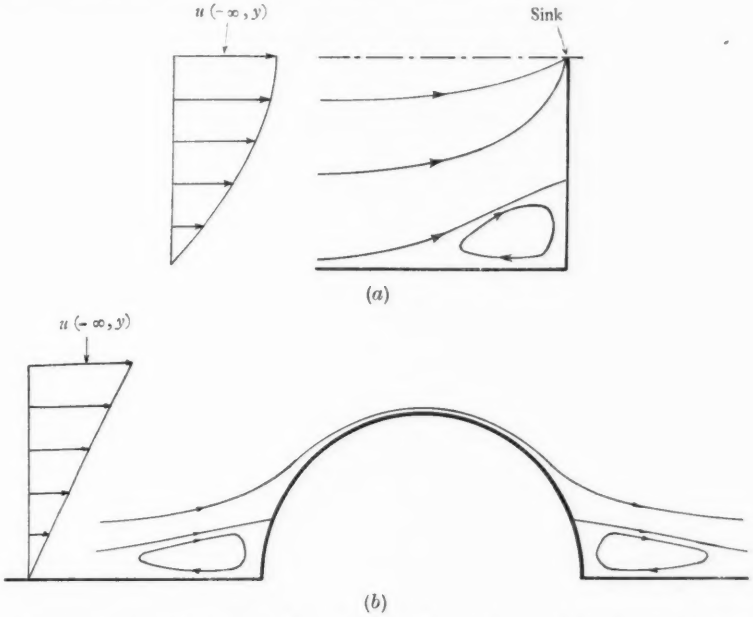

FIGURE 1. (*a*) Yih's channel flow, (*b*) shear flow past a semicircular projection.

We also expect our results to hold for the more general inviscid shear flow problem

$$\nabla^2\psi = f(\psi), \tag{2}$$

for if a corner occurs on the streamline $\psi = \psi_0$, such that $f(\psi_0) \neq 0$, it is presumably legitimate to write $f(\psi) \sim f(\psi_0)$ for the purpose of examining the flow very near the corner (where $\nabla\psi = 0$). In the Appendix it is shown that Yih's solution (of an equation of the type (2)) does in fact have the local behaviour predicted by this procedure, but no general proof of the occurrence of our corner flows in solutions of (2) will be given.

Dean (1944) has found flows containing eddies in the lee of a peak in certain solutions of the Stokes slow-motion equations; such eddies are a different species from those considered here.

2. Corner flows with constant vorticity

We seek a solution of (1) satisfying $\psi = \text{const.}$ on $\theta = \pm\frac{1}{2}\beta$ ($\beta < \frac{1}{2}\pi$). A particular integral is given by $\psi = \frac{1}{4}\omega r^2$, and the harmonic, complementary function required by the boundary condition may be found by inspection; thus

$$\psi_1 = \tfrac{1}{4}\omega r^2\left(1 - \frac{\cos 2\theta}{\cos\beta}\right) \quad (\beta < \tfrac{1}{2}\pi). \tag{3}$$

The streamlines are the hyperbolae

$$\frac{x^2}{\cos^2(\frac{1}{2}\beta)} - \frac{y^2}{\sin^2(\frac{1}{2}\beta)} = -\frac{8\psi_1 \cos\beta}{\omega \sin^2\beta},$$

and are shown in figure 2*a*: an observer moving with the fluid in the acute angles keeps the boundary on his left, as was stated above. The solution may be interpreted as a corner flow or as a stagnation-point flow; that is, either AOB or AOC

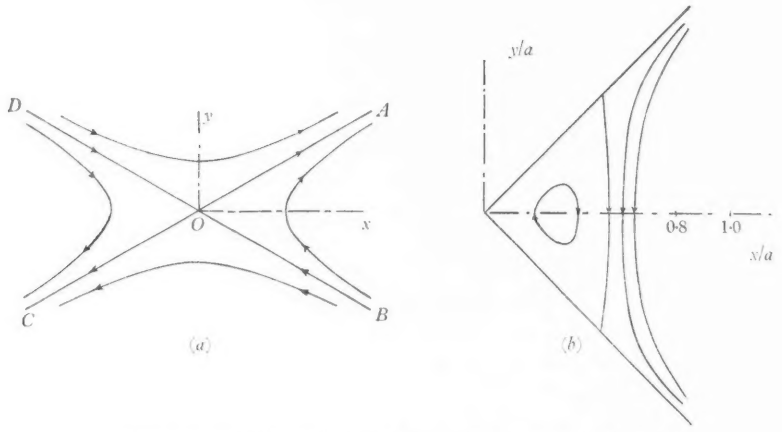

FIGURE 2. Rotational corner flows. (*a*) $\beta < \frac{1}{2}\pi$; (*b*) $\beta = \frac{1}{2}\pi$.

could be a solid boundary, or O could be a stagnation point in the body of the fluid. The solution (3) is not unique for the region $|\theta| \leqslant \frac{1}{2}\beta$, since conditions have not been specified on a closed boundary, and an irrotational flow

$$\psi_2 = Cr^{\pi/\beta} \cos\frac{\pi\theta}{\beta}, \tag{4}$$

where C is arbitrary, can be added without violating the boundary condition. However, we observe that, since $\pi/\beta > 2$, ψ_1 *dominates for sufficiently small values of* r.

The solution (3) becomes infinite for $\beta = \frac{1}{2}\pi$, and we therefore form a linear combination of ψ_1 and ψ_2 which remains finite as $\beta \to \frac{1}{2}\pi$. Writing

$$\psi_3 = \tfrac{1}{4}\omega\left(r^2 + \lim_{\beta\to\frac{1}{2}\pi} \mathscr{R}\frac{z^{\pi/\beta} - z^2}{\cos\beta}\right),$$

we obtain

$$\psi_3 = \omega\pi^{-1}(\tfrac{1}{4}\pi r^2 + r^2 \log r \cos 2\theta - r^2\theta \sin 2\theta) \quad (\beta = \tfrac{1}{2}\pi).$$

Again we may add an irrotational flow, ψ_2, with $\pi/\beta = 2$; with $C = -\omega \log a/\pi$, where a is an arbitrary length, we have

$$\psi_4 = \omega\pi^{-1}\{\tfrac{1}{4}\pi r^2 + r^2 \log(r/a) \cos 2\theta - r^2\theta \sin 2\theta\} \quad (\beta = \tfrac{1}{2}\pi). \tag{5}$$

The $r^2 \log r$ term dominates for sufficiently small values of r.

The streamlines are shown in figure 2*b*: they are not drawn for $|\theta| > \frac{1}{4}\pi$ because $r^{-1}\partial\psi_3/\partial\theta$ is discontinuous across the negative real axis (if we choose $|\theta| < \pi$), so that the flow is not a real one there.

Now let ψ be a solution of (1) for any field with a streamline which makes an acute angle at some point O, and take coordinates with origin at O and with the positive x-axis bisecting the angle. The foregoing considerations make it plausible that ψ_1 or the logarithmic part of ψ_3 provide the dominant term (apart from a constant) in the expansion of ψ about 0, in powers and logarithms of r. In the next section we shall prove this assertion.

3. The flow near acute corners on arbitrary boundaries

Consider a fluid domain $\mathscr{D}$ whose boundary $\mathscr{B}$ is a Jordan curve with a corner at O of included angle $\beta \leqslant \frac{1}{2}\pi$. Various types of domain are of interest (figure 3): here we consider only the case (figure 3*a*) in which $\mathscr{D}$ is semi-infinite and simply

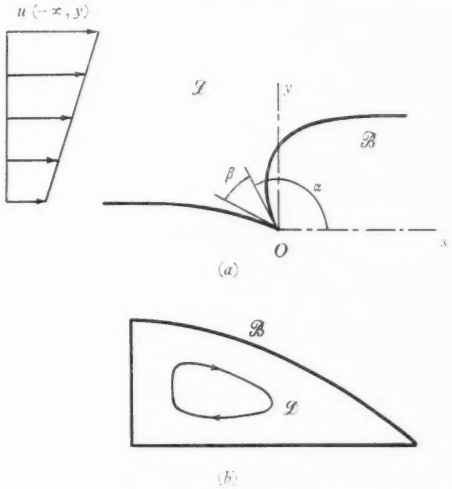

FIGURE 3. Two types of fluid domain to which the present results apply locally.

connected, since for other cases the proof only requires changes in points of detail. The domain can be mapped conformally on to the interior of a circle (Carathéodory 1932; Courant 1950) or, alternatively, on to an upper half-plane. Let

$$z = z(\zeta) = z(\xi + i\eta)$$

be one of the latter transformations, such that the corner $z = 0$ maps on to $\zeta = 0$, and $\mathscr{D}$ on to $\eta > 0$. Let $\mathscr{B}$ be so restricted that we may write, after a suitable choice of constants,

$$\left.\begin{aligned} \text{for } |\zeta| \leqslant \delta, \quad z &= e^{i\alpha}\zeta^b + o(\zeta^b) \quad (0 < b = \beta/\pi \leqslant \tfrac{1}{2}), \\ y(\xi, 0) &= |\xi|^b \sin(\alpha+\beta) + O(|\xi|^c) \quad (\xi \leqslant 0,\ c > b) \\ &= \xi^b \sin\alpha + O(\xi^c) \quad (\xi \geqslant 0). \end{aligned}\right\} \tag{6}$$

A sufficient (but by no means necessary) condition for this is that the two arcs of $\mathscr{B}$ meeting at O have bounded curvature in $-\delta \leqslant \xi \leqslant 0$ and $0 \leqslant \xi \leqslant \delta$, respectively; for then we may first apply the Schwarz–Christoffel mapping appropriate to the tangents at the corner, and then the theorem in § 152 of Carathéodory (1932). We further restrict $\mathscr{B}$ to have y finite and $dy/dx \sim O(x^{-2})$ for $|x| \to \infty$: then for $|\zeta| \to \infty$,

$$z = k_1\zeta + k_2 \log \zeta + k_3 + O(\zeta^{-1}) \quad (k_1, k_2 \text{ real}).$$

Our problem is to solve (1) with the boundary conditions

$$\left.\begin{aligned} \psi &= \text{const. on } \mathscr{B} \\ \frac{\partial \psi}{\partial x} \to 0, \quad \frac{\partial \psi}{\partial y} - \omega y - U \to 0, \quad &\text{as} \quad |z| \to \infty \text{ in } \mathscr{D}. \end{aligned}\right\} \tag{7}$$

The solution is

$$\psi = \tfrac{1}{2}\omega y^2 + U k_1 \eta + \psi_I, \tag{8}$$

where ψ_I is a harmonic function required by the boundary condition on $\mathscr{B}$. Representing it by sources on $\eta = 0$, we have

$$\begin{aligned} \psi_I(\xi_1, \eta_1) = \mathscr{I} w_I(\zeta_1) &= \mathscr{I} \frac{\omega}{2\pi} \int_{-\infty}^{\infty} \log(\zeta_1 - \xi) \frac{\partial}{\partial \xi} \{y^2(\xi, 0)\}\, d\xi \\ &= \mathscr{I} \frac{\omega}{2\pi} \left\{ \int_{-\infty}^{\xi_A} + \int_{\xi_B}^{\infty} \log(\zeta_1 - \xi) \frac{\partial}{\partial \xi} \{y^2(\xi, 0)\}\, d\xi \right. \\ &\qquad \left. + [\log(\zeta_1 - \xi)\, y^2(\xi, 0)]_{\xi_A}^{\xi_B} + \int_{\xi_A}^{\xi_B} \frac{y^2(\xi, 0)}{\zeta_1 - \xi} d\xi \right\}. \end{aligned} \tag{9}$$

Here A and B are points on $\mathscr{B}$ such that $\partial y/\partial \xi$ is continuous for $\xi \leqslant \xi_A$ and $\xi \geqslant \xi_B$ [and $O(\xi^{-2})$ for $|\xi| \to \infty$], and we confine ζ_1 to the domain $\mathscr{D}_1$: $|\zeta_1| \leqslant \epsilon$, $0 \leqslant \arg \zeta_1 \leqslant \pi$, where $\delta > \epsilon > 0$. For $|\xi| > \delta$, the integrands in (9) are continuous functions of ξ, uniformly convergent for $|\xi| \to \infty$, and regular functions of ζ_1. Hence, if $F(\zeta_1)$ denotes a function which is regular in $\mathscr{D}_1$,

$$\begin{aligned} w_I(\zeta_1) &= \frac{\omega}{2\pi} \int_{-\delta}^{\delta} \frac{y^2(\xi, 0)}{\zeta_1 - \xi} d\xi + F(\zeta_1) \\ &= \frac{\omega}{2\pi} \int_0^{\delta} \left\{ \frac{\lambda^{2b} \sin^2(\alpha + \beta) + O(\lambda^{b+c})}{\zeta_1 + \lambda} + \frac{\lambda^{2b} \sin^2 \alpha + O(\lambda^{b+c})}{\zeta_1 - \lambda} \right\} d\lambda + F(\zeta_1). \end{aligned}$$

Now, by the contour integration associated with the beta function,

$$\begin{aligned} \int_0^{\delta} \frac{\lambda^a}{\zeta \pm \lambda} d\lambda &= \mp \frac{\pi \zeta^a}{\sin \pi a} \exp\{i\pi a(-\tfrac{1}{2} \pm \tfrac{1}{2})\} \pm \delta^a \sum_{n=0}^{\infty} \frac{1}{a - n} \left(\mp \frac{\zeta}{\delta} \right)^n \quad (a \neq \text{integer}) \\ &= \zeta \log \zeta - (\zeta \pm \delta) \log(\zeta \pm \delta) \pm \delta \quad (a = 1). \end{aligned}$$

Hence

$$\left| \mathscr{I} \int_0^{\delta} \frac{O(\lambda^{b+c})}{\zeta \pm \lambda} d\lambda \right| < M \int_0^{\delta} \frac{\lambda^{b+c} \eta}{(\xi \pm \lambda)^2 + \eta^2} d\lambda = O(|\zeta|^{b+c} + |\zeta|) \quad (b + c \neq 1).$$

Omitting the trivial constant $\mathscr{I} F(0)$, we have

$$\begin{aligned} \psi_I(\xi, \eta) &= \mathscr{I} \tfrac{1}{2}\omega \frac{\zeta^{2b}}{\sin 2\beta} \{-\sin^2(\alpha + \beta) + \sin^2 \alpha\, e^{-2i\beta}\} + o(|\zeta|^{2b}) \quad (0 < b < \tfrac{1}{2}) \\ &= \mathscr{I} \frac{\omega}{2\pi} \zeta \log \zeta + O(|\zeta|) \quad (b = \tfrac{1}{2}). \end{aligned}$$

Transforming to z, writing $z = r\exp\{i(\tau+\alpha+\frac{1}{2}\beta)\}$, adding the first two terms of (8), and simplifying, we obtain

$$\psi = \tfrac{1}{4}\omega r^2\left(1-\frac{\cos 2\tau}{\cos\beta}\right)+o(r^2) \quad (0<b<\tfrac{1}{2}), \tag{10}$$

$$= \omega\pi^{-1}r^2\log r\cos 2\tau+O(r^2) \quad (b=\tfrac{1}{2}), \tag{11}$$

which is the required result. The sign of ψ yields the local flow directions described in §§ 1 and 2.

4. An example

Consider the flow past a semicircular projection, $r = 1$, $0 \leqslant \theta \leqslant \pi$, on a plane wall, $\theta = 0, \pi$, $r \geqslant 1$. The Joukowski transformation

$$\zeta = z+z^{-1} \quad (\zeta=\xi+i\eta)$$

maps the fluid domain on to $\eta > 0$ and the semicircle on to $\eta = 0$, $|\xi| \leqslant 2$. For the differential equation (1) and the boundary conditions (7), we have

$$\psi = \tfrac{1}{2}\omega y^2+U(r-r^{-1})\sin\theta+\psi_I, \tag{12}$$

where $$\psi_I = \mathscr{I}\frac{\omega}{2\pi}\int_{-2}^{2} y^2(\xi^*,0)\frac{1}{\zeta-\xi^*}d\xi^* \quad \text{and} \quad y^2(\xi,0) = 1-\tfrac{1}{4}\xi^2.$$

Hence $$\psi_I = \mathscr{I}\frac{\omega}{2\pi}\left\{\tfrac{1}{4}(\zeta^2-4)\log\frac{\zeta-2}{\zeta+2}+\zeta\right\}$$

$$= \mathscr{I}\frac{\omega}{2\pi}\left\{\frac{1}{2}\left(z-\frac{1}{z}\right)^2\log\frac{z-1}{z+1}+z+\frac{1}{z}\right\}. \tag{13}$$

The case shown in figure 1*b* is for $U = 0$; adding an irrotational flow with $U > 0$ reduces the size of the eddies, and introduces stagnation points on

$$\theta = 0, \pi, \quad 1 < r < \infty.$$

I am indebted to Miss M. Lawson for computing the streamlines of figures 1*b* and 2*b*.

Appendix: Yih's solution

Yih (1959) has considered the flow in a channel $-1 \leqslant y \leqslant 1$, $x \leqslant 0$, in which there is a sink at the origin and

$$u \to \cos\tfrac{1}{2}\pi y \quad \text{for} \quad x \to -\infty,$$

so that $$\nabla^2\psi = -\tfrac{1}{4}\pi^2\psi.$$

He gives the solution

$$\psi = \frac{2}{\pi}\sin\tfrac{1}{2}\pi y+\frac{4}{\pi^2}\sum_{n=1}^{\infty}A_n(x,y),$$

where $$A_n(x,y) = \frac{1}{n}\left\{1+\frac{(-1)^n}{4n^2-1}\right\}\exp\{(n^2-\tfrac{1}{4})^{\frac{1}{2}}\pi x\}\sin n\pi y.$$

We sum a series whose terms are asymptotically equal to A_n. For $n \to \infty$,

$$A_n(x,y) = e^{n\pi x} \sin n\pi y \left\{ \frac{1}{n} - \frac{\pi x}{8}\frac{1}{n^2} + \left(\frac{\pi^2 x^2}{128} + \frac{(-1)^n}{4} \right) \frac{1}{n^3} + O(n^{-4}) \right\}.$$

With $$e^{\pi z} = t, \quad e^{n\pi x} \sin n\pi y = \mathscr{I} t^n,$$

we have $$\sum_{n=1}^{\infty} \frac{(\pm t)^n}{n} = -\log(1 \mp t) \quad (|t| \leqslant 1, t \neq \pm 1),$$

and related series can be 'summed' by integrating both sides from 0 to t. Hence

$$\begin{aligned} \mathscr{I}\left[t + \left(1 - \frac{\pi x}{8}\right)\frac{t^2}{2} + \sum_{n=3}^{\infty} t^n \left\{ \frac{1}{n} - \frac{\pi x}{8}\frac{1}{n(n-1)} + \left(\frac{\pi x}{8} + \frac{\pi^2 x^2}{128} + \frac{(-1)^n}{4} \right) \frac{1}{n(n-1)(n-2)} \right\} \right] \\ = \mathscr{I}\left[-\log(1-t) - \tfrac{1}{8}\pi x \{(1-t)\log(1-t) + t\} \right. \\ + (\tfrac{1}{8}\pi x + \tfrac{1}{128}\pi^2 x^2) \{ -\tfrac{1}{2}(1-t)^2 \log(1-t) - \tfrac{1}{2}t + \tfrac{3}{4}t^2 \} \\ \left. + \tfrac{1}{4}\{ -\tfrac{1}{2}(1+t)^2 \log(1+t) + \tfrac{1}{2}t + \tfrac{3}{4}t^2 \} \right] \\ = g(x,y), \quad \text{say.} \end{aligned}$$

The function $\psi - (4/\pi^2)g$ has derivatives with respect to x and y up to the second order, for all $x \leqslant 0$ and all y, since the terms of its expansion are $O(t^n n^{-4})$ for $n \to \infty$, with $|t| \leqslant 1$. Hence any singularities of ψ leading to infinite values of ψ or of its first and second partial derivatives must also be present in $(4/\pi^2)g$. Near $x = 0$, $y = -1$, with

$$z + i = z^*, \quad t = e^{\pi z} = -1 - \pi z^* + O(z^{*2}),$$

the local singularity of ψ is therefore given by the $(1+t)^2 \log(1+t)$ term of g. Since $z^* = 0$ is a stagnation point, we have

$$\psi = -2/\pi - \mathscr{I} \tfrac{1}{2} z^{*2} \log z^* + O(|z^*|^2).$$

This agrees with (11), for $\omega = \frac{1}{2}\pi$ on the streamline in question.

REFERENCES

Batchelor, G. K. 1956 *J. Fluid Mech.* **1**, 117.

Carathéodory, C. 1932 *Conformal Representation.* Cambridge University Press.

Courant, R. 1950 *Dirichlet's Principle.* New York: Interscience.

Dean, W. R. 1944 *Proc. Camb. Phil. Soc.* **40**, 214.

Yih, C.-S. 1959 *J. Fluid Mech.* **5**, 36.

Yih, C.-S. 1960 *J. Fluid Mech.* **9**, 161.

The reactant concentration spectrum in turbulent mixing with a first-order reaction

By STANLEY CORRSIN
Department of Mechanics, The Johns Hopkins University

(Received 14 January 1961)

The power spectrum of a passive scalar contaminant undergoing a first-order chemical reaction and isotropic turbulent mixing is deduced for three different spectral ranges: (i) the inertial-convective range; (ii) the viscous-convective and viscous-diffusive ranges for very large Schmidt number; (iii) the inertial-diffusive range for very small Schmidt number. The analysis is restricted to stationary, locally isotropic fields, and to systems so dilute that the heat of reaction has no effect on the reaction rate.

Introduction

A clarification and extension of the stationary, locally isotropic, turbulent mixing problem has recently been given by Batchelor (1959), and Batchelor, Howells & Townsend (1959). After preserving the Obukhov (1949)–Corrsin (1951) spectral result,

$$G(k) \sim \epsilon_\theta \epsilon^{-\frac{1}{3}} k^{-\frac{5}{3}}, \tag{1}$$

with proportionality constant of order one, for the inertial-convective wave-number range, Batchelor focused attention on fluid + contaminant fields with very large 'Schmidt number' or 'Prandtl number', $\nu/\eta \gg 1$. ν is the kinematic viscosity, η is the diffusivity, k is the wave-number, ϵ is the turbulent energy-dissipation rate, ϵ_θ is the corresponding scalar contaminant field property, the rate of destruction of $\overline{\theta^2}$ by diffusion.

He pointed out that for $\nu/\eta \gg 1$ and large Reynolds number, there will be a viscous-convective wave-number range,

$$\left(\frac{\epsilon}{\nu^3}\right)^{\frac{1}{4}} \ll k \ll \left(\frac{\epsilon}{\nu\eta^2}\right)^{\frac{1}{4}}, \tag{2}$$

in which the velocity spectrum is strongly affected by viscous forces, while the scalar field spectral transfer is predominantly convective. His analysis for $k \gg (\epsilon/\nu^3)^{\frac{1}{4}}$ yielded

$$G(k) \approx 2\epsilon_\theta \frac{\nu^{\frac{1}{2}}}{\epsilon^{\frac{1}{2}}} \frac{1}{k} \exp\left\{-2\left(\frac{k}{k_B}\right)^2\right\}, \tag{3}$$

where $k_B \equiv (\epsilon/\nu\eta^2)^{\frac{1}{4}}$. This applies from the viscous-convective range (where the exponential is of order unity) all the way to $k \to \infty$.

Then Batchelor, Howells & Townsend considered the opposite extreme of a fluid-contaminant combination for which $\nu/\eta \ll 1$, in which there can exist an inertial-diffusive spectra range

$$\left(\frac{\epsilon}{\eta^3}\right)^{\frac{1}{4}} \ll k \ll \left(\frac{\epsilon}{\nu^3}\right)^{\frac{1}{4}}. \tag{4}$$

Here the turbulence spectrum is of Kolmogorov type

$$F(k) \sim \epsilon^{\frac{2}{3}} k^{-\frac{5}{3}}, \tag{5}$$

with proportionality constant of order one, while the contaminant spectrum is strongly diffusive. For this range they deduced essentially that

$$G(k) \approx \frac{1}{3} \frac{\epsilon_\theta \epsilon^{\frac{2}{3}}}{\eta^3} k^{-\frac{17}{3}}. \tag{6}$$

The present study is aimed at generalizing equations (1), (3) and (6) to include the effect of a first-order chemical reaction, assuming a system so dilute that associated temperature changes have negligible effects on the reaction rate and flow. Some preliminary results on decaying, reacting fields have been discussed (Corrsin 1958), and the formal consequences of the quasi-Gaussian hypothesis have been analysed (O'Brien 1960).

The differential equation for concentration of a dilute contaminant undergoing a first-order chemical reaction along with the convection and molecular diffusion is

$$\frac{\partial \theta}{\partial t} + u_i \frac{\partial \theta}{\partial x_i} = \eta \nabla^2 \theta - C\theta, \tag{7}$$

where C is a constant. With less dilute reactant, it will be necessary to include the heat of reaction and the temperature dependence of C. $\mathbf{u}$ is the turbulent velocity field, η is the (constant) diffusivity, t is time, $\mathbf{x}$ is the co-ordinate vector. As pointed out earlier (Corrsin 1958; O'Brien 1960), this particular reaction-rate term is not spectrally selective, so in a freely decaying field it merely multiplies the mixing wave-number spectrum by an additional (exponential) decay in time.

For stationary states, however, such simple arguments cannot be applied; we must pursue spectral elements in time as they migrate to ever larger wave numbers in the stationary spectrum. For the inertial range analysis of the turbulence itself this is essentially the approach used rather informally by Onsager (1949), arriving independently at Kolmogorov's result $F \sim k^{-\frac{5}{3}}$. For the viscous-convective spectral range in scalar mixing, this method of reasoning was introduced more rigorously by Batchelor (1959). Direct dimensional reasoning will not yield the explicit result of equation (23) because the reaction introduces an additional dimensional constant without increasing the number of dimensions.

This paper is restricted to local isotropy for both velocity and reactant fields.

Pure mixing in the inertial-convective range

As a prelude to the following section, it is instructive to re-derive the k-behaviour of (1) by a method like Onsager's. We restrict our consideration to a k-range in which the transfer of $\overline{\theta^2}$ spectral elements is purely convective. This means that

$$k \ll \left(\frac{\epsilon}{\nu \eta^2}\right)^{\frac{1}{4}}, \tag{8}$$

if $\nu/\eta \gg 1$, and that

$$k \ll \left(\frac{\epsilon}{\eta^3}\right)^{\frac{1}{4}}, \tag{9}$$

if $\nu/\eta \ll 1$.

Employing the crude concept of a spectral 'energy' cascade in which the $\overline{\theta^2}$ spectral elements 'jump' to successively larger k, we introduce the following assumptions.

(*a*) The cascade wave-number sequence is a geometrical progression, so that

$$\Delta k \approx k. \tag{10}$$

For turbulence dynamics this is suggested by the non-linearity of the Navier–Stokes equations; here we appeal to the quasi-non-linear traits of (7), due to the convective 'forcing function' coefficient $\mathbf{u}$.

(*b*) The part of $\overline{\theta^2}$ transferred in a jump at wave-number k is $G(k)\,\Delta k$. We take it to be $\approx G(k)\,k$.

(*c*) The characteristic time for each jump depends, of course, on the velocity spectrum $F(k)$, and the simplest dimensional possibility is

$$\tau(k) = k^{-\frac{3}{2}}F^{-\frac{1}{2}}. \tag{11}$$

The use of this form for the spectrally local convection time restricts us to the inertial part of the turbulence spectrum.

In the inertial-convective range, the rate of flux of $\overline{\theta^2}$ spectral content through any k must be independent of k, i.e.

$$\frac{d}{dk}\left(\frac{Gk}{\tau}\right) = 0. \tag{12}$$

Using (11), $$GF^{\frac{1}{2}}k^{\frac{5}{2}} = \text{const.} \tag{13}$$

Using $F \sim k^{-\frac{5}{3}}$ as appropriate here, we find from (13) that

$$G = Dk^{-\frac{5}{3}}, \tag{14}$$

with D a constant, consistent with (1). This approach does not immediately give the dimensional coefficients as in (1) and (5). They can be estimated by other means. For example, we may use the expression for diffusive destruction of $\overline{\theta^2}$ spectral content,

$$\epsilon_\theta = 2\eta\int_0^\infty k^2 G\,dk. \tag{15}$$

Assume that the order of the integral is given by the part between a wave-number ${}_\theta k_L$ characterizing the large structure and the wave-number $(\epsilon/\eta^3)^{\frac{1}{4}}$ (for the cases $\nu/\eta \lesssim 1$). Then

$$\epsilon_\theta \approx 2\eta D\int_{{}_\theta k_L}^{(\epsilon/\eta^3)^{\frac{1}{4}}} k^{\frac{1}{3}}\,dk. \tag{16}$$

Integrating and neglecting ${}_\theta k_L^{\frac{4}{3}}$ relative to $(\epsilon/\eta^3)^{\frac{1}{3}}$, we get

$$D \approx \tfrac{2}{3}\epsilon_\theta \epsilon^{-\frac{1}{3}}, \tag{17}$$

consistent with (1).

Reactive mixing in the inertial-convective range

In the non-diffusive spectral range, (7) can be approximated by

$$\frac{\partial\theta_n}{\partial t} + u_i\frac{\partial\theta_n}{\partial x_i} \approx -C\theta_n. \tag{18}$$

θ_n represents any '*narrow-band*' θ-field in the convective spectral range. Multiplying by θ_n and averaging, we lose the convective term by homogeneity and are left with the simple decay equation

$$\frac{\partial \overline{\theta_n^2}}{\partial t} \approx -2C\overline{\theta_n^2}. \tag{19}$$

Integrating, we obtain the result

$$\overline{\theta_n^2} = (\overline{\theta_n^2})_0 e^{-2Ct}. \tag{20}$$

The time rate of increase of wave-number for this reactively decaying spectral packet is still given by (10) and (11), since the first-order reaction has no effect on the geometry of the isoplethic surfaces, so

$$\frac{dk_n}{dt} = \frac{\Delta k_n}{\tau(k_n)} \approx \frac{k_n}{\tau} \approx k_n^{\frac{5}{2}} F^{\frac{1}{2}}(k_n). \tag{21}$$

With (20), we see that (12) generalizes to

$$\frac{d}{dk}\left\{\frac{Gk}{\tau} e^{2Ct}\right\} = 0, \tag{22}$$

or

$$e^{2Ct}\frac{d}{dk}\left\{\frac{Gk}{\tau}\right\} + \frac{Gk}{\tau}\frac{dt}{dk}\frac{d}{dt}\{e^{2Ct}\} = 0.$$

Using (21) for dk/dt, and (5) for $F(k)$, this integrates to

$$\boxed{G(k) \approx Bk^{-\frac{5}{3}} \exp\{3C\epsilon^{-\frac{1}{3}}k^{-\frac{2}{3}}\},} \tag{23}$$

which is shown qualitatively in figure 1. Evidently, for wave-numbers well above $k_c = C^{\frac{3}{2}}\epsilon^{-\frac{1}{2}}$, the effect of reaction on spectral shape is negligible. k_c locates the spectral region in which the rate of reactive loss is of the same order as the rate of convective spectral transfer.

The dimensional coefficient B in this generalization of (1) or (14) cannot be estimated by a condition as simple as (15) because $2\eta\int_0^\infty k^2 G\,dk$ no longer represents the total rate of destruction of $\overline{\theta^2}$. Of far narrower applicability than (15) would be estimation of D in (14) or B in (23) by

$$\overline{\theta^2} = \int_0^\infty G\,dk \approx \int_{{}_\theta k}^{{}_\theta k^* \text{ or } \infty} G\,dk. \tag{24}$$

Here ${}_\theta k_L$ is the 'energy-bearing' wave-number; ${}_\theta k^*$ is the end of the inertial-convective range. The limitation is, of course, that the main contribution to this integral comes from the neighbourhood of ${}_\theta k_L$, where G is unlikely to be well approximated by (14) or (23). The same limitation arises if we replace (15) by an expression for the total rate of destruction of $\overline{\theta^2}$:

$$\epsilon_\theta = 2\eta\int_0^\infty k^2 G\,dk + 2C\int_0^\infty G\,dk \tag{25}$$

$$\approx 2\eta\int_{{}_\theta k_L}^{{}_\theta k^*} k^2 G\,dk + 2C\int_{{}_\theta k_L}^{{}_\theta k^* \text{ or } \infty} G\,dk. \tag{26}$$

Having recorded these extreme doubts, but having no clearly better choice, we use (24) to estimate B. (26) is more tedious and not necessarily more reliable. Thus we write

$$\overline{\theta^2} \approx B\int_{\theta k_L}^{\theta k^*} k^{-\frac{5}{3}} \exp\{3C\epsilon^{-\frac{1}{3}}k^{-\frac{2}{3}}\}\,dk. \tag{27}$$

By integration, we get the final result

$$\overline{\theta^2} \approx -\frac{B\epsilon^{\frac{1}{3}}}{2C}[\exp\{3C\epsilon^{-\frac{1}{3}}{}_\theta k^{*-\frac{2}{3}}\} - \exp\{3C\epsilon^{-\frac{1}{3}}{}_\theta k_L^{-\frac{2}{3}}\}]. \tag{28}$$

Since ${}_\theta k^* \gg {}_\theta k_L$, we neglect the first exponential, getting the estimate

$$B \approx 2C\overline{\theta^2}\epsilon^{-\frac{1}{3}} \exp\{-3C\epsilon^{-\frac{1}{3}}{}_\theta k_L^{-\frac{2}{3}}\}. \tag{29}$$

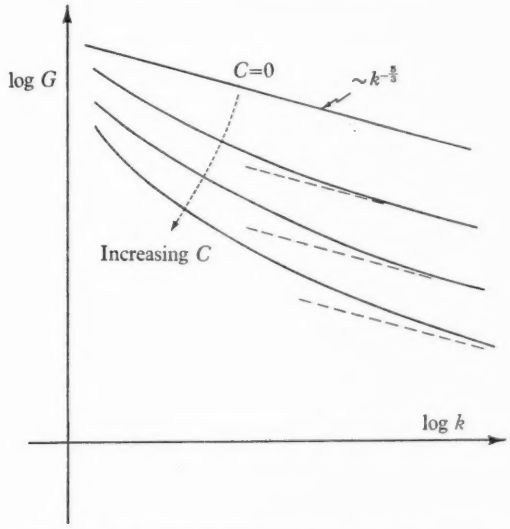

FIGURE 1. Qualitative sketch of reactant spectrum in inertial-convective range.

To gain some appreciation of (28) or (29), consider its limiting form for $C \to 0$. This is obtained most easily by putting (14) into (24), or by expanding (28) as a series, to give

$$B \to D \approx \tfrac{2}{3}\overline{\theta^2}\,{}_\theta k_L^{\frac{2}{3}}. \tag{30}$$

Equating this estimate to the better one [equation (17)], we find that

$$\epsilon_\theta \approx \overline{\theta^2}\,{}_\theta k_L^{\frac{2}{3}}\epsilon^{\frac{1}{3}}. \tag{31}$$

A similar approach to the inertial turbulent-energy spectrum gives the well-known estimate for dissipation rate in terms of large-scale parameters,

$$\epsilon \approx (\overline{u^2})^{\frac{3}{2}}\,k_L, \tag{32}$$

omitting a factor of order unity. Putting (32) into (31), we get a form looking like (32),

$$\epsilon_\theta \approx \overline{\theta^2}(\overline{u^2})^{\frac{1}{2}}\,{}_\theta k_L^{\frac{2}{3}}k_L^{\frac{1}{3}}. \tag{33}$$

If the large structures of velocity and contaminant fields are about equal,

$$\epsilon_\theta \approx \overline{\theta^2}(\overline{u^2})^{\frac{1}{2}} k_L. \tag{34}$$

In any case, we see that (29) represents the same kind of approximation as one used in obtaining (32).

Reactive mixing in the viscous-convective range and beyond

In the limiting case of mixing at very large Schmidt number, ν/η, Batchelor (1959) pointed out the possibility of a locally isotropic viscous-convective range as outlined in the Introduction. His initial arguments are unaffected by the addition of our first-order, passive chemical reaction.

This spectral range is characterized by the property that the 'smallest eddies' of the turbulent motion are much larger than the characteristic lengths of the scalar field, $(\epsilon/\nu^3)^{\frac{1}{4}} \ll k$. Therefore, if we follow a small region of fluid, the turbulent straining action can be visualized as locally uniform for a limited time. This permits analysis of the history of a Fourier element of concentration field under the joint action of turbulent straining and molecular diffusion. Inference of general spectral behaviour from a single spectral point is permissible here (unlike analysis of the turbulence field) because the diffusion equation is linear.

Batchelor chooses Cartesian axes which translate with a fluid element and are always alined with the local principal strain-rate axes. Calling these local principal strain-rates α, β, γ, equation (7) can be written as

$$\frac{\partial \theta_1}{\partial t} + \alpha x \frac{\partial \theta_1}{\partial x} + \beta y \frac{\partial \theta_1}{\partial y} + \gamma z \frac{\partial \theta_1}{\partial z} = \eta \nabla^2 \theta_1 - C\theta_1. \tag{35}$$

Presumably α, β and γ can be taken constant over distances comparable with the Kolmogorov microscale $(\nu^3/\epsilon)^{\frac{1}{4}}$, and over times comparable with the Kolmogorov time $(\nu/\epsilon)^{\frac{1}{2}}$. The subscript on θ_1 reminds us that we shall analyse the history of a single Fourier element of the full θ-field.

Following Batchelor's procedure, we get instead of his equation (4.6), the equation

$$\theta_1(\mathbf{x}, t) \doteq A_0 \exp\left\{\frac{\eta k^2}{2\gamma} - Ct\right\} \sin(kz), \tag{36}$$

where

$$k \doteq k_z = k_{0z}\, e^{-\gamma t} \tag{37}$$

and A_0 is initial amplitude (see equation (4.4) in Batchelor's paper). If we call $\theta_M(\mathbf{x}, t)$ the field with $C = 0$, and compare with Batchelor's form for θ_M, then

$$\theta_1(\mathbf{x}, t) = \theta_M(\mathbf{x}, t)\, e^{-Ct}. \tag{38}$$

To use such determinate results to infer the behaviour of a random θ-field randomly strained by isotropic turbulence, we argue that (36) applies to any Fourier element whose $k \gg (\epsilon/\nu^3)^{\frac{1}{4}}$. The magnitude of the maximum negative strain-rate is taken to be the root-mean-square value of strain-rate for the turbulence, i.e. we set

$$\gamma \approx -\tfrac{1}{2}(\epsilon/\nu)^{\frac{1}{2}}. \tag{39}$$

Supposing that the θ-field is maintained statistically steady by continuous feeding into the large structure, we use (37) to estimate the kinematic history of

any narrow slab of the broadband θ-spectrum as it migrates to larger and larger k under the convective straining of the turbulence. Then (36) tells us how fast this slab loses $\overline{\theta^2}$-content during any time interval of spectral travel.

The time required for a narrow slab to travel from k' to k follows from (37). It is

$$T = -\frac{1}{\gamma}\log\left(\frac{k}{k'}\right), \tag{40}$$

given by Batchelor. The change in slab width as it goes from k' to k is found to be

$$\delta k/k = \delta k'/k'. \tag{41}$$

During this time interval, the contribution to $\overline{\theta^2}$ carried by this slab decreases in the ratio given by the square of (36), with (40) for the travel time, or

$${}_{k'}\mathscr{R}_k = \left(\frac{k}{k'}\right)^{2C/\gamma}\exp\left\{\frac{\eta}{\gamma}(k^2-k'^2)\right\}. \tag{42}$$

To compare the actual spectral levels at k' and k, we start with

$$G(k)\,\delta k = G(k')\,\delta k'\,{}_{k'}\mathscr{R}_k. \tag{43}$$

By use of (41) and (42), this leads to

$$k^{(1-2C/\gamma)}G(k)\,e^{-\eta k^2/\gamma} = k'^{(1-2C/\gamma)}G(k')\,e^{-\eta k'^2/\gamma}. \tag{44}$$

By inspection [or by using (44) we set up a difference equation, thence a differential equation which can be solved], we arrive at the spectral form

$$G(k) = Nk^{(2C/\gamma)-1}\exp\{\eta k^2/\gamma\}, \tag{45}$$

which reduces to Batchelor's mixing form for $C = 0$. $N = \text{const.}$ Introducing (39) for γ, we derive the final result

$$\boxed{G(k) = Nk^{-(1+4C\nu^{\frac{1}{2}}\epsilon^{-\frac{1}{2}})}\exp\{-2(k/k_B)^2\},} \tag{46}$$

where $k_B \equiv (\epsilon/\nu\eta^2)^{\frac{1}{4}}$. The wave-number $k_c = C^{\frac{3}{2}}\epsilon^{-\frac{1}{2}}$ does not play a direct role in the *shape* of this part of the spectrum. It does, however, affect the entire local level through N.

In the viscous-convective range, $k^* \ll k \ll k_B$, (46) simplifies to a power law,

$$G(k) \approx Nk^{-(1+4C\nu^{\frac{1}{2}}\epsilon^{-\frac{1}{2}})}. \tag{47}$$

We note parenthetically that (47) (and Batchelor's limiting form for $C = 0$) can also be obtained by application of (22) with the spectral transfer time taken as $\tau = \text{const.} = (\nu/\epsilon)^{\frac{1}{2}}$.

Qualitatively, the combination of (23) and (45) gives a θ-spectrum like figure 2.

To evaluate N, we require that (46) [hence (47)] match the lower wave-number form, equation (23), at $k = k^* \equiv (\epsilon/\nu^3)^{\frac{1}{4}}$. This gives

$$N = Bk^{*(-\frac{5}{3}+4C\nu^{\frac{1}{2}}\epsilon^{-\frac{1}{2}})}\exp\{3C\epsilon^{-\frac{1}{3}}k^{*-\frac{2}{3}}\}, \tag{48}$$

or

$$N = B(\epsilon/\nu^3)^{(-\frac{1}{6}+C\nu^{\frac{1}{2}}\epsilon^{-\frac{1}{2}})}\exp\{3C(\nu/\epsilon)^{\frac{1}{2}}\}. \tag{48a}$$

If we take (29) as a rough approximation for B, and neglect ${}_\theta k_L^{\frac{2}{3}}$ relative to $k^{*\frac{2}{3}}$ in the exponent, (48) becomes

$$N \approx 2\overline{\theta^2} C(\nu/\epsilon)^{\frac{1}{2}} k^{*-C\nu^{\frac{1}{2}}\epsilon^{-\frac{1}{2}}} \exp\left\{-3C\left(\frac{\nu}{\epsilon}\right)^{\frac{1}{2}}\left(\frac{k^*}{{}_\theta k_L}\right)^{\frac{2}{3}}\right\}. \tag{49}$$

It should be noted that the argument of the (constant) exponential can be written as $\{-3(k_c/{}_\theta k_L)^{\frac{2}{3}}\}$ [see remarks after equation (23)]. The ubiquity of the dimensionless reaction rate $C(\nu/\epsilon)^{\frac{1}{2}}$ is notable here, as in earlier results.

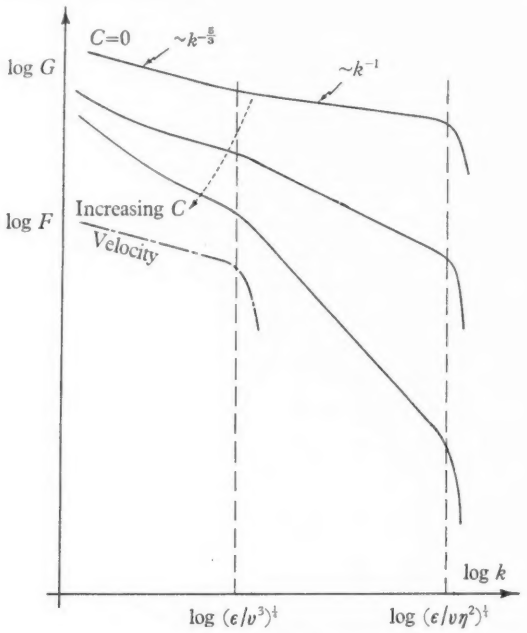

FIGURE 2. Qualitative sketch of reactant spectrum for $\nu/\eta \gg 1$.

The relation (46) reduces immediately to Batchelor's mixing case when we put $C = 0$. The corresponding simplification of the constant coefficient N follows by noting that (48) then reduces to

$$N \to Bk^{*-\frac{5}{3}}, \tag{50}$$

while

$$B \to D \approx \epsilon_\theta \epsilon^{-\frac{1}{3}}, \tag{51}$$

in accordance with (1). From (50) and (51),

$$N \to \epsilon_\theta(\nu/\epsilon)^{\frac{1}{2}}, \tag{52}$$

in essential agreement with the $C = 0$ theory.

Reactive mixing in the inertial-diffusive range

For $\nu/\eta \ll 1$, there exists an inertial-diffusive range in the θ-spectrum, its wavenumber characterized by (4). For this case we can simply follow the procedure of Batchelor *et al.* (1959), with the addition of the reactive term as in equation (7).

The Fourier transform of (7) can be written as

$$\frac{\partial P(\mathbf{k},t)}{\partial t}+i\int k'_j Q_j(\mathbf{k}-\mathbf{k}',t)\,P(\mathbf{k}',t)\,d\mathbf{k}' = -\eta k^2 P(\mathbf{k},t)-CP(\mathbf{k},t). \tag{53}$$

The simplifying theoretical arguments presented by Batchelor *et al.* (1959) can be summarized and adapted as follows.

(*a*) Since the θ-spectrum doubtless falls off much more rapidly than the **u**-spectrum in this range, the principal contribution to the integral must come at values of k' of the order of and less than $(\epsilon/\eta^3)^{\frac{1}{4}}$. It follows that over most of the spectral range of this analysis

$$k' \ll k \tag{54}$$

in the important part of the integral.

(*b*) The diffusion and reaction time for a Fourier component of θ around wave-number k is of order $(\eta k^2+C)^{-1}$, but the convective (quasi-source) effect has the inertial range characteristic time $(\epsilon k^2)^{-\frac{1}{3}}$ [which is the same as equation (11)]. With $k \gg (\epsilon/\eta^3)^{\frac{1}{4}}$, the latter time is much the larger. Therefore the time-derivative term can be neglected in equation (53) when it is applied to the wave-number range of interest here.

Neglect $\partial P/\partial t$ in (53), then multiplying the remainder by its complex conjugate, and continuing to follow the Batchelor, Howells & Townsend arguments by using (54) to justify neglecting the statistical connexion between the (spectrally) widely separated factors in this integrand ($|\mathbf{k}-\mathbf{k}'| \gg k'$), we finally get the following extension of their equation (8):

$$(\eta k^2+C)^2\,G(k) \approx \tfrac{2}{3}\epsilon_\theta^* F(k)/\eta, \tag{55}$$

where ϵ_θ^* is the rate of destruction of $\overline{\theta^2}$ by diffusion. Introducing (5) for F, we arrive at

$$\boxed{G(k) \approx \frac{1}{3}\frac{\epsilon_\theta^*\epsilon^{\frac{2}{3}}}{\eta}\frac{1}{k^{\frac{5}{3}}[\eta k^2+C]^2},} \tag{56}$$

which reduces properly for $C = 0$. With $C \neq 0$, it approximates the pure-mixing form in the wave-number range $k \gg (C/\eta)^{\frac{1}{2}}$, which is a measure of the spectral location where reactive loss rate and diffusive loss rate are comparable.

Since (56) has no arbitrary constant coefficient (except of order unity as a consequence of the various approximations *en route*), the matching of (56) with (23) at the wave-number ${}_\theta k^* = (\epsilon/\eta^3)^{\frac{1}{4}}$ just gives a relation among a number of characteristic constants in the problem. The matching leads directly to

$$B\exp\left\{3C\sqrt{\frac{\eta}{\epsilon}}\right\} \approx \frac{1}{3}\frac{\epsilon_\theta^*\epsilon^{-\frac{1}{3}}}{[1+C(\eta/\epsilon)^{\frac{1}{2}}]^2}. \tag{57}$$

With (29) as an estimate for B, this can be written as

$$\epsilon_\theta^* \approx 6C\overline{\theta^2}\left[1+C\sqrt{\frac{\eta}{\epsilon}}\right]^2\exp\left\{-3C\sqrt{\frac{\eta}{\epsilon}}\left[\left(\frac{{}_\theta k^*}{{}_\theta k_L}\right)^{\frac{2}{3}}-1\right]\right\}. \tag{58}$$

This approximation is not correct for $C \to 0$. The non-reacting limit requires that the entire expression (28) be used for B.

The qualitative characteristics of reacting spectra for $\nu/\eta \ll 1$ are sketched in figure 3. We notice in (58) that for this case the appropriate dimensionless reaction rate is $C(\eta/\epsilon)^{\frac{1}{2}}$ instead of $C(\nu/\epsilon)^{\frac{1}{2}}$.

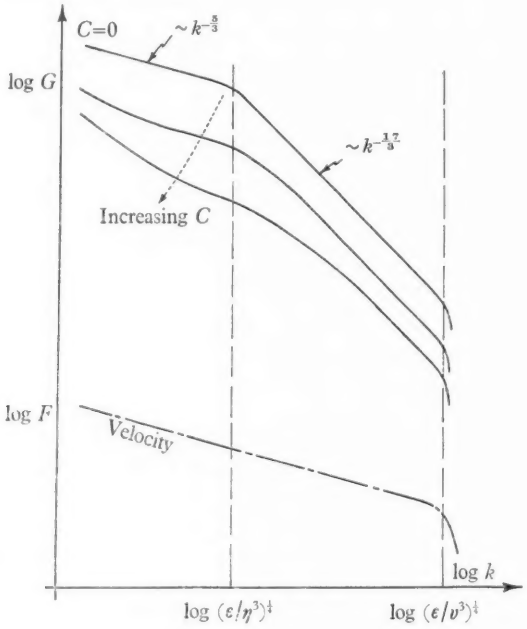

FIGURE 3. Qualitative sketch of reactant spectrum for $\nu/\eta \ll 1$.

Since (58) gives an estimate for the rate of diffusive destruction of $\overline{\theta^2}$, the total rate at which $\overline{\theta^2}$ is fed into the spectrum is just

$$\epsilon_\theta = \epsilon_\theta^* + 2C\overline{\theta^2}. \tag{59}$$

This work was supported by Fluid Dynamics Branch, U.S. Office of Naval Research.

REFERENCES

BATCHELOR, G. K. 1959 *J. Fluid Mech.* **5**, 113.
BATCHELOR, G. K., HOWELLS, I. D. & TOWNSEND, A. A. 1959 *J. Fluid Mech.* **5**, 134.
CORRSIN, S. 1951 *J. Appl. Phys.* **22**, 469.
CORRSIN, S. 1958 *Phys. Fluids*, **1**, 42.
O'BRIEN, E. E. 1960 Dissertation, The Johns Hopkins University.
OBUKHOV, A. M. 1949 *Izv. Akad. Nauk, SSSR, Geogr. i. Geofiz.*, **13**, 58.
ONSAGER, L. 1949 *Nuovo Cim.*, Suppl. 6, no. 2, 279.

Theory of unsteady flow about thin cylinders in fluids of high electrical conductivity

By LEON E. RING

Cornell University, Ithaca, N.Y.

(Received 10 June 1960 and in revised form 10 March 1961)

A theory is developed for the incompressible flow of a fluid with high electrical conductivity about thin cylinders (airfoils) in non-uniform motion. A uniform magnetic field is applied parallel to the free stream and solutions are obtained subject to the restriction of small perturbations. The effects of viscosity are included, for the most part, only through the use of the Kutta condition, where applicable, for lifting airfoils. The validity and range of applicability of the infinite-conductivity assumption are determined on the basis of an order-of-magnitude analysis; the general character of the flow is discussed at length.

The flow-field for infinite conductivity is changed from the non-magnetic case only through the new transport speed of vorticity; the forces on the airfoil are changed due to surface currents. For the case of the Alfvén speed less than the free-stream speed, the airfoil lift and pitching moment are given in integral form for general unsteady-airfoil motion and are given in closed form for harmonic ocsillations. The forces at moderate frequencies may be larger than in the corresponding non-magnetic case. The response to a unit-step change in the downwash is studied and the asymptotic form of the lift is obtained for small and large time.

For the case of the Alfvén speed greater than the free-stream speed, vorticity and current are shed from both the leading and trailing edges. Therefore the extension of the usual Kutta condition is not obvious. It is shown that if finite viscosity and/or conductivity tend to remove the trailing-edge singularity, the flow is unstable and no steady flow can be obtained.

1. Introduction

The steady magnetohydrodynamic flow of an incompressible fluid of large electrical conductivity about thin cylinders (airfoils) has been studied by Sears & Resler (1959). In the limit of infinite conductivity with a uniform magnetic field applied parallel to the free stream, the flow field is found to be irrotational and current-free and is in fact identical with the corresponding non-magnetic flow. The magnetic field inside the body is identically zero, so that the pressure on the body surface is altered due to the implied current sheet on the body surface. For large but finite conductivity, this current sheet diffuses into a thin layer. This inviscid 'magnetic-boundary-layer' has been studied by Lewellen (1959) and is found to have a thickness of the order $R_m^{-\frac{1}{2}}$, where R_m is the magnetic Reynolds number.

The results of these investigations are of sufficient general interest to suggest an analogous study of unsteady flow. In particular, since thin cylinders in asymmetric flow generally produce circulation and lift, one is led to consider the effects of unsteady circulation and vortex shedding. Thus, although ostensibly concerned with 'airfoils', the present paper is intended to cast light on phenomena that can be expected to appear in a rather general class of unsteady magneto-hydrodynamic flows around bodies. The term 'airfoil' is used since it suggests the thin cylinders being considered and since the methods of classical thin-airfoil theory are applicable to the present problem.

A free-vortex element in an incompressible and infinitely conducting fluid will travel at the Alfvén speed relative to the flow. For the aligned-fields case, this says that shed vorticity will travel parallel to the free stream, but will have a new transport speed. This suggests the use of the techniques of classical unsteady-airfoil theory, as given by Kármán & Sears (1938), with modifications for the new vortex-transport speeds and the airfoil forces due to surface currents. This is done in the present paper, so that the Sears & Resler (1959) steady solution with aligned fields is extended to include unsteady airfoil motion. Of course, this is based on the assumption, made by Sears & Resler and others, that the correct steady-flow pattern has undisturbed conditions far from the body. Other hypotheses, leading to grossly different flow patterns, have been suggested by Stewartson (1960).

2. Basic equations

The equations which govern the motion of an incompressible fluid with finite viscosity and scalar conductivity have been given by a number of authors (e.g. Resler & Sears 1958) and can be reduced to the following dimensionless form:

$$\frac{D\mathbf{q}}{Dt} + \tfrac{1}{2}\nabla(p + \alpha^2 B^2) = \alpha^2 \mathbf{B}.\nabla\mathbf{B} + \frac{1}{R_e}\nabla^2\mathbf{q}, \tag{1}$$

$$\frac{D\mathbf{B}}{Dt} = \mathbf{B}.\nabla\mathbf{q} + \frac{1}{R_m}\nabla^2\mathbf{B}, \tag{2}$$

$$\nabla.\mathbf{q} = 0, \tag{3}$$

$$\nabla.\mathbf{B} = 0. \tag{4}$$

The equations have been non-dimensionalized using the free-stream speed U_0^*, the applied magnetic field of induction B_0^*, and the body length L_0^*. M.K.S rationalized units are used, with an asterisk denoting dimensional quantities. The three parameters are defined by

$$R_m = \mu^*\sigma^* U_0^* L_0^*, \quad R_e = \frac{U_0^* L_0^*}{\nu^*}, \quad \alpha^2 = \frac{B_0^{*2}}{\mu^*\rho^* U_0^{*2}};$$

R_m is the magnetic Reynolds number and R_e the viscous Reynolds number. The parameter α^2 is the ratio of the magnetic pressure to the dynamic pressure in the free stream; it is also the square of the ratio of the speed of an Alfvén-wave in an infinitely conducting medium to the free-stream speed. The fluid is assumed to have uniform permeability μ^* and scalar conductivity σ^*. We will also use the vorticity $\boldsymbol{\Omega} = \operatorname{curl}\mathbf{q}$ and the current density $\mathbf{j} = \operatorname{curl}\mathbf{B}$.

Now consider the two-dimensional flow where small perturbations are superimposed on a uniform free-stream and a parallel magnetic field. This is represented by

$$\mathbf{q} = (1+u_x, u_y, 0), \quad u_x, u_y \ll 1;$$

$$\mathbf{B} = (1+b_x, b_y, 0), \quad b_x, b_y \ll 1.$$

For the most part, it is assumed that the flow field is described by taking zero viscosity and infinite conductivity in the linearized form of equations (1) and (2), which become

$$\frac{\partial \mathbf{u}}{\partial t} + \frac{\partial \mathbf{u}}{\partial x} + \nabla(\tfrac{1}{2}p + \alpha^2 b_x) = \alpha^2 \frac{\partial \mathbf{b}}{\partial x}, \tag{5}$$

$$\frac{\partial \mathbf{b}}{\partial t} + \frac{\partial \mathbf{b}}{\partial x} = \frac{\partial \mathbf{u}}{\partial x}. \tag{6}$$

3. General character of the flow

Steady flow

Before seeking a solution, it is well to establish the general character of the flow on the basis of order-of-magnitude arguments. In particular, the validity and range of application of the infinite-conductivity assumption (to be used later) will be established. First, let us consider flow with $R_m \ll R_e$.

By comparing the first and last terms of equation (2), one may write a characteristic magnetic diffusion time as $\tau_m = R_m \delta_m^2$, where δ_m is a characteristic diffusion distance or, in the present case, the current-penetration depth normal to the body surface. In steady flow, the time available for diffusion is the time required for current to travel the length of the body. Since the current travelling with the upstream Alfvén mechanism remains in the neighbourhood of the body longer and thus allows greater time for diffusion, the characteristic convection time is taken as $\tau_c^* = L_0^*/|U_0^* - B_0^* \mu^{*-\frac{1}{2}} \rho^{*-\frac{1}{2}}|$, which in dimensionless form becomes $\tau_c = 1/|1-\alpha|$. Equating these two times, the penetration depth for a convection-diffusion balance is given by $\delta_{mc} = (R_m|1-\alpha|)^{-\frac{1}{2}}$. This agrees with the result of Sears & Resler (1959), namely that for infinite conductivity the flow field is irrotational and current-free. It also agrees with Lary (1960), who found the penetration depth to be $|k|^{-\frac{1}{2}} \equiv \{\frac{1}{2}R_m|1-\alpha^2|\}^{-\frac{1}{2}}$, since $\frac{1}{2}(1+\alpha)$ is of order unity.

The strength of the magnetic field inside the body can be estimated by noting that the magnetic flux inside the body must be equal to that which has diffused from the fluid. The flux which has diffused from the fluid can be approximated by $\delta_m \Delta B$, where ΔB is the change in the field strength across the diffusion region. The flux inside the body can be approximated by ϵB_B, where ϵ is the body thickness ratio and B_B is a measure of the field strength inside the body. Equating these, B_B is given by $B_B = \delta_m \Delta B/\epsilon$. If $\delta_m \ll \epsilon$, i.e. if the diffusion depth is much less than the body thickness, then B_B must be nearly zero since ΔB can be no larger than order unity. This gives an effective 'no-slip' condition on **B** and results in a 'magnetic-boundary-layer', analogous to the usual viscous boundary layer. If $\delta_m \gg \epsilon$, B_B can be expected to be of the order of the free-stream value and ΔB a small quantity. This agrees with the Sears & Resler result that

the magnetic field is zero inside the body for infinite conductivity, and with Lary's result that the magnetic field is only slightly perturbed inside the body when $\epsilon \ll \{\frac{1}{2}R_m|1-\alpha^2|\}^{-\frac{1}{2}}$.

Unsteady flow

Now let us extend the above results to unsteady flow. Consider the pitching motion of a thin cylinder (insulator) which is described by the circular frequency ω. The unsteady characteristic time is taken as the 'period' $\tau_\omega = \omega^{-1}$. The penetration depth for a balance between diffusion and an unsteady input is found again by equating times to give $\delta_{m\omega} = \omega^{-\frac{1}{2}}R_m^{-\frac{1}{2}}$.

When $\delta_{m\omega} > \delta_{mc}$, the unsteady current component is carried away by the Alfvén mechanism before it can diffuse to the depth $\delta_{m\omega}$, so the essential balance remains between convection and diffusion. With this balance, the general flow character (except for the wake) can be expected to be the same as for steady flow.

For $\delta_{m\omega} < \delta_{mc}$, the unsteady current component is restricted to a smaller region than the steady component. Although there is a small-scale balance between diffusion and unsteady input, the large-scale balance remains between convection and diffusion. There are three cases depending upon the body thickness-ratio ϵ. (*a*) When $\delta_{m\omega} < \delta_{mc} \ll \epsilon$, both mechanisms tend toward a magnetic boundary layer. (*b*) When $\delta_{m\omega} \ll \epsilon \ll \delta_{mc}$, the unsteady current gives a magnetic boundary layer,while the steady solution gives a high degree of diffusion. This could be achieved for moderate values of ω with a high R_m and α sufficiently close to unity. This flow can be described by saying that the magnetic field is effectively 'frozen in the flow' during an oscillation period but can diffuse a large distance during the time that the current stays in the neighbourhood of the body. (It is also 'frozen out of the flow' or 'in the body' during an oscillation period.) (*c*) When $\epsilon \ll \delta_{m\omega} < \delta_{mc}$, both mechanisms allow a high degree of diffusion.

For the slender bodies being considered, the boundary conditions at the body-fluid interface can be satisfied by discontinuities across a singularity sheet, so the solutions are linear and superposition of solutions is possible (for thickness, camber, unsteadiness, etc.). That this is true for the limiting cases discussed above follows directly from the work of Sears & Resler (1959) and Lary (1960) except for the special case $\delta_{m\omega} \ll \epsilon \ll \delta_{mc}$. That it is also true in this case can be seen by noting that the steady solution has only small perturbations everywhere. Therefore the unsteady solution, within the linear theory, sees only an undisturbed flow. The boundary conditions for the solution of the unsteady flow field can thus be satisfied by a singularity sheet. The required unsteady current-sheet strength corresponds to the jump from the unsteady flow to the steady magnetic field inside the body, since the field strength inside the body cannot change during an oscillation period.

From the above, it is now possible to answer the question of the applicability of the infinite-conductivity theory. For the calculation of thickness effects, in general it is required that the magnetic field be approximately zero inside the body; this requires that $\epsilon \gg (R_m|1-\alpha|)^{-\frac{1}{2}}$. However, the unsteady infinite-

conductivity lifting theory only requires that the unsteady current be confined to a thin layer; thus infinite-conductivity theory is valid when *either*

$$1 \ll (R_m|1-\alpha|)^{\frac{1}{2}} \quad \text{or} \quad 1 \ll (\omega R_m)^{\frac{1}{2}}.$$

A case of particular interest occurs when $1 \ll (\omega R_m)^{\frac{1}{2}}$ and $1 \gg (R_m|1-\alpha|)^{\frac{1}{2}}$. The solution for this flow is given by the supposition of a steady contribution, calculated on the basis of Lary's (1960) theory, and an unsteady contribution calculated on the basis of the infinite-conductivity theory of the present paper.

4. Conservation laws and Kutta condition

Conservation of vorticity

Consider a body at rest which starts to move at time $t = 0$. At any finite time t, all current and vorticity must be in a finite region of the plane which can be enclosed by a curve C, where C is convected with the local flow. Since $\boldsymbol{\Omega}$ and $\mathbf{j}$ are assumed to be zero along C, Kelvin's theorem can be applied to the curve C and one can immediately write that

$$\iint \boldsymbol{\Omega}\, dx\, dy = 0, \tag{7}$$

where the integral is taken over all the vorticity, that is, the net vorticity in the system remains zero.

Conservation of current

A similar constraint will now be obtained for the current. Consider the contour C to be a circle of radius r about the body, and integrate equation (2) around C. This gives

$$\frac{d}{dt}\int_C \mathbf{B}.d\mathbf{l} = \int_C \left(-\mathbf{q}.\nabla\mathbf{B} + \mathbf{B}.\nabla\mathbf{q} + \frac{1}{R_m}\nabla^2\mathbf{B}\right).d\mathbf{l}. \tag{8}$$

Since there is no current on C, $\nabla^2\mathbf{B} = 0$ on C. The net vorticity was shown to be zero, so $\mathbf{q} = O(r^{-2})$ on C. Therefore the right-hand side of (8) is $O(r^{-1})$, which can be neglected for a sufficiently large contour. Then, applying Stokes's theorem and integrating over time, we have that

$$\iint \mathbf{j}\, dx\, dy = \text{const.} = 0, \tag{9}$$

where the integral is taken over all current, and the integration constant is evaluated at a time before the start of the body motion. This says that the net current in the system remains zero.†

† One must be a bit careful about what is meant by a two-dimensional problem, since all currents must close somehow. If there is a net current flowing, there is some question if the closing of the current (in a large wire loop, for instance) can be neglected. In the present work, the net current is zero. Therefore the current elements can close through conducting side walls, which would give an effect analogous to tip effects of classical-airfoil theory.

Kutta condition

In classical two-dimensional thin-airfoil theory, the undetermined cyclic constant (circulation) is specified, to make the solution unique, by using the Kutta condition. The criterion for small, but finite, viscosity has been discussed by a number of authors, including a recent comprehensive discussion by Sears (1956). It is because of the fact that vorticity convects with the flow (and diffuses relative thereto) that the boundary-layer vorticity leaves the airfoil at the trailing edge; therefore the Kutta condition must be applied at this edge.

For a magnetic boundary layer with $\alpha^2 < 1$, all vorticity and current must leave the airfoil from the trailing edge. Thus the Kutta condition must still be applied at the trailing edge. For $\alpha^2 > 1$, the extension is not clear. It can be shown that if the angle of attack is suddenly changed, there is an immediate flux of vorticity and current from both the leading and trailing edges. Therefore it seems that, at least in the unsteady case, the criterion should include the leading as well as the trailing edge. Since we lack such a criterion, which must come from more detailed boundary-layer considerations, this case will be treated without applying a specific condition.

5. General unsteady airfoil motion

Fluid model

Consider the unsteady two-dimensional flow about a thin cylinder (airfoil) for arbitrary values of the parameter α^2. The airfoil is taken to have zero thickness and to lie near the x-axis in the range $[0, 1]$. If the fluid has sufficiently high electrical conductivity and low viscosity, all current and vorticity are confined to thin wakes and the wakes can be represented as singularity sheets.

The fluid model used for the solution of the flow field is shown in figure 1, and consists of a current and vortex distribution in a downstream wake, over the airfoil, and when applicable, in an upstream wake. The current and vorticity in the wakes can be related by the solution of equation (5) and (6) with the condition that the wakes are force-free. This gives the well known Alfvén-wave relations,

$$\left.\begin{aligned} \epsilon_1^{(1)}(x,t) &= \alpha\epsilon_1^{(2)}(x,t) = f_1\{t - x/(1-\alpha)\}, \\ \epsilon_2^{(1)}(x,t) &= -\alpha\epsilon_2^{(2)}(x,t) = f_2\{t - x/(1+\alpha)\}, \end{aligned}\right\} \tag{10}$$

where $\epsilon^{(1)}$ is wake vorticity, $\epsilon^{(2)}$ is wake current, and the subscripts 1 and 2 refer to upstream and downstream waves respectively. These have velocities and direction of travel as shown in figure 1. For any finite time, the wakes will be of finite length and all current and vorticity will lie in the interval $-R < x < R$.

Potential relations

The flow outside the wakes can be given by a perturbation magnetic potential $\phi^{(2)}$ and a perturbation velocity potential $\phi^{(1)}$. A relation between the potentials is obtained by substitution into equation (6). Integration of the x-component with respect to x yields the result

$$\frac{\partial\phi^{(2)}}{\partial t} + \frac{\partial\phi^{(2)}}{\partial x} = \frac{\partial\phi^{(1)}}{\partial x},$$

where the integration constant is found to be zero, by evaluation at $x = \infty$. $\phi^{(2)}$ is now given explicitly in terms of $\phi^{(1)}$ by integration of the above result, following a fluid particle. This yields the integral

$$\phi^{(2)}(x, y, t) = \int_{-\infty}^{t} \frac{\partial \phi^{(1)}(x - t + \xi, y, \xi)}{\partial x} d\xi \tag{11a}$$

$$= \phi^{(1)}(x, y, t) - \int_{-\infty}^{x} \frac{\partial \phi^{(1)}(\xi, y, t + \xi - x)}{\partial t} d\xi. \tag{11b}$$

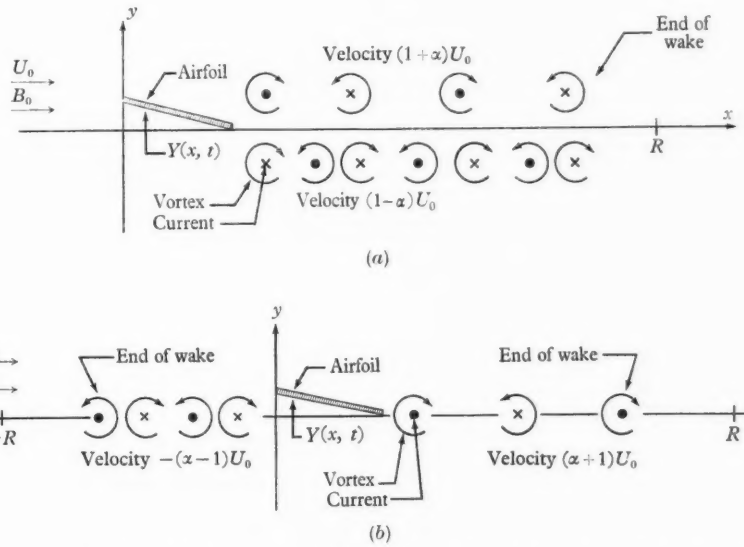

FIGURE 1. Fluid model for a lifting airfoil which has been in motion a finite time, with (*a*) $\alpha^2 < 1$, (*b*) $\alpha^2 > 1$. Wake elements have been displaced from x-axis for clarity.

The potentials are taken to be identically zero at $t = -\infty$. The magnetic and velocity potentials must satisfy equation (11) at every point in the flow field. Therefore the discontinuities must also satisfy this relation, and the current distribution $\gamma^{(2)}$ can be expressed in terms of the vortex distribution $\gamma^{(1)}$ in the same form as equation (11) (with no y dependence). The vorticity and current in the wake are expressed as

$$\gamma^{(1),(2)}(x, t) \equiv \epsilon^{(1),(2)}(x, t) \equiv \epsilon_1^{(1),(2)}(x, t) + \epsilon_2^{(1),(2)}(x, t), \tag{12}$$

where the Alfvén-wave relations are given in (10).

The circulation and total surface current are related to the distributions by

$$\Gamma^{(1),(2)}(t) = \int_0^1 \gamma^{(1),(2)}(x, t)\, dx, \tag{13}$$

where the circulation is positive in the counter-clockwise sense. The total surface current can be expressed in terms of the vortex distribution by using the current

equivalent of equation (11) in equation (13) and the functional form of the wake from equation (10). Thus we derive the result

$$\Gamma^{(2)}(t) = \int_0^1 \gamma^{(1)}(\xi, t+\xi-1)\,d\xi + \frac{1-\alpha}{\alpha}\int_{t-1}^{t} \epsilon_1^{(1)}(0^-, \eta)\,d\eta. \tag{14}$$

The first term on the right-hand side is the vortex distribution integrated in a time-lagging manner; the second is proportional to the vorticity shed from the leading edge in the previous unit of time. These indicate the general time-lagging character of the magnetic field to the velocity field.

The analogous Wagner integral equations

In classical unsteady-airfoil theory, the airfoil motion is related to the wake vorticity through the so-called Wagner integral equation. If we follow the techniques of the classical theory (e.g. von Kármán & Sears 1938), we obtain the generalization:

$$\Gamma_0^{(1)}(t) + \Gamma_k^{(1)}(t) = -\int_{\text{wake}} \epsilon^{(1)}(\xi, t)\left(\frac{\xi}{\xi-1}\right)^{\frac{1}{2}} d\xi. \tag{15}$$

Here the quasi-steady circulation is given by

$$\Gamma_0^{(1)}(t) = 2\int_0^1 \frac{DY(\xi,t)}{Dt}\left(\frac{\xi}{1-\xi}\right)^{\frac{1}{2}} d\xi, \tag{16}$$

and the airfoil surface is given by $Y(x,t)$. $\dfrac{D}{Dt} = \dfrac{\partial}{\partial t} + \dfrac{\partial}{\partial x}$ is the linearized convective derivative. $\Gamma_k^{(1)}$ represents an arbitrary circulation; if the Kutta condition is applied at the trailing edge, then $\Gamma_k^{(1)}$ is identically zero. The integration over the wake includes the forward as well as the rearward wake. It should be noted that the conservation of vorticity, equation (7), is used in the derivation of (15).

The total surface current is expressed in terms of the vortex distribution by (14). Using this, an analysis similar to that leading to equation (15) yields the result

$$\Gamma_0^{(2)}(t) + \Gamma_k^{(2)}(t) = -\int_{\text{wake}} d\xi \left\{\epsilon^{(2)}(\xi,t) - \frac{1}{\pi}\left(\frac{\xi}{\xi-1}\right)^{\frac{1}{2}} \int_0^1 \epsilon^{(1)}(\xi, t+x-1)\left(\frac{1-x}{x}\right)^{\frac{1}{2}} \frac{dx}{x-\xi}\right\}$$
$$- \frac{1-\alpha}{\alpha}\int_{t-1}^{t} \epsilon_1^{(1)}(0^-,\eta)\,d\eta, \tag{17}$$

where the quasi-steady surface current is given by

$$\Gamma_0^{(2)}(t) = -\frac{2}{\pi}\int_0^1 \left(\frac{1-x}{x}\right)^{\frac{1}{2}} dx\, \mathscr{P}\int_0^1 \frac{DY(\xi, t+x-1)}{Dt}\left(\frac{\xi}{1-\xi}\right)^{\frac{1}{2}} \frac{d\xi}{x-\xi}, \tag{18}$$

and the surface current corresponding to the arbitrary circulation is

$$\Gamma_k^{(2)}(t) = \frac{1}{\pi}\int_0^1 \Gamma_k^{(1)}(t+x-1)\,\frac{dx}{\{x(1-x)\}^{\frac{1}{2}}}. \tag{19}$$

Equation (17) is the analogue of the Wagner integral equation for current.

The problem is now reduced to the solution of the integral equations (15) and (17), with the quasi-steady terms defined by (16) and (18), with the functional form of the wake given in (10) and given some law to specify the circulation $\Gamma_k^{(1)}$ (e.g. the Kutta condition).

The lift

Consider the lift due to the vortex and current distribution over the airfoil and in the wake. Since the wake is force-free, it can introduce no net force. Divide the lift into that due to the vorticity and that due to the Lorentz force. The lift due to the Lorentz force is

$$\Delta\mathscr{L}^* = B^*\int\int j^* dx^* dy^*, \tag{20}$$

where the integral includes all current. This integration just gives the total current in the system, and, by equation (9), this is identically zero. Therefore the lift on the airfoil is equal to the force on the total vorticity in the system. The force on the vorticity can be obtained by calculating the impulse of the vortex system, as given by Kármán & Sears (1938); this gives

$$C_L(t) = \frac{\mathscr{L}^*}{\frac{1}{2}\rho^* U_0^{*2} L_0^*} = 2\frac{d}{dt}\int_{-R}^{R} (x-\tfrac{1}{2})\,\gamma^{(1)}(x,t)\,dx. \tag{21}$$

The lift is treated following the method of Kármán & Sears with modification for the change in vortex transport speeds, used by Ring (1960). The result, including arbitrary circulation and a possible forward wake, is

$$C_L(t) = A_L - 2\Gamma_0^{(1)}(t) - 2\Gamma_k^{(1)}(t) - \int_{\text{wake}} \epsilon^{(1)}(\xi,t)\left(\frac{\xi}{\xi-1}\right)^{\frac{1}{2}}\frac{d\xi}{\xi}$$
$$- 2\alpha^2\int_{\text{wake}} \epsilon^{(2)}(\xi,t)\left\{1-\frac{1}{2\xi}\right\}\left(\frac{\xi}{\xi-1}\right)^{\frac{1}{2}} d\xi, \tag{22}$$

where A_L is the lift associated with apparent mass and is given by

$$A_L \equiv 2\frac{d}{dt}\int_0^1 (x-\tfrac{1}{2})\,\gamma_0^{(1)}(x,t)\,dx. \tag{23}$$

Here $\gamma_0^{(1)}$ is the quasi-steady vortex distribution over the airfoil,

$$\gamma_0^{(1)}(x,t) = -\frac{2}{\pi}\left(\frac{1-x}{x}\right)^{\frac{1}{2}}\mathscr{P}\int_0^1 \frac{DY(\xi,t)}{Dt}\left(\frac{\xi}{1-\xi}\right)^{\frac{1}{2}}\frac{d\xi}{x-\xi}. \tag{24}$$

From equation (22), the lift can be compared to that of classical unsteady-airfoil theory. The apparent mass and the quasi-steady lift (the second term) are identical with classical theory. The third term represents the effect of an arbitrary circulation and is identically zero for a trailing-edge Kutta condition. The effect of vorticity in the wake (the fourth term) is formally the same, but is changed due to the new transport speed of vortices. The last term is new and might be called the magnetic term. The kernel of the magnetic term is seen to approach unity far from the airfoil, unlike the kernel of the wake-vorticity term which approaches ξ^{-1}. This means that the magnetic term takes into account all

current in the wake and gives a contribution even after the flow has become steady near the airfoil. In fact, it can easily be shown that the magnetic term includes the effects of surface currents in the steady solution and gives rise to the $(1-\alpha^2)$ factor of Sears & Resler (1959).

The pitching moment

As in the lift calculation, we divide the pitching moment into that due to the vorticity and that due to the currents. The pitching moment coefficient about the airfoil midchord ($x = \frac{1}{2}$), measured positive in the clockwise sense, due to the Lorentz force can be written as

$$\Delta C_m = \frac{\Delta \mathscr{M}^*}{\frac{1}{2}\rho^* U_0^{*2} L_0^{*2}} = -2\alpha^2 \int_{-R}^{R} (x-\tfrac{1}{2})\,\gamma^{(2)}(x,t)\,dx. \tag{25}$$

The current can be expressed in terms of the vorticity in a manner similar to the potential relation (11*a*), namely

$$\Delta C_m = -2\alpha^2 \int_{-R}^{R} (x-\tfrac{1}{2})\,dx \int_{-\infty}^{t} \frac{\partial \gamma^{(1)}}{\partial x}(\xi + x - t, \xi)\,d\xi. \tag{26}$$

We differentiate this with respect to time and then integrate by parts with respect to x; then, by use of (11*a*), this becomes

$$\frac{d\Delta C_m}{dt} = -2\alpha^2 \Big\{ (R-\tfrac{1}{2})\,[\gamma^{(1)}(R,t) - \gamma^{(2)}(R,t)] + (R+\tfrac{1}{2})\,[\gamma^{(1)}(-R,t) - \gamma^{(2)}(-R,t)] - \int_{-R}^{R} [\gamma^{(1)}(x,t) - \gamma^{(2)}(x,t)]\,dx \Big\}. \tag{27}$$

The first two terms on the right-hand side are zero, since they represent vorticity and current beyond the ends of the wake; the last term is the net vorticity minus the net current in the system and therefore is zero. By integration over time, the incremental pitching moment is found to be given by

$$\Delta C_m = \text{constant} = 0, \tag{28}$$

where the constant is evaluated at a time before the start of the airfoil motion. Therefore the surprising result is obtained that the pitching moment due to the total current distribution is zero. The lift due to the current is zero essentially as a consequence of the conservation law for current; however, it is not obvious why the pitching moment should have been zero.

The pitching moment due to the vorticity can be found by using impulse techniques. Again following the method of Kármán & Sears as modified by Ring, the pitching moment can be expressed as

$$C_m(t) = A_m + 2\int_0^1 (x-\tfrac{1}{2})\,\gamma_0^{(1)}(x,t)\,dx - \frac{1}{4}\int_{\text{wake}} \epsilon^{(1)}(\xi,t) \left(\frac{\xi}{\xi-1}\right)^{\frac{1}{2}} \frac{d\xi}{\xi} + 2\alpha^2 \int_{\text{wake}} \epsilon^{(2)}(\xi,t)\,\{\xi - 1 + \tfrac{1}{8}\xi^{-1}\} \left(\frac{\xi}{\xi-1}\right)^{\frac{1}{2}} d\xi, \tag{29}$$

where A_m is the pitching moment related to apparent-mass effect and is defined by

$$A_m \equiv -\frac{d}{dt}\int_0^1 [(x-\tfrac{1}{2})^2 - \tfrac{1}{8}]\,\gamma_0^{(1)}(x,t)\,dx. \tag{30}$$

The first three terms are recognized as those from classical unsteady-airfoil theory. The wake-vorticity term is formally the same but is changed because of the new transport speeds of vorticity. The last term is new and might be called the magnetic term.

As the duration of the airfoil motion becomes large, and therefore the current is far from the airfoil, it appears that the magnetic term diverges, since the integrand approaches $\xi\epsilon^{(2)}(\xi,t)$. However, that this is not actually the case can be seen by subtracting the magnetic moments due to surface current on the airfoil (expressed in terms of the wake from equations (25) and (28)). In fact, the magnetic term again gives rise to the $(1-\alpha^2)$ factor of Sears & Resler (1959).

6. Harmonic oscillations, $\alpha^2 < 1$

Calculation of wake distributions

Consider an oscillating airfoil with the upwash on the airfoil given by

$$\frac{DY(x,t)}{Dt} = g(x)\,e^{i\omega t}, \tag{31}$$

where $g(x)$ is an arbitrary function. The frequency ω is taken such that $\mathscr{R}i\omega > 0$; this corresponds to an airfoil oscillating with increasing amplitude. Clearly $\mathscr{R}i\omega$ can be put equal to zero in the final results.

Following §4, the Kutta condition is applied at the airfoil trailing edge, since $\alpha^2 < 1$. This means that $\Gamma_k^{(1)}$ must be identically zero.

The quasi-steady circulation and surface current can be expressed as

$$\Gamma_0^{(1)} = G^{(1)}e^{i\omega t}, \quad \Gamma_0^{(2)} = G^{(2)}e^{i\omega(t-\frac{1}{2})}, \tag{32}$$

where $G^{(1)}$ and $G^{(2)}$ are complex in general and are given by using equation (31) in equations (16) and (18). Thus we obtain the relations

$$G^{(1)} = 2\int_0^1 g(\xi)\left(\frac{\xi}{1-\xi}\right)^{\frac{1}{2}} d\xi, \tag{33}$$

$$G^{(2)} = -\frac{2}{\pi}\int_0^1 \left(\frac{1-x}{x}\right)^{\frac{1}{2}} e^{i\omega(x-\frac{1}{2})}\,dx\,\mathscr{P}\int_0^1 g(\xi)\left(\frac{\xi}{1-\xi}\right)^{\frac{1}{2}}\frac{d\xi}{x-\xi}. \tag{34}$$

From the functional form of the wake given in (10), the wake distributions can be written as

$$\left.\begin{aligned}\epsilon_1^{(1)}(x,t) &= \alpha\epsilon_1^{(2)}(x,t) = g_1\exp\{i\omega[t-(x-\tfrac{1}{2})/(1-\alpha)]\},\\ \epsilon_2^{(1)}(x,t) &= -\alpha\epsilon_2^{(2)}(x,t) = g_2\exp\{i\omega[t-(x-\tfrac{1}{2})/(1+\alpha)]\}.\end{aligned}\right\} \tag{35}$$

where g_1 and g_2 are complex constants to be determined. Using equations (32) and (35), equation (15) can be reduced to

$$-2G^{(1)} = g_1[K_0^{(1)} + K_1^{(1)}] + g_2[K_0^{(2)} + K_1^{(2)}], \tag{36}$$

where the integrals have been identified as Bessel functions; $K_n(z)$ is the nth-order modified Bessel function of the second kind. The superscripts are a shorthand notation to indicate the arguments, as shown below:

$$K_0^{(1)} \equiv \frac{1-\alpha}{|1-\alpha|} K_0\left(\frac{i\omega}{2|1-\alpha|}\right), \quad K_1^{(1)} \equiv K_1\left(\frac{i\omega}{2|1-\alpha|}\right), \quad K_n^{(2)} \equiv K_n\left(\frac{i\omega}{2(1+\alpha)}\right). \tag{37}$$

The factor $(1-\alpha)/|1-\alpha|$, which is unity in the present case, is included to make the definitions useful for $\alpha^2 > 1$. Similarly, equation (17) can be written as

$$-2G^{(2)} = g_1 D(\omega, \alpha) + g_2 D(\omega, -\alpha), \tag{38}$$

where D is defined by

$$D(\omega, \alpha) \equiv \frac{2}{\alpha} \exp(\tfrac{1}{2}i\omega) \int_1^\infty \exp\left\{\frac{i\omega(\xi - \frac{1}{2})}{(1-\alpha)}\right\} d\xi$$
$$-\frac{2}{\pi}\int_1^\infty \left(\frac{\xi}{\xi-1}\right)^{\frac{1}{2}} \exp\left\{-\frac{i\omega(\xi-\frac{1}{2})}{1-\alpha}\right\} d\xi \int_0^1 \left(\frac{1-x}{x}\right)^{\frac{1}{2}} \exp\{i\omega(x-\tfrac{1}{2})\} \frac{dx}{x-\xi}. \tag{39}$$

The function D has been evaluated in Ring (1960) and is

$$D(\omega, \alpha) = [J_0 - iJ_1] K_0^{(1)} + \alpha^{-1}[J_0 K_1^{(1)} + iJ_1 K_0^{(1)}], \tag{40}$$

where $J_n(z)$ is the nth-order Bessel function of the first kind. The implied arguments of J_0 and J_1 are $\frac{1}{2}\omega$. The simultaneous solution of equation (36) and (38) gives g_1 as

$$g_1 = -2G^{(1)} \frac{D(\omega, -\alpha) - G[K_0^{(2)} + K_1^{(2)}]}{D(\omega, -\alpha)[K_0^{(1)} + K_1^{(1)}] - D(\omega, \alpha)[K_0^{(2)} + K_1^{(2)}]}, \tag{41}$$

where

$$G \equiv G^{(2)}/G^{(1)}. \tag{42}$$

The constant g_2 is given by taking $\alpha \to -\alpha$ in the expression for g_1. This essentially represents the solution of the flow, since the lift, pressure distribution, etc., can easily be expressed in terms of $G^{(1),(2)}$ and $g_{1,2}$.

Force calculations

The lift has been given in equation (22); with the use of (35) and (41), this can be reduced to

$$C_L(t) = A_L - 2\Gamma_0^{(1)}(t)\, T(\tfrac{1}{2}i\omega, \alpha), \tag{43}$$

where

$$T(\tfrac{1}{2}i\omega, \alpha) \equiv \frac{(1-\alpha) K_1^{(1)}\{D(\omega, -\alpha) - G[K_0^{(2)} + K_1^{(2)}]\} - (1+\alpha) K_1^{(2)}\{D(\omega, \alpha) - G[K_0^{(1)} + K_1^{(1)}]\}}{D(\omega, -\alpha)[K_0^{(1)} + K_1^{(1)}] - D(\omega, \alpha)[K_0^{(2)} + K_1^{(2)}]}. \tag{44}$$

$T(\frac{1}{2}i\omega, \alpha)$ is the so-called Theodorsen function of classical unsteady-airfoil theory, modified to include the magnetic effects. (It should be noted that ω is the reduced frequency based on the full chord, as opposed to the usual practice of basing it on the semi-chord.) The most important change in the Theodorsen function is the appearance of G. Thus, while the classical Theodorsen function depends only on frequency, the modified Theodorsen function depends upon the mode of oscillation (and on α) as well.

In a manner similar to the life calculation, the pitching-moment is found to be

$$C_m(t) = A_m + \int_0^1 (2x-1)\,\gamma_0^{(1)}(x,t)\,dx + \tfrac{1}{2}\Gamma_0^{(1)}(t)\,S(\tfrac{1}{2}i\omega,\alpha) \tag{45}$$

where

$$S(\tfrac{1}{2}i\omega,\alpha) \equiv \frac{\begin{array}{l}(1-\alpha)\,[K_0^{(1)} - (4\alpha/i\omega)\,K_1^{(1)}]\,[D(\omega,-\alpha) - G\{K_0^{(2)} + K_1^{(2)}\}] \\ -(1+\alpha)\,[K_0^{(2)} + (4\alpha/i\omega)\,K_1^{(2)}]\,[D(\omega,\alpha) - G\{K_0^{(1)} + K_1^{(1)}\}]\end{array}}{D(\omega,-\alpha)\,[K_0^{(1)} + K_1^{(1)}] - D(\omega,\alpha)\,[K_0^{(2)} + K_1^{(2)}]}. \tag{46}$$

The function $S(\frac{1}{2}i\omega,\alpha)$ includes the wake and all magnetic effects. The appearance of G again shows that the function is not universal but depends upon the mode of oscillation considered.

Three G's are of particular interest, namely,

$$G_{\mathrm{I}} = J_0 - iJ_1, \quad G_{\mathrm{II}} = 4J_1/\omega, \quad G_{\mathrm{III}} = \tfrac{1}{2}[J_0 - iJ_1] + 2J_1/\omega. \tag{47}$$

Case I corresponds to vertical airfoil oscillations, case II to a downwash linear about the mid-chord, case III to a downwash distribution linear about the quarter-chord. The first two are of interest because of their mathematical simplicity, the last because of a special high-frequency property which will become apparent later.

Low-frequency limit

The low-frequency expansions of T and S are obtained by expanding G in a power series and by using the small-argument Bessel-function expansions. After straightforward but lengthy algebraic manipulation, the force coefficients are found to be

$$\begin{aligned} C_L(t) = {} & (1+\alpha^2)\,A_L - 2\Gamma_0^{(1)}(t)\,\{(1-\alpha^2) + \tfrac{1}{2}(1+\alpha^2)\,i\omega\ln\tfrac{1}{4}\omega + \tfrac{1}{2}[(1+\alpha^2) \\ & \times \{\gamma + \tfrac{1}{2}i\pi - \tfrac{1}{2}\ln(1-\alpha^2)\} + \alpha\ln(1+\alpha)/(1-\alpha)]\,i\omega + O(\tfrac{1}{16}\omega^2\ln^2\tfrac{1}{4}\omega)\}, \end{aligned} \tag{48}$$

$$C_m(t) = A_m + (1-\alpha^2)\int_0^1 (2x-1)\,\gamma_0^{(1)}(x,t)\,dx - \tfrac{1}{2}\Gamma_0^{(1)}(t)\,\{\tfrac{1}{2}(1+\alpha^2)\,i\omega\ln\tfrac{1}{4}\omega + O(\omega)\}. \tag{49}$$

The apparent-mass term is included in the pitching-moment although it is of order ω and some terms of order ω have been neglected.

The first thing to note from these expressions is that as $\omega \to 0$ the force coefficients become $(1-\alpha^2)$ times the values for non-magnetic flow in agreement with the Sears–Resler result. The coefficient of the $(\omega\ln\omega)$ term is increased by the factor $(1+\alpha^2)$; the coefficient of ω is also increased because of magnetic effects. Thus, although the steady forces are reduced by a factor $(1-\alpha^2)$, there is a general tendency for the unsteady contribution to be increased by the magnetic effects.

The limit $\alpha \to 0$

Taking the limit $\alpha \to 0$ (i.e. the magnetic field approaching zero), it is seen that

$$T(i\omega,\alpha) = \frac{K_1(i\omega)}{K_0(i\omega) + K_1(i\omega)} + O(\alpha^2), \tag{50}$$

and

$$S(i\omega,\alpha) = \frac{K_0(i\omega)}{K_0(i\omega) + K_1(i\omega)} + O(\alpha^2). \tag{51}$$

These limiting forms are identical with classical theory. The coefficient of the α^2 terms can be obtained; however, it turns out that the frequency dependence is of such a complicated nature as to yield little information.

High-frequency limit

As $\omega \to \infty$, it is convenient to represent G by an asymptotic expansion of the form

$$G \sim \left(\frac{4i}{\pi\omega}\right)^{\frac{1}{2}} e^{-\frac{1}{2}i\omega}\left\{\hat{G} + \frac{1}{i\omega}[-i\,e^{i\omega}\hat{\hat{G}}^{+} + \hat{\hat{G}}^{-}] + \ldots\right\}. \tag{52}$$

Using this expansion of G, the asymptotic expansion of T is

$$T(\tfrac{1}{2}i\omega, \alpha) \sim \tfrac{1}{2} \pm \tfrac{1}{2}i\alpha^2(1-2\hat{G})\,e^{-i\omega} + (4i\omega)^{-1}\{1 + 2\alpha^2 - 4\alpha^2\hat{\hat{G}}^{+} \pm i\alpha^2[1 - 5\hat{G} - 4\hat{\hat{G}}^{-}]\,e^{-i\omega} + \alpha^4(1-2\hat{G})\,e^{-2i\omega}\} + \ldots. \tag{53}$$

This expansion is valid for $-\pi \leqslant \arg\omega \leqslant 0$; the top sign is to be used for $\arg i\omega > 0$ and the bottom sign for $\arg i\omega < 0$. The expansion of S is similar. For $\alpha = 0$, T is asymptotic to the constant $\frac{1}{2}$, as is known from classical theory. However, the general case represents a decidedly different behaviour. If viewed in the complex plane, as ω becomes large (and real), T describes a circle of radius $\frac{1}{2}\alpha^2(1-2\hat{G})$ about the point $\frac{1}{2}$. It approaches this circle in an oscillating manner, as seen from the second term in the expansion. Thus, while the steady-flow theories of Lary (1960) and of Sears & Resler (1959) predict small forces in the neighbourhood of $\alpha = 1$, the present theory predicts large forces due to unsteady effects.

Case III (equation (47)) has the special property that $(1-2\hat{G}) = 0$; in fact, it is the only linear downwash distribution to have this property. The reason why this is true will be pointed out in the discussion of the Wagner problem (§ 7).

The limit $\alpha \to 1$

There is some question as to the validity of the solution for $\alpha = 1$ (e.g., the Kutta condition). However, the limiting solution is of interest since it will shed some light on the solution for α near but not equal to unity. For $\alpha \to 1^{-}$, we obtain

$$T(\tfrac{1}{2}i\omega, 1^{-}) = K_1^{(2)}\frac{J_0 - G}{J_0 K_1^{(2)} + iJ_1 K_0^{(2)}}, \tag{54}$$

$$S(\tfrac{1}{2}i\omega, 1^{-}) = T(\tfrac{1}{2}i\omega, 1^{-})\left[\frac{K_0^{(2)}}{K_1^{(2)}} + \frac{4}{i\omega}\right]. \tag{55}$$

The behaviour of these functions for large frequencies is similar to the general case, except that the radius of the asymptotic circle has been maximized. It is not valid to take the limit $\omega \to 0$ in these functions, since for α near unity we required that $1 \ll (\omega R_m)^{\frac{1}{2}}$ (§ 3). However, for large R_m, ω can be quite small. Thus we can consider small frequencies, keeping in mind the physical requirement that ω must be positive. Using the low-frequency expansions of equations (54) and (55), the force coefficients are

$$C_L(t) = 2A_L + O(\omega^2), \quad Cm(t) = O(\omega). \tag{56}$$

Thus for low frequencies and α near unity, the forces on the airfoil are small.

The circulation for $\alpha \to 1^-$ and small ω is

$$\Gamma^{(1)}(t) = -\tfrac{1}{4}i\omega \int_0^1 (2x-1)\,\gamma_0^{(1)}(x,t)\,dx\,[1+O(\omega)], \tag{57}$$

so that the circulation is small. For zero circulation, the flow pattern must correspond to classical hydrodynamic flow with a relaxed Kutta condition. Therefore the flow pattern approached by taking $\omega \to 0$ with $\alpha = 1^-$ has zero lift with zero circulation, as opposed to the limit in the Sears–Resler theory (and in the present theory), $\alpha \to 1$, with $\omega = 0$, which gives zero lift with $\Gamma^{(1)} \neq 0$. Following §3, both limits may be valid for $R_m = \infty$, with neither valid for $R_m < \infty$. However the former limit can be approached to any desired degree of accuracy by taking R_m arbitrarily large but finite.

7. The Wagner problem, $\alpha^2 < 1$

Formulation of problem

The classical problem of the response to an instantaneous change in the downwash distribution on a thin airfoil is referred to as the 'Wagner problem'. The downwash for this case may be represented by

$$\frac{DY(x,t)}{Dt} = g(x)\mathrm{H}(t), \tag{58}$$

where $\mathrm{H}(t)$ is the unit-step function defined by

$$\mathrm{H}(t) = \begin{cases} 0, & t < 0, \\ 1, & t > 0. \end{cases}$$

The downwash of equation (58) can be obtained by Fourier superposition from equation (31). Similarly, all quantities from the harmonic-oscillation solution may be superimposed to give the corresponding quantities caused by the instantaneous change of downwash.

The quasi-steady circulation is obtained from equation (32) as

$$\Gamma_0^{(1)}(t) = G^{(1)}\mathrm{H}(t) \tag{59}$$

The lift, obtained from equation (43) is

$$C_L(t) = \delta(t)\int_0^1 (2x-1)\,\gamma_0^{(1)}(x,0^+)\,dx - 2\Gamma_0^{(1)}(t)\,W(t,\alpha), \tag{60}$$

where

$$W(t,\alpha) \equiv \frac{1}{2\pi i}\int_{x_0-i\infty}^{x_0+i\infty} T(\tfrac{1}{2}s,\alpha)\frac{e^{st}}{s}\,ds, \tag{61}$$

and $\delta(t)$ is the Dirac delta function. The integral has been expressed as a Laplace-transform by taking $s = i\omega$ and x_0 to lie to the right of any singularities. The apparent mass has given an impulse lift at $t = 0$; the lift at later times is all due to the modified Wagner function $W(t,\alpha)$. Let us confine our attention to this function.

$W(t, \alpha)$ for small times

The standard method of obtaining the behaviour of W for small times is to obtain the asymptotic expansion of T for $s \to \infty$, and then relate this to the asymptotic expansion of W for $t \to 0$. The expansion of $T(\frac{1}{2}s, \alpha)$ for $s \to \infty$ is given in equation (53) and contains exponential terms. It has been shown by Ring (1960) that the e^{-s} terms give a contribution like $\exp(-1/t)$ for small times. Therefore, using known results (e.g. Doetsch 1950), the expansion of W for small times is given, from equations (61) and (53), as

$$W(t, \alpha) = \tfrac{1}{2} + (\tfrac{1}{4} + \tfrac{1}{2}\alpha^2 - \alpha^2 \hat{\hat{G}}^+)\, t + O(t^2). \tag{62}$$

The first term in W remains equal to $\frac{1}{2}$, unaffected by the magnetic field. The first magnetic effects are proportional to time and, since $\hat{\hat{G}}^+$ has appeared, depend upon the downwash distribution considered.

The result given in equation (62) will be valid even for small R_m, provided the time is taken so small that the current is still restricted to a thin layer. Following §3, this will be true for $t \leqslant 10^{-2} R_m$, where the limit on the current-penetration depth has arbitrarily been taken as $\delta_m = 10^{-1}$.

The logarithmic singularity

From the asymptotic expansion (53), it is seen that convergence of the integral in equation (61) is obtained for all time except at $t = 1$ where e^{st} balances the factor e^{-s} and gives rise to a logarithmic singularity. By extracting the coefficient of the singularity, W is found to be given by

$$W(t, \alpha) = -\tfrac{1}{2}\pi^{-1}\alpha^2(1 - 2\hat{G}) \ln|t - 1| + O(1). \tag{63}$$

This represents a marked change from the classical Wagner function, which has no singularities. The singularity is seen to arise from the high-frequency oscillating behaviour of T; having connected these phenomena, it is now possible to examine their origin.

The logarithmic singularity in W appears at time $t = 1$. At $t = 1$, the fluid at the trailing edge is that which was at the leading edge when the downwash was changed. Thus we are led to the examination of the flow near the leading edge at high frequencies. A calculation of the vortex distribution yields

$$\gamma^{(1)}(x, t) = -\pi^{-1}\Gamma_0^{(1)}(t)\{(1 - x)/x\}^{\frac{1}{2}}\{(1 - 2\hat{G}) + O(1/\omega) + O(x)\}. \tag{64}$$

Thus the coefficient of the high-frequency oscillations of $T(\frac{1}{2}i\omega, \alpha)$, the coefficient of the logarithmic singularity of $W(t, \alpha)$, and the coefficient of the leading-edge vortex singularity at high frequencies all contain the factor $(1 - 2\hat{G})$. Thus it appears that the leading-edge vortex singularity interacts with the magnetic field to produce the observed behaviour of T and W.

$W(t, \alpha)$ for large times

The asymptotic expression of T valid for $|\arg s| < \pi$ is

$$T(\tfrac{1}{2}s, \alpha) \sim \frac{1}{2}\,\frac{1 \pm i\alpha^2(1 - 2\hat{G})\, e^{-s}}{1 \pm \frac{1}{2}i\alpha^2 s^{-1} e^{-s}}. \tag{65}$$

By setting the denominator equal to zero, $T(\frac{1}{2}s, \alpha)$ is found to have infinitely many simple poles to the left of, and bounded away from, the imaginary $s-$ axis.

It is shown by Ring (1960) that the integration in equation (61) along C_3 and C_4 (figure 2) is $o(1)$ as $n \to \infty$ for $t > 1$. Therefore (61) can be written as

$$W(t, \alpha) = \frac{1}{2\pi i} \int_{C_2} \frac{e^{st}}{s} T(\tfrac{1}{2}s, \alpha)\, ds + \Sigma \operatorname{Res} \left(T(\tfrac{1}{2}s, \alpha) \frac{e^{st}}{s} \right), \tag{66}$$

where the summation is to be made over all poles to the right of C_2. The summation can be shown to converge for $t > 1$, by using the asymptotic formulation at the poles.

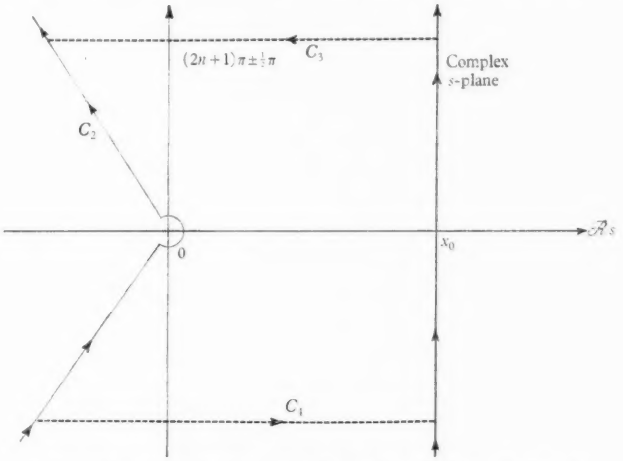

FIGURE 2. Integration contours in the evaluation of $W(t, \alpha)$.

It is now assumed that $T(\frac{1}{2}s, \alpha)$ has no poles for $\mathscr{R}s \geqslant 0$, i.e. that there are no unstable or neutrally stable solutions with $\Gamma_0^{(1)} \equiv 0$. By using the expansion of T for small s, the integral in equation (66) for large times can be given directly (e.g. Doetsch 1950). Hence,

$$W(t, \alpha) = (1-\alpha^2) - \tfrac{1}{2}(1+\alpha^2) t^{-1} + \ldots. \tag{67}$$

The summation term in equation (66) does not contribute under the asumption that there are no poles for $\mathscr{R}s \geqslant 0$ and because the effect of any poles with $\mathscr{R}s < 0$ (which do in fact exist) is exponentially small. In this connexion, it should be recalled that these poles are bounded away from the imaginary axis.

Equation (67) is seen to reduce to the classical case for $\alpha^2 = 0$. As time goes to infinity, the solution approaches the Sears–Resler solution; the time to reach the steady solution is increased by the factor $(1+\alpha^2)$. This effect might be expected in view of the lagging of the magnetic field.

8. Flow with $\alpha^2 > 1$

General relations

The theory for general unsteady-airfoil motion has been formulated in §5 in terms of an arbitrary circulation $\Gamma_k^{(1)}$, where $\Gamma_k^{(1)}$ is zero for a trailing-edge Kutta condition. For $\alpha^2 > 1$, the Kutta condition is not directly applicable; also,

the proper extension is not obvious, as noted in §4. Without a law to specify $\Gamma_k^{(1)}$, the flow cannot be determined uniquely. However, some general information regarding the stability of the flow can be obtained. For this purpose it is convenient to express $\Gamma_k^{(1)}$ in terms of the leading- and trailing-edge singularity strengths.

Let us introduce the ratio, β, of $\Gamma_k^{(1)}(t)$ to the other part of the circulation, i.e.

$$\Gamma_k^{(1)}(t) = -\beta\left\{2\int_0^1 \frac{DY(\xi,t)}{Dt}\frac{d\xi}{\xi^{\frac{1}{2}}(1-\xi)^{\frac{1}{2}}} + \int_{\text{wake}} \epsilon^{(1)}(\xi,t)\left(\frac{\xi}{\xi-1}\right)^{\frac{1}{2}}\frac{d\xi}{\xi}\right\}. \tag{68}$$

It is easily shown that

$$\frac{\gamma^{(1)}(1^-,t)}{\gamma^{(1)}(0^+,t)} = \frac{\text{trailing-edge singularity strength}}{\text{leading-edge singularity strength}} = \frac{-\beta}{1-\beta}, \tag{69}$$

so that β is a measure of the relative singularity strengths. $\beta = 0$ corresponds to a trailing-edge Kutta condition and $\beta = 1$ corresponds to a leading-edge Kutta condition. It seems reasonable to restrict β to the range $0 \leqslant \beta \leqslant 1$, since β outside this range corresponds to 'supercirculation.' This will be done here although it is not a critical assumption for the analysis.

Harmonic oscillation

Consider an oscillating airfoil with the upwash as given by equation (31). Then the quasi-steady quantities and wake distributions can again be represented as in equations (32) to (35). Using these, the analogous Wagner integral equations, (15) and (17), are treated in a manner similar to that leading to (36) and (38). The difference is that the integration over ϵ_1 is forward of the airfoil; this has the net effect of changing the sign of the K_0 terms as indicated in the definitions (37). These results can be reduced to

$$-2G^{(1)} - 2\beta G_k^{(1)} = g_1[(1-2\beta)K_0^{(1)} + K_1^{(1)}] + g_2[(1-2\beta)K_0^{(2)} + K_1^{(2)}], \tag{70}$$

$$-2G^{(2)} - 2\beta J_0 G_k^{(1)} = g_1 D_\beta(\omega,\alpha) + g_2 D_\beta(\omega,-\alpha), \tag{71}$$

where $\beta G_k^{(1)}$ corresponds to the quasi-steady contribution of equation (68),

$$G_k^{(1)} = -2\int_0^1 g(\xi)\frac{d\xi}{\xi^{\frac{1}{2}}(1-\xi)^{\frac{1}{2}}}, \tag{72}$$

and the function D (see (40)) is modified to include the wake effects associated with β, giving

$$D_\beta(\omega,\alpha) = [(1-2\beta)J_0 - iJ_1]K_0^{(1)} + \alpha^{-1}[J_0 K_1^{(1)} + iJ_1 K_0^{(1)}]. \tag{73}$$

The lift and pitching moment can be given in a form similar to equations (43) and (45). This will not be carried out in detail here; rather, let us turn our attention to the stability of the flow.

Stability of the flow

For a given airfoil motion and a given β, the wake intensities g_1 and g_2 are given by the solution of equations (70) and (71), provided the determinant of the coefficients does not vanish. If the determinant vanishes, then there is an eigensolution, i.e. there is a solution with $g(x) \equiv 0$ but $g_{1,2} \neq 0$. Let us look for such solutions.

The determinant of the coefficients of g_1 and g_2 in equations (70) and (71) is

$$\begin{vmatrix} (1-2\beta)K_0^{(1)}+K_1^{(1)} & (1-2\beta)K_0^{(2)}+K_1^{(2)} \\ D_\beta(\omega,\alpha) & D_\beta(\omega,-\alpha) \end{vmatrix} \sim 4\left\{\frac{(1-\alpha^2)\pi}{i\omega^3}\right\}^{\frac{1}{2}} \exp\left\{\tfrac{1}{2}i\omega\left(1+\frac{2\alpha}{1-\alpha^2}\right)\right\}$$

$$\times\left\{-\beta\frac{\alpha+1}{\alpha}+(1-\beta)\frac{\alpha-1}{\alpha}\,i\,e^{-i\omega}+\frac{1}{4i\omega}\left(-2\beta\alpha-\frac{(2-\beta)(\alpha-1)}{\alpha}\right.\right.$$

$$\left.\left.+\left[2\alpha(1-\beta)-\frac{(1+\beta)(\alpha+1)}{\alpha}\right]i\,e^{-i\omega}\right)+\ldots\right\}, \qquad (74)$$

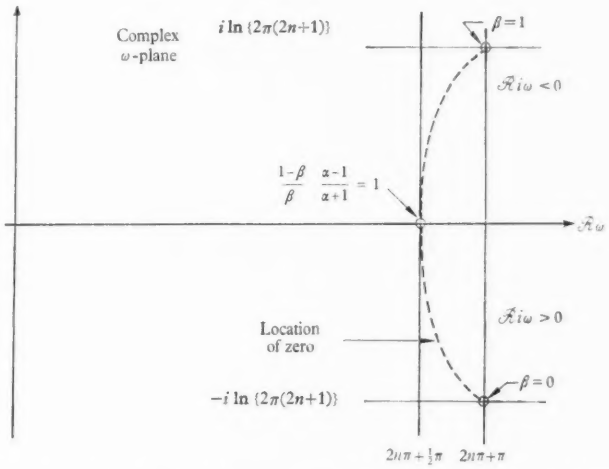

FIGURE 3. Location of an eigen-value, corresponding to a given positive integer n, in the complex ω-plane as a function of α and β. $\beta = 0$ corresponds to a trailing-edge Kutta condition; $\beta = 1$ to a Kutta condition applied at the leading-edge.

where the asymptotic expansion is valid for $|\arg\omega| < \pi$. The zeros of the determinant for large frequencies can be found by equating the largest terms in the expansion. If $0 < \beta < 1$, then we take

$$-\beta(\alpha+1)+(1-\beta)(\alpha-1)\,i\,e^{-i\omega}=0$$

which gives zeros at

$$\mathscr{R}\omega = 2\pi n+\tfrac{1}{2}\pi, \quad \mathscr{R}i\omega = \ln\{(1-\beta)(\alpha-1)/\beta(\alpha+1)\}, \qquad (75)$$

where n is a large positive integer. Continuing this analysis, it is found that a given pole will move as shown in figure 3, as β goes from 0 to 1. A similar analysis shows that there is another set of poles which corresponds to reflexion about the imaginary ω-axis in figure 3.

Therefore the determinant of equation (74) has infinitely many zeros, with corresponding eigen-solutions. For $\mathscr{R}i\omega > 0$, the solutions diverge exponentially. Thus, whenever

$$\beta(\alpha+1)/(1-\beta)(\alpha-1) < 1, \qquad (76)$$

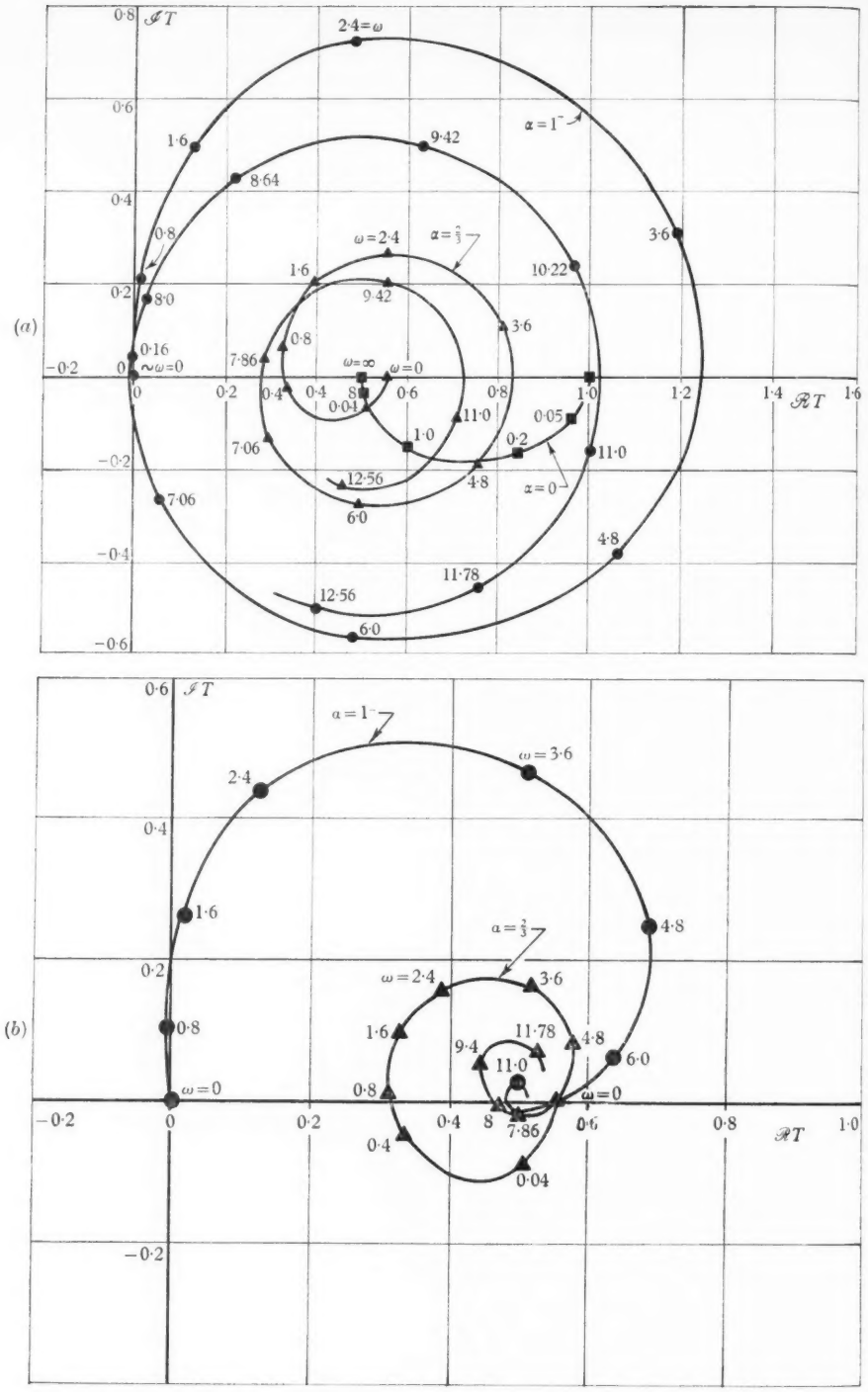

FIGURE 4(*a*). The modified Theodorsen function, $T(\frac{1}{2}i\omega, \alpha)$, for vertical oscillations, case I. This is typical of the general case. (*b*) The modified Theodorsen function, $T(\frac{1}{2}\omega, \alpha)$, for the case of a downwash distribution linear about the airfoil quarter-chord, case III. This is the special case in which the function is not asymptotic to a circle.

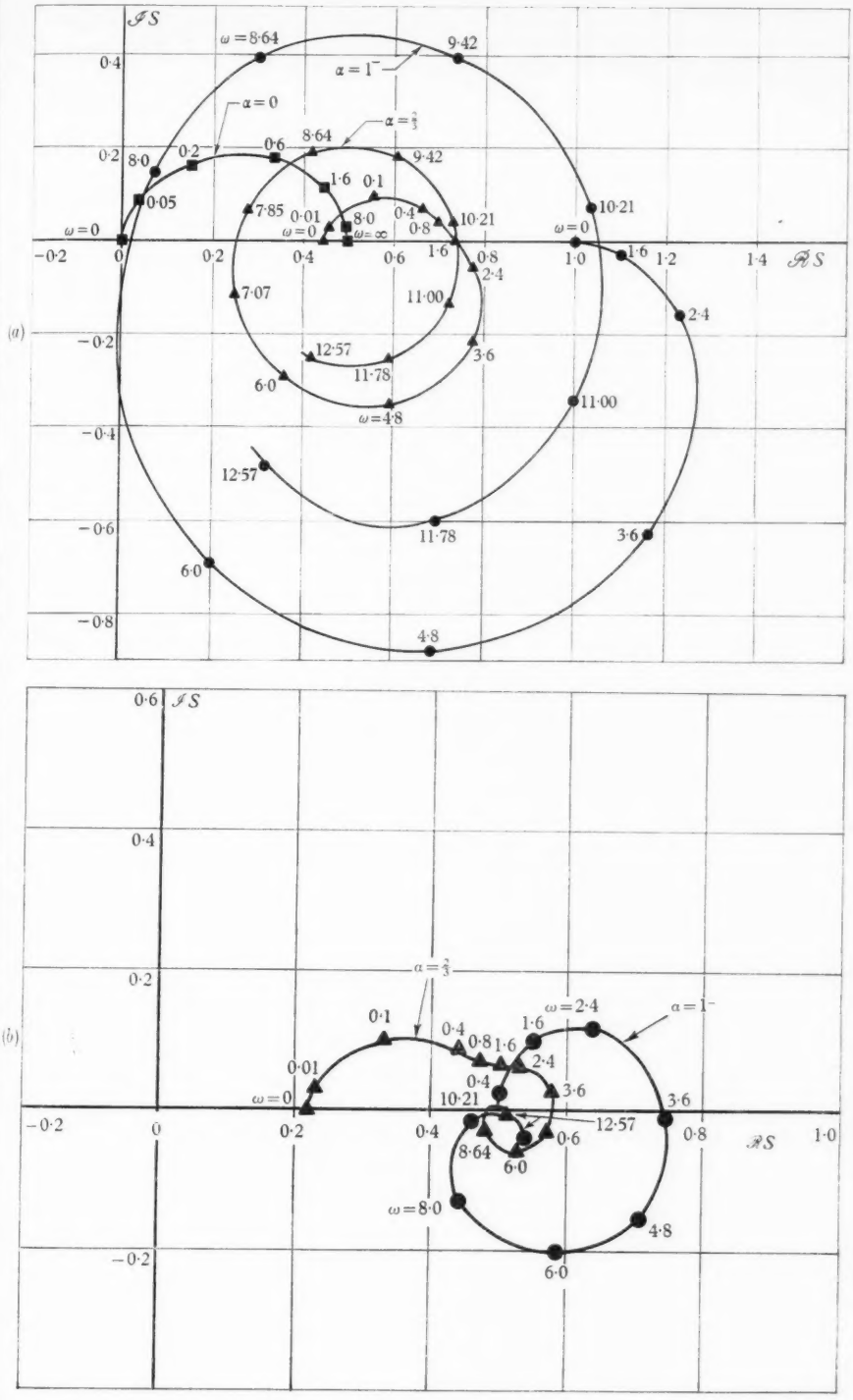

FIGURE 5(*a*). The function $S(\frac{1}{2}i\omega, \alpha)$ for vertical oscillation, case I. (*b*) The function $S(\frac{1}{2}i\omega, \alpha)$ for a downwash distribution linear about the airfoil quarter-chord, case III.

there will be diverging eigen-solutions and the flow will be unstable. Using (69), this criterion can be written as†

$$\left| \frac{\text{Trailing edge singularity strength}}{\text{Leading edge singularity strength}} \times \frac{\text{Rear wake speed}}{\text{Forward wake speed}} \right| < 1. \qquad (77)$$

We conclude, from this brief study of flow with $\alpha^2 > 1$, that steady flow must be unstable when the criterion stated in (76) and (77) is satisfied. It appears that under these conditions the vortices that move forward and rearward are capable of interacting in such a way as to induce a diverging oscillatory circulation about the stationary airfoil. Presumably such oscillation would continue until violent separation (stalling) occurs, invalidating the assumptions of the present theory.

On the other hand, it is conceivable that the resultant effect of viscosity and electrical resistance in a real fluid, when $\alpha^2 > 1$, is to enforce an effective Kutta condition at the leading, rather than at the trailing, edge. This possibility is suggested by the studies of Lary (1960), Lewellen (1959), Greenspan & Carrier (1959), and Hasimoto (1959) (all of which pertain, however, to steady flow). If this occurs, criterion (76) may not be satisfied, and we cannot conclude here that the flow is unstable. It seems clear that further study in this area must await clarification of the roles of viscous and magnetic boundary layers and separation in fixing the circulation about cylindrical bodies.

9. Conclusions

The main conclusion to be drawn from this work is that unsteady effects become more important as the magnetic field strength increases. The steady-flow theories of Lary (1960) and of Sears & Resler (1959) predict small forces for α^2 near unity; the present theory predicts large forces due to unsteady effects. In fact, figures 4 and 5 show that at moderate frequencies the forces may be larger than in the corresponding non-magnetic case.

For $\alpha^2 > 1$, there is a definite possibility that the flow will be unstable, i.e., that no steady solution exists. In particular, if the boundary layers (magnetic and/or viscous) act in such a way as to remove the trailing-edge singularity, the flow will be unstable.

This research was partially supported by the United States Air Force under Contract AF 49(638)-544, monitored by the Office of Scientific Research, Air Research and Development Command.

REFERENCES

Doetsch, G. 1950 *Handbuch der Laplace-Transforms.* Basel: Verlag Birkhauser.

Greenspan, H. P. & Carrier, G. F. 1959 The magnetohydrodynamic flow past a flat plate. *J. Fluid Mech.* **6**, 77.

Hasimoto, H. 1959 Viscous flow of a perfectly conducting fluid with a frozen magnetic field. *Phys. Fluids*, **2**, 337.

† It is interesting to examine the relative wake intensities for the eigen-solutions. This has been carried out, using the asymptotic form of (70) together with (35). It is found that the vortex flux leaving the leading edge is larger than the vortex flux leaving the trailing edge in all the unstable eigen-solutions.

KÁRMÁN, TH. VON & SEARS, W. R. 1938 Airfoil theory for non-uniform motion. *J. Aero. Sci.* **5**, 379.

LARY, E. C. 1960 A theory of thin airfoils and slender bodies in fluids of arbitrary electrical conductivity. Ph.D. Thesis, Cornell University. (Available from University Microfilms, Inc., Ann Arbor, Michigan.)

LEWELLEN, W. S. 1959 An inviscid boundary layer of magnetohydrodynamics. M. Aero. Engng Thesis, Cornell University. (Also published as AFOSR-TN-59-927.)

RESLER, E. L. & SEARS, W. R. 1958 The prospects for magneto-aerodynamics. *J. Aero. Sci.* **25**, 235.

RING, L. E. 1960 Unsteady magnetohydrodynamic flow about thin airfoils, Ph.D. Thesis, Cornell University. (Available from University Microfilms, Inc., Ann Arbor, Michigan.)

SEARS, W. R. 1956 Some recent developments in airfoil theory. *J. Aero. Sci.* **23**, 490.

SEARS, W. R. & RESLER, E. L. 1959 Theory of thin airfoils in fluids of high electrical conductivity. *J. Fluid Mech.* **5**, 257.

STEWARTSON, K. 1960 On the motion of a non-conducting body through a perfectly conducting fluid. *J. Fluid Mech.* **8**, 82.

Notes on approximations for turbulent flows with large temperature differences

By D. J. TRITTON

Department of Aeronautical Engineering, Indian Institute of Science, Bangalore

(Received 23 August 1960 and in revised form 5 May 1961)

(i) The diffusion terms in the mean velocity and temperature equations of turbulent flow are analysed to decide when variations of fluid properties can produce appreciable errors.

(ii) A theoretical demonstration is given that in the mean-flow continuity equation for a gas the error in assuming constant density is small if the flow is turbulent, even when the temperature variations are large.

(iii) Separate discussion is given of the case of local heat sources in turbulence, as large errors can occur there.

1. Introduction

In theoretical work on low-speed flows with temperature variations it is common to suppose that all temperature differences are small enough for changes in fluid properties to be neglected. In experimental work the supposition is frequently not fulfilled. In gas flows, in particular, temperature differences may well be insufficiently small compared with the absolute temperature for density variations to have no effect. In any fluid, variations of viscosity and thermal conductivity may be sizable. These notes consider, for turbulent flows, some aspects of the errors so caused. They do not give corrections—the complexity of the accurate equations precludes that—but discuss the magnitude of the errors for cases in which some analysis is necessary before this can be properly estimated. It might be thought, for instance, that for mean flows, where the direct action of molecular effects is negligible, temperature variation of viscosity would not matter, but this is seen in § 2 to be fallacious. Then, in §§ 3 and 4, attention is drawn to a respect in which theory fails less than would appear at first sight and also to a situation in which there is particular danger of large errors.

The notation is standard. An overbar ($^-$) indicates a mean value and ($'$) the difference between the instantaneous value and the mean value.

The estimation of errors is just a matter of writing the relative sizes of retained and neglected terms in terms of temperature, velocity, and length scales. During this procedure, it must be noted that there are two temperature scales (and, correspondingly, two density scales); the scale of $\overline{T}$ is that of the absolute temperature T_0, whereas that of T', or of $\overline{T}$ when it appears as a gradient, is ΔT, the difference between extremes of temperature. Strictly, a further distinction should be made between these last two and, similarly, between the scales of mean and fluctuating velocities, but this is left out of account; otherwise it is necessary

to present the analysis somewhat differently for different flows; the distinctions are unimportant in the end. The use of a single velocity scale, U, further does not allow for flows such as a wake in which the mean velocity difference has a smaller scale than the mean velocity, but it can be shown that the situations in which the results are different are of no physical importance. For length scales we distinguish between longitudinal gradients having scale L and transverse gradients having scale δ, as the results are of interest mainly for boundary-layer-type flows. (These apply, of course, to gradients of mean quantities; we shall be meeting a turbulence length scale in § 2.)

2. Mean velocity and temperature equations with variable fluid properties

Consider the term

$$A = \overline{\frac{\partial}{\partial x_i}\left(\mu \frac{\partial u_j}{\partial x_i}\right)}$$

in the mean velocity equation. If μ varies with temperature,

$$A = \underset{B}{\overline{\mu \frac{\partial^2 u_j}{\partial x_i^2}}} + \underset{C}{\overline{\frac{d\mu}{dT}\frac{\partial T}{\partial x_i}\frac{\partial u_j}{\partial x_i}}}.$$

C will behave, at least so far as the subsequent order of magnitude analysis is concerned, similarly to

$$\alpha \frac{\mu}{T}\overline{\frac{\partial T}{\partial x_i}\frac{\partial u_j}{\partial x_i}}, \quad \text{where} \quad \alpha = \frac{T}{\mu}\frac{d\mu}{dT}\,(\text{a function of } T).$$

Now

$$\overline{\frac{\partial T}{\partial x_i}\frac{\partial u_j}{\partial x_i}} = \frac{\partial \overline{T}}{\partial x_i}\frac{\partial \overline{u}_j}{\partial x_i} + \overline{\frac{\partial T'}{\partial x_i}\frac{\partial u_j'}{\partial x_i}},$$

and the length scale of the second part is a turbulent, not a mean flow, one. Consequently A can be much larger when μ is variable than when it is constant. In fact $C \simeq \alpha\mu\Delta T U/T_0\lambda^2$, where λ is the dissipation-length parameter. [There are two assumptions involved in this stage. First, no distinction is being made between the kinetic energy and $\overline{T'^2}$ dissipation-length parameters. Hence the argument as it stands does not cover the case of Prandtl number very different from 1, though it could be modified to do so (nor is the configuration considered in § 4 covered by this). Secondly, it is assumed that the correlation

$$R = \overline{\frac{\partial T'}{\partial x_i}\frac{\partial u_j'}{\partial x_i}} \Big/ \left\{\left(\overline{\frac{\partial T'}{\partial x_i}}\right)^2 \left(\overline{\frac{\partial u_j'}{\partial x_i}}\right)^2\right\}^{\frac{1}{2}}$$

(summation convention not applying here) is appreciable for at least some components. The condition for it to be so may be inferred from the equation

$$\frac{\partial}{\partial t}(\overline{u_j'T'}) + \overline{u_i'u_j'}\frac{\partial \overline{T}}{\partial x_i} + \overline{u_i'T'}\frac{\partial \overline{u}_j}{\partial x_i} + \overline{u}_i\frac{\partial}{\partial x_i}(\overline{u_j'T'}) + \frac{\partial}{\partial x_i}(\overline{u_i'u_j'T'}) + \frac{1}{\rho}\overline{T'\frac{\partial p'}{\partial x_j}}$$
$$-\kappa\overline{u_j'\frac{\partial^2 T'}{\partial x_i^2}} - \nu\overline{T'\frac{\partial^2 u_j'}{\partial x_i^2}} \,(+\text{further terms if buoyancy forces are significant}) = 0. \tag{1}$$

(That this is the constant fluid property form does not matter for the present considerations.) This represents the balance of a component of the temperature flux (see Ellison 1957, § 6 and, in particular, equations (16) and (19) for an example of this). The seventh and eighth terms indicate molecular effects on this balance; they are at least partly dissipative, the second, third, and perhaps the buoyancy force terms being the corresponding productive ones. Now these two molecular terms are closely related to the correlation under consideration, at least when the Prandtl number is near 1, because

$$\overline{u_j' \frac{\partial^2 T'}{\partial x_i^2}} + \overline{T' \frac{\partial^2 u_j'}{\partial x_i^2}} = \frac{\partial^2}{\partial x_i^2}(\overline{u_j' T'}) - 2\overline{\frac{\partial T'}{\partial x_i}\frac{\partial u_j'}{\partial x_i}}.$$

It may be inferred that R is appreciable when the balance of $\overline{u_j' T'}$ plays a role in the turbulence comparable with those of kinetic energy and $\overline{T'^2}$. Thus it is appreciable in shear flows with heat transfer but not in grid turbulence with uniform mean temperature.]

Continuing the estimation of the magnitude of C, a little manipulation of the various scales in turbulence (Hinze 1959, pp. 185–6), or a consideration of the energy balance in a shear flow, gives $\lambda^2 \simeq \delta\nu/U$. Hence

$$C \simeq \frac{\alpha \rho_0 \Delta T U^2}{T_0 \delta}.$$

We compare this with the magnitude of another term in the same equation, $\rho[\partial(\overline{u_i' u_j'})/\partial x_i]$ (D, say): $D \simeq \rho_0 U^2/\delta$; hence $C/D \simeq \alpha \Delta T/T_0$. Thus for large temperature variations in a fluid having $\alpha \simeq 1$, it is incorrect to suppose that molecular terms in a mean equation for turbulent flow are small to the order ν/ν_T (where ν_T is the eddy viscosity), as is the case when fluid properties are constant.

The reader may well be wondering why this discussion has been given in terms of variable viscosity, when it would seem that variation of thermal conductivity is a simpler case; for

$$(E =) \overline{\frac{\partial}{\partial x_i}\left(k \frac{\partial T}{\partial x_i}\right)} = \overline{k \frac{\partial^2 T}{\partial x_i^2}} + \overline{\frac{dk}{dT}\left(\frac{\partial T}{\partial x_i}\right)^2}, \tag{2}$$

and the second term is analogous to the one considered above without the complication of the correlation. However, we shall now see that the same effect does not occur here. We may make the transformation

$$\overline{\frac{\partial}{\partial x_i}\left(k \frac{\partial T}{\partial x_i}\right)} = k_0 \frac{\partial^2}{\partial x_i^2}\left(\overline{\int^T \frac{k}{k_0} dT}\right), \tag{3}$$

(k_0 is the value of k at the reference temperature T_0), showing that a term involving turbulence length scales need not be brought in and that E is of the same order of magnitude as when k is constant.

This conclusion is disguised in (2) by the correlation of k-fluctuations with T-fluctuations making $\overline{k(\partial^2 T/\partial x_i^2)}$ also large in a way that just cancels the effect of $\overline{(dk/dT)\,(\partial T/\partial x_i)^2}$. This in turn suggests that, if any other temperature-dependent

quantity is a coefficient of $\partial^2 T/\partial x_i^2$, care is again needed. Consider in this connexion the full mean temperature equation

$$\overline{u}_i \frac{\partial \overline{T}}{\partial x_i} + \overline{u_i' \frac{\partial T'}{\partial x_i}} = \overline{\frac{1}{\rho C_p} \frac{\partial}{\partial x_i} \left(k \frac{\partial T}{\partial x_i} \right)}. \tag{4}$$

We may anticipate from the above that, although the temperature variation of k does not produce appreciable terms on the right-hand side, that of ρ does. It is seen that this is indeed the case by making the transformation

$$\overline{\frac{1}{\rho C_p} \frac{\partial}{\partial x_i} \left(k \frac{\partial T}{\partial x_i} \right)} = \kappa_0 \frac{\partial^2}{\partial x_i^2} \left(\overline{\int^T \frac{\kappa}{\kappa_0} dT} \right) - \overline{k \frac{d(1/\rho C_p)}{dT} \left(\frac{\partial T}{\partial x_i} \right)^2}, \quad \left(\kappa = \frac{k}{\rho C_p} \right).$$

Analysis as before shows that the second part of this is small compared with the left-hand side of (4) only to the order $\Delta T/T_0$ when $\beta = -\rho C_p T[d(1/\rho C_p)/dT]$ is of order 1 ($\beta \equiv 1$ for a perfect gas).

It is probably misleading to regard this last result as an occasion when molecular effects are important in turbulent flow, for the same error in the usual approximation may be detected by retaining ρC_p on the left-hand side of the equation, thus:

$$\overline{\rho C_p u_i \frac{\partial T}{\partial x_i}} = \overline{\frac{\partial}{\partial x_i} \left(k \frac{\partial T}{\partial x_i} \right)}. \tag{5}$$

There is then an approximation of order $\Delta\rho/\rho_0$ in taking the left-hand side of (5) as $\rho_0 C_p \overline{u_i}(\partial \overline{T}/\partial x_i) + \rho_0 C_p \overline{u_i'(\partial T'/\partial x_i)}$, but very little approximation in dropping the right-hand side. The important point is just that it is fallacious to argue that the equation can be put in the form (4) and the right-hand side then dropped because it is a 'molecular term'.

We now return to the velocity equation. The above comments about ρ-variability apply again. But we have already seen that μ-variability also has an effect; there is no analogue to (3). Intuitively it seems probable that μ-variability will not come in if the boundary conditions on velocity and temperature are similar and if, further, $k(T)$ and $\mu(T)$ have similar functional forms. In general, however, it does come in. It is particularly important to remember this for fluids for which the variation of μ is more marked than that of ρ (α large compared with β); water is an important example in which this is strongly so. Then there may be an approximation in the velocity equation but little in the temperature equation.

All the preceding discussion has been concerned with the approximation in

$$\overline{u}_i \frac{\partial \overline{u}_j}{\partial x_i} + \overline{u_i' \frac{\partial u_j'}{\partial x_i}} = -\overline{\frac{1}{\rho} \frac{\partial p}{\partial x_j}} + \nu \frac{\partial^2 \overline{u}_j}{\partial x_i^2}$$

and

$$\overline{u}_i \frac{\partial \overline{T}}{\partial x_i} + \overline{u_i' \frac{\partial T'}{\partial x_i}} = \kappa \frac{\partial^2 \overline{T}}{\partial x_i^2}.$$

There are further approximations of the order $\Delta\rho/\rho_0$ in the common practice of replacing the second terms by $\partial(\overline{u_i' u_j'})/\partial x_i$ and $\partial(\overline{u_i' T'})/\partial x$.

3. Continuity equation of mean flow

The continuity equation of mean flow is usually taken in the form

$$\frac{\partial \overline{u}_i}{\partial x_i} = 0.$$

It will now be shown that this is a good approximation in turbulent flow of gases even when the temperature variations are large—far better than is immediately apparent. Physically this means that expansion effects shift the mean flow streamlines less than in laminar flow (for which $\partial u_i/\partial x_i = 0$ is quite a poor approximation). The result is probably most useful for the case of a boundary layer on a heated wall—the temperature difference can remain large at all distances downstream—but the treatment here will be general.

The accurate continuity equation may be written

$$\frac{\partial u_i}{\partial x_i} + \frac{1}{\rho}\frac{D\rho}{Dt} = 0. \tag{6}$$

The second term is similar to the left-hand side of the temperature equation

$$\rho C_p \frac{DT}{Dt} = \frac{\partial}{\partial x_i}\left(k\frac{\partial T}{\partial x_i}\right), \tag{7}$$

and may thus be replaced by one similar to the right-hand side. This is a molecular conductivity term and the result of this section derives in essence from the unimportance of molecular effects in turbulent flow (it will be seen that the exception to this described in § 2 does not usually arise here). Substitution of $\rho T = \rho_0 T_0$ in (7) gives

$$\frac{1}{\rho}\frac{D\rho}{Dt} = -\frac{1}{\rho_0 T_0 C_p}\frac{\partial}{\partial x_i}\left(k\frac{\partial T}{\partial x_i}\right)$$

and so from (6)

$$\frac{\partial u_i}{\partial x_i} = \frac{1}{\rho_0 T_0 C_p}\frac{\partial}{\partial x_i}\left(k\frac{\partial T}{\partial x_i}\right) = \frac{1}{\rho_0 T_0 C_p}\frac{\partial^2}{\partial x_i^2}\left(\int^T k\,dT\right) \tag{8}$$

$$= \frac{\kappa_0}{T_0}\frac{\partial^2}{\partial x_i^2}\left(\int^T \frac{k}{k_0}\,dT\right) \quad (C_p \text{ independent of } T).$$

We then obtain, on taking average values,

$$\underset{F}{\frac{\partial \overline{u}_i}{\partial x_i}} = \frac{\kappa_0}{T_0}\frac{\partial^2}{\partial x_i^2}\underset{G}{\left(\overline{\int^T \frac{k}{k_0}\,dT}\right)}. \tag{9}$$

We now consider the order of magnitude of either side of (9):

$$F \simeq U/L; \quad G \simeq \kappa \Delta T/T_0\delta^2.$$

(It is possible to think of a form of $k(T)$ for which the use of ΔT as the scale of the difference of $\overline{\int^T \frac{k}{k_0}\,dT}$ is unsatisfactory, but such is most unlikely to apply to a real fluid. This is, for instance, the correct scale for any power law.) Thus we have

$G/F \simeq \Delta T \kappa L/T_0 U\delta^2$. But $L^2/\delta^2 \simeq UL/\nu_T$. (It is because this increase in the boundary-layer thickness through an eddy viscosity replacing a molecular one is essential to the argument that it does not also apply to laminar flow.) Therefore,

$$\frac{G}{F} \simeq \frac{\Delta T}{T_0}\frac{\nu}{Pr\nu_T},$$

which will be small even if $\Delta T/T_0$ is not. The fractional error in putting $F = 0$, i.e. $\partial\overline{u}_i/\partial x_i = 0$, will be correspondingly small.

The preceding analysis made use of the perfect-gas equation. This should apply in most cases of practical importance. However, brief mention may be made of what happens if a different equation of state applies; the situation is somewhat more complicated, and it may clarify the nature of the analysis to see why. For any other equation of state, the equation corresponding to (8) has temperature-dependent quantities in the coefficient on the right-hand side. Consequently averaging cannot be carried through the differentiation and, in the same way as in § 2, a term involving turbulent length scales comes in. The magnitude of this may be estimated as before;† it is of order $(\Delta T/T_0)^2$ smaller than F, which still compares favourably with a fractional error of $\Delta T/T_0$ in laminar flow. The still smaller error in the perfect-gas case results from a coincidental cancelling of two non-linearities, that in the equation of state and that due to the temperature dependence of ρ in the term $\rho C_p(DT/Dt)$ of the temperature equation.

Expansion effects may remain important in a laminar sublayer; indeed the above argument suggests that, in view of the large gradients, they may be particularly serious there even for comparatively small $\Delta T/T_0$. However, qualitative prediction of their behaviour might be possible by analogy with flows with injection through the wall.

4. Temperature difference introduced locally into pre-existing turbulence

So far it has been supposed that the length scales of the mean velocity and temperature fields are the same. This is not so when, as in turbulent-diffusion experiments, the heat source is a small element placed in an already turbulent flow field. A full analysis for this case of all the aspects considered above is complicated and, so far as I can see, not very rewarding. However, this is a situation in which particularly large errors can arise. We therefore consider one example of the way this can happen, by examining the relative sizes of $u_j'(\partial u_i'/\partial x_i)$ (H, say) and $\partial(\overline{u_i'u_j'})/\partial x_i$ (J, say), the former being the term neglected in the usual practice of taking the latter as the gradient of the stress. If the one is not small compared with the other, the supposition that the velocity field is unchanged by the introduction of the heat source is without justification (although the ratio H/J may overestimate the change; as the temperature difference is increased, the flow might adjust itself so that the gradient of the true stress remains constant rather than the gradient of $\overline{u_i'u_j'}$).

† Though this is a point at which the distinction between the scales of mean and fluctuating quantities (see § 1) *is* necessary to the argument.

This particular example was chosen primarily because it is probably the most serious one, but also because it illustrates the way in which the unapproximated continuity equation (6), with the division into mean and fluctuating parts applied to both velocity and density, can be used for estimating the magnitude of such effects. Equation (6) may be written

$$\frac{\partial u_i}{\partial x_i} = -\frac{\partial r}{\partial t} - u_i \frac{\partial r}{\partial x_i},$$

where $r = \log \rho/\rho_0$ (and thus has $\Delta\rho/\rho_0$ as its scale and a spatial distribution similar to that of temperature). Subtraction of the average of this equation from the unaveraged form gives

$$\frac{\partial u_i'}{\partial x_i} = -\frac{\partial r'}{\partial t} - u_i' \frac{\partial \bar{r}}{\partial x_i} - \bar{u}_i \frac{\partial r'}{\partial x_i} - u_i' \frac{\partial r'}{\partial x_i} + \overline{u_i' \frac{\partial r'}{\partial x_i}}$$

and so

$$\underset{H}{\overline{u_j' \frac{\partial u_i'}{\partial x_i}}} = \underset{K}{-\overline{u_j' \frac{\partial r'}{\partial t}}} \underset{L}{- \overline{u_i' u_j'} \frac{\partial \bar{r}}{\partial x_i}} \underset{M}{- \bar{u}_i \overline{u_j' \frac{\partial r'}{\partial x_i}}} \underset{N}{- \overline{u_i' u_j' \frac{\partial r'}{\partial x_i}}}. \tag{10}$$

This can be used for estimating the size of H. The difference from previous cases is brought about by the heat wake having different length scales from the main flow; we will call its width δ_H. From (10) we get $H \simeq \Delta\rho U^2/\rho_0 \delta_H$. This is immediately indicated by the term L.† Furthermore, $J \simeq U^2/\delta$, and so

$$\frac{H}{J} \sim \frac{\Delta\rho}{\rho_0} \frac{\delta}{\delta_H},$$

which is not necessarily small. As an illustration of the possible effect in an experimental set-up, consider δ/δ_H in the region of measurement in Corrsin & Uberoi's (1951) work on local heat sources. It is about 10. These authors are not explicit about the magnitude of $\Delta\rho/\rho_0$, but it seems likely from the temperature and size of the source that it was somewhere between 0·02 and 0·1. Thus we see that H/J can be quite appreciable.

A similar analysis may be carried through for the effect of non-zero $\partial u_i'/\partial x_i$ on the use of $\partial(\overline{u_i' T'})/\partial x_i$ in the temperature equation. However, this is as usual small to the order $\Delta\rho/\rho_0$; δ_H is the length scale in all the terms. Diffusion of heat from the source is seriously affected only through changes in the mean velocity field.

I thank Dr A. A. Townsend and a referee for comments that have greatly helped with the development of these ideas. My work at Bangalore is made possible by the award by the Royal Society, to which I am most grateful, of a Rutherford Scholarship.

REFERENCES

Corrsin, S. & Uberoi, M. S. 1951 *Nat. Adv. Comm. Aero. Rep.* no. 1040.

Ellison, T. H. 1957 *J. Fluid Mech.* **2**, 456.

Hinze, J. O. 1959 *Turbulence.* New York: McGraw-Hill.

† The other terms are not so readily estimated, but there is no reason to expect either that they are any larger or that they just cancel L so as to make H smaller. In point of fact, arguments invoking the similarity of these terms to ones appearing in equation (1) suggest that K, M and N are likely to be of the same order as L.

The transverse force on a spinning sphere moving in a viscous fluid

By S. I. RUBINOW

Stevens Institute of Technology, Hoboken, New Jersey

AND JOSEPH B. KELLER

Institute of Mathematical Sciences, New York University, New York, N.Y.

(Received 13 March 1961)

The flow about a spinning sphere moving in a viscous fluid is calculated for small values of the Reynolds number. With this solution the force and torque on the sphere are computed. It is found that in addition to the drag force determined by Stokes, the sphere experiences a force $\mathbf{F}_L$ orthogonal to its direction of motion. This force is given by $\mathbf{F}_L = \pi a^3 \rho \boldsymbol{\Omega} \times \mathbf{V}[1 + O(R)]$.

Here a is the radius of the sphere, $\boldsymbol{\Omega}$ is its angular velocity, $\mathbf{V}$ is its velocity, ρ is the fluid density and R is the Reynolds number, $R = \rho\mu^{-1}Va$. For small values of R, the transverse force is independent of the viscosity μ. This force is in such a direction as to account for the curving of a pitched baseball, the long range of a spinning golf ball, etc. It is used as a basis for the discussion of the flow of a suspension of spheres through a tube.

The calculation involves the Stokes and Oseen expansions. A representation of solutions of the Oseen equations in terms of two scalar functions is also presented.

1. Introduction

We shall show that a spinning sphere moving in a viscous fluid experiences a force orthogonal to its direction of motion, which we call a lift force. It is also orthogonal to the spin axis and therefore accounts for the curving of a pitched baseball, the long range of a spinning golf ball, etc. Since we shall calculate the lift for small values of the Reynolds number, our result will not apply to these phenomena, which occur for large Reynolds numbers. Our result applies either to the slow motion of a small sphere in a fluid, such as a solid particle in a suspension, or to the motion of a satellite or other astronomical object in a gas of low density. We shall also show that the spin does not effect the drag force and that there is no correction to the retarding torque to the order we consider. Using these results we shall determine the motion of a sphere with given initial linear and angular velocities. We shall also consider the flow of a suspension of spheres through a tube, in the light of our results.

Our results are obtained by solving the Navier–Stokes equations for the motion of the fluid around the sphere. We determine the first few terms, in the expansion in terms of the Reynolds number, of the solution. This expansion consists of two parts, the Stokes and Oseen expansions, which were introduced and used by Lagerstrom & Cole (1955), and Proudman & Pearson (1957). Our method of

solution is similar to theirs with the main difference being that we obtain directly the expansion for the velocity and the pressure rather than for the stream function. This is necessary because our flow is asymmetric and therefore there is no stream function which describes it. Those authors, as well as Stokes (1851) and Oseen (1910, 1913) considered the motion of a non-spinning sphere, about which the flow is axially symmetric and describable by a stream function. The present example appears to be the first asymmetric three-dimensional case for which the flow at small Reynolds numbers has been found by using these expansions. In the appendix we prove that it is possible to represent any solution of the Oseen equations in terms of two scalar functions.

2. Formulation

We wish to consider the motion of a sphere of radius a, velocity $\mathbf{V}$ and angular velocity $\boldsymbol{\Omega}$ through an incompressible viscous fluid of density ρ and viscosity coefficient μ. The fluid is assumed to be at rest far from the sphere. It is convenient to introduce a co-ordinate system with its origin at the centre of the sphere, with the negative x'-axis pointing in the direction of $\mathbf{V}$ and with the (x', y')-plane containing $\boldsymbol{\Omega}$. In this co-ordinate system the flow is steady and the fluid has the velocity $(V, 0, 0)$ at infinity while the velocity of the surface of the sphere $r' = a$ is $\boldsymbol{\Omega} \times \mathbf{r}'$. We denote the velocity in the fluid by $\mathbf{u}'$ and the pressure in the fluid by p', taking the pressure at infinity to be zero. Now $\mathbf{u}'$ and p' satisfy the time independent Navier–Stokes equations, the equation of continuity, the condition of no slip at the sphere and the appropriate conditions at infinity. These equations and conditions are

$$\mu \Delta \mathbf{u}' - \nabla p' = \rho(\mathbf{u}' . \nabla)\, \mathbf{u}', \tag{1}$$

$$\nabla . \mathbf{u}' = 0, \tag{2}$$

$$\mathbf{u}' = \boldsymbol{\Omega} \times \mathbf{r}' \quad \text{at} \quad r' = a, \tag{3}$$

$$\mathbf{u}' = (V, 0, 0) \quad \text{at} \quad r' = \infty, \tag{4}$$

and

$$p' = 0 \quad \text{at} \quad r' = \infty. \tag{5}$$

Let us introduce the dimensionless Reynolds number R as well as the dimensionless quantities $\mathbf{u}$, p, $\boldsymbol{\omega}$, x, y, z and $\mathbf{r}$, defined by

$$\left.\begin{aligned} x = a^{-1}x', \quad y = a^{-1}y', \quad z = a^{-1}z', \quad \mathbf{r} = a^{-1}\mathbf{r}', \\ p = aV^{-1}\mu^{-1}p', \quad \mathbf{u} = V^{-1}\mathbf{u}', \quad \boldsymbol{\omega} = aV^{-1}\boldsymbol{\Omega}, \quad R = \rho\mu^{-1}Va. \end{aligned}\right\} \tag{6}$$

Upon introducing these variables into (1)–(5), we obtain

$$\Delta \mathbf{u} - \nabla p = R(\mathbf{u} . \nabla)\, \mathbf{u}, \tag{7}$$

$$\nabla . \mathbf{u} = 0, \tag{8}$$

$$\mathbf{u} = \boldsymbol{\omega} \times \mathbf{r} \quad \text{at} \quad r = 1, \tag{9}$$

$$\mathbf{u} = (1, 0, 0) \quad \text{at} \quad r = \infty, \tag{10}$$

and

$$p = 0 \quad \text{at} \quad r = \infty. \tag{11}$$

We seek the solution $\mathbf{u}$ and p of (7)–(11) as expansions in R valid for small values of R.

3. Stokes expansion

The Stokes expansion of the solution is of the form

$$\mathbf{u} = \mathbf{u}_0 + R\mathbf{u}_1 + o(R), \tag{12}$$

$$p = p_0 + Rp_1 + o(R). \tag{13}$$

Further terms beyond those shown involve powers of $\log R$ in addition to powers of R, as has been demonstrated by Proudman & Pearson (1957) for the non-rotating sphere. However, only the terms shown in (12) and (13) will be needed here. We now insert (12) and (13) into (7)–(9) and equate coefficients of R^0 in each equation, obtaining

$$\Delta\mathbf{u}_0 - \nabla p_0 = 0, \tag{14}$$

$$\nabla.\mathbf{u}_0 = 0, \tag{15}$$

and

$$\mathbf{u}_0 = \boldsymbol{\omega}\times\mathbf{r} \quad \text{at} \quad r = 1. \tag{16}$$

From the coefficients of R^1, we obtain

$$\Delta\mathbf{u}_1 - \nabla p_1 = (\mathbf{u}_0.\nabla)\,\mathbf{u}_0, \tag{17}$$

$$\nabla.\mathbf{u}_1 = 0, \tag{18}$$

and

$$\mathbf{u}_1 = 0 \quad \text{at} \quad r = 1. \tag{19}$$

We have not required of the Stokes expansion that it satisfy (10) and (11), the conditions at infinity, because this expansion is not uniformly valid in the neighbourhood of infinity. Therefore conditions at infinity on the individual terms cannot be obtained in the same way. Instead we must obtain another expansion, the Oseen expansion, which is valid at infinity. Then by matching the two expansions the necessary conditions will be obtained. To obtain the Oseen expansion we must first introduce stretched variables.

4. Stretched variables

Let us introduce the new stretched variables X, Y, Z and $\mathbf{s}$ and the new functions $\mathbf{U}$ and P, defined by

$$\left.\begin{aligned} X = Rx, \quad Y = Ry, \quad Z = Rz, \quad \mathbf{s} &= R\mathbf{r}, \\ \mathbf{U}(X,Y,Z,R) &= \mathbf{u}(R^{-1}X, R^{-1}Y, R^{-1}Z, R), \\ P(X,Y,Z,R) &= R^{-1}p(R^{-1}X, R^{-1}Y, R^{-1}Z, R). \end{aligned}\right\} \tag{20}$$

In terms of these variables, equations (7)–(11) become

$$\Delta\mathbf{U} - \nabla P = (\mathbf{U}.\nabla)\,\mathbf{U}, \tag{21}$$

$$\nabla.\mathbf{U} = 0, \tag{22}$$

$$\mathbf{U} = R^{-1}\boldsymbol{\omega}\times\mathbf{s} \quad \text{at} \quad s = R, \tag{23}$$

$$\mathbf{U} = (1,0,0) \quad \text{at} \quad s = \infty, \tag{24}$$

and

$$P = 0 \quad \text{at} \quad s = \infty. \tag{25}$$

5. Oseen expansion

The Oseen expansion of the solution $\mathbf{U}$ and P of (21)–(25) is of the form

$$\mathbf{U} = \mathbf{U}_0 + R\mathbf{U}_1 + o(R), \tag{26}$$

$$P = P_0 + RP_1 + o(R). \tag{27}$$

Upon inserting (26) and (27) into (21), (22), (24) and (25) and equating coefficients of R^0, we obtain

$$\Delta\mathbf{U}_0 - \nabla P_0 = (\mathbf{U}_0 . \nabla)\,\mathbf{U}_0, \tag{28}$$

$$\nabla . \mathbf{U}_0 = 0, \tag{29}$$

$$\mathbf{U}_0 = (1, 0, 0) \quad \text{at} \quad s = \infty, \tag{30}$$

and

$$P_0 = 0 \quad \text{at} \quad s = \infty. \tag{31}$$

Equating coefficients of R^1 yields the equations

$$\Delta\mathbf{U}_1 - \nabla P_1 = (\mathbf{U}_0 . \nabla)\,\mathbf{U}_1 + (\mathbf{U}_1 . \nabla)\,\mathbf{U}_0, \tag{32}$$

$$\nabla . \mathbf{U}_1 = 0, \tag{33}$$

$$\mathbf{U}_1 = (0, 0, 0) \quad \text{at} \quad s = \infty, \tag{34}$$

and

$$P_1 = 0 \quad \text{at} \quad s = \infty. \tag{35}$$

We have not inserted the Oseen expansion into the condition (23) on the sphere because we do not expect this expansion to be uniformly valid there. Consequently this condition must be replaced by another condition. This latter condition is that the Stokes and Oseen expansions must match since they are both expansions of the same solution expressed in different variables. This matching will be explained later.

We note that equations (28)–(31) satisfied by $\mathbf{U}_0$ and P_0 are the same as the corresponding equations for $\mathbf{U}$ and P. Therefore we cannot expect to solve them more readily than we could solve the original equations. However, we observe that a particular solution for $\mathbf{U}_0$ and P_0 is

$$\mathbf{U}_0 = (1, 0, 0), \tag{36}$$

$$P_0 = 0. \tag{37}$$

The Oseen expansion is based upon choosing this particular solution for $\mathbf{U}_0$ and P_0. With this choice (32) simplifies to

$$\Delta\mathbf{U}_1 - \nabla P_1 = \frac{\partial \mathbf{U}_1}{\partial X}. \tag{38}$$

Before determining $\mathbf{U}_1$ and P_1, let us explain the principle of matching.

6. Matching

The matching principle is that two different asymptotic expansions of a given function must be asymptotically equal in their common domain of validity, if any. We assume that the Stokes expansion is valid from the sphere out to some large distance. We also assume that the Oseen expansion is valid from infinity in to some small radius in the stretched variables. However, this radius is

considered to be large in the unstretched variables. Then the common domain of validity is a spherical shell within which the unstretched radius is large but the stretched radius is small. Therefore if the Stokes expansion is expanded for large values of the radius r while the Oseen expansion is expanded for small values of the stretched radius s, the resulting expansions must be asymptotically equal. This principle is utilized by alternately determining terms in the two expansions and matching them to the previous terms.

As a first result of applying this principle we can determine the behaviour of the zeroth-order Stokes approximation, $\mathbf{u}_0$ and p_0, for large values of r. Since $\mathbf{U}_0$ and P_0 are constant, the result is easily seen to be

$$\mathbf{u}_0 = \mathbf{U}_0 + o(1) \quad \text{as} \quad r \to \infty, \tag{39}$$

and

$$p_0 = o(1) \quad \text{as} \quad r \to \infty. \tag{40}$$

7. Zeroth-order Stokes approximation

The solution $\mathbf{u}_0$ and p_0 of (14)–(16), (39) and (40) is unique and can be found by the method explained by Lamb (1945, pp. 595, 596). Since the equations are all linear, the solution is just the sum of the known solution for a uniform flow past a non-rotating sphere and the known flow produced by a rotating sphere in a fluid at rest at infinity. Thus we have

$$\mathbf{u}_0 = \left(1 - \frac{3}{4r} - \frac{1}{4r^3}\right)(1,0,0) - \frac{3x}{4}\left(\frac{1}{r^3} - \frac{1}{r^5}\right)\mathbf{r} + \frac{1}{r^3}\boldsymbol{\omega} \times \mathbf{r}, \tag{41}$$

$$p_0 = -\frac{3x}{2r^3}. \tag{42}$$

8. First-order Oseen approximation

To determine $\mathbf{U}_1$ and P_1 we must solve (38), (33)–(35) and employ the matching condition. We begin by taking the divergence of (38) and using (33), from which it follows that $\Delta P_1 = 0$. Then, following Lamb (1945, p. 610), we introduce a scalar ϕ and a vector $\mathbf{W}$ and write

$$P_1 = \frac{\partial \phi}{\partial X}, \tag{43}$$

$$\mathbf{U}_1 = -\nabla\phi + \mathbf{W}. \tag{44}$$

Since P_1 is harmonic we require that ϕ also be harmonic, i.e.

$$\Delta\phi = 0. \tag{45}$$

Then (38) and (33) become two equations for $\mathbf{W}$:

$$\Delta\mathbf{W} - \frac{\partial}{\partial X}\mathbf{W} = 0, \tag{46}$$

$$\nabla . \mathbf{W} = 0. \tag{47}$$

In the appendix we prove the following theorem.

Theorem. If $\mathbf{W}$ satisfies (46) and (47) then there exist two scalar functions ψ and χ such that

$$\mathbf{W} = (1,0,0)\times\nabla\psi + \nabla\times[(1,0,0)\times\nabla\chi] \tag{48}$$

and

$$\Delta\psi - \frac{\partial}{\partial X}\psi = 0, \tag{49}$$

$$\Delta\chi - \frac{\partial}{\partial X}\chi = 0. \tag{50}$$

Let us define χ', which also satisfies (50), by

$$\chi' = \frac{\partial}{\partial X}\chi. \tag{51}$$

Then (48) can be written as

$$\mathbf{W} = \nabla\chi' + \left(-\chi', -\frac{\partial\psi}{\partial Z}, \frac{\partial\psi}{\partial Y}\right). \tag{52}$$

Those special solutions of the form (48) or (52) for which $\psi = 0$ were given by Lamb (1945, p. 611).

To construct $\mathbf{U}_1$ and P_1 let us make the following choices of ϕ, ψ and χ', which must be solutions of (45), (49) and (50) respectively:

$$\phi = A/s, \tag{53}$$

$$\psi = 0, \tag{54}$$

and

$$\chi' = (B/s)\exp[\tfrac{1}{2}(X-s)]. \tag{55}$$

We now compute $\mathbf{U}_1$ and P_1 from (43) and (44), using (52)–(55) and employ the matching condition. This yields $A = B = \frac{3}{2}$. Thus $\mathbf{U}_1$ and P_1 are found to be

$$\mathbf{U}_1 = \frac{3}{2s^3}(X,Y,Z) - \frac{3}{4s}\exp[\tfrac{1}{2}(X-s)](1,0,0) - \tfrac{3}{4}\exp[\tfrac{1}{2}(X-s)]\left(\frac{1}{s^2} - \frac{2}{s^3}\right)(X,Y,Z) \tag{56}$$

and

$$P_1 = -\frac{3X}{2s^3}. \tag{57}$$

This solution satisfies the condition at infinity (34) and (35). If any other choice were made for ϕ, ψ and χ', the matching condition or the conditions at infinity would have been violated.

9. First-order Stokes approximation

To determine $\mathbf{u}_1$ and p_1 we must solve (17)–(19) and employ the matching principle. We shall first find a particular solution $\mathbf{u}_{10}$ and p_{10} of (17) and (18). Then we shall add a solution $\mathbf{u}_{11}$ and p_{11} of (18) and the homogeneous form of (17) in order to satisfy the boundary condition (19). Finally we shall show that the sum of the two solutions so obtained satisfies the matching condition so no other solution need be added. To begin, we compute the inhomogeneous term $(\mathbf{u}_0\cdot\nabla)\mathbf{u}_0$ which occurs in (17). By using (41) for $\mathbf{u}_0$ we obtain

$$\begin{aligned}(\mathbf{u}_0\cdot\nabla)\mathbf{u}_0 = {}& \frac{3x}{16}\left[-\frac{3}{r^4} + \frac{8}{r^5} - \frac{6}{r^6} + \frac{1}{r^8}\right](1,0,0) + \frac{3}{16}\left[-\frac{4}{r^3} + \frac{3}{r^4} + \frac{4}{r^5} - \frac{2}{r^6} - \frac{1}{r^8}\right.\\ & \left. + x^2\left(\frac{12}{r^5} - \frac{12}{r^6} - \frac{20}{r^7} + \frac{24}{r^8} - \frac{4}{r^{10}}\right)\right]\mathbf{r} - 3x\left(\frac{1}{r^5} - \frac{1}{r^6}\right)\boldsymbol{\omega}\times\mathbf{r}\\ & - \frac{3\omega z\sin\beta}{4}\left(\frac{1}{r^6} - \frac{1}{r^8}\right)\mathbf{r} - \frac{\omega\sin\beta}{4}\left[\frac{4}{r^3} - \frac{3}{r^4} - \frac{1}{r^6}\right](0,0,1) + \frac{1}{r^6}\boldsymbol{\omega}\times(\boldsymbol{\omega}\times\mathbf{r}).\end{aligned} \tag{58}$$

Here β is the angle between $\boldsymbol{\Omega}$ and $\mathbf{U}_0$.

Let us now take the divergence of (17) and make use of (18) and (58). Then we find that

$$\Delta p_1 = -\nabla.[(\mathbf{u}_0.\nabla)\,\mathbf{u}_0] = \frac{9}{8}\left[-\frac{1}{r^4}+\frac{1}{r^8}+x^2\left(\frac{4}{r^6}-\frac{6}{r^8}+\frac{2}{r^{10}}\right)\right] - \frac{3\omega z\sin\beta}{2}\left(\frac{1}{r^6}-\frac{1}{r^8}\right)+\frac{4\omega^2}{r^6}-\frac{(\boldsymbol{\omega}.\mathbf{r})^2}{r^8}. \quad (59)$$

A particular solution of (59) is

$$p_{10} = \frac{3}{32}\left[-\frac{6}{r^2}-\frac{2}{r^4}-\frac{1}{3r^6}+x^2\left(\frac{12}{r^4}+\frac{12}{r^6}-\frac{1}{r^8}\right)\right]-\frac{\omega z\sin\beta}{8}\left(\frac{3}{r^4}-\frac{2}{r^6}\right)-\frac{\omega^2}{2r^4}+\frac{(\boldsymbol{\omega}.\mathbf{r})^2}{r^6}. \quad (60)$$

We now insert (60) into (17) and obtain for $\mathbf{u}_1$ the equation

$$\Delta\mathbf{u}_1 = \nabla p_{10}+(\mathbf{u}_0.\nabla)\,\mathbf{u}_0. \quad (61)$$

A particular solution of (61) is

$$\begin{aligned}\mathbf{u}_{10} = {}& \frac{3}{32}\left[4-x\left(\frac{4}{r}-\frac{3}{r^2}+\frac{1}{r^4}\right)\right](1,0,0)+\frac{3}{32}\left[\frac{2}{r}-\frac{3}{r^2}-\frac{1}{r^4}\right.\\ &\left.+x^2\left(-\frac{2}{r^3}+\frac{6}{r^4}+\frac{4}{r^5}+\frac{4}{r^6}\right)\right]\mathbf{r}+\frac{x}{4}(\boldsymbol{\omega}\times\mathbf{r})\left(\frac{2}{r^3}-\frac{3}{r^4}\right)\\ &+\frac{\omega\sin\beta}{16}\left[\frac{8}{r}-\frac{6}{r^2}+\frac{1}{r^4}\right](0,0,1)-\frac{\omega z\sin\beta}{16}\left[\frac{3}{r^4}+\frac{2}{r^6}\right]\mathbf{r}\\ &-\frac{\boldsymbol{\omega}\times(\boldsymbol{\omega}\times\mathbf{r})}{4r^4}-\frac{\omega^2}{2r^4}\mathbf{r}+\frac{(\boldsymbol{\omega}.\mathbf{r})^2}{r^6}\mathbf{r}. \end{aligned} \quad (62)$$

By direct computation we find that $\mathbf{u}_{10}$ satisfies (18).

Next we find $\mathbf{u}_{11}$ and p_{11} satisfying the homogeneous form of (17) and (18) and such that $\mathbf{u}_{10}+\mathbf{u}_{11}$ satisfies (19). Thus we require that

$$\mathbf{u}_{11} = -\mathbf{u}_{10} \quad \text{at} \quad r = 1. \quad (63)$$

By the method of Lamb (1945, pp. 595, 596), we find that

$$\begin{aligned}\mathbf{u}_{11} = {}& \frac{3}{32}\left[-\frac{3}{r}-\frac{1}{r^3}+\frac{2x}{r^5}\right](1,0,0)+\frac{3}{32}\left[\frac{1}{r^3}+\frac{1}{r^5}-3x\left(\frac{1}{r^3}-\frac{1}{r^5}\right)-x^2\left(\frac{7}{r^5}+\frac{5}{r^7}\right)\right]\mathbf{r}\\ &+\frac{x}{4r^5}\boldsymbol{\omega}\times\mathbf{r}-\frac{\omega\sin\beta}{16}\left(\frac{2}{r}+\frac{1}{r^3}\right)(0,0,1)-\frac{\omega z\sin\beta}{16}\left(\frac{2}{r^3}-\frac{7}{r^5}\right)\mathbf{r}\\ &+\frac{\boldsymbol{\omega}\times(\boldsymbol{\omega}\times\mathbf{r})}{4r^5}+\frac{\omega^2}{8}\left(\frac{1}{r^3}+\frac{3}{r^5}\right)\mathbf{r}-\frac{(\boldsymbol{\omega}.\mathbf{r})^2}{8}\left[\frac{3}{r^5}+\frac{5}{r^7}\right]\mathbf{r}, \end{aligned} \quad (64)$$

and

$$p_{11} = -\frac{9}{16}\frac{x}{r^3}+\frac{7}{16}\left(\frac{1}{r^3}-\frac{3x^2}{r^5}\right)-\frac{\omega z\sin\beta}{4r^3}+\frac{\omega^2}{4r^3}-\frac{3(\boldsymbol{\omega}.\mathbf{r})^2}{4r^5}. \quad (65)$$

Upon adding $\mathbf{u}_{10}$ to $\mathbf{u}_{11}$ and p_{10} to p_{11}, we obtain $\mathbf{u}_1$ and p_1. (There is no need here to write out the resulting expressions for $\mathbf{u}_1$ and p_1, but we shall presently refer to them as (66) and (67), respectively.) By employing the matching procedure we find that this solution matches the Oseen solution, and therefore it is not necessary to add anything else to it.

10. Lift, drag and torque

We shall now use the two terms of the Stokes expansion which we have found to compute the force and torque on the sphere. To do so we must first determine **f**, the force per unit area exerted by the fluid on the surface of the sphere. Lamb (1945, p. 596) gives an expression for **f** which becomes in dimensionless variables

$$\mathbf{f} = \frac{V\mu}{a}\left[-\frac{\mathbf{r}}{r}p + \left(\frac{\partial}{\partial r} - \frac{1}{r}\right)\mathbf{u} + \frac{1}{r}\nabla(\mathbf{r}\,.\,\mathbf{u})\right]. \tag{68}$$

Upon using (41), (42), (66) and (67) in (68) and integrating (68) over the surface of the sphere we obtain the total force **F** which is given in terms of the velocity **V** of the sphere by

$$\mathbf{F} = -6\pi a\mu\mathbf{V}(1+\tfrac{3}{8}R) + \pi a\mu R\boldsymbol{\omega}\times\mathbf{V} + o(a\mu VR). \tag{69}$$

The component of **F** in the direction $-\mathbf{V}$ is the drag force $\mathbf{F}_D$ and the component normal to **V** is the lift force $\mathbf{F}_L$. From (69) and the definition (6) of R, these components are

$$\mathbf{F}_D = -6\pi a\mu\mathbf{V}[1+\tfrac{3}{8}R + o(R)] \tag{70}$$

and

$$\mathbf{F}_L = \pi a^3\rho\boldsymbol{\Omega}\times\mathbf{V}[1+O(R)]. \tag{71}$$

It is interesting to note that the leading term in $\mathbf{F}_L$ is independent of μ and is similar to the lift formula for two-dimensional potential flow about an airfoil. By integrating $\mathbf{r}\times\mathbf{f}$ over the surface of the sphere we obtain for the torque **T** on the sphere the result

$$\mathbf{T} = -8\pi\mu a^3\boldsymbol{\Omega}[1+o(R)]. \tag{72}$$

The term $-6\pi a\mu\mathbf{V}$ in $\mathbf{F}_D$ was calculated by Stokes (1861) and the second term $-\frac{9}{4}\pi\mu a\mathbf{V}R$ by Oseen (1910, 1913). The expression for $\mathbf{F}_L$, which is new, is the main result of this paper. The term $-8\pi\mu a^3\boldsymbol{\Omega}$ in **T** was obtained by Kirchhoff (1876). Our results show that the spin causes no correction to the drag of order R and that there is no correction to the torque of order R.

11. The motion of a spinning sphere

Let us now consider the motion of a sphere with initial velocity $\mathbf{V}_0$ and initial angular velocity $\boldsymbol{\Omega}_0$ in a viscous fluid initially at rest. Let M denote the mass of the sphere, I its moment of inertia about any diameter, $\mathbf{V}(t)$ its linear velocity and $\boldsymbol{\Omega}(t)$ its angular velocity about a diameter at time t. We assume that the force and torque on the sphere are given by (69) and (72), ignoring the terms $o(a\mu VR)$ in (69) and $o(R)$ in (72). Then the equations of motion of the sphere are

$$M\frac{d\mathbf{V}}{dt} = -6\pi a\mu(1+\tfrac{3}{8}R)\,\mathbf{V} + \pi a^3\rho\boldsymbol{\Omega}\times\mathbf{V} \tag{73}$$

and

$$I\frac{d\boldsymbol{\Omega}}{dt} = -8\pi\mu a^3\boldsymbol{\Omega}. \tag{74}$$

The solution of (74) is

$$\boldsymbol{\Omega}(t) = \boldsymbol{\Omega}_0\exp\left[-\frac{8\pi\mu a^3}{I}t\right]. \tag{75}$$

If $\mathbf{V}^{(1)}(t)$ denotes the component of $\mathbf{V}(t)$ parallel to $\boldsymbol{\Omega}_0$, (73) yields

$$\mathbf{V}^{(1)}(t) = \mathbf{V}_0^{(1)} \exp\left[-6\pi a\mu(1+\tfrac{3}{8}R)\,M^{-1}t\right]. \tag{76}$$

Let $\mathbf{V}^{(2)}(t)$ denote the component of $\mathbf{V}(t)$ perpendicular to $\boldsymbol{\Omega}_0$. Then (73) yields

$$|\mathbf{V}^{(2)}(t)| = |\mathbf{V}_0^{(2)}| \exp\left[-6\pi a\mu(1+\tfrac{3}{8}R)\,M^{-1}t\right]. \tag{77}$$

Now we define the unit vector $\mathbf{v}(t)$ by

$$\mathbf{V}^{(2)}(t) = |\mathbf{V}^{(2)}(t)|\,\mathbf{v}(t). \tag{78}$$

From (73) it follows that $\mathbf{v}(t)$ satisfies the equation

$$\frac{d\mathbf{v}}{dt} = \frac{\pi a^3\rho}{M} \exp\left[-\frac{8\pi\mu a^3 t}{I}\right] \boldsymbol{\Omega}_0 \times \mathbf{v}. \tag{79}$$

The solution of (79) is, in rectangular components,

$$v(t) = [\cos\theta(t),\ \sin\theta(t)]. \tag{80}$$

Here the angle $\theta(t)$ is given by

$$\theta(t) = \theta_0 + \frac{I\rho\,|\boldsymbol{\Omega}_0|}{8\mu M}\left(1 - \exp\left[-\frac{8\pi\mu a^3}{I}t\right]\right). \tag{81}$$

From these results the path of the sphere can be obtained easily by integration.

12. Flow of a suspension through a tube

When a viscous fluid containing suspended particles flows through a circular tube, the particles are not uniformly distributed over the cross-section of the tube. Observations on blood flow in narrow capillaries indicate that the red blood corpuscles concentrate near the axis of the capillary. This concentration effect was explained hydrodynamically by supposing that the fluid exerted an axially directed transverse force on the particles. However, when the flow was determined by solving the linearized Stokes equations, no transverse force was found on a sphere in a shear flow, such as the Poiseuille flow in a circular tube.† A similar calculation of the force on an ellipsoid in a shear flow by Jeffery (1922) also yielded no transverse force.

To account for the effect, Jeffery proposed a new principle—that a particle moves at that distance from the axis which minimizes the rate of energy dissipation in the flow. This principle was subsequently rediscovered and generalized and has become a cornerstone of irreversible thermodynamics. If correct, Jeffery's principle should be deducible from the Navier–Stokes equations, just as all thermodynamic principles are deducible from more detailed theories. To apply it to the present problem, Jeffery utilized the result of Einstein (1906) for the excess dissipation produced by the introduction of a sphere into a uniform shear flow. Einstein has shown that the excess dissipation is proportional to

† This result can be obtained without calculation by decomposing the incident shear flow into two parts, one symmetric and the other antisymmetric about any plane through the centre of the sphere and containing the direction of the incident flow through the centre. By symmetry, neither of these flows can yield a force on the sphere normal to the plane.

the square of the vorticity of the incident flow at the particle. Since the velocity distribution in the Poiseuille flow is parabolic, the vorticity is proportional to the distance from the axis and the excess energy dissipation to the square of the distance from the axis. Thus Jeffery concluded that a particle would move along the axis.

This same conclusion was arrived at by Tollert (1954) and Saffman (1956). Tollert observed that, according to Einstein, a sphere in a shear flow $\mathbf{u}$ rotates with the angular velocity $\boldsymbol{\Omega} = \frac{1}{2}\nabla \times \mathbf{u}$. Furthermore, according to the calculation of Simha (1936), a sphere of radius a in a tube of radius R_0 lags behind the flow with the relative velocity $\mathbf{V} = -\frac{2}{3}(a^2/R_0^2)\,\mathbf{U}_0$, where $\mathbf{U}_0$ is the flow velocity at the centre of the tube. Then Tollert postulated a transverse force of the form (71) with another factor instead of $\frac{2}{3}\pi$. In a Poiseuille flow, $\nabla \times \mathbf{u} = -2\mathbf{b} \times \mathbf{U}_0/R_0^2$, where $\mathbf{b}$ denotes the radial vector from the axis. If the correct formula (71) for the transverse force on a sphere at radial position $\mathbf{b}$ were used, Tollert's argument would yield the result

$$\mathbf{F}_L = -2\pi a^5 \rho U_0^2 \mathbf{b}/3R_0^4. \tag{82}$$

Saffman derived a similar result by approximate solution of the flow equations, obtaining the numerical factor $7{\cdot}7(\frac{2}{3}\pi)$ instead of $\frac{2}{3}\pi$. The result (82) yields a force toward the axis which vanishes on the axis, in agreement with Jeffery's conclusion.

Recently Segre & Silberberg (1961) measured very accurately the distribution of spherical particles in a fluid flowing in a circular tube. They found that the particles do not concentrate along the axis. Instead they concentrate at the radius b_0 equal to about $\frac{1}{2}R_0$. Thus the previous observations were inaccurate, and the theories of Jeffery, Tollert and Saffman are incomplete. Consequently the formula (82) is incorrect, or at best incomplete. This formula and the theories referred to only account for the inward motion of spherical particles lying outside the radius b_0.

In order to understand why (82) fails, we must recognize that it is based upon (71), which applies to a sphere in a uniform flow. But the Poiseuille flow in a tube is not uniform. It is a shear flow with a parabolic velocity profile. The gradient of this profile accounts for the spin of the sphere and the curvature of the profile accounts for the lag. However, these are evidently not the only ways in which the non-uniformity of the flow affects the sphere. We therefore attempted to calculate the flow about a spinning sphere in a shear flow with a parabolic velocity profile, and from it to compute the force and torque on the sphere. We followed the procedure employed in the preceding sections and had no difficulty in obtaining the zero-order Stokes solution. We began to calculate the first-order Stokes solution and obtained some terms in it, but we did not complete the calculation because the labour became prohibitive. However, from the terms we calculated, we computed the transferse force, which came out to be given by (82). But there are many more terms in the force which we did not calculate. We expect that these further terms would modify (82) in such a way as to account for the observed effect, but this is merely a conjecture. This conjecture is strengthened by the fact that (82) yields a force of the correct order of magnitude to account for the observed effect, as we shall show below.

We have also examined the minimum-dissipation-rate analysis of Jeffery and found that it utilizes the linearized flow about a sphere in an unbounded uniform shear flow. But to zero order in the Reynolds number, the correct flow is the linearized flow about a sphere in a Poiseuille flow in a tube. If this zero-order flow were used in calculating the rate of energy dissipation, it might yield the correct equilibrium distance of the sphere from the axis.

In view of the experimental results, let us now modify (82) so that it gives an outward force for $b < b_0$. The simplest way to do this is to multiply the right-hand side of (82) by $(b-b_0)/b_0$. With this factor the force is inward for $b > b_0$ and outward for $b < b_0$. Of course this expression for the force is not correct in detail, but it is qualitatively correct.

We shall now calculate the trajectory of a sphere subject to this force. Its radial velocity $d\mathbf{b}/dt$ can be determined by equating the drag force $6\pi a\mu\, d\mathbf{b}/dt$ to $\mathbf{F}_L$. Thus

$$\frac{db}{dt} = -\frac{a^4\rho U_0^2}{9R_0^4\mu}\frac{b(b-b_0)}{b_0}. \tag{83}$$

Now the axial velocity of the sphere dx/dt is practically equal to the flow velocity $U_0(1-b^2R_0^{-2})$. Thus we have, upon dividing,

$$\frac{dx}{db} = -\frac{9R_0^2\mu b_0(R_0^2-b^2)}{a^4\rho U_0 b(b-b_0)}. \tag{84}$$

We now integrate (84) from $x = 0$, denoting the initial radius of the particle at $x = 0$ by b_1. Thus we obtain

$$x = \frac{9R_0^2\mu b_0}{a^4\rho U_0}\left[b-b_1+\frac{R_0^2}{b_0}\log\left(\frac{b}{b_1}\right)+\frac{R_0^2-b_0^2}{b_0}\log\left(\frac{b_1-b_0}{b-b_0}\right)\right]. \tag{85}$$

For b nearly equal to b_0, (85) becomes

$$x \approx \frac{9R_0^2\mu(R_0^2-b_0^2)}{a^4\rho U_0}\log\left(\frac{b_1-b_0}{b-b_0}\right). \tag{86}$$

Upon solving (86) for b and introducing the length x_0 we obtain

$$b-b_0 = (b_1-b_0)\exp[-x/x_0]. \tag{87}$$

Here x_0 is defined by

$$x_0 = \frac{9R_0^4\mu(1-b_0^2R_0^{-2})}{a^4\rho U_0}. \tag{88}$$

The concentration of particles $c(b,x)$ in the steady state is easily found, from the conservation equation, to be given by

$$c(b,x) = \frac{b_1(db_1/dt)\,c(b_1,0)}{b(db/dt)}. \tag{89}$$

By using (83) in (89), setting $c(b_1,0) = c_1$ and then using (87) to eliminate b_1 we obtain

$$\begin{aligned} c(b,x) &= \frac{b_1^2(b_1-b_0)}{b^2(b-b_0)}c_1 \\ &\approx \{b_0+(b-b_0)\exp[x/x_0]\}^2\frac{\exp[x/x_0]}{b^2}c_1, \\ &\qquad (b_0(1-\exp[-x/x_0]) < b < b_0+(R_0-b_0)\exp[-x/x_0]). \end{aligned} \tag{90}$$

Outside the range determined by the extreme initial radii $b_1 = 0$ and $b_1 = R_0$, which is given by the inequalities in (90), the concentration is zero. The concentration measured by Segre & Silberberg is in qualitative agreement with (90). Furthermore, they have found that their concentration data depend on x only through the ratio x/x_0, where x_0 is given by (88). This agreement shows that the force is of the order of magnitude given by (82). Since this force is of the first order in the Reynolds number, the actual force is also of this order and presumably would be obtained by completing the calculation of the first-order Stokes approximation to which we referred above.

The research in this paper was partially supported by the Office of Naval Research.

Appendix: on the solution of the Oseen equations

We wish to prove that every solution **W** of the reduced Oseen equations (46) and (47) can be represented in the form (48) in terms of two scalar functions ψ and χ satisfying (49) and (50). To do this we first rewrite (48) in component form after setting $\mathbf{W} = (W_1, W_2, W_3)$ and obtain

$$(W_1, W_2, W_3) = (\chi_{yy} + \chi_{zz}, -\psi_z - \chi_{xy}, \psi_y - \chi_{xz}). \tag{A 1}$$

We shall show that we can determine χ and ψ to satisfy (A 1). First we note that if χ satisfies (50) then $\chi_{yy} + \chi_{zz} = \chi_x - \chi_{xx}$. Then the first component of (A 1) becomes an ordinary differential equation for χ which has the solution

$$\chi = -e^x \int_0^x e^{-\xi} \int_0^\xi W_1(\eta, y, z)\, d\eta\, d\xi + a(y, z)\, e^x + b(y, z). \tag{A 2}$$

Here a and b are two 'constants' of integration.

To determine a and b we apply $\Delta_2 = \partial^2/\partial y^2 + \partial^2/\partial z^2$ to (A 2). From (A 1) we see that $\Delta_2 \chi = W_1$ while (46) shows that $\Delta_2 W_1 = W_{1x} - W_{1xx}$. Thus (A 2) yields

$$W_1 = e^x \int_0^x e^{-\xi} \int_0^\xi (W_{1\eta\eta} - W_{1\eta})\, d\eta\, d\xi + e^x \Delta_2 a + \Delta_2 b. \tag{A 3}$$

By evaluating the integral in (A 3) we obtain

$$W_1 = W_1 + e^x[\Delta_2 a(y, z) - W_{1x}(0, y, z)] + \Delta_2 b(y, z) + W_{1x}(0, y, z) - W_1(0, y, z). \tag{A 4}$$

In order that (A 4) hold for all values of x, y, and z it is necessary that a and b satisfy

$$\Delta_2 a(y, z) = W_{1x}(0, y, z) \tag{A 5}$$

and

$$\Delta_2 b(y, z) = W_1(0, y, z) - W_{1x}(0, y, z). \tag{A 6}$$

These equations have solutions which are determined up to additive harmonic functions. Thus (A 2) determines a class of functions χ which satisfy the first equation of (A 1).

Let us now use the second and third components of (A 1) to determine ψ. These components yield $\psi_z = -W_2 - \chi_{xy}$ and $\psi_y = W_3 + \chi_{xz}$. The integrability condition $\psi_{yz} - \psi_{zy} = 0$ is then

$$W_{3z} + \chi_{xzz} + W_{2y} + \chi_{xyy} = 0. \tag{A 7}$$

Since $\chi_{yy}+\chi_{zz}=W_1$ by (A 1), (A 7) becomes $W_{1x}+W_{2y}+W_{3z}=0$ and this equation is satisfied according to (47). Thus we may compute ψ from the relation

$$\begin{aligned}\psi(x,y,z) &= \psi(x,0,0)+\int_0^y \psi_\eta(x,\eta,0)\,d\eta+\int_0^z \psi_\zeta(x,y,\zeta)\,d\zeta \\ &= \psi(x,0,0)+\int_0^y [W_3(x,\eta,0)+\chi_{xz}(x,\eta,0)]\,d\eta \\ &\qquad -\int_0^z [W_2(x,y,\zeta)+\chi_{xy}(x,y,\zeta)]\,d\zeta. \qquad \text{(A 8)}\end{aligned}$$

We have now determined χ and ψ that satisfy (A 1). We have also verified that χ satisfies (50) since we have shown that $\chi_{yy}+\chi_{zz}=W_1$ and $\chi_x-\chi_{xx}=W_1$ so $\Delta\chi-\chi_x=0$. Therefore we need only verify that ψ satisfies (49). To do so we first observe that $\psi_{zz}=(-W_2-\chi_{yx})_z$ and $\psi_{yy}=(W_3+\chi_{xz})_y$. Thus $\psi_{yy}+\psi_{zz}=W_{3y}-W_{2z}$. Next, from (A 8) we have

$$\begin{aligned}\psi_x-\psi_{xx} &= \psi_x(x,0,0)-\psi_{xx}(x,0,0)+\int_0^y [W_{3x}-W_{3xx}+\chi_{xxz}-\chi_{xxxz}]\,d\eta \\ &\qquad -\int_0^z [W_{2x}-W_{2xx}+\chi_{xxy}-\chi_{xxxy}]\,d\zeta. \qquad \text{(A 9)}\end{aligned}$$

From (46), $W_{3x}-W_{3xx}=\Delta_2 W_3$ while from (50) and (A 1) $\chi_{xxz}-\chi_{xxxz}=\Delta_2\chi_{xz}=W_{1xz}$. Similarly, $W_{2x}-W_{2xx}=\Delta_2 W_2$ and $\chi_{xxy}-\chi_{xxxy}=W_{1xy}$. Furthermore, from (47) $W_{1xz}=-(W_{2y}+W_{3z})_z$ and $W_{1xy}=-(W_{2y}+W_{3z})_y$. Then (A 9) becomes

$$\begin{aligned}\psi_x-\psi_{xx} &= \psi_x(x,0,0)-\psi_{xx}(x,0,0)+\int_0^y [W_{3\eta\eta}-W_{2\eta z}]\,d\eta-\int_0^z [W_{2\zeta\zeta}-W_{3y\zeta}]\,d\zeta \\ &= \psi_x(x,0,0)-\psi_{xx}(x,0,0)-W_{3y}(x,0,0)+W_{2z}(x,0,0) \\ &\qquad +W_{3y}(x,y,z)-W_{2z}(x,y,z). \qquad \text{(A 10)}\end{aligned}$$

Let us now require that $\psi(x,0,0)$, which is so far arbitrary, satisfy the equation

$$\psi_x(x,0,0)-\psi_{xx}(x,0,0)=W_{3y}(x,0,0)-W_{2z}(x,0,0). \qquad \text{(A 11)}$$

Then (A 10) shows that $\psi_x-\psi_{xx}=W_{3y}-W_{2z}$ which we saw above is equal to $\psi_{yy}+\psi_{zz}$. Thus ψ satisfies (49) and the theorem is proved.

REFERENCES

Einstein, A. 1906 *Ann. Phys.* **19**, 289.

Jeffery, G. B. 1922 *Proc. Roy. Soc.* A, **102**, 161.

Kirchhoff, G. 1876 *Mechanik*, chap. 26.

Lagerstrom, P. A. & Cole, J. D. 1955 *J. Rat. Mech. Anal.* **4**, 817.

Lamb, H. 1945 *Hydrodynamics*, 6th ed. New York: Dover.

Oseen, C. W. 1910 *Ark. Mat. Astr. Fys.* **6**, no. 29.

Oseen, C. W. 1913 *Ark. Mat. Astr. Fys.* **9**, no. 16.

Proudman, I. & Pearson, J. R. A. 1957 *J. Fluid Mech.* **2**, 237.

Saffman, P. G. 1956 *J. Fluid Mech.* **1**, 540.

Segre, G. & Silberberg, A. 1961 *Nature, Lond.*, **189**, 209.

Simha, R. 1936 *Kolloid Z.* **76**, 16.

Stokes, G. G. 1851 *Camb. Phil. Trans.* **9**, 8.

Tollert, H. 1954 *Chem. Ing. Tech.* **26**, 141.

Photographic evidence of the formation and growth of vorticity behind plates accelerated from rest in still air†

By D. PIERCE

Aerodynamics Department, Royal Aircraft Establishment, Farnborough, Hampshire, England

(Received 5 May 1961)

The shedding of vorticity from the edges of a plate, which is accelerated normal to itself from rest in still air, is investigated experimentally by means of a new flow-visualization technique using spark-lighted shadowgraphs and heated air, benzene or other vapours to introduce sufficient changes in density along the surface of discontinuity.

The photographs show small-scale undulations and the formation of a number of centres of vorticity along the well known big-scale vortex sheets which roll up along their edges.

1. Introduction

Prandtl, in his well known paper of 1904, not only introduced boundary-layer theory but devoted the larger part of the discussion to the mechanism and consequences of boundary-layer separation. Using the example of the initial motion of a fluid as set up by a plate moved from rest at right angles to itself, he discussed the development of the shear layer which originates from the plate's edge, and which may be regarded as a Helmholtz surface of discontinuity, or vortex sheet, in the case of small viscosity. He pointed out that the vortex sheet tends to roll up along its free edge and, further, that such a sheet may be unstable in that small disturbances of its shape are likely to be amplified and lead to the formation of a series of centres of vorticity along the sheet. In this way, a small-scale undulation and vortex formation is superimposed upon a big-scale vortex sheet which itself may incorporate a rolled up edge with the formation of a vortex core there.

Prandtl described the flow mechanism and the resulting features from observations made in a water channel, and similar observations in water have since been made (Wedemeyer 1956). However, most of the later studies have been concerned with problems of the big-scale flow: the time-dependent development of this flow (Anton 1939; Wedemeyer 1956); the corresponding three-dimensional flow for the case of the flat triangular wing (Mangler & Smith 1959); and the features of the main core (Hall 1961). The small-scale undulations have been most extensively studied in the related case of the shear layer round a free jet (Wille 1960), and it has been noted that the formation of centres of vorticity and 'spots' in laminar layers may constitute an important phase in the mechanism of transition to turbulence.

† Crown copyright reserved.

The present study returns to Prandtl's original problem of a plate moved normal to itself from rest in still air. It is demonstrated how spark equipment, designed for the examination of unsteady supersonic flows, may be used to study time-dependent air flows at low speeds by the introduction of small quantities of a foreign vapour.

2. Equipment

The equipment used can be described in two parts: (*a*) that which concerns the acceleration of the plate from rest, and (*b*) that which enables the flow to be photographed.

2.1. *Plate acceleration*

The mechanism for accelerating the plate is shown in figure 1. The equipment consists essentially of three moving parts, with provision for the sudden application of pressure to two of the moving parts by the bursting of a diaphragm.

The plate under test is screwed to the web of a free piston which initially, by gravity, is in contact with a limited-stroke piston, as shown in figure 1. Pressure is increased in the compressed air chamber until the polyester film diaphragm

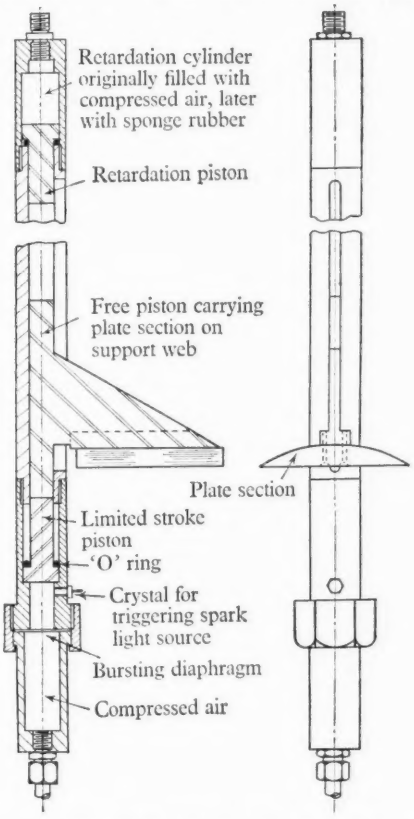
Retardation cylinder originally filled with compressed air, later with sponge rubber
Retardation piston
Free piston carrying plate section on support web
Plate section
Limited stroke piston
'O' ring
Crystal for triggering spark light source
Bursting diaphragm
Compressed air

FIGURE 1. Equipment for accelerating the plate sections.

bursts and the pressure is suddenly applied to the limited-stroke piston. This piston and the free piston carrying the plate are accelerated together until the limited-stroke piston reaches the extent of its travel. The free piston carries the plate and continues to move with roughly constant velocity (it is decelerated slightly by gravity) until after moving for a few inches it is brought to rest by the retardation piston.

Originally the retardation cylinder was filled with air from the compressed air chamber so ensuring identical pressures for acceleration and retardation. Experiments, however, showed the retardation to be too severe and the air in the retardation chamber was replaced by sponge rubber. An O-ring on the limited-travel piston acts as a buffer for its retardation and as a seal to prevent the high-pressure air from escaping. This method of suddenly applying load to the piston obviates the necessity for any breaking link or quick-release mechanism, and it has been found that 0·00025 in. thick diaphragms consistently give plate velocities of 12–13 ft./sec and 0·0005 in. thick diaphragms give 23–24 ft./sec, the variation in velocity depending mainly on slight differences in weight of the various plate sections.

The total weight of the moving parts has been kept small and is approximately 2 oz. A piezo-electric crystal is mounted in the wall of the chamber between the diaphragm and the face of the limited-stroke piston to provide a means of triggering the photographic equipment. This acceleration system is clearly capable of further development, such as to enable the plate to be accelerated to the required velocity in a shorter distance and also to provide for an increased length of travel.

2.2. *Flow visualization technique*

The present experiments were undertaken in air at room temperature and pressure, i.e. roughly 65 °F and 29 in. of mercury, and a shadowgraph system was used together with spark photography to show the details of the vortex sheet.

A spark apparatus which produces an intense light flash with a duration of 1 μsec was available. This was used as the light source of a shadowgraph system in which the parallel light beam was directed over the plate section. The spark flash was triggered at an appropriate time by the signal from the piezo-electric crystal, the signal being first passed through a pre-set delay unit. Ilford H.P.S. photographic plates were used and positioned close to the moving plate to reduce any effects due to stray light. An ordinary shadowgraph technique cannot be used directly because the density changes in the flow are too slight. Thus density changes must be artificially introduced into the flow. Several methods of doing this successfully have been developed, and in all cases the change in density was made to coincide with the surface of discontinuity in velocity so that its effect on the flow may be assumed to be small.

The first method employs a column of air heated by passing over a hot soldering iron. With the plate stationary the column was arranged to pass just outboard of the edge of the plate and was then barely discernible in the shadowgraph pictures. When the plate is moving, the heated air is drawn behind the lee side of the plate to be on the inner side of the surface of discontinuity, which is then shown up with great clarity.

Other methods employ, on the surface of the plate, fluids which evaporate. A plate of balsa wood was used and a narrow band of benzene applied by paint brush to the upper and lower surfaces. The benzene soaks into the balsa wood and then starts to vaporize. When the plate accelerates, air flowing over the surface increases vaporization of the benzene and the vapour is drawn into the vortex sheet. Because of the difference in density between the vapour and the air, the paths of their boundaries are clearly seen in the shadowgraph pictures.

When the benzene is brushed on in a narrow band across the centre of the plate, normal to the light path, the resulting photographs have the effect of showing up the flow in a plane until the vortex and vapour sheet has moved far enough from the plate to be affected by end effects of the plate.

3. Results

The plates tested were all of 3 in. square planform and each had a cross-section which was constant in the direction of the light path. A variety of plates was used, these differing in their cross-sections as may be seen in the photographs, figure 6 (*a*)–(*e*). Also visible in each figure is a scale of pins at $\frac{1}{4}$ in. intervals, the initial position of the plate tip being opposite the bottom pin. This, together with the time intervals indicated, defines the motion of the plate. Care was taken to ensure that the undulations of the vortex sheet were not caused by vibrations of the model by testing plates of different stiffness; nor were they caused by any three-dimensional periodicity across the span of the model. The absence of such periodicity was verified by simultaneously taking pictures in two planes at right angles to one another.

The main sequence of pictures in figure 2 shows the growth of the edge vortex sheets behind a plate with a convex front surface and a flat rear surface as it accelerates to, and remains at, a speed of 24 ft./sec. Figure 3 shows the distance from rest of the plate as a function of the time taken. Figure 4 shows an enlarged section at $t = 5{\cdot}41$ msec.

The sequence of photographs in figure 2 reveal the growth and the structure of the vortex sheets very clearly, and the small-scale formation of a large number of centres of vorticity within the big-scale rolled-up vortex sheet, in the manner described by Prandtl, is distinctly visible. The regularity of the process is noteworthy. Figure 3 also shows the movement of the core of the big-scale rolled-up vortex sheet. It is found that the velocity of the core is about half that of the plate. This is consistent with what is known about the corresponding three-dimensional flow past a rectangular plate of small aspect ratio where the upper edges of the tip vortex sheets are inclined to the mainstream at about half the angle of incidence (Bollay 1937, 1939; Mangler 1939; Küchemann 1955). This was also found to be the case when the plate was accelerated to half the speed, i.e. 12 ft./sec, although the initial undulations in the shear layer appear less pronounced as shown in figure 5. Future investigations may relate the change in the initial undulations to effects depending on the Reynolds number, which, at present, are not known.

The remaining photographs, figure 6, show the pronounced effect of the plate

cross-sectional shape on the regularity of the distortion of the shear layer.† The differences in the flow are of secondary nature: a round edge, figure 6(*c*), produces a less orderly flow with, possibly, two separation lines. A very pronounced shoulder, figure 6(*e*), leads to a secondary separation. Sharp edges which fix separation lines produce clean flows.

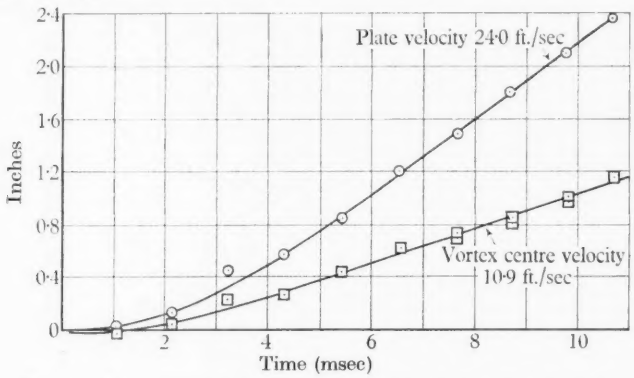

FIGURE 3. Movement of the plate and vortex centre from rest obtained from figure 2(*a*)–(*j*).

4. Conclusions

A technique has been presented which should prove useful in the examination of the development of shear layers and other time-dependent flows at low speeds. Results obtained so far clearly show the distortion of a shear layer into regular vortex filaments and finally into turbulent motion. Further experiments are necessary to understand the dependence on the Reynolds number of the regular manner in which the shear layer breaks up.

REFERENCES

ANTON, L. 1939 Formation of a vortex at the edge of a plate. *Ing.-Arch.* **10**, 411.

BOLLAY, W. 1937 A theory for rectangular wings of small aspect ratio. *J. Aero. Sci.* **4**, 294.

BOLLAY, W. 1939 A non-linear wing theory and its application to rectangular wings of small aspect ratio. *Z. angew. Math. Mech.* **19**, 21.

HALL, M. G. 1961. A theory for the core of a leading edge vortex. *J. Fluid Mech.* **11**, 209.

KÜCHEMANN, D. 1955 A non-linear lifting surface theory for wings of small aspect ratio with edge separations. *Aero. Res. Counc., Rep.* no. 17,769.

MANGLER, K. W. 1939 Der kleinste induzierte Widerstand eines Tragflügels mit kleinem Seitenverhältnis. *Jb. dtsch. Luftfahrt*, **1**, 140.

MANGLER, K. W. & SMITH, J. H. B. 1959 A theory of the flow past a slender delta wing with leading edge separation. *Proc. Roy. Soc.* A, **251**, 200.

PRANDTL, L. 1904 Über Flüssigkeitsbewegung bei sehr kleiner Reibung. *Verhandlungen des III. Internationalen Mathematiker-Kongresses, Heidelberg.* (Leipzig: B. G. Teubner, 1905.)

WEDEMEYER, E. 1956 Ausbildung eines Wirbelpaares an den Kanten einer Platte. *Max-Planck-Institut für Strömungsforschung, Bericht*, 56/B/06.

WILLE, R. 1960 Modellvorstellungen zum Übergang Laminar-Turbulent. *Deutsche Versuchsanstalt für Luftfahrt E. V. Bericht*, Nr. 113.

† In some of the pictures, particularly figure 6(*b*), some particles of balsa dust are visible; these have been shed by the plate during the acceleration phase.

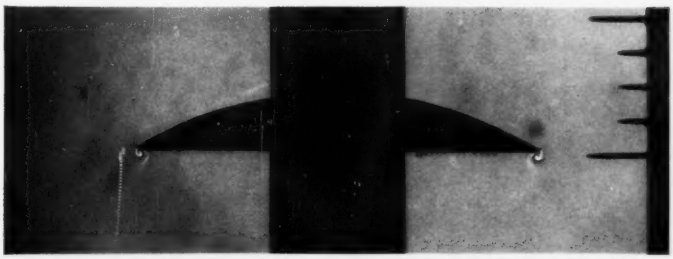

(*a*) $t = 1{\cdot}05$ msec; instantaneous velocity (v_1) = 5·5 ft./sec.

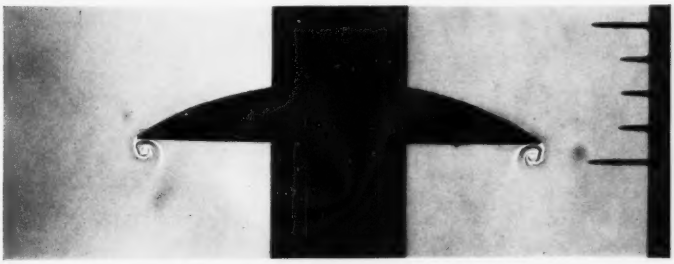

(*b*) $t = 2{\cdot}14$ msec; $v_1 = 11{\cdot}1$ ft./sec.

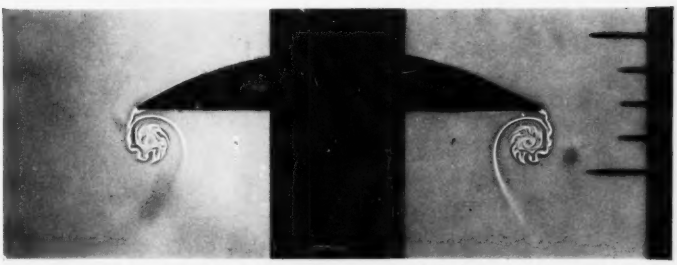

(*c*) $t = 3{\cdot}22$ msec; $v_1 = 16{\cdot}9$ ft./sec.

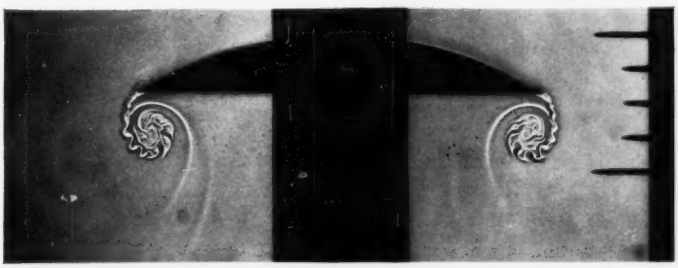

(*d*) $t = 4{\cdot}30$ msec; $v_1 = 21{\cdot}0$ ft./sec.

(*Facing p.* 464)

(*e*) $t = 5{\cdot}41$ msec; $v_1 = 23{\cdot}2$ ft./sec.

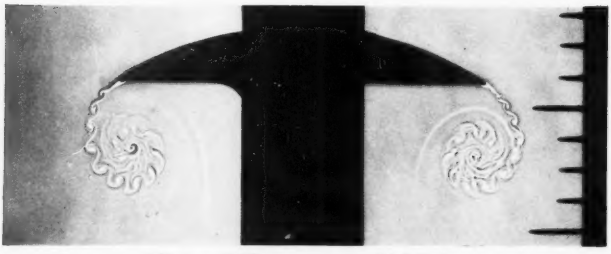

(*f*) $t = 6{\cdot}53$ msec; $v_1 = 24{\cdot}0$ ft./sec.

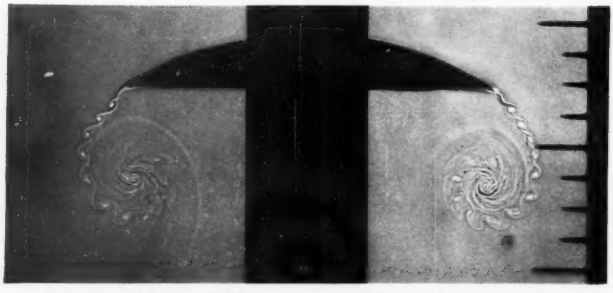

(*g*) $t = 7{\cdot}65$ msec; $v_1 = 24{\cdot}0$ ft./sec.

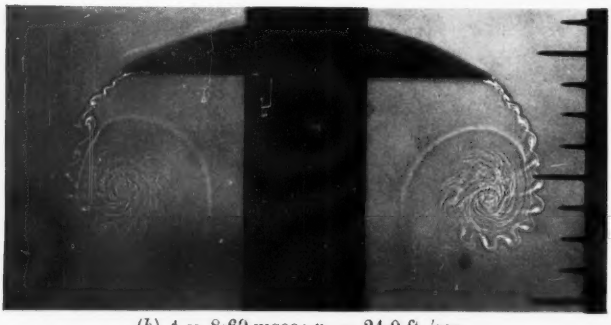

(*h*) $t = 8{\cdot}69$ msec; $v_1 = 24{\cdot}0$ ft./sec.

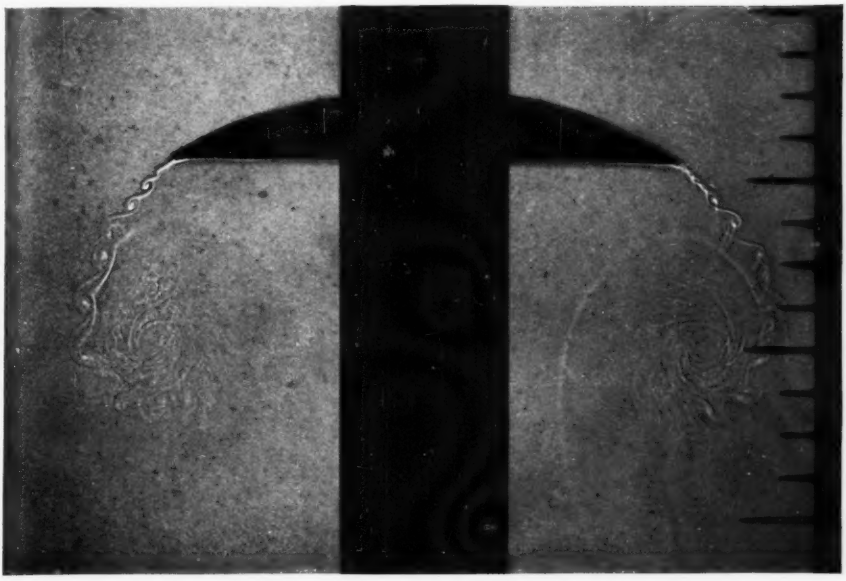

(*i*) $t = 9{\cdot}77$ msec; $v_1 = 24{\cdot}0$ ft./sec.

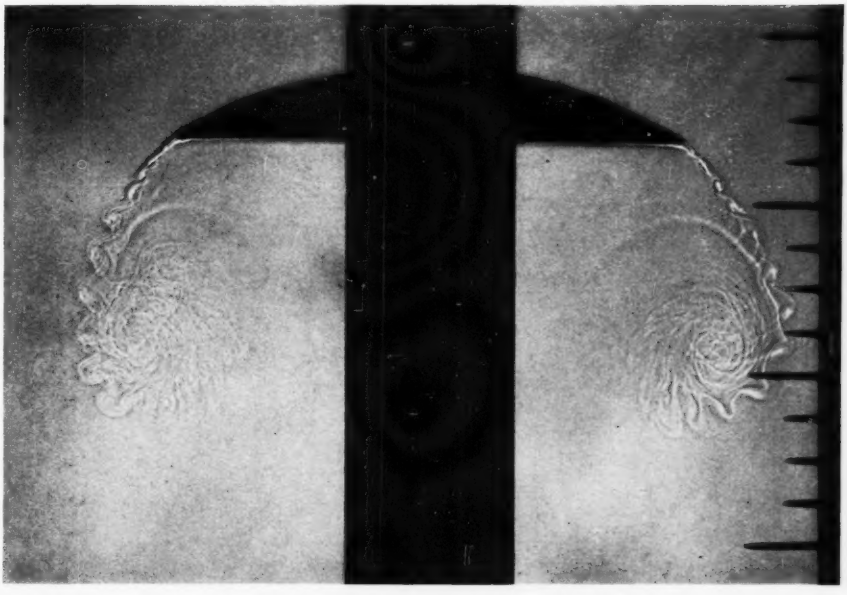

(*j*) $t = 10{\cdot}66$ msec; $v_1 = 24{\cdot}0$ ft./sec.

FIGURE 2. Sequence of shadowgraphs of convex plate section with final velocity 24 ft./sec.

FIGURE 4. Enlargement of figure 2(*e*). $t = 5{\cdot}41$ msec, $v_1 = 23{\cdot}2$ ft./sec.

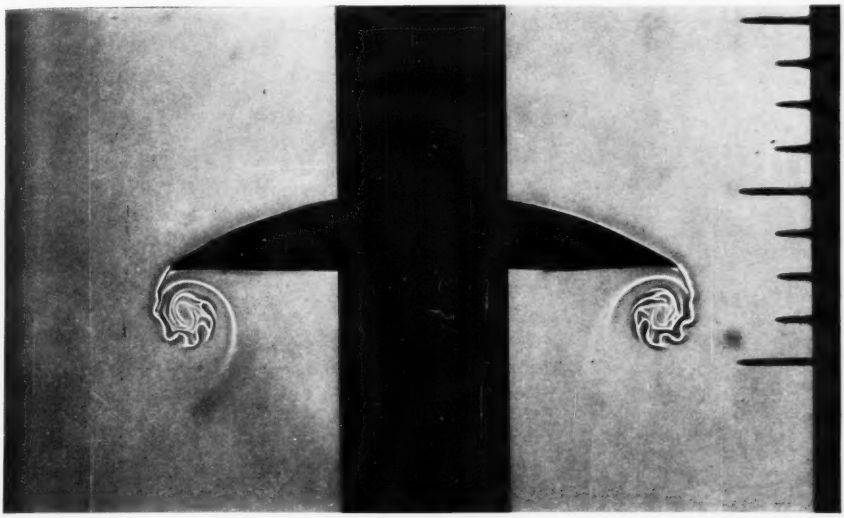

(*a*) $t = 6{\cdot}53$ msec, $v_1 = 12{\cdot}1$ ft./sec.

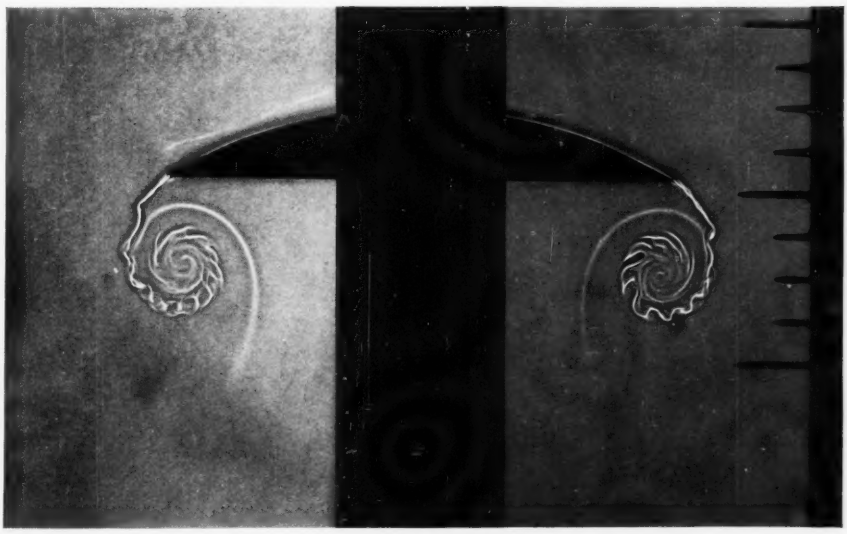

(*b*) $t = 10{\cdot}66$ msec; $v_1 = 12{\cdot}1$ ft./sec.

FIGURE 5. Shadowgraphs of convex plate section with final velocity 12·1 ft./sec.

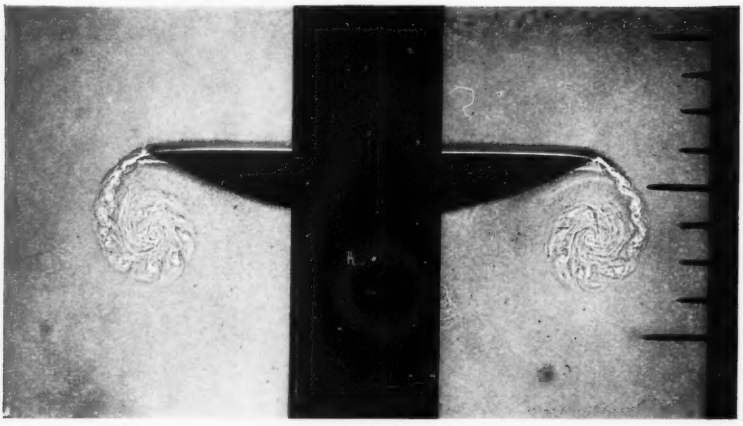

(*a*)

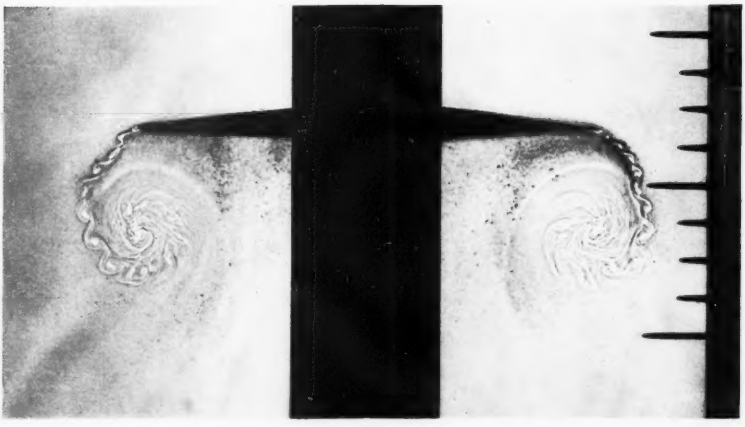

(*b*)

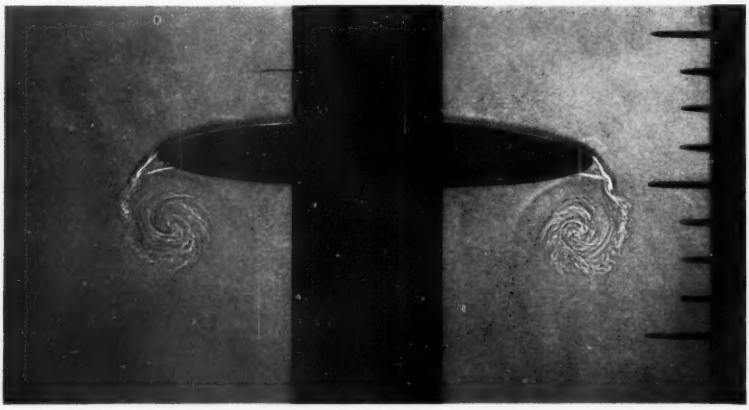

(*c*)

(*d*)

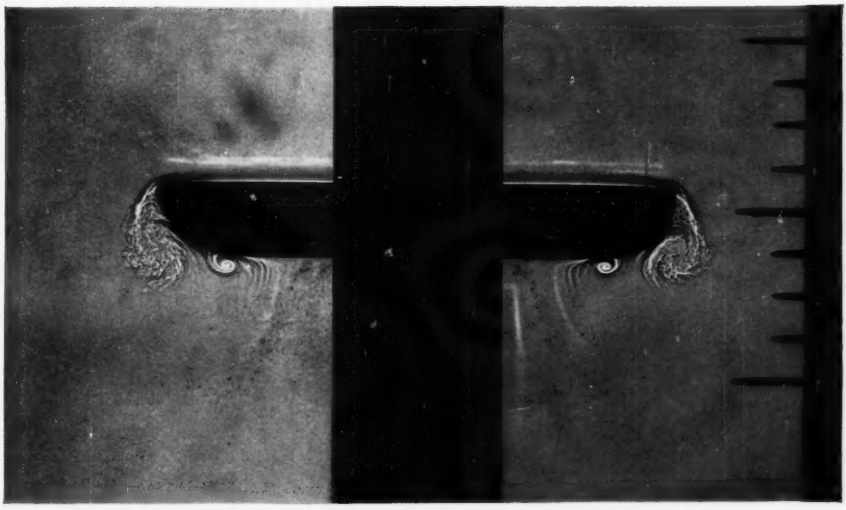

(*e*)

FIGURE 6. Shadowgraphs of various plate cross-sections at $t = 6{\cdot}53$ msec. All velocities 24 ft./sec approximately.

A turbulent equatorial jet

By ROBERT R. LONG
Department of Mechanics, The Johns Hopkins University, Baltimore

(Received 31 January 1961 and in revised form 4 April 1961)

A recent study of a laminar jet in a rotating spherical shell of fluid is extended to the case of a turbulent planetary jet at the equator of a rotating, stratified atmosphere or ocean. General forms of the velocity, density and pressure functions of both the mean motion and the turbulence are derived by a dimensional analysis applied to the mean and perturbation equations. The horizontal and vertical dimensions are estimated, based on the three characteristic constants of the problem, which are the momentum transfer, the stability and a rotation parameter. The estimates are in good agreement with the dimensions of the Cromwell current, i.e. the equatorial undercurrent of the Pacific Ocean.

To the first order of approximation, the mean axial velocity in the theory is independent of distance along the jet axis. The mean horizontal transverse velocity component is much smaller and decreases upstream. The mean vertical velocity is extremely small, also decreasing upstream. The two horizontal velocity components of the turbulence are of the same order and, in the undercurrent, are about one-fourth the mean axial velocity. The vertical turbulent component is much smaller. Finally, it is shown that the eddy-viscosity concept is inappropriate for this problem because at least one of the eddy coefficients would have to be negative.

1. Introduction

In a recent paper (Long 1960) the author investigated a laminar, two-dimensional jet in a rotating spherical shell of homogeneous, viscous fluid. The flow is predominantly zonal, or west-east, and a suggested physical mechanism is a balance of vorticity brought into the jet by the weak north-south motion and diffused by friction. The order of magnitude of the horizontal width of the theoretical jet is given by $\overline{u}/\beta\delta_y^2 \sim 1$, where δ_y is the width, $\overline{u}$ is a representative velocity, and β is the north-south rate of change of the Coriolis parameter. This expression was used to estimate the width of the Cromwell current or equatorial undercurrent. This is a west-to-east current at the equator in the Pacific Ocean, located a hundred metres or so below the surface (Cromwell, Montgomery & Stroup 1954; Fofonoff & Montgomery 1955; Hidaka & Nagata 1958; Knauss & King 1958; see also the entire volume *Deep Sea Research*, **6**, 1960). If we use values $\overline{u} = 1{\cdot}5 \times 10^2\,\mathrm{cm\,sec^{-1}}$, $\beta = 2{\cdot}6 \times 10^{-13}\,\mathrm{cm^{-1}\,sec^{-1}}$, appropriate to the Cromwell current, we obtain $\delta_y \sim 2{\cdot}6 \times 10^7$ cm. This agrees well with the observed width, 300 km, as reported by Knauss (1960).

The laminar theory had two deficiences in relation to such geophysical jet

flows as the undercurrent and the equatorial atmospheric jet (Lettau 1956): (1) the theory assumed that all quantities were independent of height, whereas the natural jets have much smaller thicknesses in the vertical than in the horizontal; (2) the motion was laminar, whereas the natural jets are no doubt fully turbulent. It was argued that the results could be applied to the undercurrent by introducing the concept of eddy viscosity, but the validity of this concept is always doubtful.

In this paper we investigate a fully turbulent jet in an infinite atmosphere or ocean. The axis of the jet is along the equator, and a general view is as pictured in figure 1. We may suppose that the flow is into a sink in the vicinity of $x = 0$, $y = 0$, $z = 0$. We confine attention, however, to the flow in the vicinity of $(-X_0, 0, 0)$ far upstream.†

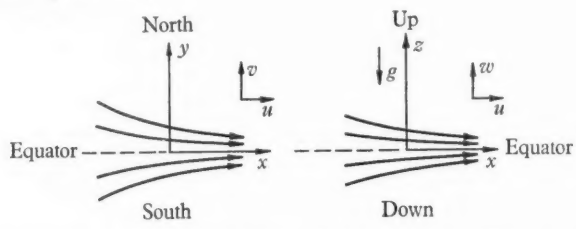

FIGURE 1. Schematic picture of mean motion in jet. The transverse velocity fields may have signs different from those suggested by this drawing.

2. Basic equations

We consider the fluid to be incompressible but inhomogeneous. At great distances vertically and horizontally from the jet axis, the gradient of density is linear in the vertical; i.e.

$$\frac{\partial \rho}{\partial z} \to -\frac{k\rho_0}{g}, \quad \frac{\partial \rho}{\partial x} \to 0, \quad \frac{\partial \rho}{\partial y} \to 0,$$

where k is a constant, g is gravity, and ρ_0 is a reference density. We also make the Boussinesq approximation (Boussinesq 1903) that density variations are negligible in their effects on the inertia of a parcel and in the equation of continuity, but of fundamental importance when they multiply gravity. Then, if we define a perturbation density ρ^* by

$$\rho = \rho_0 - \frac{kz}{g}\rho_0 + \rho^*,$$

and G, P by

$$G = -g\frac{\rho^*}{\rho_0}, \quad P = \frac{p}{\rho_0} + gz - \tfrac{1}{2}kz^2, \tag{1}$$

the equations of the problem can be written

$$u_t + uu_x + vu_y + wu_z - \beta yv = -P_x, \tag{2}$$

$$v_t + uv_x + vv_y + wv_z + \beta yu = -P_y, \tag{3}$$

$$w_t + uw_x + vw_y + ww_z - G = -P_z, \tag{4}$$

$$G_t + uG_x + vG_y + wG_z + kw = 0, \tag{5}$$

$$u_x + v_y + w_z = 0. \tag{6}$$

† We consider only westerly jets. Qualitative arguments, attributed to C. C. Lin, indicate that westerly jets are stable, easterly jets unstable to large-wavelength perturbations (Veronis 1960).

Equations (2) to (4) are the equations of motion, equation (5) expresses the incompressibility assumption, and (6) is the equation of continuity.

We have neglected molecular friction and diffusion. We know, of course, that these terms are important in so far as they affect the very small eddies, but it is well established that in fully developed turbulent flow at high Reynolds numbers, the effect on the mean motion as well as on the energy-containing eddies is negligible (Townsend 1956).

The terms $-\beta yv$ and βyu are the Coriolis accelerations, in which the Coriolis parameter $2\Omega\sin\theta$ (Ω is the angular rotation speed of the sphere, θ the latitude angle) has been approximated by $2\Omega y/a = \beta y$, where a is the radius of the sphere. This is a very good approximation if the north-south extent of the jet is sufficiently limited. Indeed, the error is of the same order as that involved in using equations in Cartesian instead of spherical co-ordinates, namely $o(\Lambda^{-2})$, where Λ is the ratio of the east-west and north-south length scales (Long 1960).

Finally we notice that in the two-dimensional theory (Long 1960), the solution described a jet motion that could exist at any latitude. In this paper the jet must be located at the equator if the equations are to have the form of (2)–(6).

We now take ensemble averages. Then, for example, we have

$$u = \overline{u} + u', \tag{7}$$

where $\overline{u}$ is the average velocity and $\overline{u'} = 0$. If we substitute into (2)–(6), we get a set of averaged and unaveraged differential equations:

$$\overline{u}\overline{u}_x + \overline{v}\overline{u}_y + \overline{w}\overline{u}_z - \beta y\overline{v} = -\overline{P}_x - (\overline{u'u'})_x - (\overline{u'v'})_y - (\overline{u'w'})_z, \tag{8}$$

$$\overline{u}\overline{v}_x + \overline{v}\overline{v}_y + \overline{w}\overline{v}_z + \beta y\overline{u} = -\overline{P}_y - (\overline{u'v'})_x - (\overline{v'v'})_y - (\overline{v'w'})_z, \tag{9}$$

$$\overline{u}\overline{w}_x + \overline{v}\overline{w}_y + \overline{w}\overline{w}_z - \overline{G} = -\overline{P}_z - (\overline{u'w'})_x - (\overline{v'w'})_y - (\overline{w'w'})_z, \tag{10}$$

$$\overline{u}\overline{G}_x + \overline{v}\overline{G}_y + \overline{w}\overline{G}_z + \overline{w}k = -(\overline{u'G'})_x - (\overline{v'G'})_y - (\overline{w'G'})_z, \tag{11}$$

$$\overline{u}_x + \overline{v}_y + \overline{w}_z = 0, \tag{12}$$

and

$$u'_t + \overline{u}u'_x + u'\overline{u}_x - (\overline{u'u'})_x + u'u'_x + \overline{v}u'_y + v'\overline{u}_y + v'u'_y - (\overline{u'v'})_y + w'u'_z + \overline{w}u'_z + w'\overline{u}_z - (\overline{u'w'})_z - \beta yv' = -P'_x, \tag{13}$$

$$v'_t + \overline{u}v'_x + u'\overline{v}_x - (\overline{u'v'})_x + u'v'_x + \overline{v}v'_y + v'\overline{v}_y - (\overline{v'v'})_y + v'v'_y + w'v'_z + \overline{w}v'_z + w'\overline{v}_z - (\overline{w'v'})_z + \beta yu' = -P'_y, \tag{14}$$

$$w'_t + \overline{u}w'_x + u'\overline{w}_x - (\overline{u'w'})_x + u'w'_x + \overline{v}w'_y + v'\overline{w}_y - (\overline{w'v'})_y + v'w'_y + w'\overline{w}_z + \overline{w}w'_z - (\overline{w'w'})_z + w'w'_z - G' = -P'_z, \tag{15}$$

$$\overset{\Lambda^{-\frac{1}{2}}}{G'_t} + \overset{\Lambda^{-\frac{1}{2}}}{\bar{u}G'_x} + \overset{\Lambda^{-\frac{1}{2}}}{u'\bar{G}_x} - \overset{\Lambda^{-\frac{1}{2}}}{(\overline{u'G'})_x} + \overset{\Lambda^{-\frac{1}{2}}}{u'G'_x} + \overset{\Lambda^{-1}}{\bar{v}G'_y} + \overset{\Lambda^{-\frac{1}{2}}}{v'\bar{G}_y} - \overset{\Lambda^{-\frac{1}{2}}}{(\overline{v'G'})_y}$$

$$+ \overset{\Lambda^{-\frac{1}{2}}}{v'G'_y} + \overset{\Lambda^{-1}}{\bar{w}G'_z} + \overset{\Lambda^{-\frac{1}{2}}}{w'\bar{G}_z} - \overset{\Lambda^{-\frac{1}{2}}}{(\overline{w'G'})_z} + \overset{\Lambda^{-\frac{1}{2}}}{w'G'_z} + kw' = 0, \quad (16)$$

$$u'_x + v'_y + w'_z = 0. \quad (17)$$

The symbols Λ^{-1}, $\epsilon^2\Lambda^{-1}$, etc., over the terms in these equations express the order of magnitude of the terms in a way which will be explained later.

If we now integrate equation (8) over a section of the jet, and assume that the velocities go to zero sufficiently fast at great distances from the jet axis, we get that

$$J = \int_{-\infty}^{\infty}\int_{-\infty}^{\infty} (\bar{P} + \bar{u}^2 + \overset{\Lambda^{-1}}{\overline{u'u'}} - \tfrac{1}{2}\beta y^2 \bar{u})\, dy\, dz \quad (18)$$

is constant, where we have used integration by parts and the equation of continuity to transform the Coriolis term. The constant J is fundamental to the problem. It is called the *momentum transfer*. If we specified the conditions at the sink precisely and all other conditions of the problem, and found the exact solution corresponding to zero motion at $|y| \to \infty$, $|z| \to \infty$, the integral (18) would be constant (independent of x), and J would be automatically determined. We confine attention, however, to the flow at large distances from the sink, and the solution we seek is not valid in the region (near the origin) where conditions are imposed that involve the precise description of the sink, say the flux Q and a linear dimension a. In adopting (18) as an alternative condition we must recognize the possibility that this may not be an adequate substitute for the two conditions involving a, Q, and that an indeterminacy may result. (Additional remarks about this point are contained below.)

3. General form of solution

We first make boundary-layer type estimates of the size of the terms in the mean equations. For example, it is plausible that the Coriolis and pressure terms alone dominate in (9), and that the vertical pressure variation is hydrostatic in (10). A first approximation for the unknowns in the equations of mean motion can then be obtained by using a generalized dimensional analysis, i.e. a search for invariance under a general affine transformation (Birkhoff 1950). We may then use the equations defining the Reynolds stresses to estimate the magnitude of such turbulent quantities as $u'v'$. A combination of these estimates of mean and turbulent quantities leads us to the general form of a first approximation to the solution and to a set of simplified differential equations that determine the first approximation. This in turn suggests a consistent scheme of successive approximations to the exact solution of the fully turbulent jet problem in the form of power series in certain small variables and parameters. We do not, to be sure, show that other expansions are not possible.

We first shift the origin of our co-ordinate system from the orifice to an origin at a great distance toward the west, X_0. Then x is the variable distance along

the x-axis from the section in question. We introduce a typical velocity and length

$$c = \beta^{\frac{1}{7}} k^{\frac{1}{7}} J^{\frac{2}{7}}, \tag{19}$$

$$L = \beta^{-\frac{3}{7}} J^{\frac{1}{7}} k^{\frac{1}{14}}, \tag{20}$$

and non-dimensional independent variables

$$\xi = x/L, \quad \eta = y/L, \quad \zeta = z/L\epsilon, \quad \tau = tc/L, \tag{21}$$

where

$$\epsilon = J^{\frac{1}{7}} \beta^{\frac{4}{7}} k^{-\frac{3}{7}}. \tag{22}$$

We also need a non-dimensional function† of x:

$$\Lambda = (X_0 - x)/L. \tag{23}$$

We assume that Λ is very large. It is of the order of the ratio of the axial scale of the mean motion to the width of the jet if we assume $\eta \sim 1$. We see that if the quantities ζ and η in (21) are both of the order of one, ϵ is the ratio of the vertical and north-south length scales. We assume that ϵ is very small. (It is of the order of 10^{-3} in the case of the equatorial undercurrent.)

We now search for solutions for the mean and turbulent quantities in the forms‡

$$\overline{u}/c = U_1 + \Lambda^{-\frac{1}{2}} U_2 + \ldots + \epsilon^2 U_{21} + \ldots, \tag{24}$$

$$\overline{v}\Lambda/c = V_1 + \Lambda^{-\frac{1}{2}} V_2 + \ldots + \epsilon^2 V_{21} + \ldots, \tag{25}$$

$$\overline{w}\Lambda/\epsilon c = W_1 + \Lambda^{-\frac{1}{2}} W_2 + \ldots + \epsilon^2 W_{21} + \ldots, \tag{26}$$

$$\overline{P}/c^2 = P_1 + \Lambda^{-\frac{1}{2}} P_2 + \ldots + \epsilon^2 P_{21} + \ldots, \tag{27}$$

$$\overline{G}\epsilon L/c^2 = G_1 + \Lambda^{-\frac{1}{2}} G_2 + \ldots + \epsilon^2 G_{21} + \ldots, \tag{28}$$

$$\overline{u'u'}\Lambda/c^2 = F_1 + \Lambda^{-\frac{1}{2}} F_2 + \ldots + \epsilon^2 F_{21} + \ldots, \tag{29}$$

$$\overline{u'v'}\Lambda/c^2 = N_1 + \Lambda^{-\frac{1}{2}} N_2 + \ldots + \epsilon^2 N_{21} + \ldots, \tag{30}$$

$$\overline{u'w'}\Lambda/c^2\epsilon = H_1 + \Lambda^{-\frac{1}{2}} H_2 + \ldots + \epsilon^2 H_{21} + \ldots, \tag{31}$$

$$\overline{v'v'}\Lambda/c^2 = K_1 + \Lambda^{-\frac{1}{2}} K_2 + \ldots + \epsilon^2 K_{21} + \ldots, \tag{32}$$

$$\overline{v'w'}\Lambda/c^2\epsilon = L_1 + \Lambda^{-\frac{1}{2}} L_2 + \ldots + \epsilon^2 L_{21} + \ldots, \tag{33}$$

$$\overline{w'w'}\Lambda/c^2\epsilon^2 = M_1 + \Lambda^{-\frac{1}{2}} M_2 + \ldots + \epsilon^2 M_{21} + \ldots, \tag{34}$$

$$\overline{u'G'}\epsilon L\Lambda/c^3 = A_1 + \Lambda^{-\frac{1}{2}} A_2 + \ldots + \epsilon^2 A_{21} + \ldots, \tag{35}$$

$$\overline{v'G'}\epsilon L\Lambda/c^3 = B_1 + \Lambda^{-\frac{1}{2}} B_2 + \ldots + \epsilon^2 B_{21} + \ldots, \tag{36}$$

† Although we define Λ with the idea in mind that X_0 represents the distance to the orifice from the section at which we perform our analysis, in fact nothing in the analysis will be changed if we regard X_0 simply as a sufficiently large positive quantity with the dimensions of length. Some consequences of this are discussed below.

‡ The first approximations to the solution represent self-preserving flow, but in the development of this paper we *show* that this type of flow is possible at great distances from the orifice by considering all equations and conditions of the problem, not simply the equations of mean motion. Since the analysis may be applied to jets and wakes in homogeneous, non-rotating fluid, the approach of this paper removes the necessity for the customary *assumption* of self-preserving flow. The point is discussed by Townsend (1956).

$$\overline{w'G'}L\Lambda/c^3 = C_1+\Lambda^{-\frac{1}{2}}C_2+\ldots+\epsilon^2C_{21}+\ldots, \tag{37}$$

$$u'\Lambda^{\frac{1}{2}}/c = u_1+\Lambda^{-\frac{1}{2}}u_2+\ldots+\epsilon^2u_{21}+\ldots, \tag{38}$$

$$v'\Lambda^{\frac{1}{2}}/c = v_1+\Lambda^{-\frac{1}{2}}v_2+\ldots+\epsilon^2v_{21}+\ldots, \tag{39}$$

$$w'\Lambda^{\frac{1}{2}}/c\epsilon = w_1+\Lambda^{-\frac{1}{2}}w_2+\ldots+\epsilon^2w_{21}+\ldots, \tag{40}$$

$$P'\Lambda^{\frac{1}{2}}/c^2 = p_1+\Lambda^{-\frac{1}{2}}p_2+\ldots+\epsilon^2p_{21}+\ldots, \tag{41}$$

$$G'\epsilon L\Lambda^{\frac{1}{2}}/c^2 = g_1+\Lambda^{-\frac{1}{2}}g_2+\ldots+\epsilon^2g_{21}+\ldots, \tag{42}$$

where the functions denoted by capital letters, U_1, V_2, etc., are functions only of η, ζ, and those denoted by small letters, u_1, v_1, etc., are functions of ξ, η, ζ, τ.

If these expressions are substituted into equations (8)–(18), we find that the sets of quantities U_1, V_1–p_1, g_1; U_2, V_2–p_2, g_2; etc., satisfy sets of equations in independent variables ξ, η, ζ, τ, from which all the constants of the problem are missing and which do not involve Λ or ϵ. If we assume, therefore, that U_1, V_1–p_1, g_1 as well as ξ, η, ζ, τ are all of order one, we may then estimate the magnitude of all terms in equations (8)–(18). A quantity such as Λ^{-1}, $\epsilon^2\Lambda^{-2}$, etc., written over a term is the ratio of that term to the dominant terms of the equation.

The first set of equations is

$$V_1\frac{\partial U_1}{\partial\eta}+W_1\frac{\partial U_1}{\partial\zeta}-\eta V_1 = -\frac{\partial N_1}{\partial\eta}-\frac{\partial H_1}{\partial\zeta}, \tag{43}$$

$$\eta U_1 = -\frac{\partial P_1}{\partial\eta}, \tag{44}$$

$$-G_1 = -\frac{\partial P_1}{\partial\zeta}, \tag{45}$$

$$V_1\frac{\partial G_1}{\partial\eta}+W_1\frac{\partial G_1}{\partial\zeta}+W_1 = -\frac{\partial B_1}{\partial\eta}-\frac{\partial C_1}{\partial\zeta}, \tag{46}$$

$$\frac{\partial V_1}{\partial\eta}+\frac{\partial W_1}{\partial\zeta} = 0, \tag{47}$$

$$1 = \int_{-\infty}^{\infty}\int_{-\infty}^{\infty}\left(P_1+U_1^2-\frac{\eta^2U_1}{2}\right)d\eta\,d\zeta, \tag{48}$$

and

$$\frac{\partial u_1}{\partial\tau}+U_1\frac{\partial u_1}{\partial\xi}+v_1\frac{\partial U_1}{\partial\eta}+w_1\frac{\partial U_1}{\partial\zeta}-\eta v_1 = -\frac{\partial p_1}{\partial\xi}, \tag{49}$$

$$\frac{\partial v_1}{\partial\tau}+U_1\frac{\partial v_1}{\partial\xi}+\eta u_1 = -\frac{\partial p_1}{\partial\eta}, \tag{50}$$

$$-g_1 = -\frac{\partial p_1}{\partial\zeta}, \tag{51}$$

$$\frac{\partial g_1}{\partial\tau}+U_1\frac{\partial g_1}{\partial\xi}+v_1\frac{\partial G_1}{\partial\eta}+w_1\frac{\partial G_1}{\partial\zeta}+w_1 = 0, \tag{52}$$

$$\frac{\partial u_1}{\partial\xi}+\frac{\partial v_1}{\partial\eta}+\frac{\partial w_1}{\partial\zeta} = 0. \tag{53}$$

These are 10 differential equations in 14 unknowns U_1, V_1, W_1, P_1, G_1, u_1, v_1, w_1, p_1, g_1, N_1, H_1, B_1, C_1. We can make the system determinate, however, by adding the four equations

$$N_1 = \lim_{\lambda\to\infty} \frac{1}{\lambda}\int_0^\lambda u_1 v_1 d\xi, \tag{54}$$

$$H_1 = \lim_{\lambda\to\infty} \frac{1}{\lambda}\int_0^\lambda u_1 w_1 d\xi, \tag{55}$$

$$B_1 = \lim_{\lambda\to\infty} \frac{1}{\lambda}\int_0^\lambda v_1 g_1 d\xi, \tag{56}$$

$$C_1 = \lim_{\lambda\to\infty} \frac{1}{\lambda}\int_0^\lambda w_1 g_1 d\xi. \tag{57}$$

Since N_1, H_1, B_1, C_1 do not vary with ξ, we substitute for the ensemble average a space average along the x-axis. The equations (43)–(47), (49)–(53) and (54)–(57) are now a complete set of equations. Notice that if we multiply (52) by g_1 and average, we get

$$B_1\frac{\partial G_1}{\partial \eta} + C_1\left(\frac{\partial G_1}{\partial \zeta} + 1\right) = 0. \tag{58}$$

This may be substituted for either (56) or (57).

The mathematical problem of the first approximation is not completely stated by the system of equations (43)–(57). Indeed, we see that if U_1, V_1, W_1, P_1, G_1, u_1, v_1, w_1, p_1, g_1, N_1, H_1, B_1, C_1 is a solution of the system, then there is an infinity of solutions U_1, $\alpha^2 V_1$, $\alpha^2 W_1$, P_1, G_1, αu_1, αv_1, αw_1, αp_1, αg_1, $\alpha^2 N_1$, $\alpha^2 H_1$, $\alpha^2 B_1$, $\alpha^2 C_1$, where α is any constant. Notice that as α is varied the solutions change in just the same way as a given solution changes when $X_0^{\frac{1}{2}}$ is varied. (The difference between $X_0 - x$ and X_0 in Λ is negligible for the purposes of the first approximation.) A similar indeterminacy arises in the non-rotating, homogeneous, turbulent jet. If the eddy-viscosity concept is used, it appears as an indeterminacy in the eddy Reynolds number (Townsend 1956).

One reason for the indeterminacy is that we have said nothing yet about our origin of time or about the turbulent velocity, pressure and density fields that exist at that instant. Something must be specified about those turbulent fields, but since we have assumed no variation with time of the mean quantities the initial fields are not completely arbitrary. For example, if we assume solutions for the turbulent quantities in the form

$$u_1 = u_{11}\cos(a\xi + b\tau) + u_{12}\sin(a\xi + b\tau),$$

$$v_1 = v_{11}\sin(a\xi + b\tau) + v_{12}\cos(a\xi + b\tau),$$

$$w_1 = w_{11}\sin(a\xi + b\tau) + w_{12}\cos(a\xi + b\tau),$$

$$p_1 = p_{11}\cos(a\xi + b\tau) + p_{12}\sin(a\xi + b\tau),$$

$$g_1 = g_{11}\cos(a\xi + b\tau) + g_{12}\sin(a\xi + b\tau),$$

where u_{11}, v_{12}, etc., are functions of η, ζ, and a, b are constants, we find from (54) to (57)

$$N_1 = \tfrac{1}{2}u_{11}v_{12} + \tfrac{1}{2}u_{12}v_{11},$$
$$H_1 = \tfrac{1}{2}u_{11}w_{12} + \tfrac{1}{2}u_{12}w_{11},$$
$$B_1 = \tfrac{1}{2}v_{11}g_{12} + \tfrac{1}{2}v_{12}g_{11},$$
$$C_1 = \tfrac{1}{2}w_{11}g_{12} + \tfrac{1}{2}w_{12}g_{11}.$$

On substitution into (43)–(53), the sine and cosine terms cancel out and we get 15 differential equations in 15 unknowns U_1, V_1, ..., u_{11}, v_{11}, ..., u_{12}, v_{12}, ... In this way we can arrive, in principle, at a solution of the first-approximation problem, but the initial conditions that are implied by this solution are very special. It is possible, of course, to assume solutions for the turbulent quantities that will satisfy more general initial conditions, but this increases the complexity of the equations that must be solved.

4. General properties of the jet

If we suppose that all the non-dimensional quantities that we have introduced (except Λ, ϵ) are of the order of 1, and if we confine attention to the first approximation in (24)–(42), we can state a number of properties of the jet:

(1) Combining $U_1 \sim 1$ and $\eta \sim 1$, we find that $\delta_y \sim \bar{u}^{\frac{1}{2}}\beta^{-\frac{1}{2}}$, where δ_y is the width of the jet. The width is small if the speed is low and if the rotation is high. In order of magnitude this is the same as the width of the laminar jet (Long 1960), although the laminar jet widens gradually with distance from the sink, whereas the width of the turbulent jet is uniform.

(2) Combining $\zeta \sim 1$, $\eta \sim 1$, we find that $\delta_z \sim \bar{u}k^{-\frac{1}{2}}$, where δ_z is the vertical thickness of the jet. Hence the vertical extent of the jet is small if the speed is low and the stability large. The vertical thickness is also independent of distance from the sink. Notice that the motion so adjusts itself that the non-dimensional numbers representing the rotation effect and the stability are of the order of one.

(3) The axial mean velocity is constant along the length of the jet.

(4) The transverse mean velocities both decrease upstream as $1/X_0$. In magnitude, $\bar{v} \ll \bar{u}$ and $\bar{w} \ll \bar{v}$.

(5) The mean-density field is independent of distance along the axis.

(6) The two horizontal turbulent velocity components are of the same order and smaller than the axial mean velocity. The vertical and horizontal transverse turbulent velocities are larger than the corresponding mean quantities. The vertical turbulent velocity is much smaller than the horizontal components.

(7) All turbulent quantities decrease rather gradually upstream as $X_0^{-\frac{1}{2}}$.

(8) The horizontal scale of the turbulence is of the order of the horizontal width of the jet; the vertical scale of the turbulence is of the order of the thickness of the jet.

An important result may be obtained concerning the eddy-viscosity concept applied to this problem. For example, if we assume the turbulent transports are proportional to the mean density gradients

$$\overline{v'G'} = -K_y\frac{\partial \bar{G}}{\partial y}, \quad \overline{w'G'} = -K_z\left(\frac{\partial \bar{G}}{\partial z} + k\right),$$

where K_y, K_z are horizontal and vertical components of eddy diffusivity, the form of (46) is preserved only if

$$K_y = \frac{1}{S_y}\Lambda^{-1}\beta^{-\frac{2}{7}}k^{\frac{3}{14}}J^{\frac{3}{7}}, \quad B_1 = -\frac{1}{S_y}\frac{\partial G_1}{\partial \eta},$$

$$K_z = \frac{1}{S_z}\Lambda^{-1}\beta^{\frac{3}{7}}k^{-\frac{9}{14}}J^{\frac{5}{7}}, \quad C_1 = -\frac{1}{S_z}\left(\frac{\partial G_1}{\partial \zeta}+1\right),$$

where S_y, S_z are non-dimensional functions of η, ζ. The coefficients of diffusion therefore decrease upstream as we would expect, and in general vary with the constants of the problem in a plausible way. But using (58) we have

$$\frac{1}{S_y}\left(\frac{\partial G_1}{\partial \eta}\right)^2+\frac{1}{S_z}\left(\frac{\partial G_1}{\partial \zeta}+1\right)^2 = 0.$$

This can only be true, however, if the diffusion coefficients are allowed to be negative. We see clearly that an analogy with molecular diffusion and friction is not useful in this problem of turbulence.

5. Circumferential equatorial jets

In the next section we apply the theory of the turbulent jet to the equatorial undercurrent. Before doing this we may mention here that westerly currents at the equator seem to be a very common feature of the atmospheres of the planets and the sun. In astrophysics it is known as the equatorial acceleration (Wasiutyński 1946; Cowling 1953; Hess 1951). In Jupiter, for example, this acceleration occurs in a band between $-7°$ and $+7°$ latitude and amounts to a relative angular velocity of about 1 % of the angular velocity of the planet ($\omega/\Omega \sim 0{\cdot}01$). In the atmosphere of the sun the acceleration is very strong, but very variable within a sunspot cycle, ω/Ω varying from 0·3 to 0·7 or so. The band containing high-speed fluid is between $-55°$ and $+55°$ when ω/Ω is a minimum; when ω/Ω is a maximum, the width of the band is very indefinite, but certainly even broader than this.

The same phenomenon occurs in our own atmosphere, although it is not yet known whether it extends round the entire globe (Lettau 1956). This jet is called the Berson westerlies by Lettau in honour of Berson who first reported the phenomenon (1910). Observations indicate that it is located in the stratosphere at around 20 km. It is about 5 km thick and 1500 km in north-south extent. The speeds are of the order of 10^3 cm sec^{-1}.

The theory of this paper can be modified to apply to this phenomenon. We need only recognize that there can be no variation of the mean quantities with longitude, so that Λ is simply an undetermined large number. The order of the width of the jet is the same, $\delta_y \sim \bar{u}^{\frac{1}{2}}\beta^{-\frac{1}{2}}$, or $\delta\theta \sim (\omega/2\Omega)^{\frac{1}{2}}$. This seems to describe in a rough way the variation in the size of the jet in the astrophysical examples.

If we apply the theory to the Berson westerlies, we get $\delta_y \sim 6\times10^7$ cm. This is considerably less than the observed width, but our knowledge of this current is still quite limited. If we use $\bar{u} = 10^3$, $k = 4\times10^{-4}$ we find $\delta_z \sim 5\times10^4$ cm which is very much too small. However, we should note that the westerly jet is im-

bedded in a belt of easterlies with a general drift of perhaps 3×10^3 cm sec^{-1}. It is more reasonable then to use for $\bar{u}$ the relative velocity of 4×10^3. This yields $\delta_z \sim 2 \times 10^5$ cm and $\delta_y \sim 1{\cdot}2 \times 10^8$ cm.

6. Application to the equatorial undercurrent

In any attempt to apply the above theory to the equatorial undercurrent we must recognize that an ocean surface exists in one case and not in the other. Our theory of a jet in an infinite fluid can be adapted to this case, however, as follows: if we guess that the mean theoretical axial velocity profile in a vertical section resembles that in figure 2 (counter currents are typical phenomena in rotating and stratified fluids), we could put in a free surface S at the indicated position without changing the situation substantially, provided the surface stress in the natural phenomenon is substituted for the stress exerted by the fluid above S in the theoretical situation. If we adopt this viewpoint, this force, supplied by the wind stress in the case of the ocean, may be related to the depth of the jet axis below the surface.

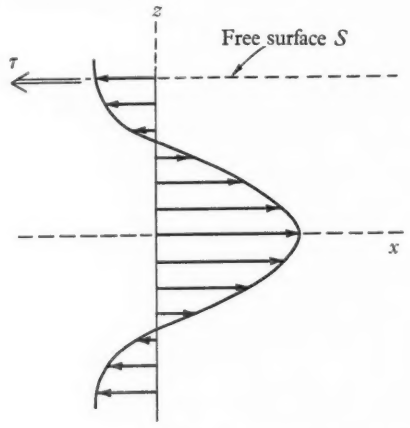

FIGURE 2. Schematic picture of vertical velocity profile of undercurrent.

In applying our theory to the Cromwell current we take as observed values (Knauss 1960) a mean velocity of $1{\cdot}5 \times 10^2$ cm sec^{-1}, width 3×10^7 cm, vertical thickness 2×10^4 cm, longitudinal length 5×10^8 cm or more, $\beta = 2{\cdot}3 \times 10^{-13}$ cm^{-1} sec^{-1}. If we use the given values of $\bar{u}$ and β, we may compute δ_y and δ_z. We get $\delta_y \sim 2{\cdot}6 \times 10^7$ cm, $\delta_z \sim 10^4$ cm, where we have estimated the stability parameter† $k = (g/\rho)\, d\rho/dz \sim 4 \times 10^{-4}$ sec^{-2}. Since the estimates are only supposed to be order of magnitude estimates, these results are remarkably close to the mark. The value of Λ is about 20 in this case, so that all turbulent quantities are $\frac{1}{4}$ to $\frac{1}{5}$ of the corresponding mean quantities.

Although we do not solve for the mean velocity and temperature fields in the jet we may make certain inferences about them. In figure 3 we picture the flow

† This estimate was supplied to me by Professor R. B. Montgomery.

in a vertical north-south cross-section. Since the motion is westerly in the jet the y- and z-equations of mean motion (or the thermal wind equation) require a temperature field in which the isotherms are roughly as drawn. This suggests the vertical and horizontal transverse velocities shown, and this is consistent with the equation of continuity (47). It is important to remark that this is precisely the observed form of the constant density surfaces in the vicinity of the Cromwell current as we see in figure 4. This transverse velocity field is also consistent with the Ekman wind-drift theory, which requires that the surface water move north and south away from the equator in this region.

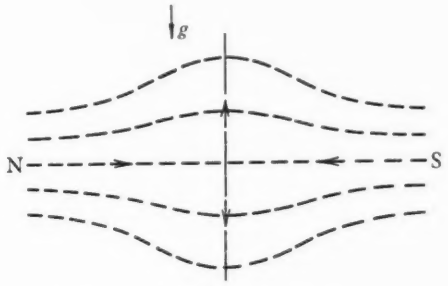

FIGURE 3. Mean temperature distribution in jet.

The author wishes to thank Professor R. B. Montgomery and Mr R. S. Arthur for a number of stimulating conversations about the undercurrent. This research was sponsored by the Office of Naval Research and the U.S. Weather Bureau.

Appendix

Jets are very common in stratified and rotating fluid systems. For example if a rotating fluid is heated, very pronounced, irregular jets occur at the free surface (Fultz *et al.* 1959). They resemble the famous Jet Stream of the atmosphere and other currents like the Gulf Stream in the oceans. In these phenomena the rotation itself, rather than the variation of the rotation, is probably the more important effect. An analysis, essentially the same as that above, can be applied to such a jet, using the same equations as (2)–(6) except that $f = 2\Omega$ replaces βy. The solutions all have the same form as (24)–(42). However, now we have $c = J^{\frac{1}{4}} f^{\frac{1}{4}} k^{\frac{1}{8}}$, $L = J^{\frac{1}{4}} f^{-\frac{3}{4}} k^{\frac{1}{8}}$, $\epsilon = fk^{-\frac{1}{2}}$, and in the differential equations of the first approximation η is missing in the terms corresponding to the Coriolis forces. We may compare these results with observations of the Jet Stream and Gulf Stream (Newton 1959; Stommel 1960). For example, Newton's data give for the ratio of depth to width 0·005 for both. We get precisely 0·005 for ϵ if we use the reasonable values $f = 10^{-4}$, $k = 4 \times 10^{-4}$. On the other hand, the theoretical estimates of the dimensions of the Jet Stream and Gulf Stream are too low by a factor of 2 or so.

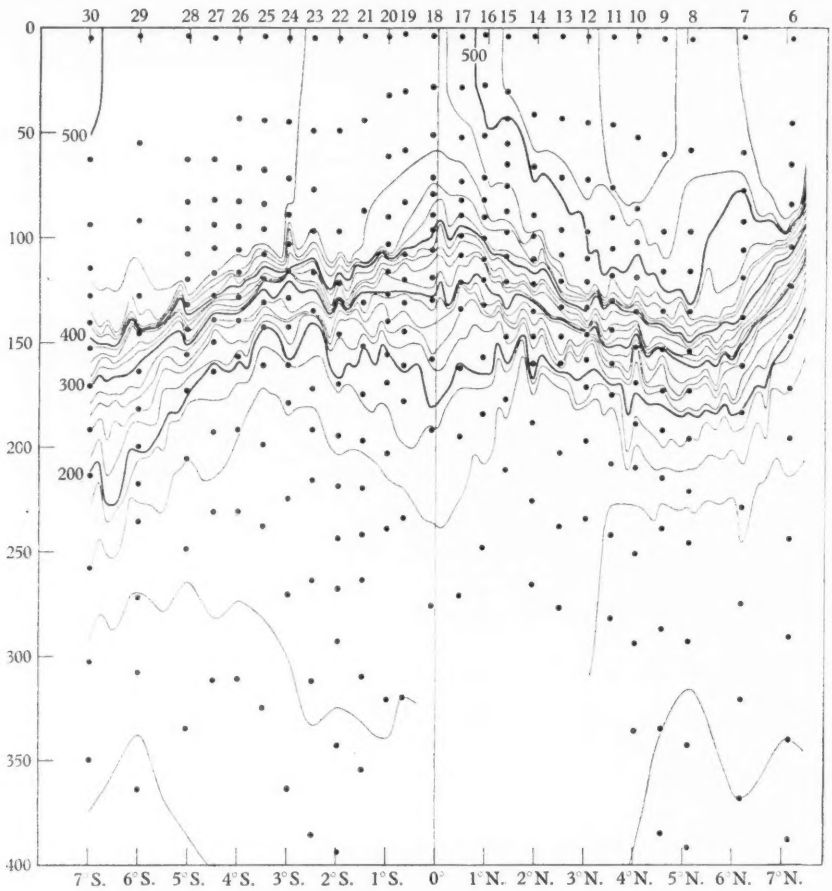

FIGURE 4. Specific-volume anomalies in centilitres per ton on vertical section in Pacific Ocean at 150° W. in July–August 1952. Observations from *Hugh M. Smith* of Pacific Ocean Fishery Investigations, U.S. Fish and Wildlife Service. Drawing from unpublished manuscript by R. B. Montgomery and E. D. Stroup.

REFERENCES

BERSON, A. 1910 Bericht über die aerologische Expedition des Königl. Aeronautischen Observatorium nach Ostafrika im Jahre 1910. *Ergebn. Arb. Preuz. Aeronaut. Obs. Lindenberg: Braunschweig.*

BIRKHOFF, G. 1950 *Hydrodynamics*, chapter IV. Princeton University Press.

BOUSSINESQ, J. 1903 *Théorie analytique de la chaleur*, Vol. **2**, p. 172. Gauthier-Villars.

COWLING, T. G. 1953 Solar electrodynamics. Article in *The Sun* (Ed. G. P. Kuiper). University of Chicago Press.

CROMWELL, T., MONTGOMERY, R. B. & STROUP, E. D. 1954 Equatorial undercurrent in Pacific Ocean revealed by new methods. *Science*, **119**, 648.

FOFONOFF, N. P. & MONTGOMERY, R. B. 1955 The equatorial undercurrent in the light of the vorticity equation. *Tellus*, **4**, 518.

FULTZ, D., LONG, R. R., OWENS, G. V., BOHAN, W., KAYLOR, R. & WEIL, J. 1959 Studies of thermal convection in a rotating cylinder with some implications for large-scale atmospheric motions. *Meteor. Monograph*, **4**.

HESS, S. L. 1951 The atmospheres of the other planets. *The Compendium of Meteorology*, p. 391.

HIDAKA, K. & NAGATA, Y. 1958 Dynamical computation of the equatorial current system of the Pacific, with special application to the equatorial undercurrent. *Geophys. J. Roy. Astr. Soc.* **1**, 198.

KNAUSS, J. A. 1960 Measurements of the Cromwell Current. *Deep Sea Res.* **6**, 265.

KNAUSS, J. A. & KING, J. F. 1958 Observations of the Pacific equatorial undercurrent. *Nature*, **182**, 601.

LETTAU, H. 1956 Theoretical notes on the dynamics of the equatorial atmosphere. *Beitr. Phys. Atm.* **29**, 107.

LONG, R. R. 1960 A laminar planetary jet. *J. Fluid Mech.* **7**, 632.

NEWTON, C. W. 1959 Synoptic comparison of Jet Stream and Gulf Stream systems. *The Atmosphere and Sea in Motion*, p. 288. New York: The Rockefeller Institute Press.

STOMMEL, H. 1960 *The Gulf Stream*, p. 202. University of California Press.

TOWNSEND, A. A. 1956 *The Structure of Turbulent Shear Flow*, p. 89. Cambridge University Press.

VERONIS, G. 1960 An approximate analysis of the equatorial undercurrent. *Deep Sea Res.* **6**, 318.

WASIUTYŃSKI, J. 1946 Hydrodynamics and structure of stars and planets. *Astrophysica Norvegica*, **4**, 497.

REVIEWS

International Summer Course in Plasma Physics. Danish Atomic Energy Commission, 1960. 645 pp. Dan.kr. 60,00.

In August 1960, the Danish Atomic Energy Commission organized a two-week course on plasma physics at their research establishment Risö. A distinguished team of a dozen lecturers was assembled from half a dozen countries, and over 130 students were enrolled. Only three months later the text of the lectures was published, in a report containing about 200,000 words. Evidently there is much interest in plasma physics these days, and there also seems to be a great deal to say about it. A brief reference, at the end of the report, lists the titles of fifteen additional seminars which took place, but whose text is not reproduced. Surely no group of students or lecturers can ever have worked harder.

Now the study of plasmas is interesting, for many reasons. At first sight a plasma may appear to resemble a gas, for it is compressible and has no structure. But the forces between the charged particles in a plasma are electromagnetic, and act over longer ranges than the forces between the molecules in a gas. Therefore we can normally consider that molecules interact only intermittently, when they approach close enough to each other, and that then they interact strongly. But it is more profitable to think of the particles in a plasma as interacting with each other the whole time, though in most cases the interaction between any pair of plasma particles is weak. Here lies the basic difference between these two states of matter: where close collisions dominate, the outcome of a particular encounter is rather uncertain, and this introduces a randomness into the mechanics of a gas, which is less pronounced in a plasma. A plasma particle interacts, essentially, with a continuum, whose behaviour is more predictable than that of a single molecule. We can therefore follow its progress in phase space more easily. A plasma thus tends to be more internally coherent, and a whole spectrum of waves becomes possible which is absent in a gas. The waves are important because they can lead to the growth of non-uniform electric and magnetic fields.

A plasma will respond strongly to an applied electric or magnetic field, and will at first try to exclude it from its interior, though in the case of a magnetic field this often leads to unstable configurations. In a plasma laced with a magnetic field the paths of the charged particles twist around the lines of force. If high-energy electrons are present, and they seem readily to be produced in such an active medium, they become powerful emitters of electromagnetic radiation.

Even the process of turning a gas into a plasma raises intriguing problems. Though they may have energy enough to detach electrons from one another, atoms and molecules are inefficient in producing ionization. But once a few free electrons exist and have picked up enough energy, the ionization sweeps on like an avalanche. Other interesting effects are the process by which neutrals and ions can exchange electrons, and the way in which contaminants, particularly

ions with one or three electrons, can be excited and then radiate. These are both important mechanisms for cooling a plasma.

Plasmas can be studied in many and widely different physical situations. They occur, for example, in radio stars and in the tails of comets, in the Van Allen belts and the curtains of the polar aurora, in lightning flashes and in television tubes. Yet none of these applications provoked the intensive modern work on plasmas. This is due to the hope that somehow one might be able to confine for a long enough time a plasma which is sufficiently hot, say at a temperature of about 10^8 degrees K. One could then set up a controlled thermonuclear reaction (C.T.R.), make helium from deuterium or tritium, and thus release a vast amount of energy. The confinement must be achieved by a skilfully designed magnetic field. The background to the Risö lectures is the question whether this can be done.

Here must be the hardest technical problem that man has yet set for himself. It is worth thinking about, for after its solution our fuel requirements will be met for the indefinite future. Though no one can reasonably maintain that it is an urgent question, it was, in the curious political circumstances of the last decade, turned into the theme of an international competition, rather like the race towards the moon. Fortunately it has now been realized that the fundamental physics must first be understood. This is quite well reflected in the various lectures. The exception is one contribution, describing a thermonuclear reactor, whose author first disarms his potential critics by admitting that plasmas are too unstable for his liking. His machine is therefore so designed that the plasma is not given time to perform its tricks properly, and by hurrying to forestall it, his machine might just scrape by with a very slight profit. It is all rather touch-and-go, like the old problem of filling a leaky bath tub with both taps full on.

In general the lecturers did not take such a point of view. They may have been thinking about thermonuclear reactors, but in doing so they felt obliged to consider almost all the different aspects of the behaviour of a plasma.

The contributors seem to have had different ideas of their responsibility to the audience. Some are represented in the report by photographic copies of papers published in well-known and highly accessible journals, none of them less than two years old at the time. Should these have been reproduced in the report? Surely anyone who wishes to read them can go to a library and do so. Surely also it is the duty of a lecturer to do more than read to his students extracts from the classics. He should produce the occasional enlightening example, point out the critical stages in an argument, be less insistent on rigour and completeness, and in general make the audience think.

Others again reported on very special studies, recently completed in their laboratories. These may indeed be most significant, but the reader does not know why and the audience was probably not certain either.

Such criticisms apply only to the minority, however. The majority of the lecturers seem to have given accounts of their subjects as proper and as balanced as our present knowledge allows. It is an engaging feature of this book that in some cases the reports reproduce the lectures almost as they must have been given, complete with the occasional slip in algebra or in spelling, and including

a few samples of typical lecture jokes. After reading them for a while one feels as though one were present oneself in the classroom at Risö.

Some of the contributions cause one to feel the same excitement that the audience must have felt on hearing physical problems discussed so lucidly and so graphically. Thus in the first lecture Rosenbluth describes, very briefly but with much insight, the basic dynamical processes of a plasma, and evaluates the characteristic quantities one has to watch. This must be the best introduction anywhere to these topics, and should be compulsory reading for all future plasma physicists.

This exceptionally high level of presentation is not reached again—after all, how could it be? But Rosenbluth scores again in an excellent account of micro-instabilities; other first-class contributions include Thompson's survey of instabilities, Simon's discussion of the collisionless Boltzmann Equation, and Wharton's three lectures on plasma waves and diagnostics.

After digesting the various reports one is deeply grateful to the lecturers for all the new points of view and amazed at the number of physical problems they have raised. Then one begins to wonder whether the material is not too much biased towards the interests of the C.T.R. physicist. To think so would be an unfair criticism. Suppose that a dozen astrophysicists had organized the course. In essence they would have had to discuss the same types of problem, for the nature of the Coulomb interaction, the Boltzmann Equation, the processes of ionization and charge exchange are quite universal. The main difference is that C.T.R. work has sometimes tended to concentrate on the study of some very special configurations, and has thereby distorted the development of the subject. Let a C.T.R. physicist have the last word (Bickerton, on page 453). 'The past experiments have been carried out in systems which were known or are now known to be unstable so that plasma behaviour has been complex and in detail incomprehensible. In the future it is to be hoped that by shifting the complexity to the external apparatus and by making a serious attempt to set up stable conditions in the plasma the resulting phenomena will be simpler and more pleasing.'

F. D. KAHN

THIRD INTERNATIONAL SYMPOSIUM ON RAREFIED GAS DYNAMICS

This symposium will be held at the University of Paris, June 26–29, 1962, and will be similar in scope and purpose to the first (Nice, 1958) and second (Berkeley, 1960) symposia with corresponding titles.

The programme will range from topics of immediate significance for upper atmosphere and space flight to basic scientific studies and will include the following areas:

Studies of the limits of the continuum theory or the quasi-equilibrium kinetic theory of gases

Problems in kinetic theory of gases, particularly attempts to solve the Boltzmann equation

Free-molecule and near-free-molecule flow in neutral and ionized gases

The physics of surface interactions between gases and solids

Boundary conditions for rarefied gas equations, and slip flow

Experimental techniques and instrumentation developments bearing on the above, whether applied to laboratory or field experiments

Edmond A. Brun (University of Paris) and Immanuel Estermann (Office of Naval Research, London) will act as co-chairmen; the editorial committee will be headed jointly by P. Germain, Paris, and L. Talbot, Berkeley. A call for papers will be distributed later.

Inquiries from the U.S. should be addressed to L. Talbot, Department of Aeronautical Sciences, University of California, Berkeley, and from Europe to Laboratoire d'Aerothermique, 4c, route des Gardes, Meudon (S & O), France.

JOURNAL OF FLUID MECHANICS

Volume 11, Part 3 November 1961

CONTENTS

The mechanism of transition in the wake of a thin flat plate placed parallel to a uniform flow
by HIROSHI SATO and KYOICHI KURIKI *page* 321

A study of natural convection above a line fire
by SHAO-LIN LEE and H. W. EMMONS 353

Experiments on the penetration of an interface by buoyant thermals
by J. M. RICHARDS 369

The effect of a sudden density change on a slightly non-uniform flow
by W. R. HAWTHORNE and P. J. BANKS 385

On corner eddies in plane inviscid shear flow
by L. E. FRAENKEL 400

The reactant concentration spectrum in turbulent mixing with a first-order reaction
by STANLEY CORRSIN 407

Theory of unsteady flow about thin cylinders in fluids of high electrical conductivity
by LEON E. RING 417

Notes on approximations for turbulent flows with large temperature differences
by D. J. TRITTON 440

The transverse force on a spinning sphere moving in a viscous fluid
by S. I. RUBINOW and JOSEPH B. KELLER 447

Photographic evidence of the formation and growth of vorticity behind plates accelerated from rest in still air
by D. PIERCE 460

A turbulent equatorial jet
by ROBERT R. LONG 465

REVIEWS
International Summer Course in Plasma Physics 478

Printed in Great Britain at the University Press, Cambridge
(Brooke Crutchley, University Printer)